



HAL
open science

Amygdala and prefrontal cortex anatomo-functional dialogue in supporting behavioral adaptation in primates

Camille Giacometti

► **To cite this version:**

Camille Giacometti. Amygdala and prefrontal cortex anatomo-functional dialogue in supporting behavioral adaptation in primates. Neuroscience. Université Claude Bernard - Lyon I, 2023. English. NNT : 2023LYO10214 . tel-04589726

HAL Id: tel-04589726

<https://theses.hal.science/tel-04589726v1>

Submitted on 27 May 2024

HAL is a multi-disciplinary open access archive for the deposit and dissemination of scientific research documents, whether they are published or not. The documents may come from teaching and research institutions in France or abroad, or from public or private research centers.

L'archive ouverte pluridisciplinaire **HAL**, est destinée au dépôt et à la diffusion de documents scientifiques de niveau recherche, publiés ou non, émanant des établissements d'enseignement et de recherche français ou étrangers, des laboratoires publics ou privés.



THÈSE de DOCTORAT
Université Claude Bernard Lyon 1

École Doctorale
ED 476 : NEUROSCIENCES ET COGNITION

Spécialité de doctorat : Biologie
Discipline : Neurosciences

**Amygdala and Prefrontal Cortex anatomo-
functional dialogue supporting behavioral
adaptation in primates**

Soutenu publiquement à Lyon le 09/11/2023, par :

Camille GIACOMETTI

Devant le jury composé de :

Pr. MACALUSO Emiliano
Dr. BOURET Sébastien
Dr. CAPPE Céline
Dr. KHAMASSI Mehdi
Dr. SLIWA Julia
Dr. AMIEZ Céline
Dr. HADJ-BOUZIANE Fadila

Université Lyon 1
CNRS, ICM Paris
CNRS, CerCo Toulouse
CNRS, ISIR Paris
CNRS, ICM Paris
CNRS, SBRI Lyon
CNRS, CRNL Lyon

Président
Rapporteur
Rapporteuse
Examinateur
Examinatrice
Directrice de thèse
Directrice de thèse

ABSTRACTS

English version

My thesis aims to explore how two crucial brain regions, the amygdala (AMG), a collection of subcortical nuclei, and the medial prefrontal cortex (mPFC), dialogue to guide behavioral adaptations in primates. Based on the literature, I highlighted three important points: 1) an expansion of one nucleus of the AMG, the lateral nucleus, in humans compared to others non-human primates, 2) the complex anatomo-functional dialogue between the heterogenous subdivisions of mPFC regions and AMG nuclei, 3) the absence of comparative studies on the functional dialogue within the AMG-mPFC network functional dialogue across primate species. The available evidence led me to hypothesized the possible existence of two distinct routes within the AMG-mPFC network that sustains behavioral adaptation and that may have diverged between macaques and humans. To test this hypothesis, I first carried out resting-state functional magnetic resonance imaging (fMRI) in humans and macaques using a similar experimental strategy to investigate the interplay between mPFC and AMG nuclei activity. My work revealed that indeed the functional connectivity of the AMG-mPFC network in macaques and humans display critical divergences that might relate to differential behavioral and emotional control abilities in line with the constraints in their respective ecological niches. Second, by means of fMRI and the development of a new adaptive task in humans, I demonstrated the engagement/disengagement of two distinct and complementary routes that sustained specific behavioral adaptation features, in line with the interplay observed at rest in the AMG-mPFC network. This thesis thus provides critical information of the nature of the dialogue in the AMG-mPFC network and its similarity and divergence between the human brain and its closest model, i.e., the macaque brain.

French version

Ma thèse vise à explorer comment deux régions cruciales du cerveau, l'amygdale (AMG), un ensemble de noyaux sous-corticaux, et le cortex préfrontal médian (mPFC), dialoguent pour guider les adaptations comportementales chez les primates. Sur la base de la littérature, j'ai souligné trois points importants : 1) l'expansion d'un noyau de l'AMG, le noyau latéral, chez l'humain comparé à d'autres primates non humains, 2) le dialogue anatomo-fonctionnel complexe entre les subdivisions hétérogènes des régions du mPFC et les noyaux de l'AMG, 3) l'absence d'études comparatives sur le dialogue fonctionnel du réseau AMG-mPFC entre les espèces de primates. Sur la base de ces résultats, j'ai émis l'hypothèse de l'existence possible de deux voies distinctes au sein du réseau AMG-mPFC qui soutiennent l'adaptation comportementale et qui pourraient avoir divergé entre les macaques et les humains. Pour tester cette hypothèse, j'ai d'abord réalisé une étude d'imagerie par résonance magnétique fonctionnelle au repos (rs-fMRI) chez l'homme et le macaque en utilisant une stratégie expérimentale similaire pour étudier l'interaction entre l'activité des noyaux de l'AMG et les régions du mPFC. Mon travail a révélé que la connectivité fonctionnelle du réseau AMG-mPFC chez les macaques et les humains présente des divergences critiques qui pourraient être liées à des capacités de contrôle comportemental et émotionnel différentielles en accord avec les contraintes de leurs niches écologiques respectives. Deuxièmement, en combinant l'approche IRMf et le développement d'une nouvelle tâche adaptative chez l'homme, j'ai démontré l'engagement/désengagement de deux voies distinctes et complémentaires qui soutiennent des caractéristiques d'adaptation comportementale spécifiques, en accord avec l'interaction observée au repos dans le réseau AMG-mPFC. Cette thèse fournit donc des informations essentielles sur la nature du dialogue dans le réseau AMG-mPFC et sur ses similitudes et divergences entre le cerveau humain et son modèle le plus proche, i.e., le cerveau du macaque.

TABLE OF CONTENTS

INTRODUCTION	5
Chapter I. Navigate through a complex and changing environment: a snippet into behavioral adaptation	6
Chapter II. Neural supports of behavioral adaptation, a specific focus on the amygdala and prefrontal cortex	11
1. The Prefrontal Cortex	11
1.1. The medial Prefrontal Cortex	13
1.1.1. The ventromedial PFC	14
1.1.2. The cingulate cortex: ACC and MCC	17
The anterior cingulate cortex	18
The midcingulate cortex	19
1.2. The lateral Prefrontal Cortex: focus on the dlPFC	23
2. The amygdala	25
Chapter III. Multiple routes of communication within the amygdala-mPFC network: A comparative approach in humans and macaques	29
Abstract	29
1. Introduction	30
2. Morphological comparison of the amygdala nuclei volumes in primates	31
3. Amygdala and medial prefrontal cortex anatomical connections in humans and macaques	36
4. Functional connectivity in the AMG-mPFC network in humans and macaques	38
5. Multiple routes of communication within the amygdala-mPFC network in macaques and humans: functional significance and future directions	42
Chapter IV. Project Overview	60
1. The functional connectivity pattern of the AMG-PFC network in primates	60
2. The functional interplay in the AMG-PFC network during behavioral adaptation in humans	61
EXPERIMENTAL PART	64
Chapter I. Frontal Cortical Functional Connectivity Is Impacted by Anaesthesia in Macaques	65
Abstract	65
Introduction	66
Materials and Methods	68
Results	78
Discussion	87
Chapter II. Differential Functional Organization of Amygdala-medial Prefrontal Cortex Networks in Macaque and Human	101
Abstract	101

Introduction	102
Results	103
Discussion	109
Methods	114
Chapter III. The Functional Interplay of the Fronto-Amygdala Network During Behavioral Adaptation in human	126
Abstract	126
Introduction	127
Materials and Methods	129
Results	137
Discussion	145
GENERAL DISCUSSION	158
Chapter I. Findings Overview	159
Chapter II. AMG-PFC anatomo-functional interplay contribution to behavioral adaptation in humans	162
1. Detection and contextual evaluation of salient events: AMG-vmPFC	162
2. Detection of learnt behaviorally significant events: MCC-dIPFC	165
Chapter III. Humans and macaques similarity and divergence within the AMG-mPFC network, a possible behavioral explanation?	169
1. Morphological evolution: LA expansion, a human feature	169
2. Resting-State interactions: a functional connectivity shift in the AMG-mPFC network	171
3. Humans and macaques: differences in behavioral expression?	172
Chapter IV. Future perspectives	177
1. Beyond the AMG-mPFC network, whole brain connectivity	177
2. Towards causally identifying AMG-PFC functional interaction	181
BIBLIOGRAPHY	187
APPENDIX	212
Supplementary Methods	213
1. Whole brain AMG parcellation and connectivity using a rs-fMRI data driven parcellation	213
2. Transcranial ultrasound stimulation approach on the whole AMG in macaques	217
Publications	220

INTRODUCTION

CHAPTER I. NAVIGATE THROUGH A COMPLEX AND CHANGING ENVIRONMENT: A SNIPPET INTO BEHAVIORAL ADAPTATION

If we go back to the origin of the words - and not the world -, from a biological, psychological and evolutionary point of view, behavior is defined as "*an observable response produced by an organism*" and adaptation as "*a process of change that an organism undergoes to be better suited to its environment*". Consequently, behavioral adaptation (BA) is defined as the ability of an organism to adjust its behavioral response in its own environment. It is important to note that an organism's adaptive behavior can only be defined in regards to its own ecological niches (*i.e.*, the external environment in which an organism evolves). Since this environment is neither fixed nor stable, behavioral adaptation is generally observed in response to environmental, expected or unexpected, changes and demands. This capacity is therefore crucial for an organism to properly navigate in its environment and interact with its peers or its surroundings and most importantly to ensure its survival. As the environment becomes more complex, an organism has to rely on higher-level cognitive functions including learning, reasoning, remembering, decision-making and attention (Staddon, 2016).

Memory is a crucial and fundamental mental process, and, without it, individuals would be limited to simple reflexive and stereotyped behaviors (Staddon, 2016). Indeed, memory plays a central role in behavioral adaptation because it allows us to record, consolidate and retrieve the history of our past experiences (*i.e.*, long-term memory). Storing a representation of the environment along with its specific context, with the response produced and the received feedback (positive or negative), allows us to respond accordingly in similar situations. As such, this process is critical to guide and optimize our future behaviors. For example, if during childhood, one accidentally -or intentionally- encounters an unpleasant event (fire, rotten and/or non-comestible food, etc.), the memory of that experience will deter any future attempts. Although, depending on the situation an individual can also rely on a more immediate memory system (*i.e.*, as short-term memory), such as working memory. It refers to the capacity of holding a small amount of information in an active, readily available state for a short interval of time and manipulate it to execute a task (Baddeley, 2003). For instance, remembering a sequence of previous choices to appropriately anticipate and choose

the next one. Therefore, memory serves as an essential foundation for behavioral adaptation, particularly for two intertwined processes: preserving our previously learnt experiences and manipulating immediate stored information.

Learning and memory are closely entwined, as learning can be broadly defined as the process of acquiring memories (Okano et al., 2000). Through a learning process we are able to acquire new knowledge, new skills, or even to develop strategies, build expectations, make predictions, as well as update and refine what we have already learnt. Learning enables us not only to respond to old challenges in our environment, but also to tackle new and unfamiliar ones more effectively (*i.e.*, notion of transfer in learning: the use of previously acquired knowledge and skills in a new learning situation; Haskell, 2004). Importantly, previously learnt associations might serve as a baseline level for processing other expected and/or unexpected events (*i.e.*, notion of uncertainty, O'Reilly, 2013; Soltani & Izquierdo, 2019). Indeed, in an uncertain environment, individuals can develop expectations, based on previous stored experiences, and thus adjust their actions accordingly. In order to adapt, and through the mechanism of learning, individuals are able to acquire and build contingencies between diverse elements of their environment: stimuli and responses, action and outcomes, action and feedback, etc. This mechanism is referred to as associative learning and is fundamental to shape behaviors (see for review Pearce & Bouton, 2000; Wasserman & Miller, 1997).

The process of making choices and selecting the most appropriate course of actions and/or strategies among a set of alternatives in a given context is defined as decision-making (Fellows, 2004; Shadlen & Kiani, 2013; Usher et al., 2013). Decision-making is an executive function involving the integration of a variety of external and internal stimuli (*i.e.*, multimodal sensory inputs, physiological and emotional states, past associations and future goals) that must be processed with information such as uncertainty, cost-benefit, risk to select the most appropriate actions (Fellows, 2004). By definition, decision-making is a vital component that coordinates behavioral adaptation. For instance, in the animal realm when confronted by danger, after a short time weighing its chances of survival (e.g., benefit/risk, past experiences), the animal action choices would be generally narrowed down to two options, the “fight or flight” or “approach or avoidance” responses. Similarly, in the case where an animal seeks to satisfy its internal needs such as hunger, it can either decide between exploring its environment for better and more valuable options or exploit its current option. In that

case, once its choice is fully depleted, it may need to explore its environment again. As humans, in our everyday life, while we may not have any predator *per se*, we are also encountering this kind of situation: wandering around trying to find a restaurant to eat, wondering whether to stick on the current known restaurant (“This Italian is always good”) or to shift for newer and/or better options further away (“This Japanese is new, it looks appealing, we should try it”). These two previous examples represent a typical example of a foraging paradigm in the neuroeconomic field where the forager must decide to leave a current research patch in search of another while evaluating the different options and balancing the cost/benefits to do so (Davidson & El Hady, 2019; Lee, 2006). Broadly, the notion of value in decision-making is conceptualized in two visions: “economic value” where value is referred to as a measure of the benefit that an individual can gain from choosing an option and “core value” that evokes the individual's own beliefs in reference to the affect, preferences, motivation and goals to achieve etc. Making a choice across several options is generally an assessment and combination of both values representations (Brosch & Sander, 2013). Indeed, it is important to emphasize that the value given to an environmental stimulus is not fixed. On the moment, it relies on the integration and combination of external factors such as the other available options values or the environmental conditions (*e.g.*, weather, the place, state of the field, peers’ opinion etc.) and internal factors such as physiological states for example the state of satiety or our level of motivation (Fellows, 2004). From a biological perspective, motivation is a fundamental process that allows individuals to effectively manage the demands of their external and internal environments. In neuroeconomics, motivation is further defined as a cost-benefit trade-off: maximizing the stimulus utility, *i.e.*, perceived value, while minimizing its associated costs such, *i.e.*, effort, delay, or uncertainty. Costs, particularly effort, primarily come into play during the initial seeking phase of motivated decision-making, where individuals must decide whether to pursue a rewarding stimulus or not (see for review Chong et al., 2016).

The notion of decision-making also implies being able to regulate the consequence of our actions on the environment to guide future behavior. The monitoring of our own action, also defined as performance monitoring, engages the notion of feedback (FB) and its direct association in time with the executed action (*i.e.*, associative learning). By definition a FB leads to an update of the situation and thus induce a necessity to adapt our behavior once again (*i.e.*, an action-FB loop; Powers,

1973). Indeed, FB can either be positive or negative and guide us to adjust our action (Powers, 1973): maintain our current options if it is beneficial or shift it if it is not (*i.e.*, for the later FB reflect an error signal, we adapt our strategy after an erroneous choice). To note, all functional explanations of behavior depend on the dichotomic notion of understanding what is good and what is bad: *i.e.*, rewards and punishments dimension (Staddon, 2016). It is important to note that given the uncertainty of the environment, our decision outcomes and their FB are also sometimes uncertain as they might change over time (*i.e.*, options and action-outcome association can rapidly evolve as the environment demands quickly shift), and by default not every outcome will influence our behavior (Soltani & Izquierdo, 2019; Staddon, 2016). Therefore, it is crucial for an individual to effectively monitor and detect, via all these aforementioned cognitive processes, environmental events and/or situations that require an adaptation.

To engage in effective decision-making and flexibility adapt our behavior in a given situation, we must first evaluate our environment in search for relevant events, assess the value of the available options by building expectations based on past learnt experiences and thus accumulate a certain quantity of evidence in time towards the available choices of action (Fellows, 2004; Lunenburg, 2010; Powers, 1973; Shadlen & Kiani, 2013). We also need to consider the motivational cost-benefit trade-off, our internal state (*i.e.*, emotional and physiological, etc.) as well as our future goals to achieve (Chong et al., 2016; Fellows, 2004). Then, once our action is selected and implemented, we have to monitor its consequences on the environment to adjust and regulate our behavior accordingly (Fellows, 2004; Lunenburg, 2010; Powers, 1973; Shadlen & Kiani, 2013).

To summarize, decision-making is a dynamic and flexible process that can be broadly divided in 4 main steps: identification of options, assessing values, choice selection, choice evaluation (Fellows, 2004; Lunenburg, 2010; Powers, 1973).

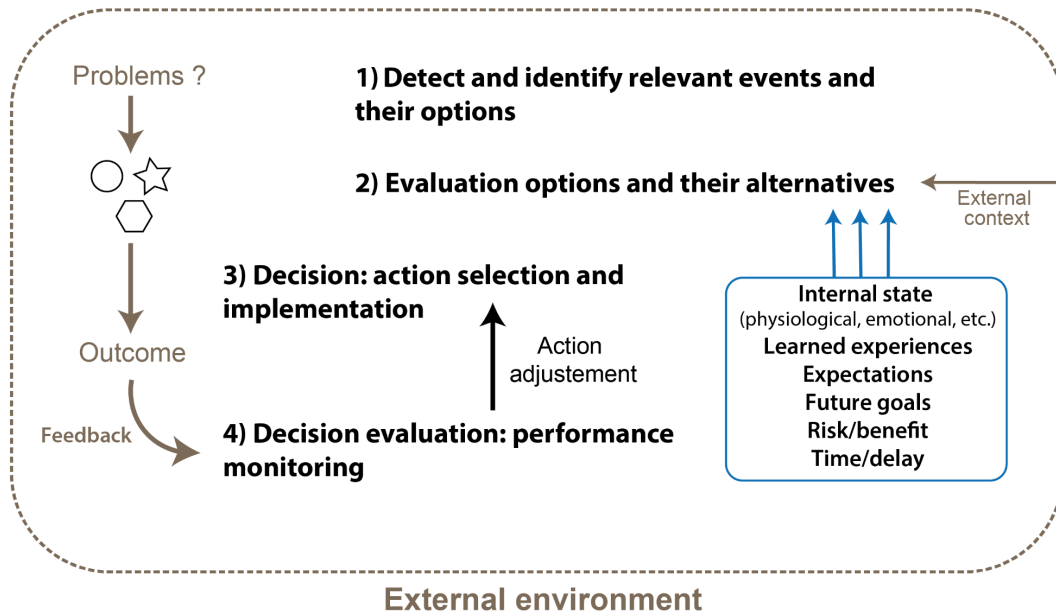


Figure 1. Schematic representation of decision-making.

Simplified representation of the 4 main steps of decision-making inspired by the representation of Powers 1973, Fellows 2004 and Lunenberg 2010 representation.

Various brain regions scattered throughout the cortex support these functions and by extension behavioral adaptation. In the context of my thesis, I will particularly focus on the decision-making process of behavioral adaptation with a particular emphasis on two interconnected brain regions: the prefrontal cortex (PFC) and the amygdala (AMG). Indeed, when adapting and taking decisions in a complex and uncertain environment the network formed by the AMG and PFC is on the front row to conceptualize the behavioral relevance of particular salient event of our environment and trigger an adaptation (Gangopadhyay et al., 2021; Murray & Fellows, 2021; Saez et al., 2015).

CHAPTER II. NEURAL SUPPORTS OF BEHAVIORAL ADAPTATION, A SPECIFIC FOCUS ON THE AMYGDALA AND PREFRONTAL CORTEX

In this section, I will first non-exhaustively discuss the structural and functional composition of the PFC (mainly the mPFC and dlPFC) and with some snippets on its evolution in primate. The second part will be dedicated to the amygdala. I will mainly and briefly focus on the origin of its complex organization and the evolution of its functional role. Indeed, AMG structural and functional composition and as well as its evolution in primates is further developed in the next chapter: ***Chapter III. Multiple routes of communication within the amygdala-mPFC network: A comparative approach in humans and macaques*** (Giacometti et al., 2023).

1. THE PREFRONTAL CORTEX

The frontal cortex is characterized by several areas that are distinguished by their unique laminar organization (*i.e.*, the organization of layers of different types of neuronal cells in the cortex, defined for example as agranular and granular cortex) in both its medial and lateral surfaces. Despite the large extension of the frontal cortex in humans (Semendeferi et al., 1997; Semendeferi & Damasio, 2000; Smaers, 2013; Smaers et al., 2011, 2017; Teffer & Semendeferi, 2012), this organization exhibits similar spatial localization within and across primate species and represents the cytoarchitectural mapping (*i.e.*, differing in the number and density of cell bodies in the cortical layers; Brodmann, 1909; Petrides & Pandya, 1994). Along the cytoarchitectonic boundary and as a consequence of cortical folding, the cortex displays gyri and sulci formations (*i.e.*, gyrification; Petrides & Pandya, 1999). The organization of cortical sulci and cytoarchitectonic areas presents a remarkably intimate relationship, as sulci are either limiting (*i.e.*, boundaries between areas) or axial to cytoarchitectonic areas (Amiez et al., 2019, 2023; Jiang et al., 2021; Novek et al., 2023; Petrides, 2005; Petrides & Pandya, 1994, 1999; Vogt et al., 1995, 2005).

In primates, the frontal lobe comprises three main areas: the motor cortex, the premotor cortex and the prefrontal cortex. Although the first two are mostly associated with motricity, from motor programming to movement production, the prefrontal cortex is neither purely motor nor sensory, but rather underlies higher-order control

processes of cognition (Fuster, 1991, 2001; Yeterian et al., 2012). The frontal cortex is the cerebral cortex that covers the lateral and medial surface of the frontal cortex anterior to the central sulcus (or Rolandic fissure) and dorsal to the lateral sulcus (or Sylvian fissure). The PFC is the part of the frontal cortex located, ventrally, anterior to the inferior precentral (IPRS) and, dorsally, the posterior part of the posteromedial frontal sulcus (PMFS-P) (Amiez et al., 2023). The PFC is a highly heterogeneous and complex structure consisting of a large number of distinct areas with different cytoarchitecture, structural and functional connectivity, and function. According to Brodmann's (1909) cytoarchitectonic map with further corrections from Petrides and Pandya (1994), it comprises the medial prefrontal cortex (mPFC), encompassing areas 9, 10, 14, 23, 24, 25 and 32, and the lateral prefrontal cortex (IPFC), comprising areas 8, 9, 9/46, 10, 44, 45, 46 and 47/12 (Brodmann, 1909; Passingham, 2021; Petrides & Pandya, 1994; Vogt & Palomero-Gallagher, 2012). It is important to note that, in accordance with Vogt and Passingham's definition of the PFC, the orbitofrontal cortex (OFC) is categorized as a distinct structure separate from the PFC and is thus not included in this chapter.

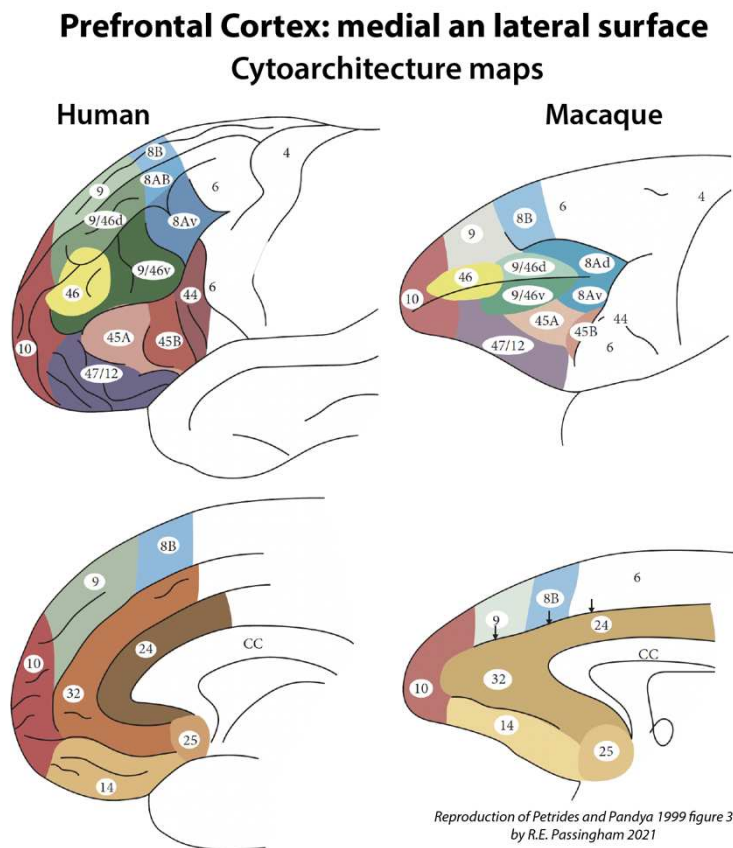


Figure 2. Prefrontal cortex cytoarchitecture organization in human and macaque. Cytoarchitecture maps of the medial and lateral prefrontal cortex (PFC) surface extracted from Passingham 2021 reproduction of Petrides and Pandya 1994.

The PFC is widely recognized as a central hub for executive functions (Fuster, 2001; Passingham, 2021). Its involvement covers most stages, if not all, of the decision-making processes, positioning the PFC as a central node of behavioral adaptation. In short, its medial ventral segment primarily focuses on stimulus evaluation, dynamically adapting based on our goals, motivations and internal states, its medial dorsal sector is dedicated to monitoring performance, involving outcome-based decisions, feedback evaluation and decision assessment and its lateral component is responsible for actively monitoring, manipulating and integrating information that is essential for planning and executing behavior (non-exhaustively: Amiez et al., 2005, 2006, 2012; Amiez & Petrides, 2014; Apps et al., 2016; Behrens et al., 2007; Boorman et al., 2013; Domenech & Koehlin, 2015; Gläscher et al., 2012; Grabenhorst & Rolls, 2011; Hiser & Koenigs, 2017; Juechems et al., 2019; Kolling et al., 2012; Loh et al., 2020; Passingham, 2021; Pelliccia et al., 2023; Procyk, Amiez, et al., 2016; Procyk, Wilson, et al., 2016; Quilodran et al., 2008; Rothé et al., 2011; Rushworth et al., 2004, 2011; Sallet et al., 2013; Scholl et al., 2015; Silvetti et al., 2013; Trudel et al., 2021; Vassena et al., 2014; Vogt & Palomero-Gallagher, 2012; Wittmann et al., 2016; Zangemeister et al., 2020).

1.1. THE MEDIAL PREFRONTAL CORTEX

The medial part is subdivided in several subregions. In humans and non-human primates (NHP), these regions are arranged ventro-dorsally along the corpus callosum (CC). Ventrally, below the genu of CC, the ventromedial prefrontal cortex (vmPFC) is occupied by cytoarchitectonic areas 14m, 25, s25 and s32 (Lopez-Persem et al., 2019; Mackey & Petrides, 2010, 2014; Palomero-Gallagher et al., 2015; Vogt, 2016; Vogt & Palomero-Gallagher, 2012). Dorsally, the cingulate cortex is composed of the gyrus situated between the CC and the cingulate sulcus (CGS) and both the dorsal and ventral banks of the CGS. In both humans and great apes (e.g., chimpanzees; Amiez et al., 2013, 2019, 2021; Miller et al., 2021), the cingulate cortex encompasses a second sulcus directly above and parallel to the CGS, the paracingulate sulcus (PCGS), that is present in 70% of cases in at least one hemisphere. The cingulate cortex is further divided in 4 subregions: the anterior (ACC), mid (MCC), posterior cingulate (PCC), and retrosplenial (RSC; *i.e.*, 4 regions models: Palomero-Gallagher et al., 2009). Located just anterior of the genu of the CC, the ACC occupies cytoarchitectonic areas 24 and 32, further divided in p24, 24c and p32 (Vogt et al.,

2016). More dorsally and posterior to the genu of the CC, the MCC encompasses cytoarchitectonic area 24 and 32, and more precisely areas a24', p24', a24c', p24c', 24d and 32' (Palomero-Gallagher et al., 2009; Vogt et al., 2003, 2005). The PCC is posterior to the MCC and is composed of cytoarchitectonic areas 23 and 31. The RSC is located along the splenium and is composed of cytoarchitectonic areas 29 and 30. Finally, above the cingulate cortex is situated the dorsomedial PFC (dmPFC), typically composed of area 9m (Passingham, 2021).

Here, I will focus exclusively on the vmPFC, ACC and MCC, as these regions are the main regions I investigated for my thesis because of their intricate anatomo-functional connection with the AMG (see **Chapter III of the Introduction**) and their role in behavioral adaptation through decision-making dimension.

1.1.1. THE VENTROMEDIAL PFC

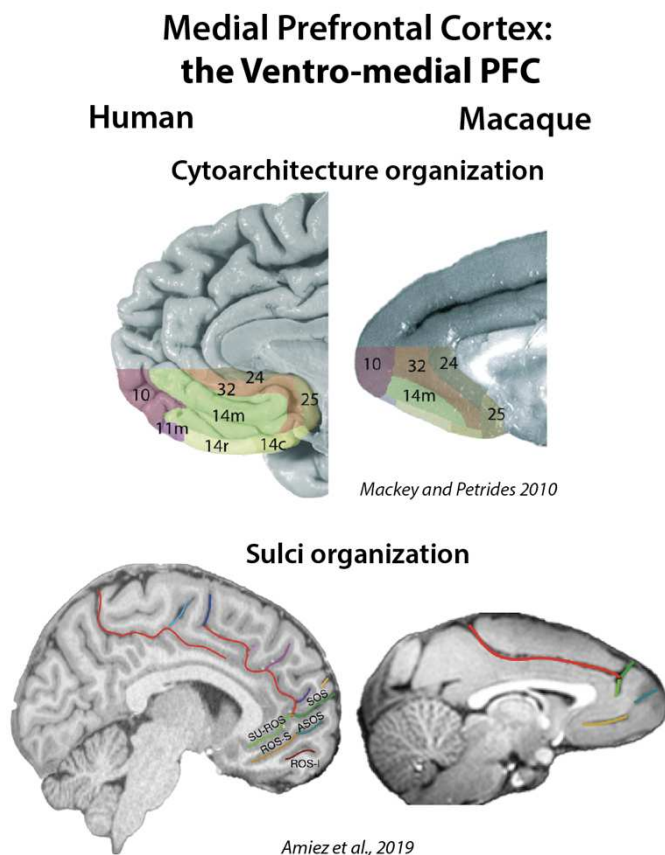


Figure 3. Medial prefrontal cortex: ventro-medial division Prefrontal cortex cytoarchitecture and sulci organization in human and macaque. Cytoarchitecture maps extracted from Mackey and Petrides 2010 and sulci organization from Amiez et al., 2019.

Structural distinction and boundaries of the vmPFC region is tricky, as “vmPFC” refers to a functionally-defined region (Lopez-Persem et al., 2019). It occupies a large portion of the ventral part of the mPFC and contains several cytoarchitectonic areas 14m, 25, s25 and s32 (Lopez-Persem et al., 2019; Mackey & Petrides, 2010, 2014;

Palomero-Gallagher et al., 2015; Vogt, 2016; Vogt & Palomero-Gallagher, 2012) with debated boundaries (Mackey & Petrides, 2010; Wallis & Rich, 2011). Indeed, the limitation between vmPFC and the frontopolar cortex, and with the orbitofrontal cortex (OFC), is still vague. Moreover, for quite a long time it has been associated as a part of the ACC, often refers as subgenual ACC (sgACC or sACC) as opposed to perigenual ACC (pgACC, pACC or rACC, see next section), but vision changes as these two regions differs in terms of cytoarchitecture, neurochemistry, structural and functional connections as well a function (Palomero-Gallagher et al., 2015; Vogt & Palomero-Gallagher, 2012). In the context of my thesis, I will use the terminology vmPFC to refer to this region.

Lopez-Persem et al., (2019), attempt to better characterize the vmPFC on the basis of sulcal morphology and resting-state fMRI in humans (rs-fMRI; Lopez-Persem et al., 2019). Understanding the sulcal pattern of a region is essential to properly interpreted its function as in most case 1) sulci are limitant between two defined cytoarchitectonic -and functional- regions and 2) the location an activation in fMRI can variate depending on the absence or presence of a sulcus (Amiez et al., 2012, 2013, 2019, 2023; Jiang et al., 2021; Loh et al., 2020; Mackey & Petrides, 2010, 2014). They found that 1) vmPFC is functionally organized around two principal sulci (superior rostral sulcus and suprarostal sulcus, ROS-S and SU-ROS respectively) and mainly encompass area 14m and 25 and 2) vmPFC morphology and functional organization (i.e., vmPFC peak within the default mode network, a network define in rs-fMRI and homologous in both humans and macaques, Hutchison & Everling, 2012; Miranda-Dominguez et al., 2014) is impacted by the interindividual variability of the sulcal patterns (i.e., secondary and/or supplementary sulci presence and location).

Numerous studies in comparative neuroscience have provided important insights into structural and functional homology of the vmPFC between humans and NHP (Mackey & Petrides, 2010, 2014; Neubert et al., 2015). More precisely, Mackey and Petrides (2010, 2014) conducted histological quantitative analyses that revealed analogous architectonic areas within the vmPFC of human and macaque monkeys. From a functional perspective, Neubert et al. (2015) combined rs-fMRI with a comparative approach that match the functional connectivity profiles of a given region from one specie to another (i.e., matching fingerprint analysis, Mars et al., 2016, 2018; Neubert et al., 2015), highlighting the functional similarity of the vmPFC between the two species. Furthermore, Amiez et al., (2019) have shown that the superior border of

the vmPFC with the ACC is defined as the junction of 2 sulci forming a fork shape at the rostral extremity of the CGS: the supra-orbital sulcus (SOS) pointing in upwards and the SU-ROS pointing downwards (of note, in human when a PCGS is present, the fork is more frequently located at the rostral end of the PCGS; Amiez et al., 2019). Although this fork shape is always present in primates, some divergences appeared between the *Hominidae* group (great apes and humans) and the Old-World monkeys (baboons and macaques). Indeed, the form and orientation of these folds is highly variable between species: in humans and chimpanzees, the fork is pointing downwards while in macaques the fork is pointing forwards in the majority of cases. This has been suggested to reflect the extension of the mPFC in *Hominidae* (Amiez et al., 2019).

Except from its strong structural and functional connection with the AMG (see **Chapter III of the Introduction** for more details), tracer studies in macaques have demonstrated strong structural connections of vmPFC with the cingulate cortex region (including ACC, MCC, and PCC), temporal cortices including the entorhinal cortex, parahippocampal cortex, superior temporal sulcus and gyrus (STS, STG), the hippocampus (HPC), striatum, insula, and OFC (Barbas & Pandya, 1989; Carmichael & Price, 1995; Joyce & Barbas, 2018; Kondo et al., 2005; Vogt & Pandya, 1987; Wang et al., 2021). Similarly, in humans, data-driven parcellation of the mPFC (diffusion MRI associated with deep brain stimulation and rs-fMRI) as shown that the vmPFC corresponding cluster shares strong functional connections with the striatum (stronger connection with the ventral division than for the dorsal division of the striatum), hypothalamus (HP), hippocampus (HPC) the OFC (medial and lateral) and weaker connection for the parietal cortex (Beckmann et al., 2009; Johansen-Berg et al., 2008; Margulies et al., 2007; Vergani et al., 2016).

In primates, vmPFC appears to be involved in a wide range of functions closely related to decision-making and especially in monitoring current environment options and its updates. VmPFC lesions studies specifically demonstrated a deficit in emotional state regulation and in value representation with an absence and/or a weakened ability to process the affective attribute of stimuli and its updates, a particularly inability to anticipate future consequences following a decision and social behavior inadequacy (Bechara et al., 1999, 2000; Clark et al., 2008; Gläscher et al., 2012; Hampton et al., 2007; Schneider & Koenigs, 2017). Further neuroimaging studies in humans, have shown its involvement in value-based decision-making:

representing and assessing the value of a current stimulus/choices, expected choices, track of previous choices and rewards associated to a decision (Behrens et al., 2007; Boorman et al., 2013; A. Harris et al., 2011; Hiser & Koenigs, 2017; Kolling et al., 2012; Mehta et al., 2019; Rushworth et al., 2011; Spalding et al., 2018; Trudel et al., 2021; Vassena et al., 2014). Finally, vmPFC is also a key region in social decision-making (Dang et al., 2019; Hiser & Koenigs, 2017; Olsson et al., 2020; Van Den Bos & Güroğlu, 2009).

1.1.2. THE CINGULATE CORTEX: ACC AND MCC

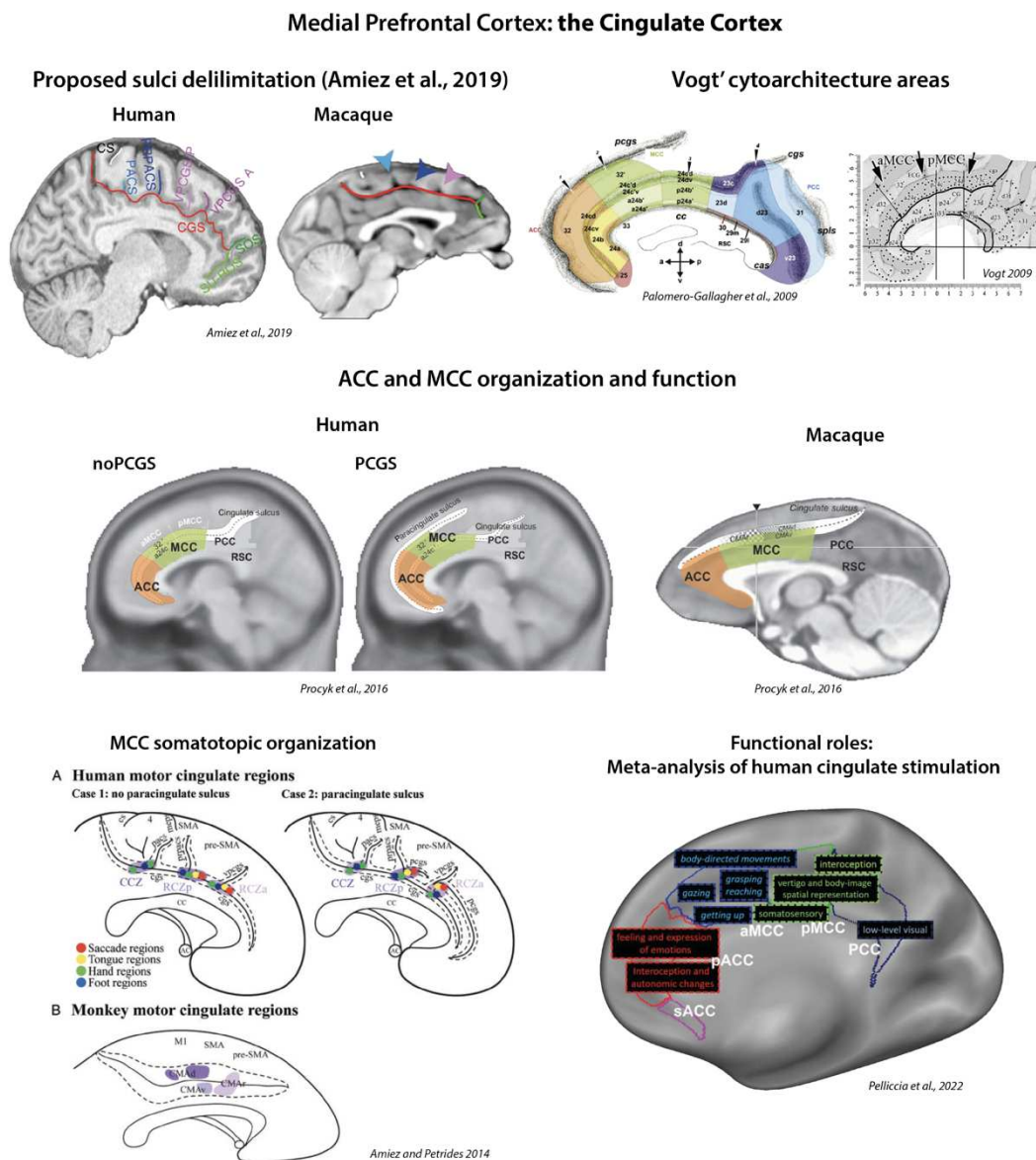


Figure 4. Medial prefrontal cortex: cingulate cortex region cytoarchitecture, sulci organization and function in human and macaque. *Top panel:* general sulci organization extracted from Amiez et al., 2019 and cytoarchitecture maps extracted from Palomero-Gallagher et al., 2009 and Vogt 2009. *Bottom panel:* in the top and right bottom corner, specific organization of the ACC and MCC in humans

and macaque monkeys (extracted from *Procyk et al., 2016* and *Amiez and Petrides 2014*). In the bottom left corner, ACC and MCC functional roles extracted from the meta-analysis of human cingulate stimulation by *Pelliccia et al., 2022*.

Based on the cytoarchitecture, the cingulate cortex has been divided in 4 main regions, from rostral to dorsal: the ACC, the MCC, the PCC and the retrosplinal cortex (RSC; 4 regions models: (Palomero-Gallagher et al., 2009; Vogt, 2009; Vogt & Palomero-Gallagher, 2012). Although, only the ACC and MCC regions belong to the mPFC. As seen in the vmPFC section above, sulci have been proposed as boundaries between brain regions. Concerning the cingulate cortex, Amiez et al. (2019) proposed that the sulci extending from the CGS perpendicularly towards the brain superior surface delimited the 3 cingulate cortex regions in primates (Amiez et al., 2019). More precisely, the anterior vertical paracingulate sulcus (VPCGS-A), located at the level of the rostral limit of the genu of the CC would delimitate the ACC and MCC and the paracentral sulcus (PACS), located at the level of the rostral limit of the pons, is the limit between MCC and PCC (Loh et al., *in prep*). It is important to emphasize that, while the PCGS is strictly found in *Hominidae* (humans, great apes), all the other sulci present in human brains on the medial surface of the brain are also present, fully or as precursors (e.g., dimples or spurs) in Old-World monkeys' brains (macaques, baboons). Here, I will specifically focus on the ACC and MCC.

THE ANTERIOR CINGULATE CORTEX

Compared to vmPFC region, the ACC, situated rostrally to the genu of the CC, contains less cytoarchitecture areas, mainly composed of regions 24 and 32, more precisely, 24abc and 32p (Palomero-Gallagher et al., 2008; Vogt, 2009). In the literature, it either refers to pgACC/pACC or rACC (stands for rostral, compared to dACC see next section on MCC). In the context of my thesis, I will use Vogt's nomenclature and refer to this region as ACC (Palomero-Gallagher et al., 2008; Vogt, 2009, 2016; Vogt & Palomero-Gallagher, 2012).

Expect the slight divergence of the vmPFC/ACC limit between Great Apes and humans vs. Old-World Monkeys, the ACC appears to be structurally and functionally conserved across primate' species (Amiez et al., 2019; Neubert et al., 2015; Passingham, 2021; Vogt & Palomero-Gallagher, 2012). Monkey tracer studies have shown that ACC is structurally interconnected with the AMG (see **Chapter III of the Introduction**), the hippocampus (HPC), the striatum, the Locus Coeruleus (LC), the hypothalamus (HP), the periaqueductal gray region (PAG), the PCC, and prefrontal

regions including dorsomedial PFC (dmPFC), dlPFC, OFC and vmPFC (Barbas & Pandya, 1989; Carmichael & Price, 1995; Chiba et al., 2001; Morecraft et al., 2012; Vogt & Pandya, 1987; Wang et al., 2021). In terms of structural connections, one particular connection that differentiates ACC from MCC, is an absence or very light structural connections between the ACC and the parietal cortex compared to MCC (Vogt & Palomero-Gallagher, 2012). Functional connectivity studies using rs-fMRI in both humans and monkeys have confirmed that the ACC shares functional connectivity strength with the dlPFC, striatum, PCC and hippocampus (Beckmann et al., 2009; Margulies et al., 2007; Neubert et al., 2015).

From my knowledge, the ACC shares a mixed function in between vmPFC and MCC, respectively involved in value-based decision-making/emotion regulation and goal-directed behavior/performance monitoring respectively (see previous section for vmPFC and next section on MCC for more details). This complexity might also stem from the lack of consensus regarding its nomenclature, which in turn complicates the demarcation of this region from the vmPFC and MCC in neuroimaging studies (Vogt & Palomero-Gallagher, 2012). Indeed, neuroimaging studies in humans have shown that ACC is often activated alongside with the vmPFC in value-based decision-making especially during the monitoring of choices and expected choices values (Behrens et al., 2007; Klein-Flügge et al., 2022; Rushworth et al., 2011). ACC also co-activated with MCC during conflictual information detection and behavioral switch (see for review Klein-Flügge et al., 2022).

Regardless, through its functional and structural connections with autonomic center, the ACC has been suggested to have a pivotal role in internal-guided behaviors (Etkin et al., 2011; Palomero-Gallagher et al., 2008; Vogt & Palomero-Gallagher, 2012). Neuroimaging and intracerebral electrical stimulation studies of ACC has notably demonstrated its important contribution to autonomic outflow regulation as well as emotion expression and regulation in humans (see for review Pelliccia et al., 2023).

THE MIDCINGULATE CORTEX

The growing interest of MCC as an important center of executive function further accelerated its consideration as a single functional and structural unit and not just a subdivision of the ACC (Vogt, 2009, 2016). As a result, in the literature a lot of studies and still up today referred to the MCC as the dorsal ACC (Procyk, Wilson, et al., 2016; Vogt, 2009, 2016). For the rest of my thesis, I will use Vogt's nomenclature.

The MCC is a complex and heterogeneous region of its own and has been further subdivided, based on cytoarchitecture, in an anterior and posterior part namely the aMCC and the pMCC respectively (Vogt, 2009, 2016; Vogt et al., 1995, 2003). In primates, the structural boundary between these two MCC subregions is defined by the pre-paracentral sulcus (Amiez et al., 2019). Importantly, the MCC encompasses cingulate motor areas (CMA; Dum & Strick, 1991, 1992, 2002; He et al., 1995). CMAs were originally discovered in monkeys using intracortical micro-stimulation, as well as by anatomical demonstration of connection to the premotor cortex, the primary motor cortex, and the spinal cord (Dum & Strick, 1991, 1992, 2002; He et al., 1995). Three main CMA divisions have been defined: CMAr, CMA_d, and CMA_v (for rostral, dorsal, and ventral CMAs), the more rostral one CMAr belonging to the aMCC while the two more dorsal ones belonging to the pMCC and PCC respectively (Dum & Strick, 1991, 2002; He et al., 1995a; Luppino et al., 1991; Morecraft et al., 1996, 2007). In the monkey, CMAr occupies both banks of the CGS, while the two others, CMA_d and CMA_v, are located on the dorsal and ventral banks of the CGS respectively (Dum & Strick, 2002). Although humans and monkeys have been suggested to be homologous (Procyk, Wilson, et al., 2016; Vogt, 2016), monkeys CMAs' nomenclature is not used and they are rather referred as rostral cingulate zones anterior and posterior, RCZa and RCZp respectively for CMAr and CMA_d, and caudal cingulate zone (CCZ) for the CMA_v. Similarly, to monkeys, the 3 human CMAs are located along a rostro-caudal axis along the CGS and PCGS with RCZa situated the most rostral followed by RCZp and CCZ (Amiez & Petrides, 2014; Picard & Strick, 2001). In both humans and monkeys, the CMAs contain face and body somatomotor representations. More precisely, whereas both the two anterior CMAs (CMAr/RCZa and CMA_v/RCZp) contain one hand, one foot and one face motor representation each, the posterior CMA (CMA_v/CCZp) contains two hand and a foot representation (Amiez & Petrides, 2014; He et al., 1995b; Luppino et al., 1991). In humans, Amiez's team further precise that when a PCGS was present, the face motor representations in RCZa and RCZp would be reliably found in the PCGS, but, when it was absent, they would be always located in the CGS (Amiez et al., 2013; Loh et al., 2018, 2020). Related to the presence of PCGS in humans, Palomero-Gallagher and Vogt (2008), highlighted that this secondary sulcus is closely related to the presence of the area 32' in the MCC. Macaque monkeys do not present a PCGS and thus do not seem to have an area 32' (Amiez et al., 2019; Palomero-Gallagher et al., 2008; Vogt & Palomero-Gallagher,

2012). However, note that great apes such as Chimpanzee do present both a PCGS and an area 32', thus it seems that is a morphological brain characteristic that appeared after the split between Hominidae and Old-World monkeys (Amiez et al., 2021).

The 3 CMAs anatomo-functional connections are organized along a rostro-caudal gradient with fronto-lateral regions. Tracer studies in monkeys have shown that the most anterior CMA (CMAr) has strong structural connections with the prefrontal cortex and pre-SMA and weaker structural links with the premotor and motor areas, whereas the caudal CMAs (CMAAd and CMAv) show reversed pattern with stronger connections with motor-related and weaker links with prefrontal areas (Dum & Strick, 1991; He et al., 1995b; Luppino et al., 1993; Morecraft et al., 2012; Petrides & Pandya, 2006). MCC's CMAs rostro-caudal organization has been further evidenced with rs-fMRI in humans and awake macaques monkeys: the most rostral CMA (CMAr/RCZa) exhibited stronger correlation strength with rostral (Area 10, dlPFC, Broca area) compared to caudal lateral frontal cortical areas (Motor region M1 Hand and Face, Frontal eye field) while the more caudal CMAs (CMAAd/RCZp and CMAv/CCZ) displayed stronger correlation strength with caudal compared to anterior lateral frontal cortical areas (Giacometti et al., 2022; Loh et al., 2018). All together this rostro-caudal connectivity pattern among MCC in both humans and macaques, suggests a differential functional involvement of rostral vs. caudal CMAs where the former is more implicated in high-order cognitive function and the later in lower order motor control function (Loh et al., 2018). Note that tracer studies in macaques also demonstrated that the CMAs also present structural connections with the AMG (see **Chapter III of the Introduction** for more details), the superior temporal gyrus and sulcus (STG and STS), the parietal cortex, the insula, OFC, PCC, preSMA, ACC, and vmPFC (Barbas & Pandya, 1989; Carmichael & Price, 1995; Morecraft et al., 2012; Vogt & Pandya, 1987). Further rs-fMRI studies in humans and macaques have shown functional connections of the CMAs with the striatum, premotor cortex, SMA, M1, the operculum, the parietal cortex, PCC, and hippocampus (Beckmann et al., 2009; Neubert et al., 2015).

Several studies in both humans and macaques have shown that the MCC has a crucial role in goal-directed behavior and performance monitoring including errors predictions, conflict, behavioral switch, and actions-FB detection exclusively when they trigger a need to adapt for future behaviors (Amiez et al., 2005, 2006, 2012, 2013;

Amiez & Petrides, 2014; Loh et al., 2020; Pelliccia et al., 2023; Procyk, Amiez, et al., 2016; Procyk, Wilson, et al., 2016; Quilodran et al., 2008; Rothé et al., 2011; Rushworth et al., 2004; Scholl et al., 2015; Vogt, 2016; Wittmann et al., 2016). Concerning the latter, several of these studies have demonstrated that the somatotopic organization of MCC' CMAs reflects fields devoted to the detection and evaluation of motor domain-specific FB relevant for adaptations: gustatory FB (e.g., juice reward) recruits the orofacial motor representation of the rostral CMA (Procyk, Wilson, et al., 2016), auditory FB (e.g., vocal and verbal) involves the face motor representation of the CMA (Loh et al., 2020), and somesthetic FB on the hand (e.g., air puff) recruits the hand motor representation of the CMA (Amiez et al., 2013; Amiez & Petrides, 2014). To note, MCC also appears to partake in autonomic system regulation: MCC activation correlates with the recruitments of both the sympathetic and parasympathetic autonomous systems; this activation recruits the same sulcal regions as the one involves in FB evaluation (Amiez & Procyk, 2019).

Altogether, these 3 regions within the mPFC, *i.e.*, vmPFC, ACC and MCC, appear to display complementary functions in the decision-making process. This functional synergy follows a hierarchical and progressive pattern, ranging from the evaluation and analysis of environmental stimuli and internal states to the detection of actionable feedback. As we move caudally along the corpus callosum and along a strengthened connection with motor regions, the relationships of these regions to action monitoring and sensorimotor functions becomes more pronounced. To note, the PCC situated caudally to the MCC (include area 23d and 31) is involved in visuospatial orientation and adjustments (Vogt & Palomero-Gallagher, 2012). Conversely, more ventral and rostral regions appear to be more predisposed to subjective contextual understanding of both internal and external environments (Calderazzo et al., 2021; Juechems et al., 2019; Pelliccia et al., 2023; Shen et al., 2023; Vogt & Palomero-Gallagher, 2012).

1.2. THE LATERAL PREFRONTAL CORTEX: FOCUS ON THE dlPFC

The IPFC covers the lateral surface of the brain on both sides, it is divided in two components, a dorsal and a ventral part, respectively named dlPFC and vlPFC. The dlPFC include cytoarchitectonics areas 8, 9/46, 46 and 9 and the vlPFC comprise areas 44, 45 and 47/12. The inferior frontal dimple is the limiting sulcus situated between these two regions, more precisely it separates area 45 from area 9/46 (Amiez et al., 2023; Petrides, 2005; Petrides & Pandya, 1994, 2002). Despite the large enlargement of the frontal lobe and particularly its lateral part (Semendeferi et al., 1997; Semendeferi & Damasio, 2000; Smaers, 2013; Smaers et al., 2011, 2017; Teffer & Semendeferi, 2012), the IPFC presents comparable organization across primates species in terms of cytoarchitecture and sulci (Amiez et al., 2023; Petrides, 2005; Petrides & Pandya, 1994, 2002). Recently, Amiez et al., (2023) highlighted sulci organization difference between *Hominidae* and Old-World monkeys, 3 sulci appeared only in great apes and humans compared to macaques and baboons and has been suggested to reflect the expansion of the dlPFC cytoarchitectonic areas 10, 46 and 9 (Amiez et al., 2023). In the context of my thesis, we were mostly interested in dlPFC, thus I will mostly focus the following paragraphs on this subregion.

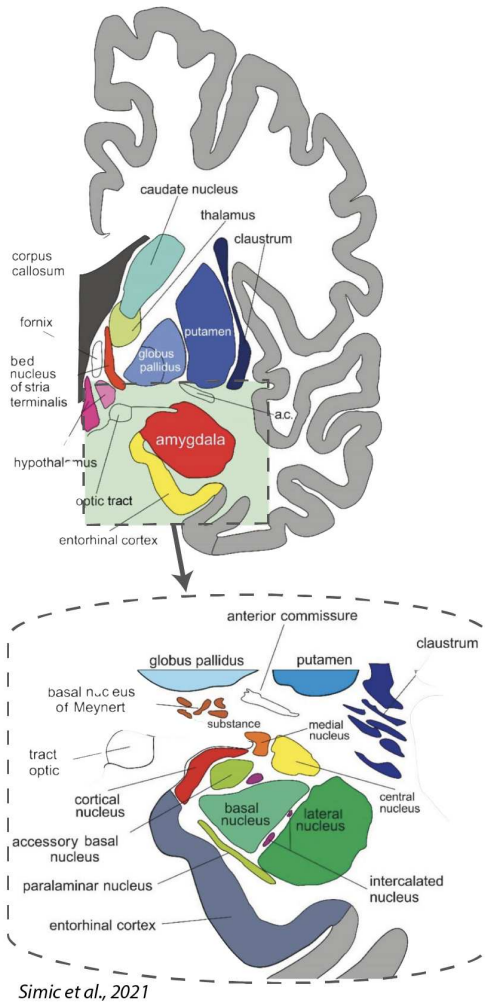
In the macaque brain, on the dlPFC surface lies the principal sulcus that encompasses along to its rostro-caudal axis cytoarchitectonic areas 10, 46 and 9/46 in both its dorsal and ventral banks sulci (Petrides, 2005; Petrides & Pandya, 1994, 1999, 2002). Consistent with Petrides and Pandya's definition, when referring to the dlPFC in humans and monkeys, the majority of studies have considered exclusively the lower half of the dlPFC, constituted by area 46 and 9/46 (Petrides & Pandya, 1999). Note that 9/46 can be further divided in a dorsal and ventral part relative to the principal sulcus dorsal and ventral banks (d9/46 and v9/46; Petrides & Pandya, 1999). Sallet et al. (2013) further identified functionally these two areas in humans and their correspondences in macaques based on their profile of functional connectivity from rs-fMRI. Results corroborated with previous cytoarchitecture definition and structural connection via tracer studies in macaques (Sallet, Mars, et al., 2013). Overall, dlPFC is connected to the STS, frontal eye field (FEF), the lateral intraparietal cortex, motor cortex, premotor cortex, preSMA, MCC and its CMAs and RSC (Borra et al., 2019; Gerbella et al., 2013; Morecraft et al., 2012; Petrides, 2005; Petrides & Pandya, 1999).

According to its connectivity profile, the dlPFC has access to multimodal and processed sensory inputs from the temporal and parietal cortices, memory systems through the retrosplenial cortex and towards the hippocampus, and motor outputs. This supports the commonly accepted role of the dlPFC in cognitive control, monitoring, manipulation and integration of different types of information for behavior planning and execution, as well as working memory and language processing (Gläscher et al., 2012; Hertrich et al., 2021; Loh et al., 2020; MacDonald et al., 2000; Panikratova et al., 2020; Petrides, 2000, 2005; Pochon, 2001; Tanji & Hoshi, 2008).

2. THE AMYGDALA

In this section, I will have a few words about the origin and function of the AMG as its morphology, structural and functional connectivity with the mPFC is further discussed in details in the next Chapter of the Introduction (**Chapter III. Multiple routes of communication within the AMG-mPFC network: A comparative approach in humans and macaques**; Giacometti et al., 2023).

Amygdala location and composition



Amygdala connectivity

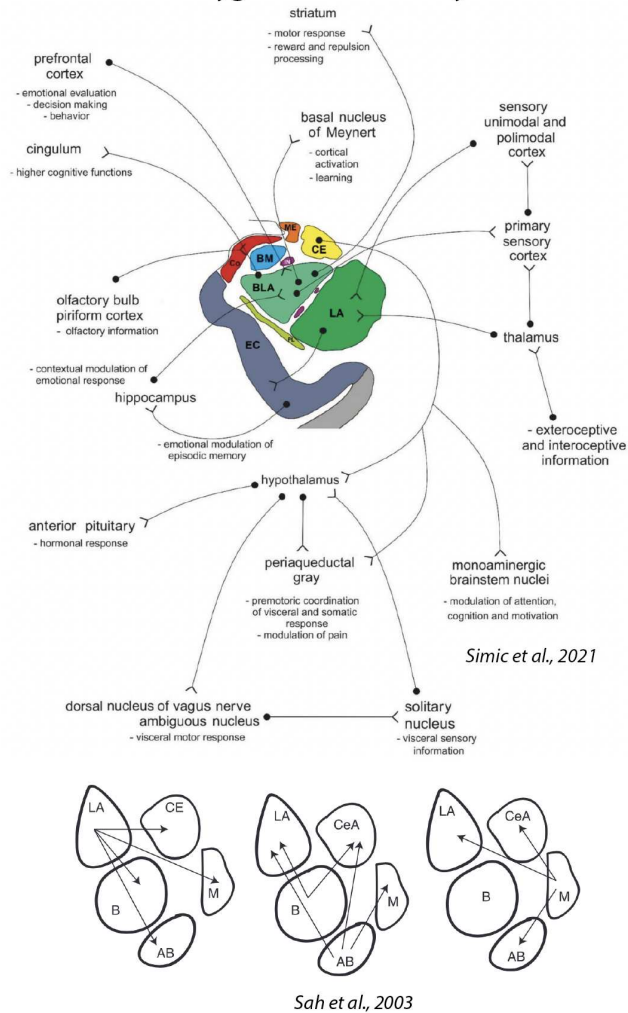


Figure 5. Schematic and simplified representation of the amygdala location, composition and connectivity. Left column and top right images are modified schema extracted from Simic et al., 2021. The bottom right schema is extracted from Sah et al., 2003. Nomenclature: AB and BM respectively accessory basal or basomedial nucleus represent the same nucleus under different terminology; same apply to B or BLA/BL respectively basal and basolateral nucleus; CE/CeA: central nucleus; M/Me: medial nucleus; LA: lateral nucleus.

Nested deep in the temporal lobe, the AMG lies at the anterior border of the hippocampal formation and the anterior aspect of the lateral ventricle's inferior horn.

In neuroimaging study in both humans and macaques the amygdala is often seen as a single brain unit. However, AMG is a heterogeneous and highly complex mosaic-like structure composed of an ensemble of nuclei, approximately 13, with distinct neurochemistry, cytoarchitecture, structural and functional connections. As such, the AMG is often referred to as “the amygdaloïd complex” (Aggleton, 2000; Medina et al., 2011; Sah et al., 2003; Šimić et al., 2021; Swanson & Petrovich, 1998).

Briefly, in primates, AMG nuclei can be broadly parcellated into deep and superficial groups. The deep group is composed of the lateral (LA), basal (B), and accessory basal nuclei (AB) (Aggleton, 2000; LeDoux, 2007; Price et al. 1987). It can also be referred to as the basolateral and/or laterobasal subdivision in neuroimaging (Amunts et al., 2005). Certain studies used different terminology: the basal and accessory basal nuclei can also be referred to as basolateral and basomedial nuclei respectively (BL and BM; Barbas & de Olmos, 1990). Anatomically, the superficial group consists in the majority of the medial (ME) and cortical (CO) nuclei, letting aside remaining nuclei including the central (CE) nucleus (the term corticomедial complex can also be found in the literature to refer to this group). According to the basolateral/laterobasal subdivision terminology, further studies use the centromedial and superficial subdivision for the remaining nuclei subdivision to refer to the grouping of the central and medial nucleus (Amunts et al., 2005). Note that each nucleus can be further divided into several portions, *e.g.*, medial and lateral. Another important part of the AMG is a ribbon of inhibitory neurons between the central and basolateral nuclei, the intercalated masses (IM), thought to gate information flow from the basolateral to the central nucleus (Royer et al., 1999).

This complex and rich organization of AMG nuclei is the result of embryological differentiation during development (Humphrey, 1968; Medina et al., 2011; Swanson & Petrovich, 1998). Based on genoarchitecture in mammals (*i.e.*, gene expression and composition patterns within a neural structure, see Puelles & Ferran, 2012) combined with neurochemistry and connectomics studies, it has been suggested that the AMG originated from the caudal pole of two main embryonic divisions of the telencephalon: the pallial (*i.e.*, similar to cerebral cortex) and subpallial parts (*i.e.*, similar to basal ganglia; Humphrey, 1968; Medina et al., 2011; Swanson & Petrovich, 1998). Broadly, the basolateral and cortical nuclei group are thought to derive from the ventral and lateral sections of the pallial division while the centromedial nuclei group including the intercalated mass derives from the subpallial division (Medina et al., 2011; Swanson

& Petrovich, 1998). Note that the extended AMG, composed notably of the bed nucleus of the stria terminalis and central nucleus, has some hypothalamic origins (Medina et al., 2011).

Lastly, it is worth noting that these nuclei are intricately interconnected, forming a microcircuit within the AMG. In particular, it has been proposed that sensory information enters the AMG via the basolateral division, with a strong emphasis on the lateral nucleus as a sensory receiver and the basal and basomedial nucleus as receivers of more complex information from associative cortices. Once processed, information then follows a predominantly lateral-to-medial trajectory to the centromedial division, which acts as an output station (Aggleton, 2000; Sah et al., 2003). This micro-network suggests extensive local processing of information that contributes to the integrated functioning of the AMG as a whole in supporting the production of appropriate behavioral outcomes.

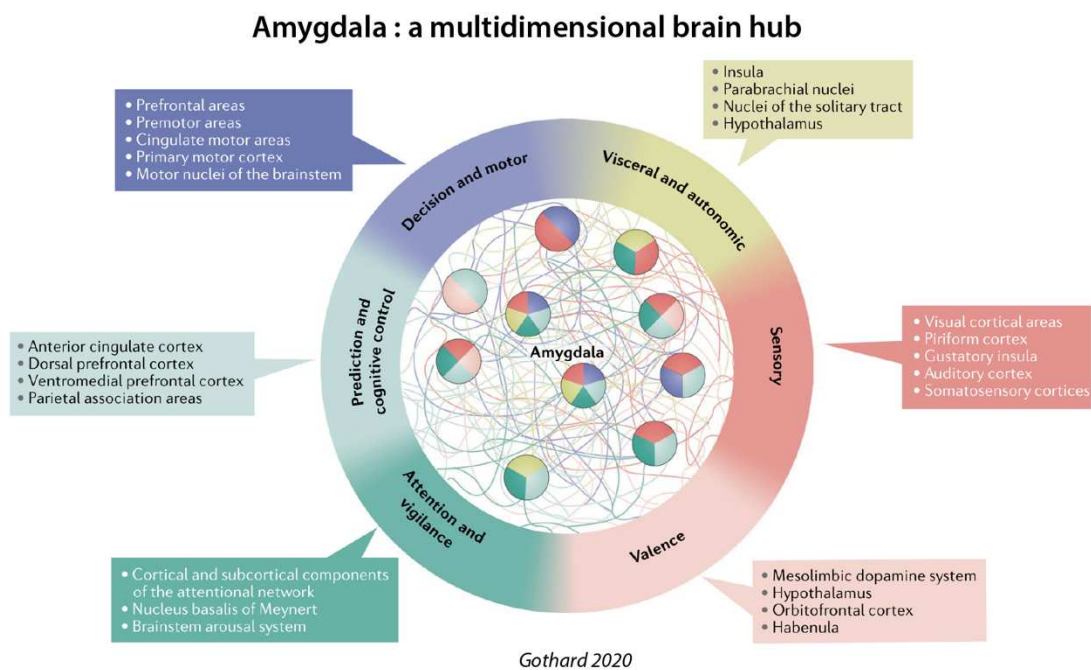


Figure 6. New perspective of AMG functional role: a multidimensional structure at the intersection of brain-wide circuits. Extracted from *Gothard 2020*.

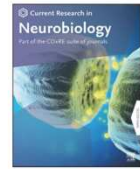
For many years, the AMG has been almost exclusively seen as a fear processing center in humans and non-human primates. Yet, in the last two decades other perceptions of the roles of the AMG have emerged. Through its widely cortical and subcortical structural and functional connections and accumulating evidence from lesions and neuroimaging studies, the AMG has been suggested to participate in a wide range of cognitive processes non-exhaustively including learning, value and

reward processing during decision making, goal-directed behavior, attentional and vigilance processes notably in the detection of salient events, emotion and a wide range of processes in social cognition (non-exhaustively: Amir et al., 2015; Bechara et al., 1999, 2003; Belova et al., 2008; Bermudez & Schultz, 2010; Bickart et al., 2012, 2014; Dal Monte et al., 2015, 2022; Grabenhorst et al., 2019; Grabenhorst & Schultz, 2021; Morrison & Daniel Salzman, 2010; Morrow et al., 2019; Ousdal et al., 2008, 2014; Putnam & Chang, 2021; Rudebeck et al., 2013, 2017; Seymour & Dolan, 2008; Taswell et al., 2021; Tottenham, 2015; Wassum & Izquierdo, 2015; Zangemeister et al., 2016). Recently, a new model for AMG functions has been proposed, placing the AMG as an important multidimension processing hub in the brain, i.e, a central structure at the intersection of brain-wide networks (Gothard, 2020).

The next chapter aims at describing the evolution in the primate order of the morphology, structural and functional connectivity of the AMG-mPFC network and its potential behavioral implications. This chapter has been published as a review (Giacometti et al., 2023).

Contents lists available at [ScienceDirect](https://www.sciencedirect.com)

Current Research in Neurobiology

journal homepage: www.sciencedirect.com/journal/current-research-in-neurobiology

CHAPTER III. MULTIPLE ROUTES OF COMMUNICATION WITHIN THE AMYGDALA-MPFC NETWORK: A COMPARATIVE APPROACH IN HUMANS AND MACAQUES

Camille Giacometti^{1,}, and Céline Amiez^{1,*} and Fadila Hadj-Bouziane^{1,*}*

¹ Equal contributions

* Corresponding author

ABSTRACT

The network formed by the amygdala (AMG) and the medial Prefrontal Cortex (mPFC), at the interface between our internal and external environment, has been shown to support some important aspects of behavioral adaptation. Whether and how the anatomo-functional organization of this network evolved across primates remains unclear. Here, we compared AMG nuclei morphological characteristics and their functional connectivity with the mPFC in humans and macaques to identify potential homologies and differences between these species. Based on selected studies, we highlight two subsystems within the AMG-mPFC circuits, likely involved in distinct temporal dynamics of integration during behavioral adaptation. We also show that whereas the mPFC displays a large expansion but a preserved intrinsic anatomo-functional organization, the AMG displays a volume reduction and morphological changes related to specific nuclei. We discuss potential commonalities and differences in the dialogue between AMG nuclei and mPFC in humans and macaques based on available data

Key words: Amygdala, Medial Prefrontal Cortex, Anatomo-functional connectivity, Human, Non-human primate.

1. INTRODUCTION

From the exploration of the environment to the regulation of mood and decision making, the amygdala (AMG) and its dynamic interactions with the medial prefrontal cortex (mPFC) encompass a wide range of functions that support behavioral adaptation in primates (see for review [Gangopadhyay et al., 2021](#); [Murray and Fellows, 2021](#)). These interactions are thought to allow us to react to relevant salient information from our environment and to regulate, control, and adjust these reactions when necessary ([Kim et al., 2011](#)). Accordingly, clinical studies in humans ([Johnstone et al., 2007](#); [Price and Drevets, 2010](#); [Likhtik and Paz, 2015](#); [Mukherjee et al., 2016](#); [Dong et al., 2019](#); [Paul et al., 2019](#); [Li et al., 2021](#)) and lesion studies in the most studied model of the human brain, i.e., the macaque rhesus ([Málková et al., 1997](#); [Bechara et al., 1999](#); [Rudebeck et al., 2013](#); [Wellman et al., 2016](#); [Elorette et al., 2020](#); [Taswell et al., 2021](#)), have shown that such behavioral adaptation abilities depend, at least in part, on the integrity of this network. In particular, a dysregulation of the top-down control of the mPFC onto the AMG, present in a wide range of pathologies, leads to inappropriate and maladaptive behavioral reactions ([Johnstone et al., 2007](#); [Dong et al., 2019](#)).

Over the course of primate evolution, behavioral adaptation has evolved to permit the proper navigation of each species in their respective ecological niches. In humans, this ability reaches its highest level of complexity to face highly complex environments and social interactions ([Henke-von der Malsburg et al., 2020](#)). However, whether and how the anatomo-functional interactions of this AMG-mPFC network changes in the primate order to subserve behavioral adaptation with increasing complexity is still currently poorly understood. In the present review article, we aimed at providing insights toward that question by identifying, in humans and macaques, homologies and differences of the morphological characteristics of the AMG nuclei and their functional connectivity with the medial prefrontal cortex, two aspects that are often considered separately. Regarding the functional organization of these networks, we deliberately focus on resting-state functional Magnetic Resonance Imaging (rs-fMRI), a powerful tool increasingly used to study functional networks in comparative neuroscience. By doing so, we sought to identify the potential relationships between anatomical and functional organizations in AMG-mPFC circuitries across species, despite their difference in spatial resolution.

First, although the frontal cortex displays an increase of volume from the last common ancestor of humans and old- world monkeys to humans (Semendeferi et al., 2002; Smaers et al. 2011, 2017; Barrett et al., 2020), a large body of evidences point towards a preserved anatomo-functional organization of the mPFC (Petrides and Pandya, 2002; Petrides et al., 2012; Neubert et al., 2015; Procyk et al., 2016; Amiez et al., 2019). Specifically, the mPFC is composed of several regions arranged on the medial part of the brain along the corpus callosum (Fig. 1B). A similar topographical organization can be found along the anterior/ventral-postero/dorsal axis in both macaques and humans, including the ventromedial prefrontal cortex (vmPFC), the anterior cingulate cortex (ACC), the anterior midcingulate cortex (amCC), and the posterior mid-cingulate cortex (pmCC) (Procyk et al., 2016; Vogt, 2016; Lopez-Persem et al., 2019). From vmPFC to MCC in both macaques and humans, the literature points toward a functional organization sustaining different aspects of behavioral adaptation, i.e., from the evaluation of both our internal and external environment, the evaluation and update of our goals, to the evaluation of our decisions and of their outcomes (Quilodran et al., 2008; Grabenhorst and Rolls, 2011; Amiez et al., 2012; Boorman et al., 2013; Scholl et al., 2015; Procyk et al., 2016; Wittmann et al., 2016; Juechems et al., 2019). Comparatively, as detailed more thoroughly below, the AMG displays the reverse pattern, i.e., a decreased brain occupation volume from the last common ancestor of humans and old-world monkeys to humans that is accompanied by morphological changes of the nuclei forming the AMG (Barger et al. 2007, 2014; Chareyron et al., 2011).

2. MORPHOLOGICAL COMPARISON OF THE AMYGDALA NUCLEI VOLUMES IN PRIMATES

In both macaques and humans, the AMG is an almond-shaped structure nested deep in the medial temporal lobe of the brain, and composed of an ensemble of nuclei displaying distinct anatomical and connectivity features (see details in next sections) (Stephan et al., 1987; Aggleton, 2000; Amunts et al., 2005). In primates, AMG nuclei are broadly parcellated into a deep and a superficial group. The deep group is composed of the lateral (LA), basal (B) and accessory basal (AB) nuclei (Aggleton, 2000). In the literature, the latter two nuclei are also found under the abbreviations BL and BM, respectively.

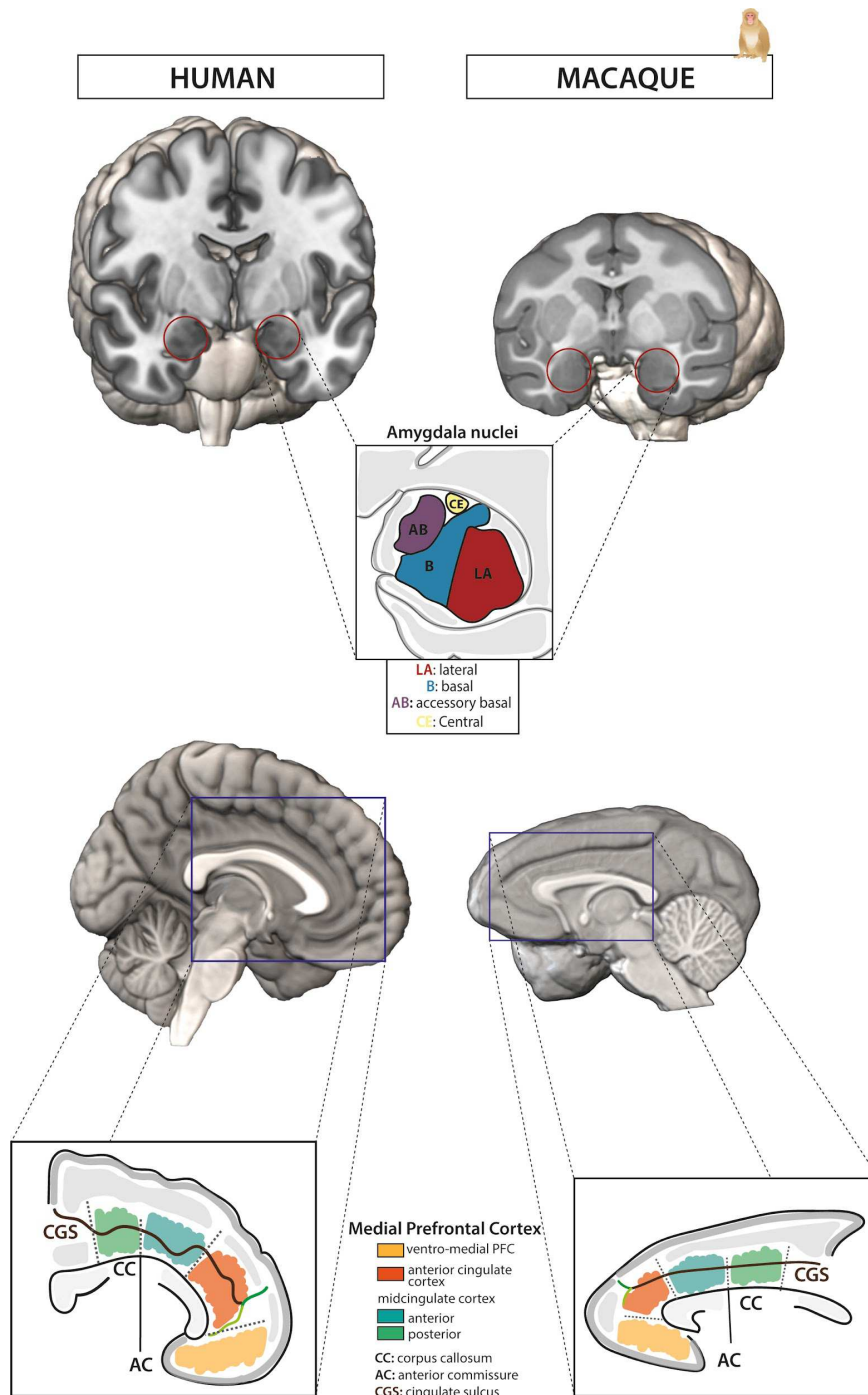


Figure 1. Amygdala and medial prefrontal cortex organization in humans and macaques.

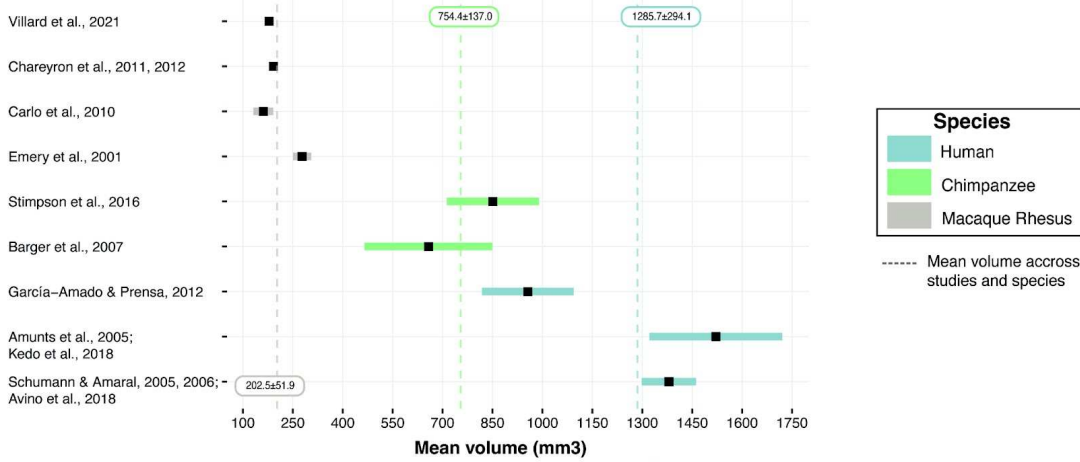
Human brain sections, from the MNI averaged ICBM152 brain, are displayed in the left column. Macaque rhesus brain sections, from the NMT macaque atlas, are displayed in the right column. **A.** The amygdala (AMG) is outlined (red circle) on the coronal sections of both species. A schematic representation of the AMG main nuclei subdivisions are represented in the center of the figure: Lateral (LA, in red), Basal (B or BL, in blue), Accessory Basal (AB or BM, in purple), and Central (CE, in yellow) nuclei. **B.** The mPFC organization is displayed on sagittal sections in both species. The mPFC encompasses the ventro-medial Prefrontal Cortex (vmPFC, which includes area 25, and parts of area 14m, 10m, and 32, yellow area), the Anterior Cingulate Cortex (ACC, i.e., which includes areas 32 and 24 abc, orange area), the anterior and posterior Mid-Cingulate Cortex (MCC, which includes areas 24a'b'c', 32', anterior MCC: teal area, posterior MCC: green area).

LA nucleus is situated on the lateral part of the AMG complex and is ventrally and caudally bounded by the temporal horn of the lateral ventricle (red, Fig. 1A). B nucleus (blue, Fig. 1A) is bounded laterally by LA and medially by AB nucleus (purple, Fig. 1A). The superficial group is composed of the medial (ME) and cortical nuclei (CO), while excluding the central (CE) nucleus. The CE nucleus, also part of the extended AMG (Fox and Shackman, 2019; Holley and Fox, 2022), lies dorsally and caudally within the AMG complex above the AB nucleus (yellow, Fig. 1A). All these AMG nuclei

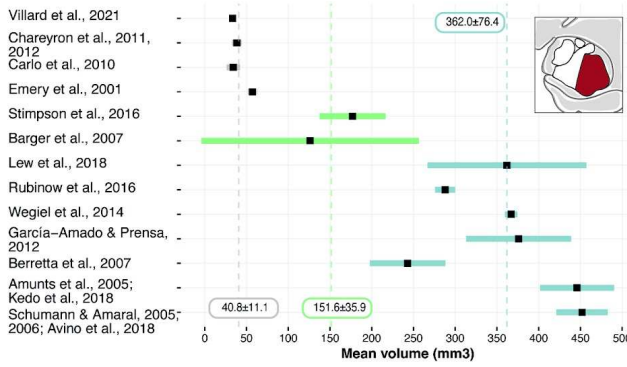
are strongly interconnected, creating a micro-circuit within the AMG itself, where LA is considered as a sensory gateway, receiving inputs from sensory association cortices, then the flux of information circulates to the other AMG nuclei. Therein, as discussed below, B and AB are more heavily connected to mPFC while CE is connected to autonomic centers nuclei (Aggleton, 2000), and the amygdalar inhibitory intercalated masses contribute to regulatory processes within the AMG (Royer et al., 1999).

The first question we addressed here is whether and how AMG main nuclei, LA, B, AB and CE, have evolved after the split of humans and macaques from their last common ancestor. In that goal, we gathered studies that have examined the volume of AMG and AMG main nuclei in humans and rhesus macaques (see Fig. 2, Table S1 and methods in supplementary material for the studies selected and associated references). As an intermediate species between humans and macaques, we selected studies including chimpanzees (great apes) to understand whether any changes between humans and macaques are proper to the “homo” genus or to the Hominidae family (comprising great apes and humans’ genii) (Pozzi et al., 2014). In the 3 species, we only considered ex-vivo stereological studies that specifically reported the volume of the whole AMG and AMG main nuclei. We excluded MRI volumetry studies given the lack of consensus and precision in particular regarding the identification of AMG nuclei on MRI images. Note that potential lateralization, sex and age effects were not assessed because 1) several studies reported non-significant volume variations across hemispheres (Brabec et al., 2010; Kedo et al., 2018), and 2) most studies included only one hemisphere. We first created forest plots comprising each of the selected studies for the whole AMG (AMG, Fig. 2A) and its nuclei separately: LA (Fig. 2B), B (Fig. 2C), AB (Fig. 2D) and CE (Fig. 2E). Results showed that the absolute AMG volume is higher in humans (mean across studies, blue dotted line, 1285.6 ± 294.1 mm³), compared to chimpanzees (green dotted line, 754.4 ± 137 mm³, 1.8 times smaller than humans), and macaques (brown dotted line, 202.5 ± 51.9 mm³, 6 times smaller than humans).

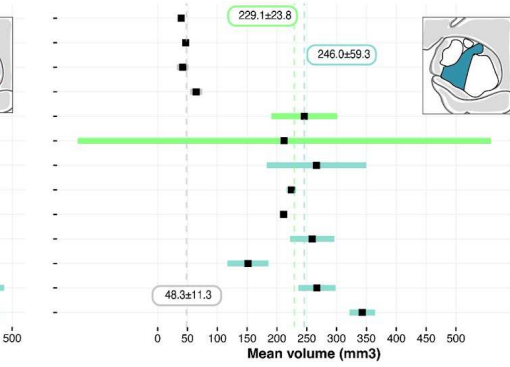
A. Amygdala absolute volume



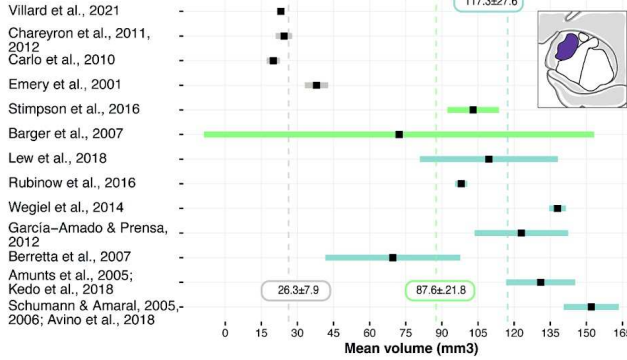
B. Lateral nucleus absolute volume



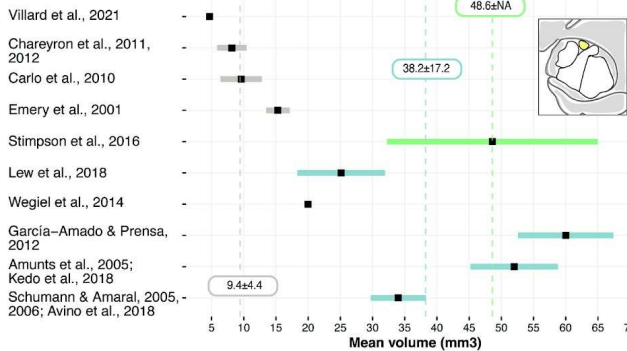
C. Basal nucleus absolute volume



D. Accessory Basal nucleus absolute volume



E. Central nucleus absolute volume



F. Relative volume occupied by each nucleus in the whole amygdala (percentage)

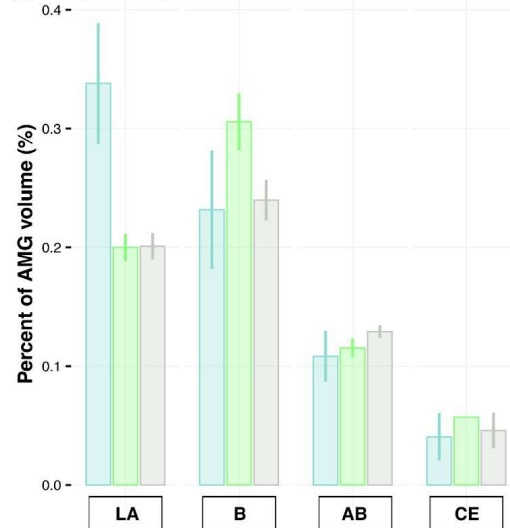


Figure 2. Volumetric analysis of whole amygdala and amygdala nuclei (LA, B, AB, and CE) in primates. Humans in blue and non-human primates, (chimpanzees and macaques) in green and brown, respectively. The analysis is performed exclusively on ex-vivo stereological studies in which we extracted mean volumes, standard deviations and sample size. The majority of studies either include

only one hemisphere or did not specify; for the few studies indicating AMG volumes in both hemispheres, we calculated the average volume across hemispheres. A. Forest plots displaying the mean volume of the whole AMG in each selected study (black square) and 95% confidence interval around the mean (wide line) for each species. Mean \pm sd volume across species and studies are represented by dashed vertical lines and displayed in rectangles. B.C.D.E. Mean absolute volumes of LA (B), B (C), AB (D) and CE (E) nuclei across studies and species. Note that the studies included in C are those included in B. F. Because the absolute volume cannot be used to compare the 3 primate species, we calculated the percentage of volume occupied by each nucleus in the whole AMG volume (volume nuclei/volume AMG*100) in each study indicating the volume of the whole AMG. Results are displayed on a bar plot representing the relative volume of LA, B/BL, AB/BM and CE within the AMG for each species (error bars represent interstudy variability). The LA nucleus displays a large expansion in humans compared to macaques and chimpanzees.

When accounting for differential brain size between species using telencephalic absolute volume as a reference ([Semendeferi et al., 1997](#): humans (1 125 492 mm³), chimpanzees (305 521 mm³), and macaques (62 737 mm³)), we identified that the volume occupied by the AMG volume occupies in the whole brain is 0.11%, 0.24%, and 0.34% in human, chimpanzee, and macaque brains, respectively. In other words, although the absolute volume of the AMG increased in humans compared to the other species, the percentage of volume it represents occupied volume of the AMG in the whole brain decreased compared to the other species. Importantly, among the AMG nuclei, the LA displays the largest expansion relative to the other nuclei in humans, compared to chimpanzees and macaques ([Fig. 2B and F](#)). It represents 34% of the whole AMG volume in humans whereas it represents 20% and 21% in chimpanzees and macaques, respectively. These results are in agreement with previous findings that either compared humans and great apes or humans and macaques ([Barger et al., 2007](#); [Chareyron et al., 2011](#)), suggesting that the expansion of LA appeared after the split of humans and chimpanzees from their last common ancestor. In the next sections, we will successively summarize the current state of knowledge regarding the anatomical and functional relationships of the different AMG nuclei in humans and macaques before discussing the potential functional significance of the expansion of the LA nucleus in humans (see last section).

3. AMYGDALA AND MEDIAL PREFRONTAL CORTEX ANATOMICAL CONNECTIONS IN HUMANS AND MACAQUES

Pioneer lesion studies in macaques showed causal evidences of bidirectional anatomical connections between AMG and mPFC: 1) broad lesions of AB and LA nuclei induce an axonal degeneration in the rostral cingulate cortex, and, 2) reciprocally, lesions in various areas of the cingulate cortex and vmPFC are associated with degenerated cells in B nucleus (Pandya et al., 1973; Nauta, 1993). Tracers' studies in NHP further refined the topological organization of the anatomical connections between AMG and mPFC. First, they demonstrate that these connections were strictly ipsilateral. Second, AMG efferent fibers preferentially terminate in the deep layer II and I of mPFC regions while mPFC efferences towards AMG arose mainly from layer V (Jacobson and Trojanowski, 1975; Aggleton et al., 1980; Porrino et al., 1981; Amaral and Price, 1984; Vogt and Pandya, 1987; Barbas and de Olmos, 1990; Carmichael and Price, 1995; Stefanacci and Amaral, 2000; Ghashghaei and Barbas, 2002; Ghashghaei et al., 2007; Morecraft et al., 2007; Cho et al., 2013; Zikopoulos et al., 2017; Kim et al., 2018; Sharma et al., 2020; Calderazzo et al., 2021; Kelly et al., 2021). In addition, mPFC projections toward the AMG are denser compared to AMG projections toward mPFC, qualifying the mPFC as a "sender" region (Fig. 3A) (Ghashghaei et al., 2007). These connections display a peculiar rostro-caudal organization from low to high density in mPFC regions along the corpus callosum: the connection density is stronger between the most caudal part of vmPFC (area 25), then decreases rostrally in ACC (area 32), and increases with MCC regions (area 24; Fig. 3A) (Ghashghaei et al., 2007; Sharma et al., 2020; Calderazzo et al., 2021).

Finally, with their fine-grained spatial resolution, these latter studies also revealed a gradient with a varying density of connections between AMG nuclei and mPFC regions. Specifically, among the AMG nuclei, LA and CE share few direct connections with mPFC (Barbas and de Olmos, 1990; Zikopoulos et al., 2017; Kim et al., 2018; Kelly et al., 2021) as they are mainly connected to sensory association cortices (inferior temporal areas TE and TEO, Superior Temporal Sulcus, etc.) and autonomic centers (hypothalamus or brainstem), respectively (Aggleton, 2000; Stefanacci and Amaral, 2000). By contrast, the B and AB nuclei present the densest reciprocal anatomical connections with mPFC regions. Quantitative histological studies further revealed a differential pattern of efferent connections from these two

AMG nuclei (AB and B) toward mPFC regions. Rostral and dorsal mPFC regions, namely ACC and aMCC, receive more projections from B nucleus compared to AB nucleus with a proportional ratio of 90-80% and 10–20%, respectively. Note that pMCC appears to receive sparser projections from the AMG (Morecraft et al., 2007). By contrast, vmPFC receives a similar proportion of projections from both B and AB nuclei (Barbas and de Olmos, 1990; Morecraft et al., 2007; Kim et al., 2018; Sharma et al., 2020), yet, relative to ACC and MCC, its inputs from nucleus AB are denser (Sharma et al., 2020). A similar topographical organization is also present when considering efferences from mPFC toward those AMG nuclei: whereas both MCC and ACC project heavily to B nucleus compared to AB nucleus (Ghashghaei and Barbas, 2002; Ghashghaei et al., 2007; Morecraft et al., 2007; Cho et al., 2013; Zikopoulos et al., 2017; Kelly et al., 2021), vmPFC sends efferences to both B and AB nuclei (Ghashghaei and Barbas, 2002; Ghashghaei et al., 2007; Cho et al., 2013).

Knowledge about the structural connectivity in humans comes from either post-mortem (ex vivo) dissection or from non-invasive diffusion MRI performed in- vivo or ex- vivo (Diffusion tensor imaging -DTI). DTI refers to analytic methods using diffusion weighting imaging (DWI) MRI sequence that provides information about the orientation, the strength and integrity of white fiber tracts at the macroscopic level (Basser and Pierpaoli, 1996). DTI can inform on the orientation and pathway of white fiber tracts and the strength and integrity of fiber tracts (Basser and Pierpaoli, 1996). DTI is an indirect measure with limited spatial resolution and accuracy compared to ex-vivo tracer studies in animal studies (Sarwar et al., 2021). Direct comparisons in macaques between anatomical connectivity as estimated with ex- vivo tracer studies and DTI studies using at 3T show that these connectivity measures display only moderate correspondances (e.g. Grier et al., 2020; Yendiki et al., 2022). This becomes even trickier when considering the intricate structural connectivity pattern of each individual amygdala nucleus with mPFC. However, DTI has the advantage of allowing the comparison of structural connections in both human and non- human primates using the same approach. These studies have shown that the principal white matter tracts connecting AMG with mPFC, i.e., the uncinate fasciculus, the amygdalofugal pathway, and the cingulum, are highly conserved between humans and macaques (Thiebaut de Schotten et al., 2012; Folloni et al., 2019a; Barrett et al., 2020). In addition, Mars et al. (2018) have developed a connectional blueprint based on the main bundles of white matter tracts that can be anatomically matched across species (i.e.,

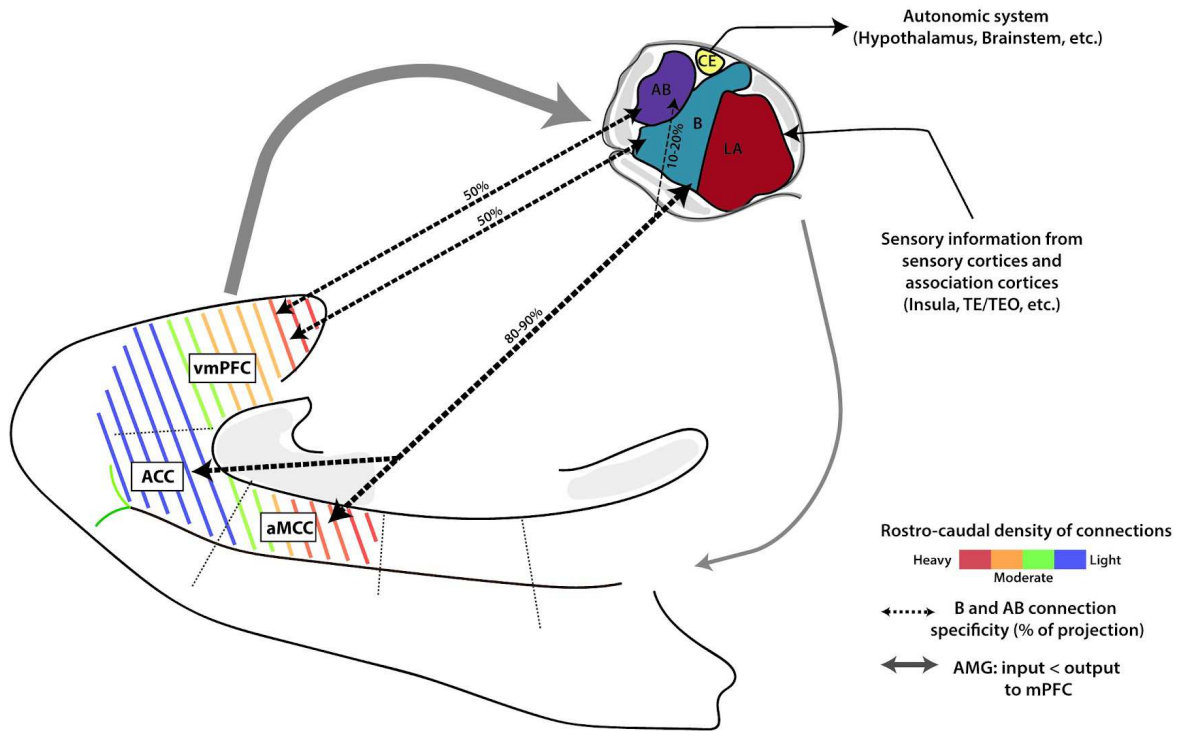
the uncinate fasciculus) to identify homologous brain areas (Mars et al., 2018). In humans, DTI has also been used to delineate the AMG in two subdivisions based on their differential structural connections with other brain regions, i.e. the basolateral and the centromedial subdivision (defined by Amunts et al., 2005 in humans, see next section), coherently with macaque ex- vivo tracer studies (Aggleton, 2000; Solano-Castiella et al., 2010; Bzdok et al., 2013; Balderston et al., 2015). Finally, more recent development in the field provides a finer segmentation of the AMG nuclei at different times during adolescence (Azad et al., 2021). While DTI is a promising tool, future developments using for instance ultra-high- resolution MRI and advances in analytical tools will undoubtedly help overcome the current limitations and hopefully provide more finer-grained cross-species comparisons (Sotiropoulos and Zalesky, 2019; Grier et al., 2022).

In summary, although the literature suggests preserved fiber tracts between macaques and humans at the macroscopic level, differential connectivity profiles between the various AMG nuclei and mPFC regions are observed in macaques at the microscopic level. Importantly, whether these latter highly specific patterns do exist in humans remains to be elucidated. In the next section, we tackle the question of the functional dialogue between AMG nuclei and mPFC regions, as measured at rest using functional Magnetic Resonance Imaging (rs-fMRI).

4. FUNCTIONAL CONNECTIVITY IN THE AMG-MPFC NETWORK IN HUMANS AND MACAQUES

Rs-fMRI measures the temporal correlation of spontaneous low-frequency fluctuations of the BOLD signals between different brain regions in the absence of any specific task or stimulus (Biswal et al., 1995). It has the great advantage to provide *in-vivo* information on brain network functional connectivity as well as the connectivity profile of a particular brain region. While the spatial resolution of fMRI does not permit direct comparisons with the tract-tracing anatomical studies described above, it can provide key information about the functional relationships between anatomically interconnected regions (Greicius et al., 2009).

A. Structural connection: macaque *rhesus* tracer studies



B. Functional connectivity in human resting-state fMRI study

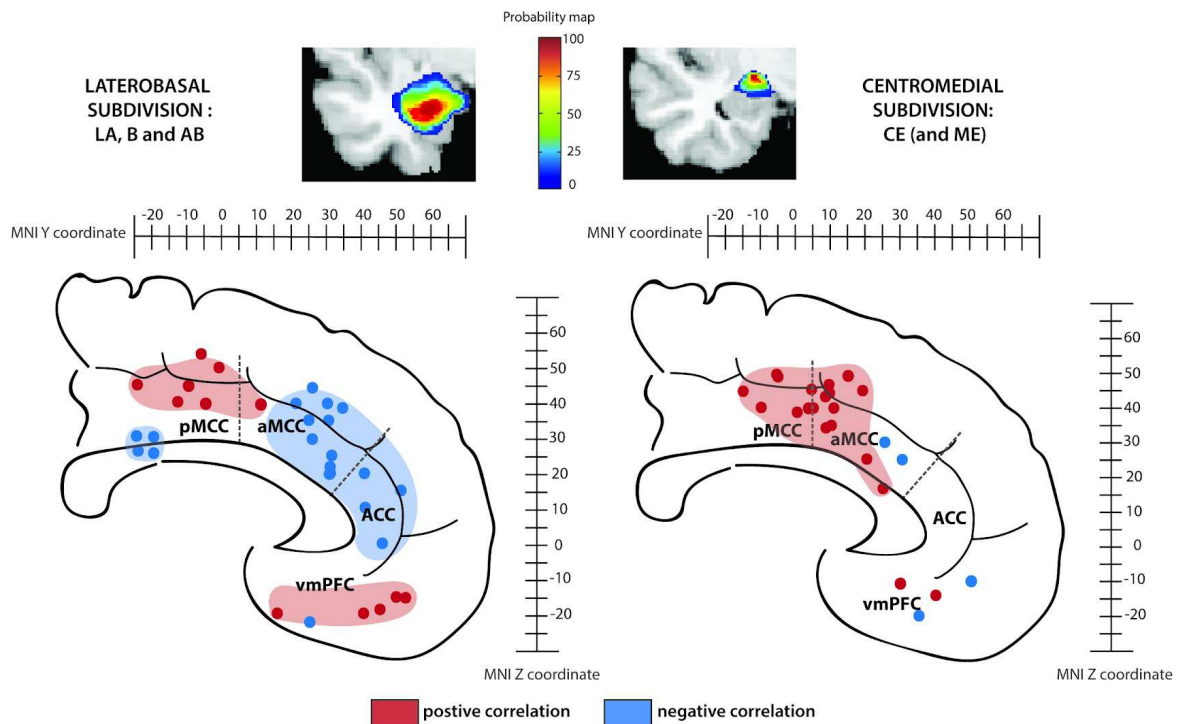


Figure 3. AMG-mPFC dialogue: two different levels of analysis between macaque structural connectivity and human functional connectivity. A. Diagram representing the structural connectivity based on tract-tracing studies in macaques between the AMG nuclei, i.e., LA, B/BL, AB/BM, CE, and the various mPFC regions. AMG and mPFC share strictly ipsilateral and bidirectional connections. The

mPFC sends more projections to the AMG than it received (i.e., “senders”, wide gray arrows). The colored dotted lines in the mPFC represent the rostro-caudal gradient of density of structural connections between AMG and mPFC, i.e., high density (red-orange) with vmPFC and MCCa to low density with ACC (green-blue). The dotted arrows in black represent the preference of connectivity between B/BL and MCC/ACC on one hand, and between AB/BM with vmPFC on the other hand. B. Correlation peaks for each selected study between mPFC and the laterobasal (LB, which includes LA, B/BL, and AB/BM nuclei) and centromedial (CM, which includes CE and ME nuclei) AMG subdivisions as defined by Amunts et al. (2005) in humans. We selected studies identifying significant peaks of activation with MNI coordinates and we focused on ipsilateral connectivity. Note that some studies did not directly use Amunts et al. (2005) parcellation, they instead used it as a reference for their own clustering of the AMG. Location (Y, and Z MNI stereotaxic coordinates values) of significant correlation peak values are displayed on a medial sagittal section of the human brain. Negative correlations are represented in blue and positive correlations in red. Results show a differential functional connectivity pattern between the 2 AMG subdivisions.

Numerous studies in humans have described the functional dialogue between AMG and mPFC while considering the whole extent of the AMG or focusing on AMG subdivisions (Amunts et al., 2005). These studies have shown that the fluctuations of activity in the whole AMG is positively correlated with those in more ventral mPFC regions and negatively correlated with those in more dorsalmPFC regions (Roy et al., 2009; Kim et al., 2011). To identify the respective FC of AMG nuclei with mPFC (see Table 2 in supplementary material), we focused on human rs-fMRI studies (described in supplementary materials) that relied on the most widely used nomenclature in the field: laterobasal subdivision (LB, composed of LA, B, AB nuclei), and centromedial subdivision (CM, composed of CE and ME) (Amunts et al., 2005; Eickhoff et al., 2005). Our intent was to identify the FC organization pattern and the regulatory interactions between AMG nuclei and mPFC focusing on the sign of correlation (positive vs negative) (Gopinath et al., 2015). Note that we only targeted correlations within hemispheres and we did not take into consideration any lateralization effect as this was outside the scope of the present review (see Table S2). The corresponding correlation peaks for each selected study is displayed on sagittal brain diagrams between Y MNI coordinates from -26 to 52 and Z coordinates from -22 to 50 for LB and CM nuclei (blue and red correspond to negative and positive correlations, respectively; Fig. 3B).

Not surprisingly, as LB subdivision occupies the major portion of AMG, we confirm that it displays a similar FC pattern with mPFC subregions than when considering the whole AMG (Roy et al., 2009; Kim et al., 2011): positive correlations with vmPFC, negative correlations with ACC and aMCC, and positive correlations

with pMCC. A recent study that used a finer data-driven parcellation of AMG and high-resolution data further suggested that the strongest FC was observed between AB/B nuclei -as compared to LA nucleus-with mPFC regions, with a trend toward a preferential functional coupling between the AB nucleus and vmPFC (area 25) on one hand and between the B nucleus and aMCC on the other hand (Klein-Flügge et al., 2022). By contrast, the activity of CM subdivision appeared to display a very distinct functional connectivity pattern with mPFC: positive correlations with mPFC regions, more specifically with the MCC regions (both aMCC and pMCC). These patterns of connectivity between the various AMG nuclei and mPFC regions point toward the existence of complex relationships that might be dynamically and differentially adjusted depending on the environmental context.

How are the functional relationships organized between AMG and mPFC in macaques at rest? To the best of our knowledge, only a handful of studies have examined this interplay in macaques (Neubert et al., 2015; Grayson et al., 2016; Folloni et al., 2019b; Morin et al., 2020; Reding et al., 2020). Two points need to be raised. Firstly, these studies have been carried out under anaesthesia (e.g., isoflurane). Yet, several studies have demonstrated that anaesthesia strongly affects brainactivity, and in particular the functional dialogue within the frontal cortex (Hutchison et al., 2014; Barttfelda et al., 2015; Uhrig et al., 2018; Giacometti et al., 2022). Anaesthesia notably causes a global decrease of negative correlations in the brain (Hutchison et al., 2014; Barttfelda et al., 2015; Uhrig et al., 2018; Hori et al., 2020; Giacometti et al., 2022), thus calling for some caution when directly comparing studies conducted in anaesthetized macaques *versus* in awake humans using similar parameters. Furthermore, to the best of our knowledge, so far macaques rs-fMRI studies have only examined the FC of the whole extent of AMG. These studies showed 1) positive correlations between the AMG, and the vmPFC, the ACC (Neubert et al., 2015; Folloni et al., 2019b; Reding et al., 2020), and the ACC/aMCC limit, and 2) negative correlation between the AMG and aMCC (Neubert et al., 2015).

Overall, the current available evidence from anaesthetized macaques suggests that the FC between vmPFC and AMG share similarities with awake humans while the FC between ACC and AMG displays some differences between the two species. Whether these differences are driven by the state (anaesthesia vs awake) or represents mere interspecies differences is further discussed in the last section of the review.

5. MULTIPLE ROUTES OF COMMUNICATION WITHIN THE AMYGDALA-MPFC NETWORK IN MACAQUES AND HUMANS: FUNCTIONAL SIGNIFICANCE AND FUTURE DIRECTIONS

The goal of the review was to scrutinize anatomical and functional relationships within AMG-mPFC circuitries and identify potential homologies and differences between macaques and humans. We highlighted in particular: 1) differences between AB and B nuclei structural connectivity with mPFC regions from tract tracing studies in macaques (Fig. 3A), and 2) differential pattern of functional connectivity between the mPFC regions and the laterobasal (LA, B and AB) or centromedial AMG subdivisions (CE and ME) from rs-fMRI studies in humans (Fig. 3B). These evidences suggest multiple routes of communications between AMG nuclei -or subdivisions- and mPFC. Below we discuss how these different AMG-mPFC routes might enable the integration of information from the internal and external environments to support flexible behavior (Saez et al., 2015). Specifically, we propose that two routes within the AMG-mPFC network support distinct temporal dynamics of integration necessary for behavioral adaptation, the former dealing with long-term contextual adaptation (vmPFC-LB) and the latter dealing with online monitoring of actions (LB-MCCa and CM-MCCa). In addition, we highlight an expansion of the LA nucleus in humans compared to macaques and discuss potential commonalities and differences between both species in AMG-mPFC circuits.

5.1 Two routes with distinct behavioral adaptation temporalities within AMG-mPFC

Among the LB subdivision, B and AB nuclei share strong bidirectional structural connections with mPFC regions, especially with vmPFC and aMCC (Fig. 3A). Of note, the projections from mPFC towards AMG nuclei are denser than their counterparts (Ghashghaei et al., 2007), suggesting a moderating role of mPFC onto the AMG, that is gradually setup from the end of infancy to adolescence (Gee et al. 2013, 2022; Tottenham, 2015). While evidence of the functional relationships between AMG nuclei and mPFC using rs-fMRI remain elusive to date in macaque, evidence from human studies show a differential functional relationship with two particular regions of mPFC in humans: 1) a positive versus negative functional coupling at rest between the LB subdivision and the vmPFC versus the aMCC, respectively, and 2) a positive functional coupling between the CM subdivision and

the aMCC (Fig. 3B). Interestingly, vmPFC and MCC sustain different and complementary aspects of flexible decision-making necessary for behavioral adaptation (Quilodran et al., 2008; Grabenhorst and Rolls, 2011; Amiez et al., 2012; Boorman et al., 2013; Scholl et al., 2015; Procyk et al., 2016; Wittmann et al., 2016; Juechems et al., 2019), that might in part be reflected in their differential dialogue with the LB and CM subdivisions.

On one hand, vmPFC is thought to integrate contextual and value information with previous knowledge to update decisions accordingly (Grabenhorst and Rolls, 2011; Boorman et al., 2013; Vassena et al., 2014; Scholl et al., 2015; Wittmann et al., 2016; Schneider and Koenigs, 2017; Juechems et al., 2019; Dal Monte et al. 2020, 2022; Gangopadhyayet al., 2021). This integration depends, at least in part, on information processed within the LB subdivision associated with choices, value and rewards evaluation in both social and non-social contexts coded in abstract conceptual format (Gupta et al., 2011; Wellman et al., 2016; O'Neill et al., 2018; Grabenhorst et al., 2019; Dal Monte et al., 2020; Elorette et al., 2020; Jezzini and Padoa-Schioppa, 2020; Grabenhorst and Schultz, 2021; Dal Monte et al., 2022). For instance, the level of complexity in the social network enhances the strength of connectivity between vmPFC and LB (Bickart et al., 2012). Beyond its interactions with the LB subdivision (B and AB nuclei), vmPFC also received inputs from the entorhinal cortex (EC), a gateway to the hippocampus, mediating long-term contextual and episodic memory functions (Joyce and Barbas, 2018; Calderazzo et al., 2021). Through these connections, the LB-vmPFC circuit might thus be in an ideal position to update decisions based on stored information and support longer term (as opposed to short-term) behavioral adaptation. Previous studies have suggested strong interactions between another region of the PFC (the orbitofrontal cortex) and the LB subdivision in shaping behavioral responses depending on the environment (Saez et al., 2017; Zikopoulos et al., 2017). Here, we further suggest that the circuit formed by the vmPFC and the LB subdivision also participate in these processes and it would be interesting in future studies to disentangle the contribution of these pathways in behavioral adaptation.

On the other hand, MCC (often referred as dACC) strongly interacts with the premotor cortex and the dorso-lateral PFC (Morecraft et al., 2012; Calderazzo et al., 2021) involved in action planning, cognitive control, and feedback-based decision, critical to rapidly adapt behaviors when required by the environment (Amiez et al.,

2012; Boorman et al., 2013; Vassena et al., 2014; Procyk et al., 2016; Wittmann et al., 2016; Juechems et al., 2019). The evidences based on rs-fMRI in humans that we presented above suggests two distinct ways by which AMG and MCC might interact: 1) a negative functional coupling between the activity of MCC and the LB subdivision and 2) a positive functional coupling between the activity of MCC and the CM subdivision. While the LB-MCC route is sustained by massive direct anatomical projections, characterized in particular by dense projections between the B nucleus and the MCC (Sharma et al., 2020), the CM-MCC route presumably reflects indirect interactions. Yet, both are likely to participate in functions that require fast stimulus-response adaptations to face immediate changes in the environment (Bickart et al., 2012; Klavir et al., 2013; Aryeh Hai Taub et al., 2018; Aryeh H. Taub et al., 2018; Terburg et al., 2018; Leitão et al., 2022). For example, during aversive learning, electrophysiological recordings in monkeys have shown that stimulus processing rapidly occurs within LB before reaching the MCC and propagates back to the LB (Klavir et al., 2013; Aryeh Hai Taub et al., 2018; Aryeh H. Taub et al., 2018). In the CM subdivision, the CE nucleus is mainly connected with autonomic centers such as the hypothalamus and brainstem regions (Aggleton, 2000; Cardinal et al., 2002). Lesion study in non-human primates has demonstrated its implication in defensive and physiological responses in anxiety-related and stress-related situations (Kalin, 2004). In humans, studies showed strong coupling between CE and MCC at rest (Bickart et al., 2012; Tillman et al., 2018). The MCC also participates in sympathetic and parasympathetic responses (Amiez and Procyk, 2019). One might thus hypothesize that the, MCC, through its functional interactions with the CM, including CE, and more largely the central extended AMG, may shape avoidance-approach responses, based on previous negative and/or positive feedback-based experiences, that might have been previously integrated by LB-vmPFC circuit. Such regulation likely depends on dynamic and flexible interactions between AMG nuclei involving inhibitory neurons such as the intercalated interneurons masses and top-down regulation from the mPFC (McDonald and Augustine, 1993; Zikopoulos et al., 2017).

It is therefore possible that these two routes within the AMG-mPFC network support distinct temporal dynamics of integration, the former dealing with long-term contextual adaptation (vmPFC-LB) and the latter dealing with online monitoring of actions (LB-MCCa and CM-MCCa). A balance between these different circuits within the AMG-mPFC network would be essential to support decision-making flexibility in

various environmental contexts in light to our internal state to promote behavioral adaptation. The AMG, formed by a collection of nuclei, is often viewed as a hub sustaining a high degree of information integration coordinating multiple brain circuits during behavior adaptation (Morrow et al., 2019; Putnam and Gothard, 2019). Accordingly, in humans, a disruption within these AMG-mPFC circuits leads to a various mental illnesses characterized by a maladaptive behavioral responses, i.e. exaggerated, reduced, or even an absence, and/or an atypical behavior (Blair, 2008; Kim et al., 2011; Murray et al., 2011; Swartz et al., 2013; Likhtik and Paz, 2015; Nicholson et al., 2015; Mukherjee et al., 2016; Dong et al., 2019; Li et al., 2021; Cao et al., 2022; Gao et al., 2022). In particular, the LA nucleus in humans is a very sensible target to a large number of neuropsychiatric diseases. Several postmortem studies comparing patients with healthy subjects have reported morphological alterations of the LB with a special focus on the LA nucleus (e.g. volume and neurons numbers) in autism spectrum disorder, Williams syndrome, major depression disorder, panic disorder, schizophrenia, and bipolar disorders (Schumann and Amaral, 2006; Berretta et al., 2007; Bezchlibnyk et al., 2007; Kreczmanski et al., 2007; Schumann et al., 2011; Wegiel et al., 2014; Rubinow et al., 2016; Asami et al., 2018; Lew et al., 2018). The studies highlighted above deciphering the AMG-mPFC circuitries at the nuclei subdivisions level will undoubtedly help us to better understand these maladaptive behaviors and hopefully help to refine therapeutic strategies to help these patients.

5.2 Towards a comparison of AMG-mPFC networks in macaques and humans

Our objective was to identify potential homologies and differences in AMG-mPFC circuitries between macaques and humans. First, the CE nucleus, part of the CM and central extended AMG together with the bed nucleus of the stria terminalis (BST), is thought to have been conserved throughout the course of evolution, with limited differences between rodents and primates, hence between macaques and humans (Chareyron et al., 2011), as confirmed with the volumetric analysis presented above. Comparatively, we highlighted in humans a selective expansion of the LA nucleus, part of the LB subdivision, and tightly connected with sensory and higher order association cortices (Stefanacci and Amaral, 2000). This volume expansion has also been associated with an increase of neuron numbers in humans (Barger et al., 2012). It is possible that this expansion allows the integration of a higher amount of multi-sensorial information that humans are facing in their daily life including their

highly complex social interactions compared to macaques (see also [Barger et al., 2012](#)). Several neuroimaging studies reported an increase in AMG volume related to complex social networks ([Dziura and Thompson, 2014](#)) and the size of the social group ([Sallet et al., 2011](#); [Kanai et al., 2012](#)). Although these studies refer to the whole AMG, and confirmation needs to be brought by, it is possible that this increase concerns in particular the LA nucleus. A recent study using electrical stimulation in epileptic patients showed that stimulation of the LA nucleus evoked an earlier response in ACC/aMCC compared to that of the B or AB nucleus ([Sawada et al., 2022](#)). While in macaques, LA only shares few direct projections with mPFC compared to AB and B, it remains to be determined whether the LA expansion might have led to differences in the organization of anatomical projections between AMG and mPFC in humans.

Regarding the rs-fMRI functional connectivity of AMG nuclei and/or subdivisions with mPFC regions, the current state of the art, especially in light with very limited evidences focusing essentially on the whole AMG functional connectivity under anaesthesia in macaques, does not allow to draw firm conclusions about potential homologies or differences between humans and macaques. Nevertheless, one could relate the FC involving vmPFC and aMCC with the whole AMG in anaesthetized macaques and whole AMG and LB subdivision in awake humans and the similarities between the two species in terms of structural connectivity of the CE nucleus. It is possible thus that the two routes described above are present in both humans and macaques to support distinct temporal dynamics of integration necessary for behavioral adaptation, yet with some differences. Indeed, the FC between the region located between the vmPFC and aMCC, namely the ACC, and the AMG displays some differences between the two species: the activity of this region is mainly negatively correlated with that of the AMG in humans while the available evidence in macaques points toward a positive correlational relationship between these two regions. While these conclusions await further evidences, we propose tentative interpretations that might be related to these functional differences across species. One possibility is that this difference is driven by the state (anaesthesia vs awake). Alternatively, this difference might reflect mere differences between species: although the macaque mPFC possesses all the sulcal precursors of the human mPFC, the region interfacing with vmPFC and MCC (which contains ACC) is the one displaying the most notable sulcal changes across primate species (the fork composed by two sulci situated at the rostral of the cingulate sulcus 1) faces downwards in

humans versus forward in macaques and baboons, and 2) is located more dorsal in non-human than in human primates; [Amiez et al., 2019](#)). Whether and how these morphological changes would affect the functional relationships between mPFC and AMG nuclei is yet to be determined. With novel tools giving access to the fine-grained parcellation of the AMG in macaque ([Hartig et al., 2021](#)), it would be possible for future studies to further refine our knowledge about the AMG nuclei FC profiles with mPFC in awake macaques, therefore providing more direct comparisons with available evidence in humans.

5.3 Limitation and further perspectives

We mainly focused the scope of the review in the adult brain, not taking into account several factors that might also affect the anatomical and functional interplay within AMG-mPFC circuits such as sex, age or personality traits (see for instance [Tottenham, 2015](#); [Reber and Tranel, 2017](#); [Kenwood and Kalin, 2021](#); [Ferrara and Opendak, 2023](#)). Another limitation of our hypotheses is that evidences come from different species (humans vs macaques) and from different approaches with different spatial scales: a microscopic scale providing structural connectivity of each AMG nuclei in macaques versus a macroscopic scale in humans using rs-fMRI or DWI. In comparative neurosciences, the gap between invasive -but highly precise- techniques used in non-human primates and non-invasive -but less precise- techniques used in humans is called the “macroscopic–microscopic divide” ([Barron et al., 2021](#)). Cross-species neuroimaging comparison approaches have emerged to bridge this gap as they have the advantage to be applicable in both human and non-human primates and in particular in macaques ([Barron et al., 2021](#); [Friedrich et al., 2021](#)). With higher field strength at 7T or even 10.5 T in macaques ([Thanh Vu et al., 2017](#); [Yacoub et al., 2020](#)), this approach can provide a finer-grained description of brain networks. As such, future works may apply this strategy to consider the respective whole-brain functional coupling of each AMG nuclei within and across species (e.g. [Torrise et al., 2015](#); [Elvira et al., 2022](#)). The implementation of effective connectivity in these studies might also provide important insights about the directionality of the interplay within these networks ([Liu et al., 2016](#); [Berboth and Morawetz, 2021](#)). Our further understanding of the temporal and dynamic interactions between the AMG nuclei and the mPFC in primates may also benefit from interventional optogenetic and electrophysiological approaches similar to those carried out in mice (e.g. [Kopell et al.,](#)

2014; Felix-Ortiz et al., 2016). Some electrophysiological studies, although rare, have already provided key information about similarities and differences of the efficiency and robustness of the functioning of the mPFC-AMG networks in humans versus macaques (Pryluk et al., 2019). Combining these different and complementary techniques in future studies will be essential to understand how the different AMG nuclei interact with the mPFC and other brain networks such as the fronto-amygdala-striatal circuitry (Cho et al., 2013) to subserve differential behavioral adaptation capacities in humans and monkeys and shed light on the evolution of this network (Henke-von der Malsburg et al., 2020).

CRedit authorship contribution statement

C. Giacometti : Conceptualization, Investigation, Writing – original draft. **C. Amiez** : Conceptualization, Writing – review & editing. **F. Hadj-Bouziane** : Conceptualization, Writing – review & editing.

Declaration of competing interest

The authors declare that they have no known competing financial interests or personal relationships that could have appeared to influence the work reported in this paper.

Acknowledgments

This work was funded by the French National Research Agency (ANR-18-CE37-0012 to C.A, ANR-15-CE37- 0003 to F.H.-B.). C.A. and F.H.-B. are employed by the Centre National de la Recherche Scientifique (CNRS). C.A. and C.G. were also supported by Laboratoire d'excellence (LabEx) CORTEX ANR-11-LABX-0042 of Université de Lyon. Note that a CC-BY public copyright license has been applied by the authors to the present document and will be applied to all subsequent versions up to the Author Accepted Manuscript arising from this submission, in accordance with the grant's open access conditions. *Conflict of Interest*: None declared.

Appendix A Supplementary data

Supplementary data to this article can be found online at <https://doi.org/10.1016/j.crneur.2023.100103>.

References

Aggleton JP. 2000. The amygdala: a functional analysis. 2nd ed. Aggleton JP, editor. Oxford, OX; New York: Oxford University Press. <https://global.oup.com/academic/product/the-amygdala-9780198505013?cc=us&lang=en&>.

Aggleton JP, Burton MJ, Passingham RE. 1980. Cortical and subcortical afferents to the amygdala of the rhesus monkey (*Macaca mulatta*). *Brain Res.* 190(2):347–368. doi:10.1016/0006-8993(80)90279-6. <https://linkinghub.elsevier.com/retrieve/pii/0006899380902796>.

Amaral DG, Price JL. 1984. Amygdalo-cortical projections in the monkey (*Macaca fascicularis*). *J Comp Neurol.* 230(4):465–496. doi:10.1002/cne.902300402. <http://doi.wiley.com/10.1002/cne.902300402>.

Amiez C, Procyk E. 2019. Midcingulate somatomotor and autonomic functions. In: *Handbook of Clinical Neurology.* Vol. 166. p. 53–71. <https://linkinghub.elsevier.com/retrieve/pii/B9780444641960000042>.

Amiez C, Sallet J, Hopkins WD, Meguerditchian A, Hadj-Bouziane F, Ben Hamed S, Wilson CRE, Procyk E, Petrides M. 2019. Sulcal organization in the medial frontal cortex provides insights into primate brain evolution. *Nat Commun.* 10(1). doi:10.1038/s41467-019-11347-x. <http://dx.doi.org/10.1038/s41467-019-11347-x>.

Amiez C, Sallet J, Procyk E, Petrides M. 2012. Modulation of feedback related activity in the rostral anterior cingulate cortex during trial and error exploration. *Neuroimage.* 63(3):1078–1090. doi:10.1016/j.neuroimage.2012.06.023. <http://dx.doi.org/10.1016/j.neuroimage.2012.06.023>.

Amunts K, Kedo O, Kindler M, Pieperhoff P, Mohlberg H, Shah NJ, Habel U, Schneider F, Zilles K. 2005. Cytoarchitectonic mapping of the human amygdala, hippocampal region and entorhinal cortex: intersubject variability and probability maps. *Anat Embryol (Berl).* 210(5–6):343–352. doi:10.1007/s00429-005-0025-5. <http://link.springer.com/10.1007/s00429-005-0025-5>.

Asami T, Nakamura R, Takaishi M, Yoshida H, Yoshimi A, Whitford TJ, Hirayasu Y. 2018. Smaller volumes in the lateral and basal nuclei of the amygdala in patients with panic disorder. Yamasue H, editor. *PLoS One.* 13(11):e0207163. doi:10.1371/journal.pone.0207163. <https://dx.plos.org/10.1371/journal.pone.0207163>.

Avino TA, Barger N, Vargas M V., Carlson EL, Amaral DG, Bauman MD, Schumann CM. 2018. Neuron numbers increase in the human amygdala from birth to adulthood, but not in autism. *Proc Natl Acad Sci U S A.* 115(14):3710–3715. doi:10.1073/pnas.1801912115.

Azad A, Cabeen RP, Seppehrband F, Kim R, Campbell CE, Lynch K, Tyszka JM, Herting MM. 2021. Microstructural properties within the amygdala and affiliated white matter tracts across adolescence. *Neuroimage.* 243. doi:10.1016/j.neuroimage.2021.118489.

Balderston NL, Schultz DH, Hopkins L, Helmstetter FJ. 2015. Functionally distinct amygdala subregions identified using DTI and high-resolution fMRI. *Soc Cogn Affect Neurosci.* 10(12):1615–1622. doi:10.1093/scan/nsv055.

Barbas H, de Olmos J. 1990. Projections from the amygdala to basoventral and mediodorsal prefrontal regions in the rhesus monkey. *J Comp Neurol.* 300(4):549–571. doi:10.1002/cne.903000409. <https://onlinelibrary.wiley.com/doi/10.1002/cne.903000409>.

Barger N, Stefanacci L, Semendeferi K. 2007. A comparative volumetric analysis of the amygdaloid complex and basolateral division in the human and ape brain. *Am J Phys Anthropol.* 134(3):392–403. doi:10.1002/ajpa.20684.

Barger N, Hanson KL, Teffer K, Schenker-Ahmed NM, Semendeferi K. 2014. Evidence for evolutionary specialization in human limbic structures. *Front Hum Neurosci.* 8(MAY). doi:10.3389/fnhum.2014.00277.

Barger N, Stefanacci L, Schumann CM, Sherwood CC, Annese J, Allman JM, Buckwalter JA, Hof PR, Semendeferi K. 2012. Neuronal populations in the basolateral nuclei of the amygdala are differentially increased in humans compared with apes: A stereological study. *J Comp Neurol.* 520(13):3035–3054. doi:10.1002/cne.23118. <https://onlinelibrary.wiley.com/doi/10.1002/cne.23118>.

Barger N, Stefanacci L, Semendeferi K. 2007. A comparative volumetric analysis of the amygdaloid complex and basolateral division in the human and ape brain. *Am J Phys Anthropol.* 134(3):392–403. doi:10.1002/ajpa.20684.

Barrett RLC, Dawson M, Dyrby TB, Krug K, Ptito M, D’Arceuil H, Crosson PL, Johnson PJ, Howells H, Forkel SJ, et al. 2020. Differences in frontal network anatomy across primate species. *Journal of Neuroscience.* 40(10):2094–2107. doi:10.1523/JNEUROSCI.1650-18.2019.

Barron HC, Mars RB, Dupret D, Lerch JP, Sampaio-Baptista C. 2021. Cross-species neuroscience: closing the explanatory gap. *Philosophical Transactions of the Royal Society B: Biological Sciences.* 376(1815):20190633. doi:10.1098/rstb.2019.0633.

Barttfeld P, Uhriga L, Sitta JD, Sigmane M, Jarraya B, Dehaene S. 2015. Signature of consciousness in the dynamics of resting-state brain activity. *Proc Natl Acad Sci U S A.* 112(3):887–892. doi:10.1073/pnas.1418031112.

Basser PJ, Pierpaoli C. 1996. Microstructural and Physiological Features of Tissues Elucidated by Quantitative-Diffusion-Tensor MRI. *J Magn Reson B.* 111(3):209–219. doi:10.1006/jmrb.1996.0086.

Bechara A, Damasio H, Damasio AR, Lee GP. 1999. Different contributions of the human amygdala and ventromedial prefrontal cortex to decision-making. *Journal of Neuroscience.* 19(13):5473–5481. doi:10.1523/jneurosci.19-13-05473.1999.

Berboth S, Morawetz C. 2021. Amygdala-prefrontal connectivity during emotion regulation: A meta-analysis of psychophysiological interactions. *Neuropsychologia.* 153:107767. doi:10.1016/j.neuropsychologia.2021.107767.

Berretta S, Pantazopoulos H, Lange N. 2007. Neuron Numbers and Volume of the Amygdala in Subjects Diagnosed with Bipolar Disorder or Schizophrenia. *Biol Psychiatry.* 62(8):884–893. doi:10.1016/j.biopsych.2007.04.023. <https://linkinghub.elsevier.com/retrieve/pii/S0006322307003575>.

Bezchlibnyk YB, Sun X, Wang J-F, MacQueen GM, McEwen BS, Young LT. 2007. Neuron somal size is decreased in the lateral amygdalar nucleus of subjects with bipolar disorder. *J Psychiatry Neurosci.* 32(3):203–10. <http://www.ncbi.nlm.nih.gov/pubmed/17476367>.

Bickart KC, Hollenbeck MC, Barrett LF, Dickerson BC. 2012. Intrinsic amygdala-cortical functional connectivity predicts social network size in humans. *Journal of Neuroscience.* 32(42):14729–14741. doi:10.1523/JNEUROSCI.1599-12.2012.

Biswal B, Zerrin Yetkin F, Haughton VM, Hyde JS. 1995. Functional connectivity in the motor cortex of resting human brain using echo-planar mri. *Magn Reson Med.* 34(4):537–541. doi:10.1002/mrm.1910340409. <https://onlinelibrary.wiley.com/doi/10.1002/mrm.1910340409>.

Blair RJR. 2008. Review. The amygdala and ventromedial prefrontal cortex: Functional contributions and dysfunction in psychopathy. *Philosophical Transactions of the Royal Society B: Biological Sciences.* 363(1503):2557–2565. doi:10.1098/rstb.2008.0027.

Boorman ED, Rushworth MF, Behrens TE. 2013. Ventromedial prefrontal and anterior cingulate cortex adopt choice and default reference frames during sequential multi-alternative choice. *Journal of Neuroscience.* 33(6):2242–2253. doi:10.1523/JNEUROSCI.3022-12.2013.

Brabec J, Rulseh A, Hoyt B, Vizek M, Horinek D, Hort J, Petrovicky P. 2010. Volumetry of the human amygdala — An anatomical study. *Psychiatry Res Neuroimaging.* 182(1):67–72. doi:10.1016/j.pscychresns.2009.11.005. <https://linkinghub.elsevier.com/retrieve/pii/S0925492709002716>.

Bzdok D, Laird AR, Zilles K, Fox PT, Eickhoff SB. 2013. An investigation of the structural, connectional, and functional subspecialization in the human amygdala. *Hum Brain Mapp.* 34(12):3247–3266. doi:10.1002/hbm.22138.

Calderazzo SM, Busch SE, Moore TL, Rosene DL, Medalla M. 2021. Distribution and overlap of entorhinal, premotor, and amygdalar connections in the monkey anterior cingulate cortex. *Journal of Comparative Neurology.* 529(4):885–904. doi:10.1002/cne.24986.

Cao L, Li H, Liu J, Jiang J, Li B, Li X, Zhang S, Gao Y, Liang K, Hu Xinyue, et al. 2022. Disorganized functional architecture of amygdala subregional networks in obsessive-compulsive disorder. *Commun Biol.* 5(1). doi:10.1038/s42003-022-04115-z.

Cardinal RN, Parkinson JA, Hall J, Everitt BJ. 2002. Emotion and motivation: the role of the amygdala, ventral striatum, and prefrontal cortex. *Neurosci Biobehav Rev.* 26(3):321–352. doi:10.1016/S0149-7634(02)00007-6.

<https://linkinghub.elsevier.com/retrieve/pii/S0149763402000076>.

Carmichael ST, Price JL. 1995. Limbic connections of the orbital and medial prefrontal cortex in macaque monkeys. *J Comp Neurol.* 363(4):615–641. doi:10.1002/cne.903630408. <http://doi.wiley.com/10.1002/cne.903630408>.

Chareyron LJ, Banta Lavenex P, Amaral DG, Lavenex P. 2011. Stereological analysis of the rat and monkey amygdala. *Journal of Comparative Neurology.* 519(16):3218–3239. doi:10.1002/cne.22677. <https://onlinelibrary.wiley.com/doi/10.1002/cne.22677>.

Cho YT, Ernst M, Fudge JL. 2013. Cortico-Amygdala-Striatal Circuits Are Organized as Hierarchical Subsystems through the Primate Amygdala. *Journal of Neuroscience.* 33(35):14017–14030. doi:10.1523/JNEUROSCI.0170-13.2013.

Dal Monte O, Chu CCJ, Fagan NA, Chang SWC. 2020. Specialized medial prefrontal–amygdala coordination in other-regarding decision preference. *Nat Neurosci.* 23(4):565–574. doi:10.1038/s41593-020-0593-y.

Dal Monte O, Fan S, Fagan NA, Chu C-CJ, Zhou MB, Putnam PT, Nair AR, Chang SWC. 2022. Widespread implementations of interactive social gaze neurons in the primate prefrontal-amygdala networks. *Neuron.* 110(13):2183-2197.e7. doi:10.1016/j.neuron.2022.04.013.

Dong M, Xia L, Lu M, Li C, Xu K, Zhang L. 2019. A failed top-down control from the prefrontal cortex to the amygdala in generalized anxiety disorder: Evidence from resting-state fMRI with Granger causality analysis. *Neurosci Lett.* 707:134314. doi:10.1016/j.neulet.2019.134314.

<https://linkinghub.elsevier.com/retrieve/pii/S0304394019303945>.

Dziura SL, Thompson JC. 2014. Social-Network Complexity in Humans Is Associated With the Neural Response to Social Information. *Psychol Sci.* 25(11):2095–2101. doi:10.1177/0956797614549209.

Eickhoff SB, Stephan KE, Mohlberg H, Grefkes C, Fink GR, Amunts K, Zilles K. 2005. A new SPM toolbox for combining probabilistic cytoarchitectonic maps and functional imaging data. *Neuroimage.* 25(4):1325–1335. doi:10.1016/j.neuroimage.2004.12.034.

Elorette C, Aguilar BL, Novak V, Forcelli PA, Malkova L. 2020. Dysregulation of behavioral and autonomic responses to emotional and social stimuli following bidirectional pharmacological manipulation of the basolateral amygdala in macaques. *Neuropharmacology.* 179:108275. doi:10.1016/j.neuropharm.2020.108275. <https://linkinghub.elsevier.com/retrieve/pii/S0028390820303439>.

Elvira UKA, Seoane S, Janssen J, Janssen N. 2022. Contributions of human amygdala nuclei to resting-state networks. Cristofori I, editor. *PLoS One.* 17(12):e0278962. doi:10.1371/journal.pone.0278962. <https://dx.plos.org/10.1371/journal.pone.0278962>.

Felix-Ortiz AC, Burgos-Robles A, Bhagat ND, Leppla CA, Tye KM. 2016. Bidirectional modulation of anxiety-related and social behaviors by amygdala projections to the medial prefrontal cortex. *Neuroscience*. 321:197–209. doi:10.1016/j.neuroscience.2015.07.041.

Ferrara NC, Opendak M. 2023. Amygdala circuit transitions supporting developmentally-appropriate social behavior. *Neurobiol Learn Mem*. 201. doi:10.1016/j.nlm.2023.107762.

Folloni D, Sallet J, Khrapitchev AA, Sibson N, Verhagen L, Mars RB. 2019a. Dichotomous organization of amygdala/temporal-prefrontal bundles in both humans and monkeys. *Elife*. 8. doi:10.7554/eLife.47175. <https://elifesciences.org/articles/47175>.

Folloni D, Verhagen L, Mars RB, Fouragnan E, Constans C, Aubry JF, Rushworth MFS, Sallet J. 2019b. Manipulation of Subcortical and Deep Cortical Activity in the Primate Brain Using Transcranial Focused Ultrasound Stimulation. *Neuron*. 101(6):1109-1116.e5. doi:10.1016/j.neuron.2019.01.019. <https://linkinghub.elsevier.com/retrieve/pii/S0896627319300467>.

Fox AS, Shackman AJ. 2019. The central extended amygdala in fear and anxiety: Closing the gap between mechanistic and neuroimaging research. *Neurosci Lett*. 693:58–67. doi:10.1016/j.neulet.2017.11.056.

Friedrich P, Forkel SJ, Amiez C, Balsters JH, Coulon O, Fan L, Goulas A, Hadj-Bouziane F, Hecht EE, Heuer K, et al. 2021. Imaging evolution of the primate brain: the next frontier? *Neuroimage*. 228:117685. doi:10.1016/j.neuroimage.2020.117685. <https://linkinghub.elsevier.com/retrieve/pii/S1053811920311708>.

Gangopadhyay P, Chawla M, Dal Monte O, Chang SWC. 2021. Prefrontal–amygdala circuits in social decision-making. *Nat Neurosci*. 24(1):5–18. doi:10.1038/s41593-020-00738-9. [accessed 2021 Feb 1]. <https://doi.org/10.1038/s41593-020-00738-9>.

Gao Y, Sun J, Cheng L, Yang Q, Li J, Hao Z, Zhan L, Shi Y, Li M, Jia X, et al. 2022. Altered resting state dynamic functional connectivity of amygdala subregions in patients with autism spectrum disorder: A multi-site fMRI study. *J Affect Disord*. 312:69–77. doi:10.1016/j.jad.2022.06.011.

Gee DG, Hanson C, Caglar LR, Fareri DS, Gabard-Durnam LJ, Mills-Finnerty C, Goff B, Caldera CJ, Lumian DS, Flannery J, et al. 2022. Experimental evidence for a child-to-adolescent switch in human amygdala-prefrontal cortex communication: A cross-sectional pilot study. *Dev Sci*.(January):1–16. doi:10.1111/desc.13238.

Gee DG, Humphreys KL, Flannery J, Goff B, Telzer EH, Shapiro M, Hare TA, Bookheimer SY, Tottenham N. 2013. A developmental shift from positive to negative connectivity in human amygdala-prefrontal circuitry. *Journal of Neuroscience*. 33(10):4584–4593. doi:10.1523/JNEUROSCI.3446-12.2013. <https://www.jneurosci.org/lookup/doi/10.1523/JNEUROSCI.3446-12.2013>.

Ghashghaei HT, Barbas H. 2002. Pathways for emotion: Interactions of prefrontal and anterior temporal pathways in the amygdala of the rhesus monkey. *Neuroscience*. 115(4):1261–1279. doi:10.1016/S0306-4522(02)00446-3. <https://linkinghub.elsevier.com/retrieve/pii/S0306452202004463>.

Ghashghaei HT, Hilgetag CC, Barbas H. 2007. Sequence of information processing for emotions based on the anatomic dialogue between prefrontal cortex and amygdala. *Neuroimage*. 34(3):905–923. doi:10.1016/j.neuroimage.2006.09.046. <https://linkinghub.elsevier.com/retrieve/pii/S105381190600989X>.

Giacometti C, Dureux A, Autran-Clavagnier D, Wilson CRE, Sallet J, Dirheimer M, Procyk E, Hadj-Bouziane F, Amiez C. 2022. Frontal cortical functional connectivity is impacted by anaesthesia in macaques. *Cerebral Cortex*. 32(18):4050–4067. doi:10.1093/cercor/bhab465.

Gopinath K, Krishnamurthy V, Cabanban R, Crosson BA. 2015. Hubs of anticorrelation in high-resolution resting-state functional connectivity network architecture. *Brain Connect*. 5(5):267–275. doi:10.1089/brain.2014.0323.

Grabenhorst F, Báez-Mendoza R, Genest W, Deco G, Schultz W. 2019. Primate Amygdala Neurons Simulate Decision Processes of Social Partners. *Cell*. 177(4):986-998.e15. doi:10.1016/j.cell.2019.02.042.

Grabenhorst F, Rolls ET. 2011. Value, pleasure and choice in the ventral prefrontal cortex. *Trends Cogn Sci*. 15(2):56–67. doi:10.1016/j.tics.2010.12.004. <https://linkinghub.elsevier.com/retrieve/pii/S1364661310002561>.

Grabenhorst F, Schultz W. 2021. Functions of primate amygdala neurons in economic decisions and social decision simulation. *Behavioural Brain Research*. 409. doi:10.1016/j.bbr.2021.113318.

Grayson DS, Bliss-Moreau E, Machado CJ, Bennett J, Shen K, Grant KA, Fair DA, Amaral DG. 2016. The Rhesus Monkey Connectome Predicts Disrupted Functional Networks Resulting from Pharmacogenetic Inactivation of the Amygdala. *Neuron*. 91(2):453–466. doi:10.1016/j.neuron.2016.06.005.

Greicius MD, Supekar K, Menon V, Dougherty RF. 2009. Resting-State Functional Connectivity Reflects Structural Connectivity in the Default Mode Network. *Cerebral Cortex*. 19(1):72–78. doi:10.1093/cercor/bhn059. <https://academic.oup.com/cercor/article-lookup/doi/10.1093/cercor/bhn059>.

Grier MD, Yacoub E, Adriany G, Lagore RL, Harel N, Zhang RY, Lenglet C, Uğurbil K, Zimmermann J, Heilbronner SR. 2022. Ultra-high field (10.5T) diffusion-weighted MRI of the macaque brain. *Neuroimage*. 255. doi:10.1016/j.neuroimage.2022.119200.

Grier MD, Zimmermann J, Heilbronner SR. 2020. Estimating Brain Connectivity With Diffusion-Weighted Magnetic Resonance Imaging: Promise and Peril. *Biol Psychiatry Cogn Neurosci Neuroimaging*. 5(9):846–854. doi:10.1016/j.bpsc.2020.04.009.

Gupta R, Koscik TR, Bechara A, Tranel D. 2011. The amygdala and decision-making. *Neuropsychologia*. 49(4):760–766. doi:10.1016/j.neuropsychologia.2010.09.029. <http://dx.doi.org/10.1016/j.neuropsychologia.2010.09.029>.

Hartig R, Glen D, Jung B, Logothetis NK, Paxinos G, Garza-Villarreal EA, Messinger A, Evrard HC. 2021. The Subcortical Atlas of the Rhesus Macaque (SARM) for neuroimaging. *Neuroimage*. 235:117996. doi:10.1016/j.neuroimage.2021.117996. <https://linkinghub.elsevier.com/retrieve/pii/S1053811921002731>.

Henke-von der Malsburg J, Kappeler PM, Fichtel C. 2020. Linking ecology and cognition: does ecological specialisation predict cognitive test performance? *Behav Ecol Sociobiol*. 74(12):154. doi:10.1007/s00265-020-02923-z. <http://link.springer.com/10.1007/s00265-020-02923-z>.

Holley D, Fox AS. 2022. The central extended amygdala guides survival-relevant tradeoffs: Implications for understanding common psychiatric disorders. *Neurosci Biobehav Rev*. 142. doi:10.1016/j.neubiorev.2022.104879.

Hori Y, Schaeffer DJ, Yoshida A, Cléry JC, Hayrynen LK, Gati JS, Menon RS, Everling S. 2020. Cortico-Subcortical Functional Connectivity Profiles of Resting-State Networks in Marmosets and Humans. doi:10.1523/JNEUROSCI.1984-20.2020. [accessed 2021 Mar 1]. <https://doi.org/10.1523/JNEUROSCI.1984-20.2020>.

Hutchison RM, Hutchison M, Manning KY, Menon RS, Everling S. 2014. Isoflurane induces dose-dependent alterations in the cortical connectivity profiles and dynamic properties of the brain's functional architecture. *Hum Brain Mapp*. 35(12):5754–5775. doi:10.1002/hbm.22583.

Jacobson S, Trojanowski JQ. 1975. Amygdaloid projections to prefrontal granular cortex in rhesus monkey demonstrated with horseradish peroxidase. *Brain Res*. 100(1):132–139. doi:10.1016/0006-8993(75)90248-6. <https://linkinghub.elsevier.com/retrieve/pii/0006899375902486>.

Jezzini A, Padoa-Schioppa C. 2020. Neuronal activity in the primate amygdala during economic choice. *Journal of Neuroscience*. 40(6):1286–1301. doi:10.1523/JNEUROSCI.0961-19.2019.

Johnstone T, Van Reekum CM, Urry HL, Kalin NH, Davidson RJ. 2007. Failure to regulate: Counterproductive recruitment of top-down prefrontal-subcortical circuitry in major depression. *Journal of Neuroscience*. 27(33):8877–8884. doi:10.1523/JNEUROSCI.2063-07.2007.

Joyce MKP, Barbas H. 2018. Cortical connections position primate area 25 as a keystone for interoception, emotion, and memory. *Journal of Neuroscience*. 38(7):1677–1698. doi:10.1523/JNEUROSCI.2363-17.2017.

Juechems K, Balaguer J, Herce Castañón S, Ruz M, O'Reilly JX, Summerfield C. 2019. A Network for Computing Value Equilibrium in the Human Medial Prefrontal Cortex. *Neuron*. 101(5):977-987.e3. doi:10.1016/j.neuron.2018.12.029.

Kalin NH. 2004. The Role of the Central Nucleus of the Amygdala in Mediating Fear and Anxiety in the Primate. *Journal of Neuroscience*. 24(24):5506–5515. doi:10.1523/JNEUROSCI.0292-04.2004. <https://www.jneurosci.org/lookup/doi/10.1523/JNEUROSCI.0292-04.2004>.

Kanai R, Bahrami B, Roylance R, Rees G. 2012. Online social network size is reflected in human brain structure. *Proceedings of the Royal Society B: Biological Sciences*. 279(1732):1327–1334. doi:10.1098/rspb.2011.1959.

Kedo O, Zilles K, Palomero-Gallagher N, Schleicher A, Mohlberg H, Bludau S, Amunts K. 2018. Receptor-driven, multimodal mapping of the human amygdala. *Brain Struct Funct*. 223(4):1637–1666. doi:10.1007/s00429-017-1577-x.

Kelly EA, Thomas VK, Indraghanty A, Fudge JL. 2021. Perigenual and Subgenual Anterior Cingulate Afferents Converge on Common Pyramidal Cells in Amygdala Subregions of the Macaque. *The Journal of Neuroscience*. 41(47):9742–9755. doi:10.1523/jneurosci.1056-21.2021.

Kenwood MM, Kalin NH. 2021. Nonhuman Primate Models to Explore Mechanisms Underlying Early-Life Temperamental Anxiety. *Biol Psychiatry*. 89(7):659–671. doi:10.1016/j.biopsych.2020.08.028.

Kim M. J., Gee DG, Loucks RA, Davis FC, Whalen PJ. 2011b. Anxiety Dissociates Dorsal and Ventral Medial Prefrontal Cortex Functional Connectivity with the Amygdala at Rest. *Cerebral Cortex*. 21(7):1667–1673. doi:10.1093/cercor/bhq237. <https://academic.oup.com/cercor/article-lookup/doi/10.1093/cercor/bhq237>.

Kim M. J., Loucks RA, Palmer AL, Brown AC, Solomon KM, Marchante AN, Whalen PJ. 2011a. The structural and functional connectivity of the amygdala: From normal emotion to pathological anxiety. *Behavioural Brain Research*. 223(2):403–410. doi:10.1016/j.bbr.2011.04.025.

Kim Y, Sakata H, Nejime M, Konoike N, Miyachi S, Nakamura K. 2018. Afferent connections of the dorsal, perigenual, and subgenual anterior cingulate cortices of the monkey: Amygdalar inputs and intrinsic connections. *Neurosci Lett*. 681:93–99. doi:10.1016/j.neulet.2018.05.028.

Klavir O, Genud-Gabai R, Paz R. 2013. Functional connectivity between amygdala and cingulate cortex for adaptive aversive learning. *Neuron*. 80(5):1290–1300. doi:10.1016/j.neuron.2013.09.035.

Klein-Flügge MC, Jensen DEA, Takagi Y, Priestley L, Verhagen L, Smith SM, Rushworth MFS. 2022 Sep 22. Relationship between nuclei-specific amygdala connectivity and mental health dimensions in humans. *Nat Hum Behav*. doi:10.1038/s41562-022-01434-3. <https://www.nature.com/articles/s41562-022-01434-3>.

Kopell NJ, Gritton HJ, Whittington MA, Kramer MA. 2014. Beyond the Connectome: The Dynome. *Neuron*. 83(6):1319–1328. doi:10.1016/j.neuron.2014.08.016.

Kreczmanski P, Heinsen H, Mantua V, Woltersdorf F, Masson T, Ulfing N, Schmidt-Kastner R, Korr H, Steinbusch HWM, Hof PR, et al. 2007. Volume, neuron density and total neuron number in five subcortical regions in schizophrenia. *Brain*. 130(3):678–692. doi:10.1093/brain/awl386. <https://academic.oup.com/brain/article-lookup/doi/10.1093/brain/awl386>.

Leitão J, Burckhardt M, Vuilleumier P. 2022. Amygdala in Action: Functional Connectivity during Approach and Avoidance Behaviors. *J Cogn Neurosci*. 34(5):729–747. doi:10.1162/jocn_a_01800.

Lew CH, Groeniger KM, Bellugi U, Stefanacci L, Schumann CM, Semendeferi K. 2018. A postmortem stereological study of the amygdala in Williams syndrome. *Brain Struct Funct*. 223(4):1897–1907. doi:10.1007/s00429-017-1592-y.

Li L, He C, Jian T, Guo X, Xiao J, Li Y, Chen Heng, Kang X, Chen Huafu, Duan X. 2021. Attenuated link between the medial prefrontal cortex and the amygdala in children with autism spectrum disorder: Evidence from effective connectivity within the “social brain.” *Prog Neuropsychopharmacol Biol Psychiatry*. 111. doi:10.1016/j.pnpbp.2020.110147.

Likhtik E, Paz R. 2015. Amygdala-prefrontal interactions in (mal)adaptive learning. *Trends Neurosci*. 38(3):158–166. doi:10.1016/j.tins.2014.12.007. <https://linkinghub.elsevier.com/retrieve/pii/S0166223614002355>.

Liu N, Hadj-Bouziane F, Moran R, Ungerleider LG, Ishai A. 2016 Jan 11. Facial Expressions Evoke Differential Neural Coupling in Macaques. *Cerebral Cortex*:bhv345. doi:10.1093/cercor/bhv345.

Lopez-Persem A, Verhagen L, Amiez C, Petrides M, Sallet J. 2019. The Human Ventromedial Prefrontal Cortex: Sulcal Morphology and Its Influence on Functional Organization. *The Journal of Neuroscience*. 39(19):3627–3639. doi:10.1523/JNEUROSCI.2060-18.2019. <https://www.jneurosci.org/lookup/doi/10.1523/JNEUROSCI.2060-18.2019>.

Málková L, Gaffan D, Murray EA. 1997. Excitotoxic lesions of the amygdala fail to produce impairment in visual learning for auditory secondary reinforcement but interfere with reinforcer devaluation effects in rhesus monkeys. *Journal of Neuroscience*. 17(15):6011–6020. doi:10.1523/jneurosci.17-15-06011.1997. <https://www.jneurosci.org/lookup/doi/10.1523/JNEUROSCI.17-15-06011.1997>.

Mars RB, Sotiropoulos SN, Passingham RE, Sallet J, Verhagen L, Khrapitchev AA, Sibson N, Jbabdi S. 2018. Whole brain comparative anatomy using connectivity blueprints. *Elife*. 7. doi:10.7554/eLife.35237. [/pmc/articles/PMC5984034/](https://pmc/articles/PMC5984034/).

Mcdonald AJ, Augustine JR. 1993. LOCALIZATION OF GABA-LIKE IMMUNOREACTIVITY IN THE MONKEY AMYGDALA.

Morecraft RJ, Mcneal DW, Stilwell-Morecraft KS, Gedney M, Ge J, Schroeder CM, Van Hoesen GW. 2007. Amygdala interconnections with the cingulate motor cortex in the rhesus monkey. *Journal of Comparative Neurology*. 500(1):134–165. doi:10.1002/cne.21165.

Morecraft RJ, Stilwell-Morecraft KS, Cipolloni PB, Ge J, McNeal DW, Pandya DN. 2012. Cytoarchitecture and cortical connections of the anterior cingulate and adjacent somatomotor fields in the rhesus monkey. *Brain Res Bull*. 87(4–5):457–497. doi:10.1016/j.brainresbull.2011.12.005. <https://linkinghub.elsevier.com/retrieve/pii/S0361923011003650>.

Morin EL, Howell BR, Feczko E, Earl E, Pincus M, Reding K, Kovacs-Balint ZA, Meyer JS, Styner M, Fair D, et al. 2020. Developmental outcomes of early adverse care on amygdala functional connectivity in nonhuman primates. *Dev Psychopathol*. 32(5):1579–1596. doi:10.1017/S0954579420001133.

Morrow J, Mosher C, Gothard K. 2019. Multisensory neurons in the primate amygdala. *Journal of Neuroscience*. 39(19):3663–3675. doi:10.1523/JNEUROSCI.2903-18.2019. [accessed 2021 Feb 3]. <https://doi.org/10.1523/JNEUROSCI.2903-18.2019>.

Mukherjee P, Sabharwal A, Kotov R, Szekely A, Parsey R, Barch DM, Mohanty A. 2016. Disconnection between amygdala and medial prefrontal cortex in psychotic disorders. *Schizophr Bull.* 42(4):1056–1067. doi:10.1093/schbul/sbw012.

Murray EA, Fellows LK. 2021. Prefrontal cortex interactions with the amygdala in primates. *Neuropsychopharmacology.*(July):1–17. doi:10.1038/s41386-021-01128-w.

Murray EA, Wise SP, Drevets WC. 2011. Localization of Dysfunction in Major Depressive Disorder: Prefrontal Cortex and Amygdala. *Biol Psychiatry.* 69(12):e43–e54. doi:10.1016/j.biopsych.2010.09.041.

Nauta WJH. 1993. Fibre Degeneration Following Lesions of the Amygdaloid Complex in the Monkey. *Neuroanatomy.*:202–219. doi:10.1007/978-1-4684-7920-1_12.

Neubert F-X, Mars RB, Sallet J, Rushworth MFS. 2015. Connectivity reveals relationship of brain areas for reward-guided learning and decision making in human and monkey frontal cortex. *Proceedings of the National Academy of Sciences.* 112(20):E2695–E2704. doi:10.1073/pnas.1410767112. <http://www.pnas.org/lookup/doi/10.1073/pnas.1410767112>.

Nicholson AA, Densmore M, Frewen PA, Théberge J, Neufeld RW, McKinnon MC, Lanius RA. 2015. The Dissociative Subtype of Posttraumatic Stress Disorder: Unique Resting-State Functional Connectivity of Basolateral and Centromedial Amygdala Complexes. *Neuropsychopharmacology.* 40(10):2317–2326. doi:10.1038/npp.2015.79. <http://www.nature.com/articles/npp201579>.

O'Neill P-K, Gore F, Salzman CD. 2018. Basolateral amygdala circuitry in positive and negative valence. *Curr Opin Neurobiol.* 49:175–183. doi:10.1016/j.conb.2018.02.012.

Pandya DN, Van Hoesen GW, Domesick VB. 1973. A cingulo-amygdaloid projection in the rhesus monkey. *Brain Res.* 61:369–373. doi:10.1016/0006-8993(73)90540-4. <https://linkinghub.elsevier.com/retrieve/pii/0006899373905404>.

Paul S, Beucke JC, Kaufmann C, Mersov A, Heinzl S, Kathmann N, Simon D. 2019. Amygdala-prefrontal connectivity during appraisal of symptom-related stimuli in obsessive-compulsive disorder. *Psychol Med.* 49(2):278–286. doi:10.1017/S003329171800079X.

Petrides M, Pandya DN. 2002. Comparative cytoarchitectonic analysis of the human and the macaque ventrolateral prefrontal cortex and corticocortical connection patterns in the monkey. *European Journal of Neuroscience.* 16(2):291–310. doi:10.1046/j.1460-9568.2001.02090.x. <http://doi.wiley.com/10.1046/j.1460-9568.2001.02090.x>.

Petrides M, Tomaiuolo F, Yeterian EH, Pandya DN. 2012. The prefrontal cortex: Comparative architectonic organization in the human and the macaque monkey brains. *Cortex.* 48(1):46–57. doi:10.1016/j.cortex.2011.07.002. <https://linkinghub.elsevier.com/retrieve/pii/S0010945211002279>.

Porrino LJ, Crane AM, Goldman-Rakic PS. 1981. Direct and indirect pathways from the amygdala to the frontal lobe in rhesus monkeys. *J Comp Neurol.* 198(1):121–136. doi:10.1002/cne.901980111. <https://onlinelibrary.wiley.com/doi/10.1002/cne.901980111>.

Pozzi L, Hodgson JA, Burrell AS, Sterner KN, Raaum RL, Disotell TR. 2014. Primate phylogenetic relationships and divergence dates inferred from complete mitochondrial genomes. *Mol Phylogenet Evol.* 75(1):165–183. doi:10.1016/j.ympev.2014.02.023.

Price JL, Drevets WC. 2010. Neurocircuitry of mood disorders. *Neuropsychopharmacology.* 35(1):192–216. doi:10.1038/npp.2009.104. <http://www.nature.com/articles/npp2009104>.

Procyk E, Wilson CRE, Stoll FM, Faraut MCM, Petrides M, Amiez C. 2016. Midcingulate Motor Map and Feedback Detection: Converging Data from Humans and Monkeys. *Cerebral Cortex.* 26(2):467–476. doi:10.1093/cercor/bhu213.

Pryluk R, Kfir Y, Gelbard-Sagiv H, Fried I, Paz R. 2019. A Tradeoff in the Neural Code across Regions and Species. *Cell.* 176(3):597–609.e18. doi:10.1016/j.cell.2018.12.032.

Putnam PT, Gothard KM. 2019. Multidimensional neural selectivity in the primate amygdala. *eNeuro.* 6(5):1–13. doi:10.1523/ENEURO.0153-19.2019.

Quilodran R, Rothé M, Procyk E. 2008. Behavioral Shifts and Action Valuation in the Anterior Cingulate Cortex. *Neuron*. 57(2):314–325. doi:10.1016/j.neuron.2007.11.031.

Reber J, Tranel D. 2017. Sex differences in the functional lateralization of emotion and decision making in the human brain. *J Neurosci Res*. 95(1–2):270–278. doi:10.1002/jnr.23829.

Reding KM, Grayson DS, Miranda-Dominguez O, Ray S, Wilson ME, Toufexis D, Fair DA, Sanchez MM. 2020. Effects of social subordination and oestradiol on resting-state amygdala functional connectivity in adult female rhesus monkeys. *J Neuroendocrinol*. 32(2). doi:10.1111/jne.12822.

Roy AK, Shehzad Z, Margulies DS, Kelly AMC, Uddin LQ, Gotimer K, Biswal BB, Castellanos FX, Milham MP. 2009. Functional connectivity of the human amygdala using resting state fMRI. *Neuroimage*. 45(2):614–626. doi:10.1016/j.neuroimage.2008.11.030. <https://linkinghub.elsevier.com/retrieve/pii/S1053811908012214>.

Royer S, Martina M, Paré D. 1999. An Inhibitory Interface Gates Impulse Traffic between the Input and Output Stations of the Amygdala. *The Journal of Neuroscience*. 19(23):10575–10583. doi:10.1523/JNEUROSCI.19-23-10575.1999. <https://www.jneurosci.org/lookup/doi/10.1523/JNEUROSCI.19-23-10575.1999>.

Rubinow MJ, Mahajan G, May W, Overholser JC, Jurjus GJ, Dieter L, Herbst N, Steffens DC, Miguel-Hidalgo JJ, Rajkowska G, et al. 2016. Basolateral amygdala volume and cell numbers in major depressive disorder: a postmortem stereological study. *Brain Struct Funct*. 221(1):171–184. doi:10.1007/s00429-014-0900-z.

Rudebeck PH, Mitz AR, Chacko RV, Murray EA. 2013. Effects of Amygdala Lesions on Reward-Value Coding in Orbital and Medial Prefrontal Cortex. *Neuron*. 80(6):1519–1531. doi:10.1016/j.neuron.2013.09.036.

Saez A, Rigotti M, Ostojic S, Fusi S, Salzman CD. 2015. Abstract Context Representations in Primate Amygdala and Prefrontal Cortex. *Neuron*. 87(4):869–881. doi:10.1016/j.neuron.2015.07.024. <http://dx.doi.org/10.1016/j.neuron.2015.07.024>.

Saez RA, Saez A, Paton JJ, Lau B, Salzman CD. 2017. Distinct Roles for the Amygdala and Orbitofrontal Cortex in Representing the Relative Amount of Expected Reward. *Neuron*. 95(1):70–77.e3. doi:10.1016/j.neuron.2017.06.012.

Sallet J, Mars RB, Noonan MP, Andersson JL, O'Reilly JX, Jbabdi S, Croxson PL, Jenkinson M, Miller KL, Rushworth MFS. 2011. Social Network Size Affects Neural Circuits in Macaques. *Science* (1979). 334(6056):697–700. doi:10.1126/science.1210027.

Sarwar T, Ramamohanarao K, Zalesky A. 2021. A critical review of connectome validation studies. *NMR Biomed*. 34(12). doi:10.1002/nbm.4605.

Sawada M, Adolphs R, Dlouhy BJ, Jenison RL, Rhone AE, Kovach CK, Greenlee JDW, Howard III MA, Oya H. 2022. Mapping effective connectivity of human amygdala subdivisions with intracranial stimulation. *Nat Commun*. 13(1). doi:10.1038/s41467-022-32644-y.

Schneider B, Koenigs M. 2017. Human lesion studies of ventromedial prefrontal cortex. *Neuropsychologia*. 107(July):84–93. doi:10.1016/j.neuropsychologia.2017.09.035. <https://doi.org/10.1016/j.neuropsychologia.2017.09.035>.

Scholl J, Kolling N, Nelissen N, Wittmann MK, Harmer CJ, Rushworth MFS. 2015. The good, the bad, and the irrelevant: Neural mechanisms of learning real and hypothetical rewards and effort. *Journal of Neuroscience*. 35(32):11233–11251. doi:10.1523/JNEUROSCI.0396-15.2015.

Schumann CM, Amaral DG. 2006. Stereological Analysis of Amygdala Neuron Number in Autism. *Journal of Neuroscience*. 26(29):7674–7679. doi:10.1523/JNEUROSCI.1285-06.2006. <https://www.jneurosci.org/lookup/doi/10.1523/JNEUROSCI.1285-06.2006>.

Schumann CM, Bauman MD, Amaral DG. 2011. Abnormal structure or function of the amygdala is a common component of neurodevelopmental disorders. *Neuropsychologia*.

49(4):745–759. doi:10.1016/j.neuropsychologia.2010.09.028.
<https://linkinghub.elsevier.com/retrieve/pii/S0028393210004185>.

Semendeferi K, Damasio H, Frank R, Van Hoesen GW. 1997. The evolution of the frontal lobes: a volumetric analysis based on three-dimensional reconstructions of magnetic resonance scans of human and ape brains. Academic Press.

Semendeferi K, Lu A, Schenker N, Damasio H. 2002. Humans and great apes share a large frontal cortex. *Nat Neurosci.* 5(3):272–276. doi:10.1038/nn814.
<http://www.nature.com/articles/nn814>.

Sharma KK, Kelly EA, Pfeifer CW, Fudge JL. 2020. Translating Fear Circuitry: Amygdala Projections to Subgenual and Perigenual Anterior Cingulate in the Macaque. *Cerebral Cortex.* 30(2):550–562. doi:10.1093/cercor/bhz106.

Smaers JB, Gómez-Robles A, Parks AN, Sherwood CC. 2017. Exceptional Evolutionary Expansion of Prefrontal Cortex in Great Apes and Humans. *Current Biology.* 27(5):714–720. doi:10.1016/j.cub.2017.01.020.

Smaers JB, Steele J, Case CR, Cowper A, Amunts K, Zilles K. 2011. Primate Prefrontal Cortex Evolution: Human Brains Are the Extreme of a Lateralized Ape Trend. *Brain Behav Evol.* 77(2):67–78. doi:10.1159/000323671. <https://www.karger.com/Article/FullText/323671>.

Solano-Castiella E, Anwender A, Lohmann G, Weiss M, Docherty C, Geyer S, Reimer E, Friederici AD, Turner R. 2010. Diffusion tensor imaging segments the human amygdala in vivo. *Neuroimage.* 49(4):2958–2965. doi:10.1016/j.neuroimage.2009.11.027.

Sotiropoulos SN, Zalesky A. 2019. Building connectomes using diffusion MRI: why, how and but. *NMR Biomed.* 32(4). doi:10.1002/nbm.3752.

Stefanacci L, Amaral DG. 2000. Topographic Organization of Cortical Inputs to the Lateral Nucleus of the Macaque Monkey Amygdala: A Retrograde Tracing Study.

Stephan H, Frahm HD, Baron G. 1987. Comparison of brain structure volumes in Insectivora and primates. VII. Amygdaloid components. *J Hirnforsch.* 28(5):571–584. <http://www.ncbi.nlm.nih.gov/pubmed/3693895>.

Swartz JR, Wiggins JL, Carrasco M, Lord C, Monk CS. 2013. Amygdala habituation and prefrontal functional connectivity in youth with autism spectrum disorders. *J Am Acad Child Adolesc Psychiatry.* 52(1):84–93. doi:10.1016/j.jaac.2012.10.012.

Taswell CA, Costa VD, Basile BM, Pujara MS, Jones B, Manem N, Murray EA, Averbeck BB. 2021. Effects of Amygdala Lesions on Object-Based Versus Action-Based Learning in Macaques. *Cerebral Cortex.* 31(1):529–546. doi:10.1093/cercor/bhaa241.

Taub Aryeh Hai, Perets R, Kahana E, Paz R. 2018. Oscillations Synchronize Amygdala-to-Prefrontal Primate Circuits during Aversive Learning. *Neuron.* 97(2):291–298.e3. doi:10.1016/j.neuron.2017.11.042.

Taub Aryeh H., Shohat Y, Paz R. 2018. Long time-scales in primate amygdala neurons support aversive learning. *Nat Commun.* 9(1). doi:10.1038/s41467-018-07020-4.

Terburg D, Scheggia D, Triana del Rio R, Klumpers F, Ciobanu AC, Morgan B, Montoya ER, Bos PA, Giobellina G, van den Burg EH, et al. 2018. The Basolateral Amygdala Is Essential for Rapid Escape: A Human and Rodent Study. *Cell.* 175(3):723–735.e16. doi:10.1016/j.cell.2018.09.028.

Thanh Vu A, Jamison K, Glasser MF, Smith SM, Coalson T, Moeller S, Auerbach EJ, Uğurbil K, Yacoub E. 2017. Tradeoffs in pushing the spatial resolution of fMRI for the 7T Human Connectome Project. *Neuroimage.* 154:23–32. doi:10.1016/j.neuroimage.2016.11.049.

Thiebaut de Schotten M, Dell'Acqua F, Valabregue R, Catani M. 2012. Monkey to human comparative anatomy of the frontal lobe association tracts. *Cortex.* 48(1):82–96. doi:10.1016/j.cortex.2011.10.001.

Tillman RM, Stockbridge MD, Nacewicz BM, Torrisi S, Fox AS, Smith JF, Shackman AJ. 2018. Intrinsic functional connectivity of the central extended amygdala. *Hum Brain Mapp.* 39(3):1291–1312. doi:10.1002/hbm.23917.

Torrisi S, O'Connell K, Davis A, Reynolds R, Balderston N, Fudge JL, Grillon C, Ernst M. 2015. Resting state connectivity of the bed nucleus of the stria terminalis at ultra-high field. *Hum Brain Mapp.* 36(10):4076–4088. doi:10.1002/hbm.22899.

Tottenham N. 2015. Social scaffolding of human amygdala-mPFC circuit development. *Soc Neurosci.* 10(5):489–499. doi:10.1080/17470919.2015.1087424.

Uhrig L, Sitt JD, Jacob A, Tasserie J, Barttfeld P, Dupont M, Dehaene S, Jarraya B. 2018. Resting-state Dynamics as a Cortical Signature of Anesthesia in Monkeys. *Anesthesiology.* 129(5):942–958. doi:10.1097/ALN.0000000000002336.

Vassena E, Krebs RM, Silvetti M, Fias W, Verguts T. 2014. Dissociating contributions of ACC and vmPFC in reward prediction, outcome, and choice. *Neuropsychologia.* 59:112–123. doi:10.1016/j.neuropsychologia.2014.04.019.

<https://linkinghub.elsevier.com/retrieve/pii/S0028393214001419>.

Vogt BA. 2016. Midcingulate cortex: Structure, connections, homologies, functions and diseases. *J Chem Neuroanat.* 74:28–46. doi:10.1016/j.jchemneu.2016.01.010. <http://dx.doi.org/10.1016/j.jchemneu.2016.01.010>.

Vogt BA, Pandya DN. 1987. Cingulate cortex of the rhesus monkey: II. Cortical afferents. *J Comp Neurol.* 262(2):271–289. doi:10.1002/cne.902620208. <http://doi.wiley.com/10.1002/cne.902620208>.

Wegiel J, Flory M, Kuchna I, Nowicki K, Ma SY, Imaki H, Wegiel Jarek, Cohen IL, London E, Wisniewski T, et al. 2014. Stereological study of the neuronal number and volume of 38 brain subdivisions of subjects diagnosed with autism reveals significant alterations restricted to the striatum, amygdala and cerebellum. *Acta Neuropathol Commun.* 2(1):141. doi:10.1186/s40478-014-0141-7.

Wellman LL, Forcelli PA, Aguilar BL, Malkova L. 2016. Bidirectional Control of Social Behavior by Activity within Basolateral and Central Amygdala of Primates. *The Journal of Neuroscience.* 36(33):8746–8756. doi:10.1523/JNEUROSCI.0333-16.2016. <https://www.jneurosci.org/lookup/doi/10.1523/JNEUROSCI.0333-16.2016>.

Wittmann MK, Kolling N, Akaishi R, Chau BKH, Brown JW, Nelissen N, Rushworth MFS. 2016. Predictive decision making driven by multiple time-linked reward representations in the anterior cingulate cortex. *Nat Commun.* 7(1). doi:10.1038/ncomms12327.

Yacoub E, Grier MD, Auerbach EJ, Lagore RL, Harel N, Adriany G, Zilverstand A, Hayden BY, Heilbronner SR, Uğurbil K, et al. 2020. Ultra-high field (10.5 T) resting state fMRI in the macaque. *Neuroimage.* 223:117349. doi:10.1016/j.neuroimage.2020.117349.

Yendiki A, Aggarwal M, Axer M, Howard AFD, van Walsum AM van C, Haber SN. 2022. Post mortem mapping of connective anatomy for the validation of diffusion MRI. *Neuroimage.* 256. doi:10.1016/j.neuroimage.2022.119146.

Zikopoulos B, Höistad M, John Y, Barbas H. 2017. Posterior orbitofrontal and anterior cingulate pathways to the amygdala target inhibitory and excitatory systems with opposite functions. *Journal of Neuroscience.* 37(20):5051–5064. doi:10.1523/JNEUROSCI.3940-16.2017. <http://www.jneurosci.org/lookup/doi/10.1523/JNEUROSCI.3940-16.2017>.

CHAPTER IV. PROJECT OVERVIEW

In this final chapter of the introduction, I will outline how the experimental part of my thesis is organized. To understand the anatomo-functional organization of the connections between the AMG and the PFC in primates, which supports various aspects of behavioral adaptation, I employed a combination of complementary functional MRI (fMRI) methods in both humans and *rhesus* macaques: resting-state fMRI and task-based fMRI. The utilization of MRI methods in my thesis offers several crucial advantages: 1) the outstanding spatial resolution allows for comprehensive brain coverage and 2) fMRI can be employed in both humans and macaques under similar conditions, facilitating comparative analyses. Consequently, it participates in bridging the microscopic, i.e., macaques studies scale, and macroscopic, i.e., humans studies scale, gap (Barron et al., 2021; Miranda-Dominguez et al., 2014).

My research was thus divided into two parts. The first one aiming to characterize the functional connectivity pattern between AMG and PFC in primates and tackle whether it evolved with rs-fMRI. The second one aiming to understand how this functional pattern sustains some features of behavioral adaptation in humans.

1. THE FUNCTIONAL CONNECTIVITY PATTERN OF THE AMG-PFC NETWORK IN PRIMATES

Following-up the extensive review of the literature (***Chapter III of the Introduction***; published paper in *Current Research in Neurobiology* journal, Giacometti et al., 2023), several unsolved queries emerged and built the first two chapters of my thesis.

First, in macaques, the majority of rs-fMRI studies, assessing AMG or mPFC functional connectivity, are realized when macaques are under an anaesthetized state. However, 1) anaesthesia has been shown to strongly affect rs-fMRI signals (Hutchison et al., 2014; Uhrig et al., 2018), and 2) most comparative studies in the field have compared humans and macaques' connectivity using awake human and anaesthetized monkeys, preventing proper interspecies comparisons. We thus first investigated the effect of the awareness state (anaesthesia vs. awake) within the same

group of macaque monkeys on the rs-fMRI functional connectivity organization of a well- characterized network in the human brain, i.e., the PFC network (Loh et al., 2018). This constitutes the first chapter of the experimental part of my thesis entitled: **“Chapter I: Frontal Cortical Functional Connectivity Is Impacted by Anaesthesia in Macaques”**. This work has been published in *Cerebral Cortex* journal: Giacometti et al., 2022.

Second, to the extent of my observations, no studies, whether conducted under anaesthetized or awake conditions, have yet examined the functional connectivity with rs-fMRI between the AMG nuclei and the mPFC in macaques and nor ventured into comparing the functional connectivity within the AMG-mPFC network between human and macaque monkey. Therefore, after establishing the impact of anaesthesia on PFC connectivity (Giacometti et al., 2022), to fill this gap, I investigated the functional connectivity pattern of the AMG-mPFC network in humans and awake macaque monkeys using the same approach. I hypothesized that this pattern would be mostly preserved in macaques and humans given the known strong homology between these species (Chareyron et al., 2011; Petrides & Pandya, 1994, 2002). This constitutes the second chapter of the experimental part of my thesis entitled: **“Chapter II: Differential Functional Organization of Amygdala-medial Prefrontal Cortex Networks in Macaque and Human”**. This work is under a second revision process in *Communication Biology* journal: Giacometti et al., 2023, *in revision*.

2. THE FUNCTIONAL INTERPLAY IN THE AMG-PFC NETWORK DURING BEHAVIORAL ADAPTATION IN HUMANS

Behavioral adaptation can be necessary for a number of reasons, making the study of the process challenging. A particularly challenging aspect in our environment is to identify events, related or not to our own actions, that require an adaptation (see **Chapter I of the Introduction**). Two classes of events can be defined: 1) events caused by one’s own actions and specifically *FeedBack –FB–* from those actions (e.g., we adapt our strategy after an erroneous choice), and 2) events not temporally- and causally- linked to our actions, specifically *Action-Independent Events –AiDE–*. For example, we adapt our strategy after a change of rule. It should be emphasized here that an AiDE is an unknown event that has an impact onto FB processing and on the selection of the appropriate behavioral adaptation but that does not necessarily

indicate what response to select. It only indicates a need to keep the current strategy or to select another strategy (shift or stay for instance). Therefore, it is not just an irrelevant sensory event (e.g., a plane passing overhead), nor a conditional cue because an AiDE does not dictate what action to execute (i.e., a conditional cue relies on if/then conditions: if cue A and B select response W and X, respectively), and not a switching cue because an AiDE does not necessarily indicate a need to switch response or strategy. In our everyday life, these two types of information – FB and AiDE – will frequently occur concurrently, and a critical and difficult part of adapting appropriately involves resolving the difference between these two. Where it gets more complicated is that the dynamics of accumulating evidence when facing a FB vs. an AiDE are very different. FB has a direct temporal and causal link to an executed action; we are thus certain to derive information about a given action from a given FB. *A contrario*, an AiDE has no such contiguity and no initial relation to our actions meaning that we must accumulate evidence to identify the appropriate adaptation to an AiDE. So, the crucial dilemma is this: after an undesirable outcome, should we adapt as if we had made a mistake and received a negative FB, or should we continue to accumulate evidence as if there had been an AiDE that we need to understand and learn to adapt to? Primates in general and humans in particular are able to resolve this credit assignment problem, as evidenced by their ability to appropriately adapt their behavior. Yet the neural basis of this process is currently unknown. More specifically, how the learning of the relationships between FB, AiDE, and behavioral adaptation is built in the brain. In order to tackle this issue, I scanned with fMRI a group of 42 human participants while they performed a novel behavioral adaptation task involving both FB and AiDEs. I hypothesized that the dynamic within the AMG-mPFC network would be modulated by the stage of learning (AiDE significance). This constitutes the third chapter of the experimental part of my thesis entitled: “**Chapter III: The Functional interplay of the fronto-amygdala network during behavioral adaptation in humans**” (Giacometti et al., *in preparation*).

Note that I also participated in additional studies aiming at identifying how the medial and lateral frontal cortex evolved in the primate order on the basis of the sulcal and the cytoarchitectonic organization (Amiez, Sallet, Novek, Hadj-Bouziane, Giacometti et al., 2021; Amiez, Sallet, Giacometti et al. 2023, see Appendix Publications section).

In the general discussion of my thesis, I will provide an in-depth summary of my thesis' findings and their implications. In a first chapter, I will discuss about the AMG-mPFC network dynamic functional interactions as support for behavioral adaptation in humans. The comparative aspect between primate species is also further explored in a second chapter to envision how differential organization of the AMG-mPFC network in primates may be encountered for differential behavioral adaptation abilities. Finally, I will highlight future research directions, complemented by preliminary results with a focus on two main subjects. Firstly, I will examine the AMG nuclei whole-brain level functional interactions and investigate their specificities rs-fMRI data-driven clustering method. Secondly, in an effort to understand the causal role of the AMG, I will present future approaches with a special focus on rs-fMRI associated transcranial ultrasound stimulation (TUS) perturbations of the AMG.

EXPERIMENTAL PART



CHAPTER I. FRONTAL CORTICAL FUNCTIONAL CONNECTIVITY IS IMPACTED BY ANAESTHESIA IN MACAQUES

Camille Giacometti^{1}, Audrey Dureux^{*}, Delphine Autran-Clavagnier, Charles R. E. Wilson, Jérôme Sallet, Manon Dirheimer, Emmanuel Procyk, Fadila Hadj-Bouziane and Céline Amiez*

* Camille Giacometti and Audrey Dureux have contributed equally to this work and are co-first authors

** Fadila Hadj-Bouziane and Céline Amiez have contributed equally to this work and are co-last authors

ABSTRACT

A critical aspect of neuroscience is to establish whether and how brain networks evolved across primates. To date, most comparative studies have used resting-state functional magnetic resonance imaging (rs-fMRI) in anaesthetized nonhuman primates and in awake humans. However, anaesthesia strongly affects rs-fMRI signals. The present study investigated the impact of the awareness state (anaesthesia vs. awake) within the same group of macaque monkeys on the rs-fMRI functional connectivity organization of a well- characterized network in the human brain, the cingulo-frontal lateral network. Results in awake macaques show that rostral seeds in the cingulate sulcus exhibited stronger correlation strength with rostral compared to caudal lateral frontal cortical areas, while more caudal seeds displayed stronger correlation strength with caudal compared to anterior lateral frontal cortical areas. Critically, this inverse rostro-caudal functional gradient was abolished under anaesthesia. This study demonstrated a similar functional connectivity (FC) organization of the cingulo-frontal cortical network in awake macaque to that previously uncovered in the human brain pointing toward a preserved FC organization from macaque to human. However, it can only be observed in awake state suggesting that this network is sensitive to anaesthesia and warranting significant caution when comparing FC patterns across species under different states.

Keywords: anaesthesia, awake, frontal cortex, macaque monkey, resting-state fMRI

INTRODUCTION

A critical aspect of neuroscience is to identify whether and how brain networks evolved across primates in order to 1) establish the putative uniqueness of the human brain and 2) to allow an optimal transfer of results obtained in nonhuman primates (NHP) to humans. Most comparative studies in the past decade have used resting-state functional magnetic resonance imaging (rs-fMRI), a noninvasive approach focusing on the assessment of spontaneous low-frequency fluctuations of blood-oxygen-level-dependent (BOLD) signal (<0.1 Hz) at rest (Biswal et al. 1997). This method reveals temporal correlations of activity between brain areas (Biswal et al. 2010) and allows to compare brain anatomo-functional connectivity (FC) organization across primate species (Vincent et al. 2007; Hutchison et al. 2011, 2012, 2013, 2015; Mars et al. 2011, 2013, 2016, 2018; Hutchison and Everling 2012; Sallet et al. 2013; Hadj-Bouziane et al. 2014; Neubert et al. 2015, 2014; Van Essen et al. 2016; Folloni et al. 2019; Yin et al. 2019; Lopez-Persem et al. 2020; Amiez et al. 2021; Barron et al. 2021; Friedrichet al. 2021; Thomas et al. 2021). For example, it has been shown that large-scale resting-state networks (e.g., the default-mode network [DMN]) are topographically and functionally comparable between humans and macaques (Hutchison et al. 2011; Mars et al. 2012). Although these rs-fMRI studies have provided evidence of functional homologies between humans and NHP, a critical issue is that they were performed in anaesthetized macaques and awake humans (Vincent et al. 2007; Hutchison et al. 2012, 2013, 2015; Sallet et al. 2013; Neubert et al. 2014, 2015; Milham et al. 2018; Folloni et al. 2019; Yin et al. 2019; Lopez-Persem et al. 2020; Amiez et al. 2021; Thomas et al. 2021). There is a growing literature showing that anaesthetic drugs alter brain FC patterns both in humans (see for review Alkire and Miller 2005; Hudetz 2012) and NHP (Li et al. 2013; Hutchison et al. 2014; Bartfelda et al. 2015; Lv et al. 2016; Wu et al. 2016; Rao et al. 2017; Uhrig et al. 2018; Hori et al. 2020; Areshenkoff et al. 2021; Signorelli et al. 2021). In the case of isoflurane, one of the most commonly used anaesthetic agents, several major impacts on brain function have been described: 1) a global FC (i.e., correlation of activity between brain regions) breakdown when using a concentration in the inhaled air >1.5%, 2) a decrease of anticorrelations, and 3) a stronger alteration of interhemispheric compared with intrahemispheric FC (Hutchison et al. 2014; Bartfelda et al. 2015; Uhrig et al. 2018; Xu et al. 2018; Hori et al. 2020).

In the present study, we sought to determine the extent to which anaesthesia affects frontal cortical network connectivity. To do so, we identified in the same group of macaque monkeys the impact of the awareness state (anaesthesia vs. awake) on the rs-fMRI FC organization of the cingulo-frontal lateral cortical network (Loh et al. 2018). This network was chosen because 1) it is well characterized in human where it presents a rostro-caudal organization (i.e., the most anterior regions compute the highest levels of cognitive processing and the most caudal regions compute the most basic level of motor processing) (Loh et al. 2018; Petrides, 2005a, 2005b; Koechlin and Summerfield, 2007; Badre and D'Esposito, 2009) and 2) multidimensional studies converge toward a preserved organization from macaque to human. First, its FC organization is also observed in chimpanzees (Amiez et al. 2019, 2021). Second, anatomical studies (e.g., Amiez et al. 2019; Petrides and Pandya 1994) and electrophysiological studies (e.g., Rothé et al. 2011; Quilodran et al. 2008; Stoll et al. 2016) in macaque strongly suggest that the anatomical and functional signatures of the various areas composing this network are similar to those observed in humans.

In awake humans, three cingulate motor zones occupy the cingulate cortex along a rostro-caudal axis: the most rostral one is anterior Rostral Cingulate Zone (RCZa), posterior Rostral Cingulate Zone (RCZp) is observed caudally to RCZa, and finally Caudal Cingulate Zone (CCZ) occupies the most caudal location. RCZa and RCZp/CCZ have been shown to display a linear inverse FC gradient with the lateral prefrontal cortex and motor regions. RCZa displays stronger positive correlations with rostromedial prefrontal areas (e.g., frontopolar cortical area 10, Broca area [BA], dorsolateral prefrontal cortical Areas 46 and 9/46) and weaker ones with the caudal lateral-frontal motor areas (e.g., frontal eye field [FEF], primary tongue, and primary hand motor areas, called M1Face and M1Hand, respectively). Conversely, RCZp and CCZ display the opposite pattern, that is, weaker correlation strength with more rostral lateral-prefrontal areas and stronger correlation strength with more caudal lateral motor frontal areas (Loh et al. 2018). Macaque cingulate motor areas, named rostral Cingulate Motor Area (CMAr), ventral Cingulate Motor Area (CMAv), and dorsal Cingulate Motor Area (CMA_d) have been suggested to be homologous to the human RCZa, RCZp, and CCZ, respectively (Picard and Strick 2001; Amiez and Petrides 2014; Procyk et al. 2016). Furthermore, macaque brains do present homologues of a set of rostromedial frontal areas studied in humans (i.e., area 10, area 46, area 9/46, BA, FEF, M1Face, and M1Hand areas; Petrides and Pandya 1994). Based on these

findings, we tested whether, in macaques, 1) the FC within the cingulo-frontal lateral network would follow a similar rostro-caudal functional gradient to that uncovered in the human brain and 2) this functional organization would be impacted by anaesthesia.

Three *rhesus* macaques underwent rs-fMRI sessions in both anaesthetized and awake states. Results revealed that 1) the inverse functional gradient displayed by rostral cingulate versus caudal cingulate regions with rostrolateral prefrontal regions and caudal lateral motor frontal regions is highly preserved from awake macaques to humans and 2) it is abolished in anaesthetized state compared with awake state in macaques.

MATERIALS AND METHODS

Macaque Monkey Subjects

For this study, we included three monkeys: two females (Monkeys C, 21 years old and N, 9.5 years old) and one male (Monkey L, 9.5 years old) *rhesus* monkeys (*Macaca mulatta*, 5–8 kg). Animals were maintained on a water and food regulation schedule, individually tailored to maintain a stable level of performance for each monkey. All procedures follow the guidelines of European Community on animal care (European Community Council, Directive No.86–609, November 24, 1986) and were approved by French Animal Experimentation Ethics Committee #42 (CELYNE).

Surgical Procedure

Macaque monkeys were surgically implanted with a PEEK MR-compatible head post (Rogue Research). The surgical procedure was conducted under aseptic conditions. Animals were sedated prior to intubation and they were maintained under gas anaesthesia with a mixture of O₂ and air (isoflurane 1–2%). After an incision of the skin along the skull midline, the head fixation device was positioned under stereotaxic guidance on the skull and maintain in place using ceramic sterile screws (Thomas RECORDING products) and acrylic dental cement (Palacos® Bone cements, Heraeus company). Throughout the surgery, heart rate, respiration rate, blood pressure, expired CO₂, and body temperature were continuously monitored. At the completion of the surgery, the wound was closed in anatomical layers. Analgesic and antibiotic treatment were administered for 5 days postoperatively and monkeys recovered for at least 1 month.

Awake-State Experimental Setup

Beginning at ~4 weeks after the surgery, the monkeys were acclimatized to the head-fixation system and the MRI environment. In an effort to compare human and monkey rs-fMRI data, the monkeys were engaged in a similar protocol that the one used in humans in [Loh et al. \(2018\)](#), that is, performing ocular fixation. The difference was indeed the motivation used: liquid reward throughout the runs for monkeys, and monetary rewards at the end of the fMRI session for human subjects. Specifically, monkeys were trained to sit in a sphinx position in an MRI compatible plastic chair (Rogue Research) with their heads fixed, in a mock scanner mimicking the actual MRI environment. During the training, each animal was habituated to view a central cross presented on a screen in front of them. During the scanning sessions, monkeys sat in a sphinx position in the plastic chair positioned within a horizontal magnet (3-T MR scanner; Siemens Healthcare). Monkeys faced a translucent screen placed 57 cm from their eyes and a white cross ($4^\circ \times 4^\circ$) was presented in the center of a black background on the screen at eye level, aligned with their sagittal axis. Eye position was monitored at 1000 Hz during scanning using an eye-tracking system (Eyelink 1000 Plus Long Range, SR research). The horizontal (X) and vertical (Y) eye positions from the right eye of each monkey were recorded for each run and each monkey (12 runs for Monkeys C and N and 8 runs for Monkey L as eye movements from 4 runs were not recorded due to technical issues). The calibration procedure involved the central cross and 4 additional crosses (5 degrees of eccentricity), placed in the same plane as the fixation cross. Each point appeared sequentially on the screen and the monkeys were rewarded for orienting and maintaining their gaze toward the cross. The task and all behavioral parameters were controlled by the Presentation[®] program (Neurobehavioral System). Visual stimulations were projected onto the screen with a projector (CHRISTIE LX501).

Monkeys were rewarded with liquid dispensed by a computer-controlled reward delivery system (Crist[®]) through a plastic tube placed in their mouth. They were rewarded when their eye gaze was within a 4° window around the cross. In the reward schedule and to promote long period of fixation, the frequency of reward delivery increased as the duration of fixation increased ([Hadj-Bouziane et al. 2012](#)). For each run, we computed the percentage of time the animals spent with their eyes open or fixating. The mean time with eyes open across runs was, respectively, 69%, 69%, and 84% for Monkeys L, N, and C. Within this time, the percentage of fixation

varied from 36% to 69%, 2% to 58%, and 5% to 98% for Monkeys L, N, and C, respectively.

Rs-fMRI Images Acquisition

Table 1 provides an overview of the protocols and scanning parameters under both states, namely, awake and anaesthetized (and was generated using BioRender, see BioRender.com). The data from both states were acquired from the same scanner, in a 3T Siemens Magnetom Prisma MRI scanner (Siemens Healthcare). Due to the specific constraints in the anaesthetized (stereotaxic frame) and awake (MRI chair) states, we could not use the same coil systems in the two conditions.

Anaesthetized State.

Prior to anaesthesia, monkeys were injected with glycopyrrolate, an anticholinergic agent that decreases salivary secretion (Robinul; 0.06 mg/kg). Twenty minutes after, anaesthesia was induced with an intramuscular injection of tiletamine and zolazepam (Zoletil; 7 mg/kg). The animals were then intubated and ventilated with oxygen enriched air and 1% Isoflurane (for Monkeys N and L) or 1.5% Isoflurane (for Monkey C) through- out the duration of the scan. The isoflurane was set at 1.5% for Monkey C because this monkey presented a lower sensitivity to isoflurane. Note that the critical point of isoflurane when the FC is really impacted is >1.5% (Hutchinson et al. 2014). An MRI-compatible stereotaxic frame (Kopf) was used to secure the head and reduce variability in the measure. Monkeys were placed in a sphinx position with their head facing the back of the scanner. Breathing volume and frequency were set based on the animal weight. During the scan, physiological parameters including heart rate and ventilation parameters (spO₂ and CO₂) were monitored. Body temperature was also measured and maintained using warm- air circulating blankets. The anaesthetized resting-state acquisitions were performed about 2 h after anaesthesia induction and at least 1 h after first inhalation of isoflurane. Three received loop coils were used for the acquisition: 2 L11 Siemens ring coils were placed on each side of the monkey's head and 1 L7 Siemens above the monkey's head. A high-resolution T_1 -weighted anatomical scan was first acquired for each of the three monkeys MPRAGE, 0.5-mm³ isotropic voxels, 144 slices, TR (Repetition Time) = 3000 ms, TE (Echo Time)= 366 ms). Resting- state functional images were obtained in an ascending order with a T_2^* -weighted gradient echo planar images (EPI) sequence with the following parameters: for Mon- keys L and N, TR = 1700 ms, TE = 30 ms, flip angle = 75°, FOV = 400 × 300

mm, 25 slices, voxel size: 1.7 mm^3 and for Monkey C, TR = 2000 ms, TE = 30 ms, flip angle = 75° , FOV = 480×336 , 31 slices, voxel size: 1.8 mm^3 . We collected six runs for Monkeys L and C and five runs for Monkey N due to technical problems during the acquisition (Monkey N started to awaken in the sixth run). Note that Monkey C has slightly different rs-fMRI parameters because this monkey presented a bigger head and we wanted to preserve a whole brain acquisition. We obtained 400 volumes per run (12 min each) for a total of 6800 volumes across the 3 animals. The different runs were acquired during the same session for each animal.

Awake State

Data were acquired using a custom-made eight channel receive surface coil positioned around the head, and a circular transmit coil positioned above the head (Mareyam et al. 2011). Functional images were acquired in an ascending order with a total of 12 runs of 12 min per monkey (400 volumes/run, corresponding to a total of 4800 volumes per monkey) across different scan sessions. We used a BOLD-sensitive T_2^* -weighted echo planar sequence with the following parameters: TR = 1800 ms, TE = 27 ms, flip angle = 75° , FOV = 480×336 mm, voxel size = 1.8 mm isotropic, 30 slices. Throughout the scan duration, macaques were either fixating the central cross presented on the screen or eyes opened for the duration of the run. Each functional imaging acquisition was preceded by a T_1 -weighted low-resolution anatomical scan with a MPRAGE sequence (TR = 2500 ms, TE = 2.44 ms, flip angle = 8° , FOV = 128×128 mm, voxel size = 0.9 mm isotropic, 64 volumes).

Table 1. Overview of the experimental design

Species	Conditions	fMRI	Coils	Parameters	Run
3 Rhesus macaques: C, L, and N	Anaesthetized 1–1.5% isoflurane	3T	3 loops receive coils: Siemens ring coils (L11x2 and L7)	TR = 1.7–2 s, voxel = $1.7\text{--}1.8 \text{ mm}^3$, 400 vol/run	6 runs
	Awake		8 loops received coil 1 transmit loop	TR = 1.8 s, voxel = 1.8 mm^3 , 400 vol/run	12 runs

rs-fMRI Images Preprocessing

The preprocessing of resting-state scans was then performed with SPM 12. The first five volumes of each run were removed to allow for T_1 equilibrium effects. First, we

performed a slice timing correction using the time center of the volume as reference. The head motion correction was then applied using rigid body realignment. Then, images were skull-stripped using the best tool from the FSL software (Jenkinson et al. 2005, <https://fsl.fmrib.ox.ac.uk/fsl/fslwiki/BET>). Using the Analysis of Functional NeuroImage (AFNI) software (Cox 1996), the segmentation of each brain of each session (anaesthetized and awake sessions) was performed on skull-stripped brains. To ensure optimized intersession and inter subject comparisons, both anatomical and functional images were then registered in a common atlas space, CHARM/SARM (Seidlitz et al. 2018; Jung et al. 2021 https://afni.nimh.nih.gov/pub/dist/doc/html/doc/nonhuman/macaque_template/atlas_charm.html). Temporal filtering was then applied to extract the spontaneous slowly fluctuating brain activity (0.01–0.1 Hz). Finally, linear regression was used to remove the following nuisance variables: the cerebrospinal fluid, white matter signals from the segmentation, and volumes containing artifacts as detected by the ART toolbox (https://www.nitrc.org/projects/artifact_detect/). A global signal regression was not used because it has been shown that this approach might introduce bias in functional connectivity analysis (Saad et al. 2012, Power et al. 2017). Finally, a spatial smoothing with a 4-mm full width at half maximum (FWHM) Gaussian kernel was applied to the output of the regression. Note this latter smoothing was chosen in an effort to optimize the comparison between macaque and human. Indeed, in our reference paper in human (Loh et al. 2018), we used a 6-mm FWHM Gaussian kernel, which represents ~ 2 * the voxel size resolution of the EPI images (i.e., 2.7-mm^3 isotropic). In macaque, our voxel size being 1.8 mm^3 (awake state) and 1.6 mm^3 (anaesthetized state) isotropic; we therefore used also ~ 2 * the voxel size resolution of the EPI images, that is, a 4-mm FWHM Gaussian kernel. Importantly, in both states, we chose not to concatenate the runs and rather to average FC data across runs by using a similar rs-fMRI acquisition procedure in awake and anaesthetized conditions. The reason was 2-fold: 1) concatenate runs in awake macaques is hardly feasible given the fact that data are acquired on multiple days and 2) given the reliability to assess FC provided with runs lasting more than at least 6 min (Birn et al. 2013).

Seeds and Regions of Interest Selection

Seeds Selection in the MCC

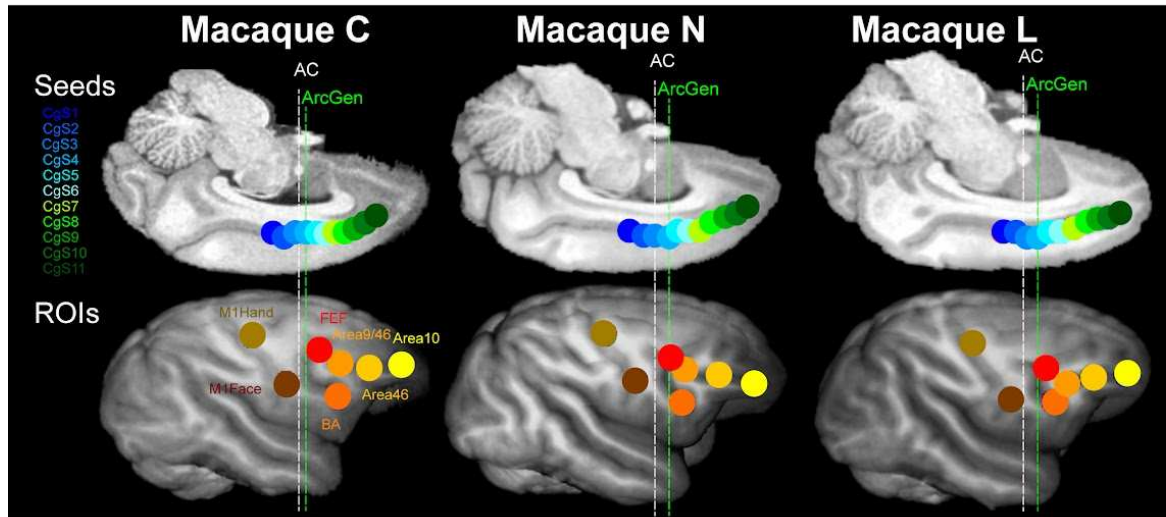
The seeds consisted of 2.5-mm radius spheres positioned in the cingulate sulcus (covering both ventral and dorsal banks of the cingulate sulcus) in both hemispheres, starting 10 mm posterior to the anterior commissure (AC) to the rostral end of the cingulate sulcus, and spaced from 2.5 mm each, for a total of 11 seeds (CgS1, CgS2, CgS3, CgS4, CgS5, CgS6, CgS7, CgS8, CgS9, CgS10, and CgS11, see [Fig. 1](#) for the positioning of seeds in the right hemisphere and [Fig. 2](#) for the left hemisphere). We used overlapping seeds to capture the correlation pattern of both banks of the cingulate sulcus along the rostro-caudal axis in order to improve the identification of the location of the various CMA as they are not precisely described in the literature. Given that, in macaques, CMAr is located about 10 mm anterior to the genu of the arcuate, we anticipated that this subdivision would roughly correspond to CgS8 ([Procyk et al. 2016](#)). Caudal seeds CgS1– CgS7 correspond to Y values –5 to +10 (with AC at Y0), whereas CgS8–CgS11 correspond to Y values +12.5 to +20. As it can be appreciated in [Figures 1 and 2](#), the genu of the arcuate sulcus (ArcGen) is at the level of CgS4 (i.e., at Y = +2.5). According to our previous metaanalysis aiming at identifying the location of the rostral cingulate motor area (CMAr) in macaques ([Procyk et al. 2016](#)), the face motor area CMAr is located about 10 mm anterior to ArcGen.

Regions of Interest Selection

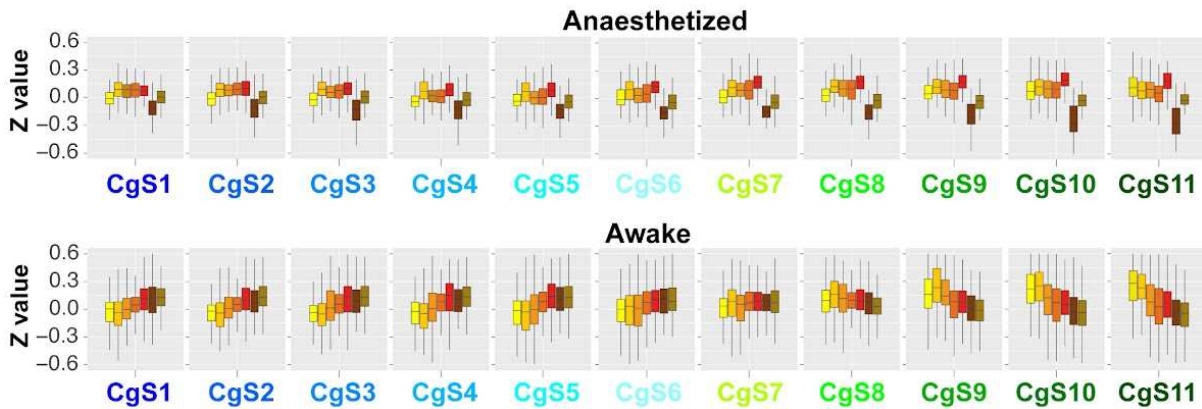
For a stricter comparison of the present results with results obtained in our previous studies which assessed the FC of the cingulate sulcus in the human ([Loh et al. 2018](#)) and in the chimpanzee ([Amiez et al. 2021](#)), we used the same regions of interest (ROIs) (see [Fig. 1](#) for the positioning of ROIs in the right hemisphere and [Fig. 2](#) for the left hemisphere). Each ROI consisted of a sphere with a 2.5-mm radius.

ROIs Selection in Motor Cortical Areas. For each subject, three ROIs within the motor cortex of both hemispheres were identified based on sulcal morphology. These included the hand motor region— M1Hand—and the primary face motor region within the ventral part of the posterior part of the precentral gyrus—M1Face ([He et al. 1993](#); [Luppino and Rizzolatti 2000](#); [Graziano et al. 2002](#)). We also included the FEF, located in the rostral bank of the arcuate sulcus, at the level of the ArcGen ([Bruce et al. 1985](#); [Amiez and Petrides 2009](#)).

A. Right hemisphere: Seeds and ROIs in all macaques



B. Connectivity between each seed and ROIs



C. Linear Trend of connectivity of each seed with all ROIs

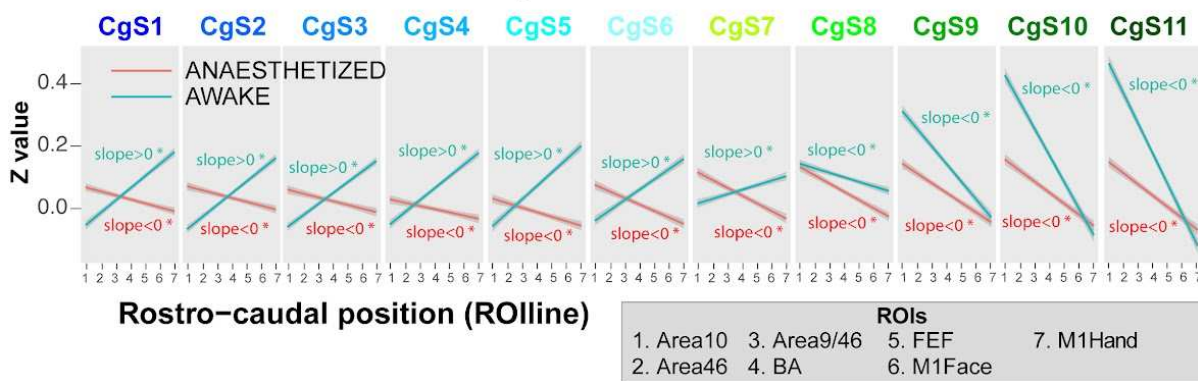


Figure 1. Anaesthesia altered the functional gradient inversion between cingulate regions and lateral prefrontal and motor regions in the right hemisphere. (A) Position of the seeds and ROIs for the three macaques in the right hemisphere. Top part represents the 11 seeds along the cingulate sulcus in an inverse midsagittal section and the bottom part the 7 ROIs in the lateral surface of the brain. The color conventions are maintained through the rest of the figure. (B) Boxplots represent the FC between each of the 11 seeds, more caudal in blue to more rostral in green, and the ROIs. At the top is the anaesthetized condition and at the bottom is the awake condition. In the anaesthetized state, seeds CgS1–CgS11 show stronger connectivity with rostral lateral prefrontal seeds and weaker connectivity with posterior frontal motor ROIs, whereas in the awake state, there is a gradient

*inversion at CgS7/CgS8 level where caudal seeds CgS8–CgS11 are stronger connected to caudal frontal motor regions and weaker with rostral lateral prefrontal regions. (C) Linear trend of connectivity between each seed and ROline in both conditions (ROIs ranked based on their rostro-caudal position). Error bars represent the 95% confidence level interval. No inversion gradient in the anaesthetized state compared with the awake state at the CgS7 and CgS8 transition (GLMM: STATE effect: $F = 12.469$, $P < 0.0004142$, SEED effect: $F = 380.666$, $P < 2.2e-16$; ROline effect: $F = 410.959$, $P < 2.2e-16$, and effect of STATE*SEED*ROLine interactions $df = 10$, $F = 157.147$, $P < 2.2e-16$).*

ROIs Selection in the Prefrontal Cortex. For each subject, four ROI locations within the left prefrontal cortex were identified based on local anatomy. On a rostro-caudal axis:

- 1) The frontopolar cortex—Area 10: It occupies the rostral part of the principalis sulcus (Petrides and Pandya 1994).
- 2) Areas 46 and 9/46 of the dorsolateral prefrontal cortex—DLPFC: Area 9/46 occupies the caudal part of the sulcus principalis, and Area 46 occupies the sulcus principalis between Area 9/46 and Area 10 (Petrides and Pandya 1994).
- 3) Broca's region: Area 44 has been shown to occupy the fundus of the ventral part of the arcuate sulcus (Petrides et al. 2005a).

More details about the coordinate of both ROIs and seeds are displayed in tables for each monkey in the supplementary materials ([Supplemental Table 2](#)).

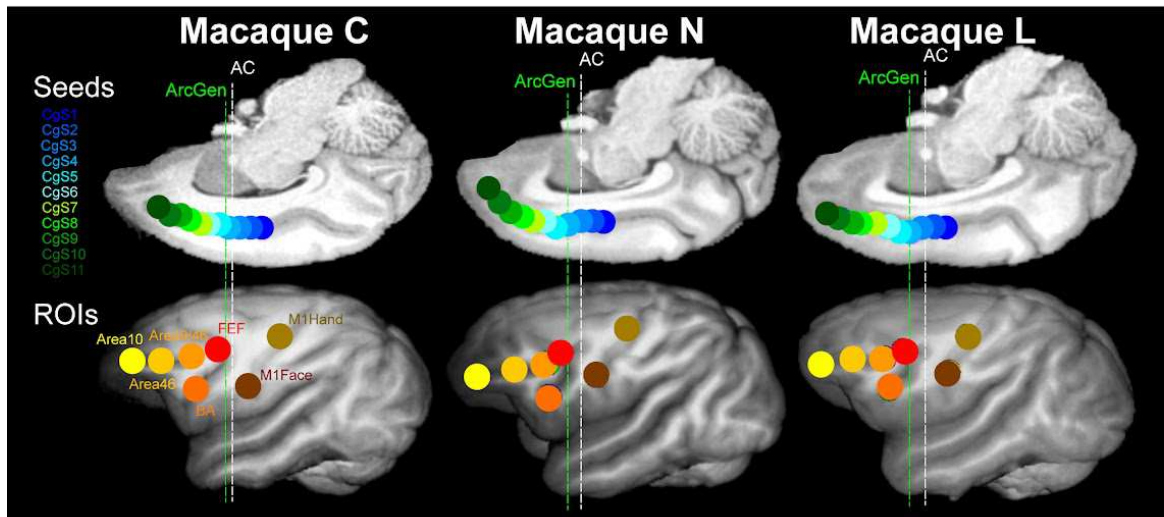
Correlations between Seeds and ROIs

For each hemisphere of each animal, Pearson correlation coefficients between the seeds with the various ROIs in the prefrontal cortex and the motor cortex were computed and normalized using the Fisher's r -to- Z transform formula. The significant threshold at the individual subject level was set to $Z = 0.1$ ($P < 0.05$). These normalized correlation coefficients, which corresponded to the FC strength between each seed and each ROI in individual brains, were subsequently processed with R software for all the following analyses. Note that our small sample size ($n = 3$) prevented us to address the effect of lateralization within this network.

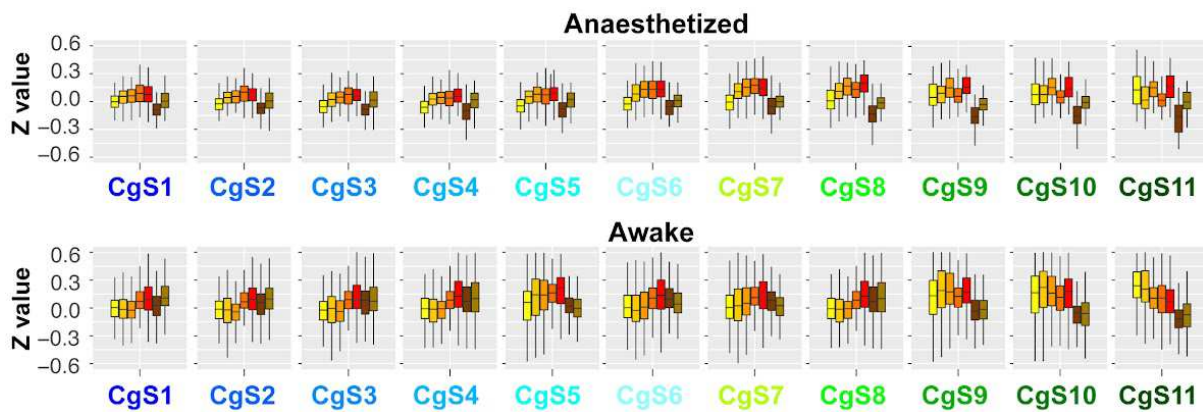
To identify the impact of the state (awake or anaesthetized) on the connectivity profile of each seed with the various lateral frontal ROIs, we constructed boxplots representing the correlation strength of each seed location with each of the ROIs in each state and in each hemisphere. As carried out previously in humans (Loh et al. 2018), we then characterized, in both states, the rostro-caudal functional axis based on the correlation profiles of each seed with the lateral frontal cortex by estimating

linear trends in their correlation strength (for details, see Methods in Loh et al. 2018). The seven ROIs were first ranked along a rostro-caudal axis based on their averaged Y coordinate values across macaque brains and recoded into a numeric axis variable (ROLine): 1) Area 10 (most anterior), 2) Area 46, 3) Area 9/46, 4) Area 44, 5) FEF, 6) M1Face, and 7) M1Hand (most posterior).

A. Left hemisphere: Seeds and ROIs in all macaques



B. Connectivity between each seed and ROIs



C. Linear Trend of connectivity of each seed with all ROIs

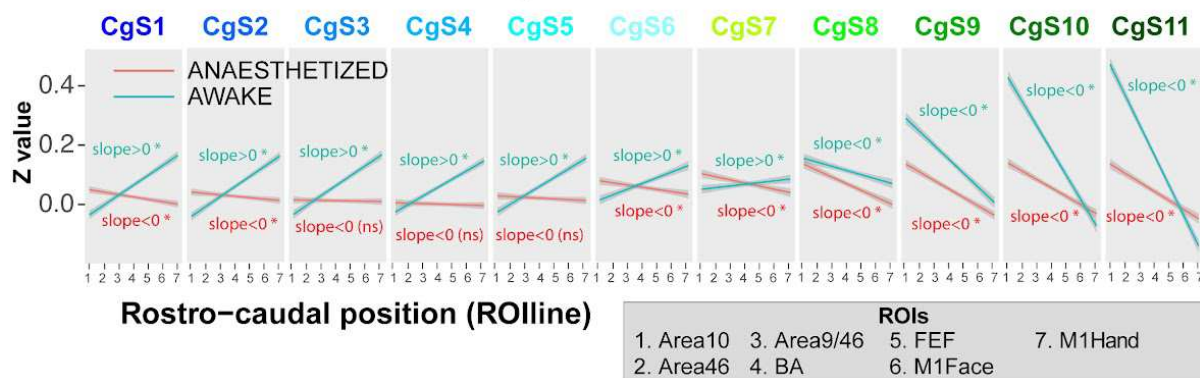


Figure 2. Anaesthesia altered the functional gradient inversion between cingulate regions and lateral prefrontal and motor regions in the left hemisphere. (A) Position of the seeds and ROIs for the three macaques in the left hemisphere. Top part represents the 11 seeds along the cingulate sulcus in an inverse midsagittal section and the bottom part the 7 ROIs in the lateral surface of the brain. (B) Boxplots represent the FC between each of the 11 seeds, more caudal in blue to more rostral in green, and the ROIs. At the top is the anaesthetized condition and at the bottom is the awake condition. In the anaesthetized state, seeds CgS1–CgS11 show stronger connectivity with rostral lateral prefrontal seeds and weaker connectivity with posterior frontal motor ROIs, whereas in the awake state, there is gradient inversion at CgS7/CgS8 level where caudal seeds CgS8–CgS11 are stronger connected to caudal frontal motor regions and weaker with rostral lateral prefrontal regions. (C) Linear trend of connectivity strength between each seed and ROIline (ROIs ranked based on their rostral-to-caudal position) in both conditions. Error bars represent the 95% confidence level interval. No inversion gradient in the anaesthetized state compared with the awake state at the CgS7 and CgS8 transition (GLMM: STATE effect: $F = 28.84$, $P < 7.901e-08$; SEED effect: $F = 330.973$, $P < 2.2e-16$; ROIline effect: $F = 294.497$, $P < 2.2e-16$, and effect of STATE-SEED-ROIline interactions $df = 10$, $F = 112.782$, $P < 2.2e-16$).

We then performed multiple linear regressions on the correlation Z values with seed identity (CgS1–CgS11), state (awake or under anaesthesia), and the linear axis variable (ROIline) as predictors for each hemisphere separately or considering hemisphere as an additional factor. We assessed whether the linear trends (slopes) observed for each seed were identical or not in each sulcal morphology using generalized linear mixed models—GLMM—with ROI identity (Area 10, etc.), state (anaesthetized/awake), and the linear axis variable (ROIline, values 1–7) as fixed effect and the macaque identity and run identity as random intercept factors, followed by post hoc Tukey comparisons (performed with lsmeans package, <https://cran.r-project.org/web/packages/lsmeans/lsmeans.pdf>). We also assessed the correlation Z values between each ROI and all seeds separately for each hemisphere using a GLMM with seed identity (CgS1–CgS11) and state (awake or under anaesthesia) as fixed effect and the macaque identity as random factor followed by post hoc Tukey comparisons.

Correlations within the Frontal Cortex and Hierarchical Clustering

To assess the impact of anaesthesia on the overall functioning of the network composed by the various seeds and ROIs, in each hemisphere, we averaged the normalized correlation coefficients for each seed–seed, seed–ROI, and ROI–ROI pairing across runs and macaques. Correlation heatmaps were then generated in both states, anaesthetized and awake. Note that autocorrelations were not considered in the statistical analysis. Then, unsupervised hierarchical clustering was performed for the 11 seeds within the cingulate sulcus and the 7 ROIs within the

lateral frontal cortex (method described in [Loh et al. 2018](#)). To summarize, this clustering method defines the cluster distance between two clusters to be the maximum distance between their individual components (using the `hclust` function in R, see <http://www.r-tutor.com/gpu-computing/clusteri ng/hierarchical-cluster-analysis>). At every stage of the clustering process, the two nearest clusters are merged into a new cluster. The process is repeated until the whole data set is agglomerated into one single cluster. The outcome was used to construct dendrograms and heatmaps. To better display clusters across ROIs, values in the heatmaps were normalized (Z-scored) by column. Therefore, values (and sign) in the heatmap do not represent actual connectivity measures.

Quality Check of rs-fMRI Signal: Motion Estimation and Temporal Signal-to-Noise Ratio

Temporal Signal-to-Noise Ratio. The mean signal from seeds and ROIs was extracted using the AFNI software. For each run and each monkey, we computed the temporal signal-to-noise ratio (tSNR— average intensity of time series divided by the standard deviation) across the brain, in each seed and in each ROI, in both states, anaesthetized and awake. The tSNR within the whole brain, within each seed and each ROI in awake versus anaesthetized state was compared using GLMM for each hemisphere separately (package `lme4`, R statistical software: <https://www.r-project.org/>) with the anaesthetized/awake state as fixed effect and the macaque identity as a random factor.

Estimated Brain Movements. For each session, we also computed the six temporal derivatives of the estimated brain movements (three translations and three rotations) in each session of all monkeys ([Power et al. 2012](#)). These temporal derivatives in awake versus anaesthetized state were compared using GLMM (package `lme4`, R statistical software: <https://www.r-project.org/>) with the anaesthetized/awake state as fixed effect and the macaque identity as a random factor.

RESULTS

We compared the FC pattern within the cingulo-frontal lateral network of three *rhesus* macaques under two states, awake and anaesthetized, using rs-fMRI. As summarized in [Table 1](#), for each animal, we acquired six runs under anaesthesia (1–1.5% isoflurane) and 12 runs while the animals were awake. Each run comprised of 400

volumes (see [Materials and Methods](#)). We assessed FC (Pearson correlation strengths) between 11 seeds located along the cingulate sulcus and 7 ROIs along a rostro-caudal axis in the lateral frontal cortex. Seeds were positioned in an anteroposterior extent that would fairly encompass all cingulate motor areas. ROIs were selected based on the known homologies between humans and macaques ([Petrides and Pandya 1994](#)).

Anaesthesia Impacts the Correlation Strength between Cingulate Seeds and Lateral Frontal ROIs

For each hemisphere of each animal and in each state, we computed the correlation coefficients between the mean signal of cingulate seeds and ROIs in the prefrontal cortex and the motor cortex ([Figs 1A and 2A](#)). In [Figures 1B and 2B](#), the results are displayed on boxplots with each seed represented on the horizontal axis and correlation strength (Z value) on the vertical axis. In [Figures 1C and 2C](#), the plots represent the correlation strength linear trend between each seed and ROIs numbered and ranked from 1 to 7 based on their rostro-to-caudal position (renamed ROline). The ranking was based on their averaged Y coordinate values across macaque brains and recoded into a numeric axis variable (ROline): 1) Area 10 (mean Y value across both hemispheres of the 3 macaques = 42, most anterior); 2) Area 46 (mean Y value = 35); 3) Area 9/46 (mean Y value = 28.3); 4) Area 44 (mean Y value = 27.5); 5) FEF (mean Y value = 24.2); 6) M1Face (mean Y value = 16.5); and 7) M1Hand (mean Y value = 9.2, most posterior). Statistical analysis show that Z values were higher in the awake versus anaesthetized runs (main effects of STATE in the left hemisphere: $F = 28.53$, $P < 9.274e-08$; in the right hemisphere: $F = 14.182$, $P < 0.0002$). In both the right ([Fig. 1](#)) and the left hemispheres ([Fig. 2](#)), the interaction among the STATE (anaesthetized/awake), the SEED identity (CgS1–CgS11), and the ROline (1–7) was statistically significant (left hemisphere: $df = 10$, $F = 112.683$, $P < 2.2e-16$; right hemisphere: $df = 10$, $F = 155.259$, $P < 2.2e-16$, GLMM with three factors [ROline, SEED, STATE] and one random factor [Macaque ID]). Note that we observed a main effect of SEED and of ROline, both in the left (SEED effect: $F = 330.681$, $P < 2.2e-16$; ROline effect: $F = 294.134$, $P < 2.2e-16$) and the right hemispheres (SEED effect: $F = 376.094$, $P < 2.2e-16$; ROline effect: $F = 405.607$, $P < 2.2e-16$). When considering hemispheres as an additional factor, the results show a significant interaction between STATE (anaesthetized, awake), SEED

(CgS1–CgS11), ROline (1–8), and HEMISPHERE (left/right) (GLMM, fixed effects = hemisphere, seeds, ROline, and state, random effect = macaque ID, $F = 3.88$, $P < 2.757e-05$). However, given the small sample size and the lack of a priori hypothesis regarding lateralization, we refrain from discussing further this result.

In the awake state, results show that, in both hemispheres, caudal cingulate seeds CgS1–CgS7 display stronger connectivity strength with caudal frontal motor ROIs and weaker connectivity strength with rostral prefrontal cortical seeds. Conversely, the rostral cingulate seeds CgS8–CgS11 display stronger connectivity strength with rostral lateral prefrontal cortical seeds and weaker connectivity strength with caudal frontal motor ROIs. This gradient inversion at the CgS7/CgS8 transition can be visually appreciated in both hemispheres on the boxplots of [Figures 1B](#) and [2B](#) and the slopes of the linear trends in the correlation strength for each cingulate seed with the rostro-caudal lateral frontal ROIs ([Figs 1C](#) and [2C](#), see also [Supplemental Table 1](#) which displays the values of the slopes and corresponding P -values for each seed). In contrast, in the anaesthetized state, in both hemispheres, all cingulate seeds CgS1–CgS11, regardless of their position, display stronger correlation strength with rostral lateral prefrontal cortical seeds and weaker correlation strength with caudal frontal motor ROIs (see Boxplots in [Figs 1B](#) and [2B](#) and the linear trend of connectivity between each seed and the set of ROIs in [Figs 1C](#) and [2C](#)). Contrasting with the awake condition, there was no apparent gradient inversion along the axis in the anaesthetized condition.

To better identify the impact of the state (anaesthetized/awake) on the connectivity between each ROIs and all seeds, we performed GLMM with two fixed factors (SEED, STATE) and one random factor (Macaque ID). The interaction between STATE and SEED was significant for all ROIs in both the right and left hemispheres (RIGHT: Area 10: $df = 10$, $F = 49.54$, $P < 2.2e-16$; Area 46: $df = 10$, $F = 110.11$, $P < 2.2e-16$; Area 9/46: $df = 10$, $F = 9.6$, $P < 5.044e-16$; BA: $df = 10$, $F = 7.26$, $P < 1.6e-11$; FEF: $df = 10$, $F = 14.27$, $P < 2.2e-16$; M1Face: $df = 10$, $F = 2.96$, $P < 0.001$; M1Hand: $df = 10$, $F = 39.724$, $P < 2.2e-16$; LEFT: Area 10: $df = 10$, $F = 21.15$, $P < 2.2e-16$; Area 46: $df = 10$, $F = 74.02$, $P < 2.2e-16$; Area 9/46: $df = 10$, $F = 30.53$, $P < 2e-16$; BA: $df = 10$, $F = 6.2$, $P < 1.713e-09$; FEF: $df = 10$, $F = 5.13$, $P < 1.66e-07$; M1Face: $df = 10$, $F = 8.11$, $P < 0.78e-13$; and M1Hand: $df = 10$, $F = 30.011$, $P < 2.2e-16$). Post hoc Tukey comparisons revealed that the increased correlation

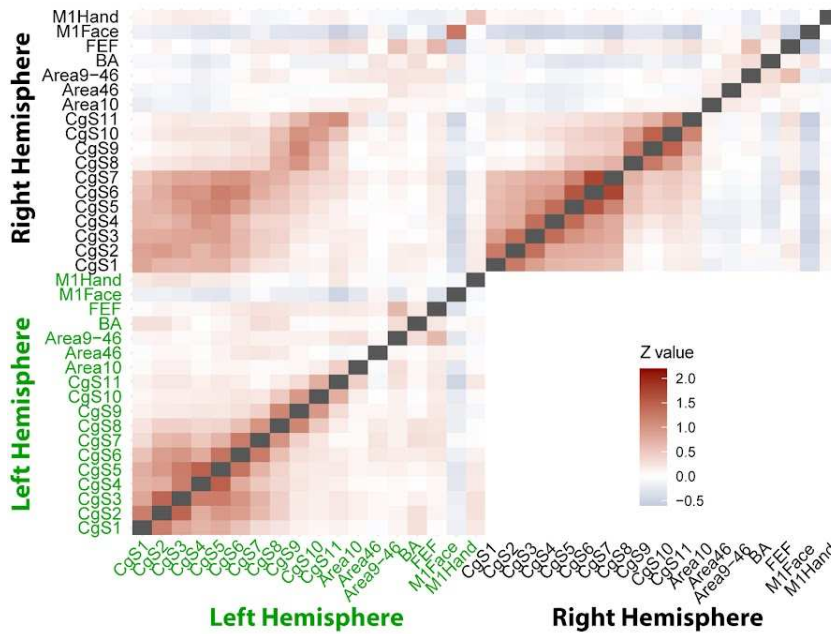
strength between the most caudal cingulate seeds and the motor cortical areas M1Face and M1Hand, and between the most rostral cingulate seeds and the lateral prefrontal cortical Areas 10, 46, and 9/46, were only present in awake condition, in both hemispheres (left hemisphere: [Supplemental Fig. 4](#), right hemisphere: [Supplemental Fig. 5](#)). These results suggest that the rostro-to-caudal inversion of gradient was present only in the awake state. The inversion of gradient occurred on average, across the three macaques, at the CgS7/CgS8 transition (i.e., at 10 mm anterior to the AC and on average at 9 mm anterior to the ArcGen). Note that, despite a small variability across monkeys and runs, results show that the gradient of FC is reversed from caudal to rostral seeds in awake state but not in anaesthetized macaques in each run (see Supplemental Fig. 7). Note also that the analysis of each monkey individually reveals that the transition was observed at slightly different levels in the two hemispheres: Macaque C displays the inversion of gradient at the CgS7/CgS8 transition (at 12.5 mm from AC and 10.5 mm from the ArcGen) in both hemispheres ([Supplemental Fig. 1](#)). Macaque N displays this inversion at the CgS7/CgS8 transition in the left hemisphere (at 12.5 mm from AC and 7.5 mm from ArcGen) and at the CgS8/CgS9 transition (at 15 mm from AC and 10 mm from ArcGen) in the right hemisphere ([Supplemental Fig. 2](#)). Macaque L displays this inversion at the CgS5/CgS6 transition (at 7.5 mm from AC and 3.5 mm from ArcGen) in the left hemisphere and at the CgS6/CgS7 transition (at 10 mm from AC and 6 mm from ArcGen) in the right hemisphere ([Supplemental Fig. 3](#)). As such, the inversion of the gradient occurs in a cingulate zone ranging from $Y = 3.5$ to $Y = 10.5$ mm from ArcGen.

Anaesthesia Impacts the Network Connectivity Pattern between Cingulate Seeds and Lateral Frontal ROIs

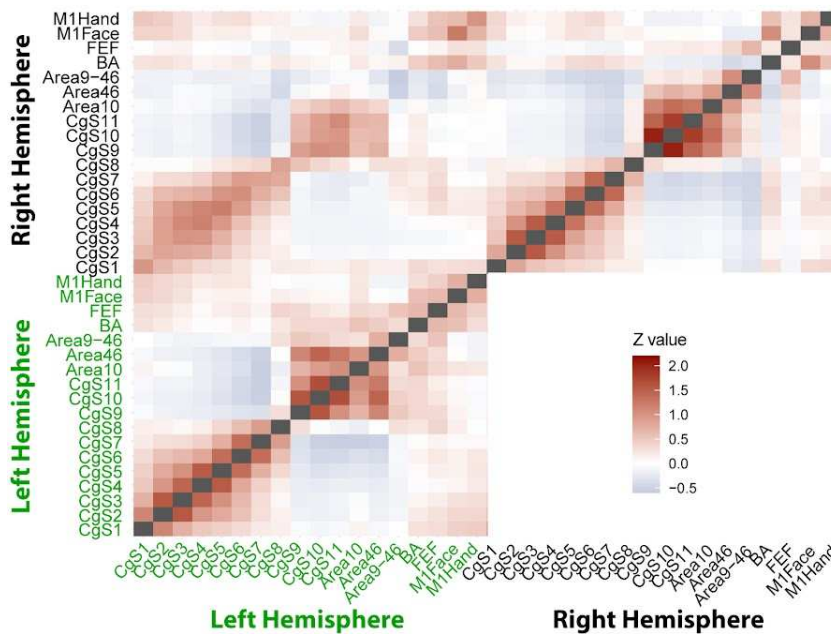
To identify the effect of the state (anaesthesia/awake) across the mediolateral frontal networks, we computed a correlation matrix between all regions defined as seeds and ROIs (i.e., SEED-ROI Z correlations; SEED- SEED Z correlations and ROI-ROI Z correlations; see [Materials and Methods](#), part Statistical Analysis, Correlations within the Frontal Cortex and Hierarchical Clustering). The correlation heatmaps are displayed in [Figures 3A,B](#) for the anaesthetized and awake states, respectively. Visual inspection of the heatmaps suggests that the pattern of connectivity observed unilaterally is similar to that observed bilaterally and that negative and positive

correlations are not distributed in a similar fashion in anaesthetized and awake states. We further analyzed the distribution of the correlation coefficients (Z values, positive or negative) within these heatmaps. First, results revealed that the distribution of the Z values was narrower and the peak of distribution was shifted toward positive values in anaesthetized state compared with awake state (peaks at -0.07 and 0.12 in awake and anaesthetized states, respectively, see also histogram of Z values density in anaesthetized vs. awake states, [Fig. 3C](#)). In other words, there were more negative correlations in the awake compared with the anaesthetized state (37.5% vs. 21.3%, respectively, $\chi^2 = 27.57$, $P < 1.5e-7$, proportion test) and conversely more positive correlations in the anaesthetized compared with the awake state (78.7% vs. 62.5%, respectively, $\chi^2 = 11.703$, $P < 6.2e-4$, proportion test, [Fig. 3D](#)). Second, we found an interaction between the state (anaesthetized/awake) and the sign of the correlation values (positive/negative) on Z values ($df = 1$, $F = 9.96$, $P < 0.002$, GLM, fixed effect = Z value valence and STATE, [Fig. 3E](#)). Although the mean negative Z values across these networks were not impacted by the state (estimate = -0.005 , $P = 0.75$, post hoc Tukey), positive Z values were higher in the awake than in the anaesthetized state (estimate = 0.055 , $P < 0.0001$, post hoc Tukey).

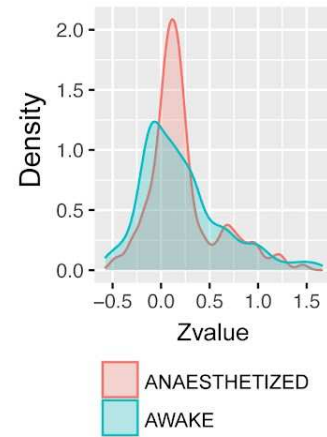
A. Heatmap - Anaesthetized state



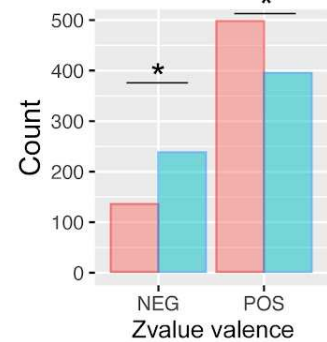
B. Heatmap - Awake state



C.



D.



E.

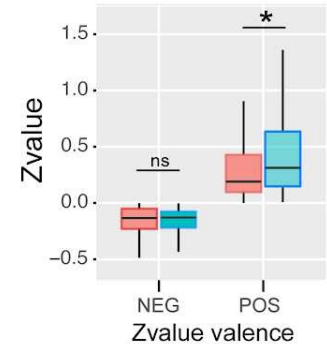


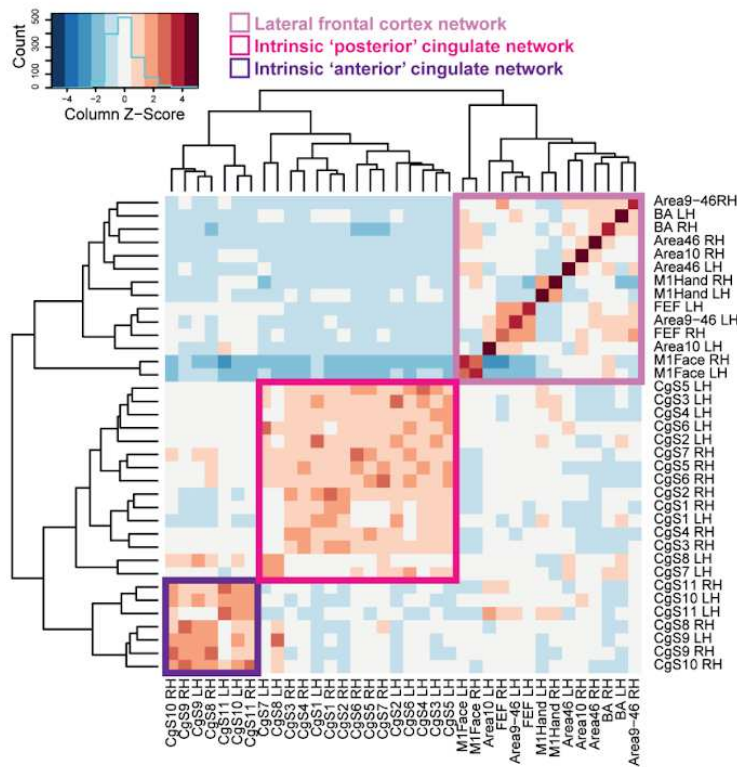
Figure 3. Anaesthesia impacts the Medio-lateral frontal network global network connectivity pattern. (A, B) Heatmaps of the functional correlations (Z value) between all seeds and ROIs unilaterally and bilaterally in the anaesthetized (A) and awake (B) state. Color gradient from red to blue, with red representing positive Z values and blue negative Z values. Negative and positive Z values are differently distributed in awake versus anaesthetized state. The gray diagonal represents auto-correlations. (C) Density plot representing the distribution of Z value in both conditions: anaesthetized (in pink) peaked in negative Z value and awake (in blue) in positive Z values. (D) Number of positive and negative Z values: more negative Z values in awake versus anaesthetized (26.2% vs. 39.8%, respectively, $\chi^2 = 35.145$, $P < 3.1e-9$) and more positive Z values in the anaesthetized than awake (73.8% vs. 60.2%, respectively, $\chi^2 = 17.323$, $P < 3.2e-5$). (E) Boxplots representing the mean Z values in both positive and negative in each condition. Positive Z values

mean is increased in the awake state (estimate = 0.047, $P < 0.0001$, post hoc Tukey) and no difference on mean negative Z value (estimate = -0.001, $P = 0.92$, post hoc Tukey).

Cingulo-Lateral Frontal Networks are Differently Organized in the Awake versus the *Anaesthetized* State

To assess whether the state (anaesthetized/awake) had an impact on the FC in the cingulo-lateral frontal networks, unilaterally, and bilaterally, we performed an unsupervised hierarchical clustering of the seeds and ROIs based on their intercorrelations across all macaques in the awake and anaesthetized states (see [Materials and Methods](#)). Resulting dendrograms from the seed and ROI clustering are displayed in [Figure 4](#) along with a heatmap reflecting the correlation strengths between each pair of seed–seed, seed–ROI, and ROI– ROI clusters. In the anaesthetized state, this analysis demonstrated two functional networks between regions of the cingulate cortex (pink square for the posterior network and lighter pink square for the anterior network, [Fig.4A](#)) and a functional network between regions of the lateral frontal cortex (blue square, [Fig. 4A](#)), suggesting poor functional interplay between these two entities. In contrast, in the awake state, we found three main functional networks: 1) an anterior cingulate– lateral prefrontal network (dark green square, [Fig. 4B](#)) encompassing Areas 10, 46, and 9/46, and the three most anterior cingulate areas (CgS9, CgS10, CgS11); 2) a posterior cingulate–lateral prefrontal network (light green square, [Fig. 4B](#)) including Area 9/46, BA, FEF, M1Face, and M1Hand, and CgS8 (where the gradient inversion is observed, [Figs 1 and 2](#)), and a posterior intrinsic cingulate network (brown square, [Fig. 4B](#)) comprising cingulate seeds from Cgs1 to CgS7. Note that all these networks are unilaterally and bilaterally organized. In sum, the analysis provides evidence of different functional interactions in the cingulo-frontal lateral networks between the awake and anaesthetized states.

A. Anaesthetized state



B. Awake state

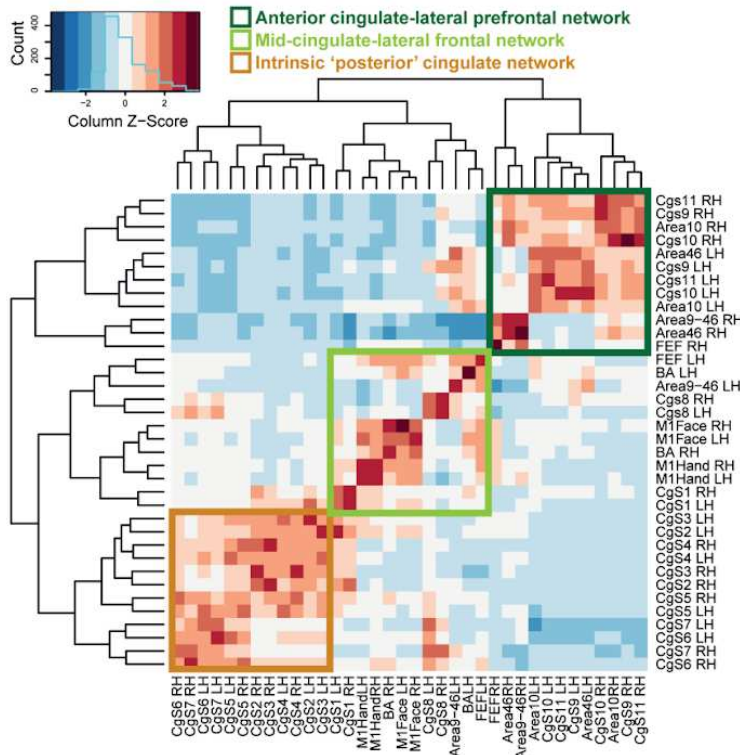
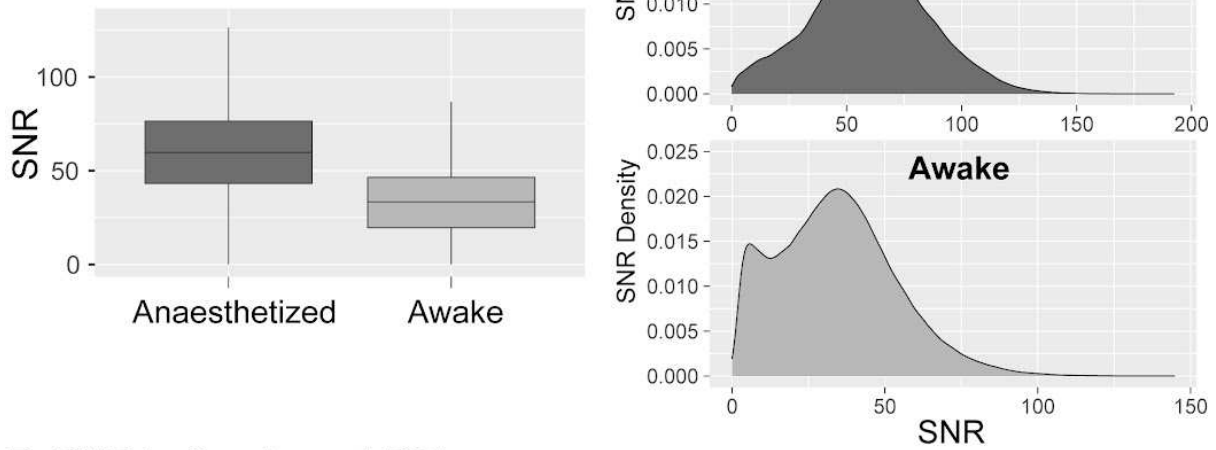
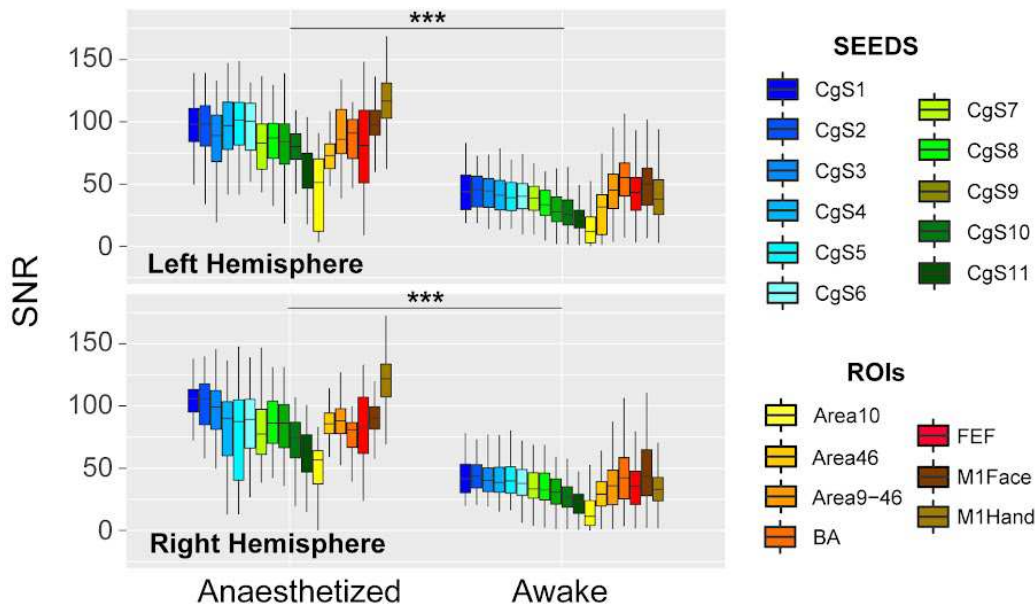


Figure 4. In the large mediolateral network, clustering dissociates three main networks in the awake state versus two main networks in anaesthetized state. Hierarchical clustering of all seeds and ROIs based on their intercorrelations in anaesthetized (A) and awake (B) state. Dendrograms are represented on the left and top side of the heatmap. (A) In the anaesthetized state, two main clusters: lateral frontal cortex network (purple) and cingulate network (pink). (B) Three clusters are sorted for the awake state: anterior cingulate-lateral network (dark green), posterior cingulate-lateral prefrontal network (light green), and posterior intrinsic cingulate network (light brown).

A. Whole brain SNR



B. SNR in Seeds and ROIs



C. Temporal derivatives of motion parameters

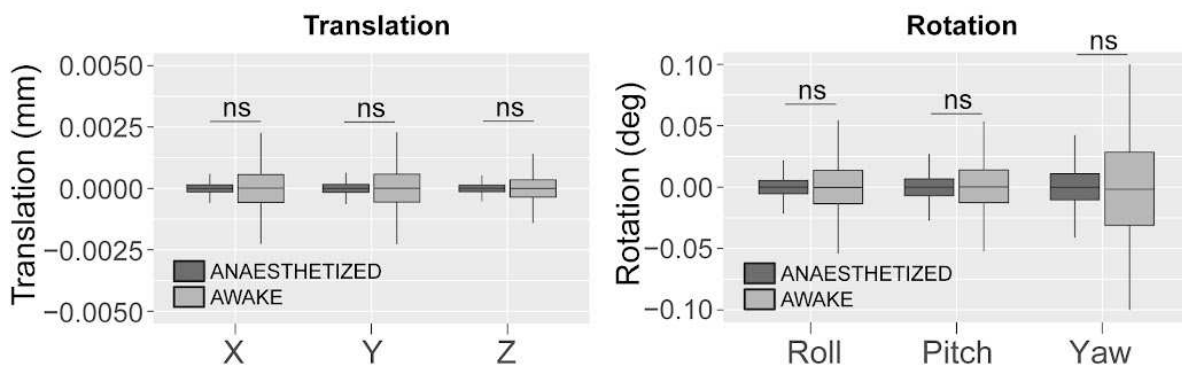


Figure 5. tSNR ratio and estimated brain movement in the awake and anaesthetized states. (A) Whole-brain tSNR. Right panel: boxplot representing the tSNR mean in both conditions. GLMM ($df = 8.654e+05$, t value = -535.16 , $P < 2e-16$) shows a greater tSNR in the anaesthetized state

compared with the awake state. Left panel represents the distribution of tSNR values in the whole brain. (B) tSNR in each seed and ROI in both hemispheres and conditions: GLMM ($df = 17$, $F = 44.42$, $P < 2.2e-16$) shows a greater tSNR in the anaesthetized state compared with the awake state. (C) Boxplot represents the temporal derivatives of estimated brain movements (translation and rotation) in the X, Y, and Z directions, with no significant effect of movement across conditions (GLMM, $df = 5$, $F = 0.0049$, $P > 0.05$).

rs-fMRI Signal Quality Check: Motion Estimation and tSNR

We assessed the quality of our two data sets to rule out potential confounding effects. We first extracted mean signal from seeds and ROIs and then computed for each run and each monkey the tSNR (see Material and Methods section). The tSNR was higher in anaesthetized compared with awake sessions (GLMM, fixed effect = state [anaesthetized, awake], random effect [macaque ID], $df = 8.654e+05$, t value = -535.16 , $P < 2e-16$, Fig. 5A). For each of our predefined seeds and ROIs, the tSNR was also higher in anaesthetized compared with awake sessions both in the left and right hemispheres (LEFT:GLMM, fixed effects = state [anaesthetized/awake] and Seeds/ROIs [CgS1–CgS11, Area 10, Area 46, Area 9/46, BA, FEF, M1Face, M1Hand], random effect [macaque ID], $df = 17$, $F = 44.42$, $P < 2.2e-16$; RIGHT: $df = 17$, $F = 59.03$, $P < 2.2e-16$, GLMM, Fig. 5B). The difference in tSNR is reasonably related to the different coils used in the awake versus anaesthetized states due to technical limitations (see Material and Methods section). Yet, importantly, these differences in tSNR between both states cannot be attributed to variations in estimated brain movements (GLMM, fixed effects = STATE [anaesthetized/awake] or movement types [translations in X, Y, and Z directions; yaw, roll, and pitch rotations], random effect [macaque ID], $df = 5$, $F = 0.0049$, ns, Fig. 5C). Importantly, all results presented above, obtained in awake macaques, are similar to those obtained in awake humans with a different coil.

DISCUSSION

In the present study, we investigated the FC organization between the cingulate cortex and the lateral frontal cortex in monkeys under two states, awake and anaesthetized states, using rs-fMRI. In the awake state, we consistently observed for the three monkeys a FC organization that follows a rostro-caudal functional gradient such that rostral cingulate regions were more functionally correlated with rostral lateral prefrontal regions (i.e., areas 10, 46, and 9/46) compared with frontolateral motor

regions. Inversely, caudal cingulate regions were more functionally correlated with frontal lateral motor regions (i.e., M1Face and M1Hand) compared with rostrolateral prefrontal regions. This FC organization is similar to that previously described in humans (Loh et al. 2018). More importantly, our results reveal that, in the anaesthetized state, 1) this functional gradient inversion was not apparent and 2) the number of negative correlations and the strength of positive correlations within the different parts of the networks were reduced compared with the awake state. These results provide evidence that anaesthesia impacts the FC between the cingulate cortex and the lateral frontal cortex.

Functional versus Structural Organization of the Cingulo-Frontal Cortical Network

The present rs-fMRI FC results in awake macaque, that is, the particular rostro-to-caudal FC organization of the cingulo-frontal lateral network, are consistent with structural connectivity literature in macaque. Indeed, it has been shown that whereas CMAr displays denser structural connections with medial and lateral prefrontal cortex and weaker connections with dorsal premotor and primary motor cortex, CMAc displays a higher density of connections with motor regions and spinal cord (Dum and Strick 1991; He et al. 1995; Morecraft et al. 2012). These results are supported by several studies reporting a high correspondence between rs-fMRI FC and ex vivo tracer-measured structural connectivity in macaque monkeys (Miranda-Dominguez et al. 2014) as well as a robust correlation (Straathof et al. 2019). This organization supports the hypothesis that primate frontal cortical areas are organized along a rostro-caudal axis with progressively rostral areas implementing more abstract and higher order levels of behavioral control and progressively caudal areas performing more motor processing (Fuster 2001; Koehlin 2003; Domenech and Koehlin 2015).

Similar Rostro-Caudal Functional Gradient in the Cingulo-Frontal Lateral Network in Awake Humans and Monkeys

As discussed above, Loh et al. (2018) recently reported a particular rostro-caudal FC organization within the cingulo-frontal lateral network using rs-fMRI in awake humans. Anterior cingulate regions displayed stronger positive correlations with rostrolateral prefrontal regions and weaker ones with the lateral caudal motor regions whereas more caudal cingulate regions displayed the reverse pattern. Interestingly, the present

study reveals a similar FC organization of the cingulo-frontal lateral network when rhesus macaques were awake and an altered organization when they were anaesthetized.

While in the study of [Loh et al. \(2018\)](#), seeds in the cingulate cortex regions and ROIs in the motor cortical areas were defined based on activation peaks from a fMRI motor mapping task and ROIs in the lateral prefrontal cortex were defined based on local anatomy, all the seeds and the ROIs in the monkey of the present study were identified based on local anatomy. Specifically, based on a previous metanalysis suggesting that the face motor area of CMa is located about 10 mm anterior to the genu of the arcuate ([Procyk et al. 2016](#)), we anticipated that this subdivision would roughly correspond to CgS8. Interestingly, the FC profile of this region and that of more anterior cingulate seeds, CgS8–CgS11, that we uncovered in the present study display a similar pattern than that found previously in human and chimpanzee, RCZa (homologue of the macaque CMa). In the present study and as previously reported in human and chimpanzee ([Loh et al. 2018](#); [Amiez et al. 2021](#)), these seed regions display functional coupling with BA, FEF, M1Face, M1Hand in the awake state ([Supplemental Figs 4 and 5](#)). Altogether, these data suggest that our seed CgS8 might represent the caudal limit of the homologous of RCZa in human, that is, CMa.

Concerning CMac, it is subdivided into CMAv and CMAr ([Dum and Strick, 2002](#)), and these regions are thought to correspond to human RCZp and CCZ ([Amiez and Petrides 2014](#); [Loh et al. 2018](#)). We have shown that, in humans, the gradient of connectivity of RCZp and CCZ with the same set of ROIs in frontal cortex displays the reverse pattern of RCZa, that is, increased connectivity with caudal motor lateral frontal cortical seeds and decreased connectivity with rostral lateral prefrontal cortical seeds. Our results show that this reversed gradient in the awake macaque can be observed from the most caudal seed (CgS1) and CgS7 (+10 mm from AC, +8 mm from ArcGen, see [Figs 1 and 2](#)). We can therefore reasonably conclude that the macaque homologues of the human RCZp and CCZ are both located within these caudal cingulate seeds (CgS1–CgS7) but that we cannot identify their respective location on the sole basis of our ROI analysis. Importantly, in humans, we were also unable to dissociate RCZp and CCZ on the basis of their correlation profile using the same chosen set of ROIs ([Loh et al. 2018](#)).

In sum, based on their FC signatures with the lateral prefrontal and motor cortex in rs-fMRI, we could identify homologies between humans and monkeys cingulate

motor regions but only when considering data from the awake state. Note that the FC of the rostral cingulate seeds displays similarities between human awake and chimpanzees anaesthetized with propofol (Amiez et al. 2021). As we did not investigate the FC profile for caudal cingulate seeds, we do not know whether a rostro-caudal gradient inversion is also present in chimpanzees. However, it is likely that, as propofol also strongly alters FC (Barttfeld et al. 2015; Uhrig et al. 2018), the resulting gradient would be abolished but future studies should shed light on this matter. In other words, the state— awake versus anaesthetized—matters when comparing FC patterns using rs-fMRI across species, and the present study shows that a careful attention should be given to interpreting FC patterns in particular of motor and premotor cortex collected under anaesthesia.

Anaesthesia Alters rs-fMRI-Identified FC Pattern in Cingulo-Frontal Lateral Networks

Anaesthesia is characterized by an alteration of the level of consciousness, decreased muscle tone, and altered autonomic responsiveness (Scharf and Kelz 2013). The degree to which each of these effects is achieved depends both on the anaesthetic agent and its dose. Isoflurane is a volatile inhalation anaesthetic agent, commonly used in surgical procedures and in vivo neuroimaging studies in animals, at concentrations varying between 0.75% and 1.5%. In NHP, increased cerebral blood flow (CBF) has been reported with a dose-dependent effect such that higher dose of isoflurane increases CBF due to larger vasodilation (Matta et al. 1999). Not surprisingly, these changes in CBF induce various alterations of FC in the brain, as measured using rs-fMRI. First, at the whole brain level, the comparison between awake and anaesthetized conditions in both humans and monkeys, suggest that interhemispheric correlations exhibited more pronounced reduction compared with intrahemispheric ones (Hutchison et al. 2014; Hori et al. 2020) and that this effect was dependent on the dose of anaesthetics (Hutchison et al. 2014). Second, anaesthesia is also characterized by weaker correlation strength in addition to a decrease in negative correlations or anticorrelations (Hutchison et al. 2014; Barttfeld et al. 2015; Uhrig et al. 2018; Xu et al. 2019; Hori et al. 2020). Our results on the cingulo-frontal lateral networks reveal no difference in interhemispheric or intrahemispheric correlations. Yet, we found a significant decrease of the positive

correlation strength (Fig. 3E) and a decrease in the number of negative correlations (Fig. 3D) in the anaesthetized state compared with the awake state. Note that the tSNR significantly differed between the two states, likely because of the different coils used in the two conditions (see [Materials and Methods](#)). However, the decrease in correlation strength under anaesthesia might not result from a lower ability to detect a signal change because the tSNR was higher than in the awake state, and despite the lower tSNR in the awake state, the positive correlations strengths were higher. In addition, it is unlikely that motion, as measured from the estimated brain movements, could explain the differences between the two states as we did not find any significant difference between them. Negative correlations in rs-fMRI studies are highly debated, in particular on whether they artifactually result from data preprocessing strategies (following global signal regression, see for instance [Saad et al. 2012](#); [Murphy et al. 2009](#)). In the present study, we did regress out CSF and WM signals, but not the global signal. Therefore, the reduction of negative correlation reported here is a mere feature of the impact of isoflurane on FC patterns in macaque frontal cortex. Importantly, more recent evidence suggests instead that these negative correlations have biological significance. They might highlight regulatory interactions between brain networks and regions ([Barttfeld et al. 2015](#); [Gopinath et al. 2015](#); [Uhrig et al. 2018](#)) and that they may represent a relevant biomarker in some diseases ([Ramkiran et al. 2019](#)). Therefore, the larger number of negative correlations found in the awake state compared with anaesthetized state might participate in the configuration of the FC signature within the cingulo-frontal lateral networks.

Beyond the general effect of anaesthesia on brain activity at rest, [Hutchison et al. \(2011\)](#), showed in anaesthetized macaques that most of the large-scale resting-state networks are topographically and functionally comparable to human ones ([Hutchison et al. 2011](#)). However, they also revealed major differences, especially the lack of a dorsomedial PFC component in the DMN. The same group subsequently showed that in anaesthetized marmosets, the coactivation strength decreased within large-scale resting-state networks and that the DMN network was particularly impacted, also exhibiting a lack of frontal component compared with the awake state ([Hori et al. 2020](#)). On the contrary, in awake NHP, frontal and prefrontal components of the DMN are not altered ([Hori et al. 2020](#); [Mantini et al. 2011](#)). These results underlie the impact of anaesthesia, on large-scale brain functional brain networks,

and suggest that regions of the frontal cortex might be particularly sensitive to anaesthetic agents. Similarly, our clustering results have shown that the functional interplay between cingulate and lateral frontal cortex can be observed only in the awake state. In the anaesthetized state, only local FC persists as lateral frontal cortical regions and cingulate regions appear in separate clusters. These results are in line with the hypothesis stipulating that anaesthetics alter cortical activity by biasing spontaneous fluctuations of cortical activity to a more local brain configuration that is highly shaped by brain anatomy (Uhrig et al. 2018). Therefore, anaesthesia might be a potential confound factor that should be considered carefully when comparing FC patterns across species and under different awareness states, especially when considering frontal motor regions (Schroeder et al. 2016; Ma et al. 2019). In our study, anaesthesia strongly affects M1 activity and its functional dialogue with the cingulo-prefrontal network (Supplemental Figs 4 and 5). This is in line with other findings showing disrupted FC between M1 region and the cingulate cortex, the somatosensory cortex, the FEF with several anaesthetic drugs (Schroeder et al. 2016; Uhrig et al. 2018). As supported by several studies, the FC alteration within our network might be caused by thalamocortical pathway disruption occurring under anaesthesia. Indeed, the thalamus is seen as the on–off switch for consciousness and gate of information flux and consequently is one of the main targets of anaesthetic drugs (see for review White and Alkire 2003; Hudetz et al. 2012; Mashour et al. 2013). Future studies may assess further the effect of anaesthesia on the FC organization of the thalamo-cingulo-frontal network.

Limitations

A potential limitation of the present study is the use of different coils in awake and anaesthetized conditions because of technical constraints specific to each setup. However, the differential FC results obtained in these conditions cannot reasonably be attributed to this aspect given that, although the tSNR was higher in the anaesthetized than in the awake condition, the modulation of FC connectivity within this network was observed only in the awake condition. Another potential limitation is the heterogeneity of the ages of the three monkeys participating in the study (one monkey of 21 years old and two monkeys of 9.5 years old). However, the FC results were highly similar across the three monkeys (see Supplemental Figs 1–

3), suggesting that the age is not impacting the anatomo functional organization of this specific network as assessed with the present rs-fMRI methodology. Finally, another limitation is the fact that monkeys received liquid reward throughout each run to maintain a good level of motivation. Although this is a methodological difference between the two states, it should be emphasized that our results were highly similar in sessions in which monkeys were less engaged in the task (notfixating and/or eye closed) and therefore received less juice (Supplemental Fig. 6). Furthermore, our results are similar to those obtained in humans (Loh et al.2018) where the motivation during rs-fMRI runs is not primary reward (liquid) but still exists in the form of monetary reward. Two hypotheses therefore emerge: 1) networks underlying motivation modulates activity in the studied cingulo-frontal cortical network in a similar way in human and macaque; 2) rs-fMRI in awake human and macaque tackled structural connectivity of this network and FC is not sensitive to the impact of the motivation type. Future studies may address these two hypotheses.

Conclusions

The present study revealed a similar FC signature in cingulo-frontal lateral networks in awake macaque comparable to that previously described in awake human subjects (Loh et al. 2018) using rs-fMRI, suggesting a persevered FC organization of this network from macaque to human. Specifically, rostral seeds in the cingulate sulcus exhibited stronger correlation strength with rostral compared with caudal lateral prefrontal ROIs, while caudal seeds in the cingulate sulcus displayed stronger correlation strength with caudal compared with lateral prefrontal ROIs. By comparing this cingulo-frontal lateral network pattern in awake or anaesthetized animals, we found that the inverse rostro-caudal functional gradient was abolished under anaesthesia, suggesting caution when comparing FC patterns across species under different states.

Supplementary Material

[Supplementary material](#) can be found at *Cerebral Cortex* online.

Authors' Contributions

C.A. and F.H.-B. organized the project. A.D., C.G., and D.A.-C. trained monkeys to perform ocular fixation in the MRI environment. A.D., C.A., C.G., and F.H.-B. acquired neuroimaging data in awake macaques; E.P., C.W., M.D., J.S., C.A., and F.H.-B. acquired neuroimaging data in anaesthetized macaques. C.A. and F.H.-B. analyzed data. C.G., A.D., C.A., and F.H.-B. interpreted data and wrote the article.

Funding

French National Research Agency (ANR-18-CE37-0012-01 to C.A, ANR-15-CE37-0003 to F.H.-B.).

Notes

C.A., F.H.-B., and E.P. are employed by the Centre National de la Recherche Scientifique. C.G., C.A., D.A.-C., E.P., C.W., and J.S. are supported by the labex CORTEX ANR-11-LABX-0042 of Université de Lyon. We thank Gislène Gardechaux for technical assistance in training awake macaques. We also thank Franck Lambertson for technical help in acquiring neuroimaging data in awake macaques.

Conflict of Interest: None declared.

References

- Alkire MT, Miller J. 2005. General anaesthesia and the neural correlates of consciousness. *Prog Brain Res.* 150:229–244.
- Amiez C, Petrides M. 2009. Anatomical organization of the eye fields in the human and non-human primate frontal cortex. *Prog Neurobiol.* 89(2):220–230.
- Amiez C, Petrides M. 2014. Neuroimaging evidence of the anatomofunctional organization of the human cingulate motor areas. *Cereb Cortex.* 24(3):563–578.
- Amiez C, Sallet J, Hopkins WD, Meguerditchian A, Hadj-Bouziane F, Ben Hamed S, Wilson CRE, Procyk E, Petrides M. 2019. Sulcal organization in the medial frontal cortex provides insights into primate brain evolution. *Nat Commun.* 10(1):3437.
- Amiez C, Sallet J, Novek J, Hadj-Bouziane F, Giacometti C, Andersson J, Hopkins WD, Petrides M. 2021. Chimpanzee histology and functional brain imaging show that the paracingulate sulcus is not human-specific. *Commun Biol.* 4(1):1–12.
- Areshenkoff CN, Nashed JY, Hutchison RM, Hutchison M, Levy R, Cook DJ, Menon RS, Everling S, Gallivan JP. 2021. Muting, not fragmentation, of functional brain networks under general anaesthesia. *Neuroimage.* 231(January):117830.
- Badre D, D'Esposito M. 2009. Is the rostro-caudal axis of the frontal lobe hierarchical? *Nature Reviews Neuroscience.* 10(9):659–669.

- Barron HC, Mars RB, Dupret D, Lerch JP, Sampaio-Baptista C. 2021. Cross-species neuroscience: closing the explanatory gap. *Philos Trans R Soc B Biol Sci.* 376(1815):20190633.
- Barttfeld P, Uhriga L, Sitta JD, Sigmane M, Jarraya B, Dehaene S. 2015. Signature of consciousness in the dynamics of resting-state brain activity. *Proc Natl Acad Sci U S A.* 112(3):887–892.
- Birn RM, Molloy EK, Patriat R, Parker T, Meier TB, Kirk GR, Nair VA, Meyerand ME, Prabhakaran V. 2013. The effect of scan length on the reliability of resting-state fMRI connectivity estimates. *NeuroImage.* 83:550–558.
- Biswal BB, Van KJ, Hyde JS. 1997. Simultaneous assessment of low and BOLD signals in resting-state functional connectivity maps. *NMR Biomed.* 10(4–5):165–170.
- Biswal BB, Mennes M, Zuo X-N, Gohel S, Kelly C, Smith SM, Beckmann CF, Adelstein JS, Buckner RL, Colcombe S, et al. 2010. Toward discovery science of human brain function. *Proc Natl Acad Sci.* 107(10):4734–4739.
- Bruce CJ, Goldberg ME, Bushnell MC, Stanton GB. 1985. Primate frontal eye fields. II. Physiological and anatomical correlates of electrically evoked eye movements. *J Neurophysiol.* 54(3):714–734. Cox RW. 1996. AFNI: software for analysis and visualization of functional magnetic resonance neuroimages. *Comput Biomed Res.* 29(3): 162–173.
- Domenech P, Koechlin E. 2015. Executive control and decision- making in the prefrontal cortex. *Curr Opin Behav Sci.* 1:101–106.
- Dum RP, Strick PL. 1991. The origin of corticospinal projections from the premotor areas in the frontal lobe. *J Neurosci.* 11(3):667–689.
- Dum RP, Strick PL. 2002. Motor areas in the frontal lobe of the primate. *Physiol Behav.* 77:677–682.
- Fuster JM. 2001. The prefrontal cortex - an update: time is of the essence. *Neuron.* 30(2):319–333.
- Folloni D, Verhagen L, Mars RB, Fouragnan E, Constans C, Aubry JF, Rushworth MFS, Sallet J. 2019. Manipulation of subcortical and deep cortical activity in the primate brain using transcranial focused ultrasound stimulation. *Neuron.* 101(6):1109–1116.
- Friedrich P, Forkel SJ, Amiez C, Balsters JH, Coulon O, Fan L, Goulas A, Hadj-Bouziane F, Hecht EE, Heuer K, et al. 2021. Imaging evolution of the primate brain: the next frontier? *Neuroimage.* 228: 117685.
- Gopinath K, Krishnamurthy V, Cabanban R, Crosson BA. 2015. Hubs of anticorrelation in high-resolution resting-state functional connectivity network architecture. *Brain Connect.* 5(5):267–275.
- Graziano MS, Taylor CS, Moore T. 2002. Complex movements evoked by microstimulation of precentral cortex. *Neuron.* 34(5):841–851.
- Hadj-Bouziane F, Liu N, Bell AH, Gothard KM, Luh WM, Tootell RBH, Murray EA, Ungerleider LG. 2012. Amygdala lesions disrupt modulation of functional MRI activity evoked by facial expression in the monkey inferior temporal cortex. *Proc Natl Acad Sci U S A.* 109(52):E3640–E3648.

- Hadj-Bouziane F, Monfardini E, Guedj C, Gardechaux G, Hynaux C, Farnè A, Meunier M. 2014. The helmet head restraint system: a viable solution for resting state fMRI in awake monkeys. *Neuroimage*. 86:536–543.
- He SQ, Dum RP, Strick PL. 1993. Topographic organization of corticospinal projections from the frontal lobe: Motor areas on the lateral surface of the hemisphere. *J Neurosci*. 13(3):952–980.
- He S, Dum R, Strick P. 1995. Topographic organization of corticospinal projections from the frontal lobe: motor areas on the medial surface of the hemisphere. *J Neurosci*. 15(5):3284–3306.
- Hori Y, Schaeffer DJ, Gilbert KM, Hayrynen LK, Cléry JC, Gati JS, Menon RS, Everling S. 2020. Altered resting-state functional connectivity between awake and isoflurane anaesthetized macaques. *Cereb Cortex*. 30(11):5943–5959.
- Hudetz AG. 2012. General anaesthesia and human brain connectivity. *Brain Connect*. 2(6):291–302.
- Hutchison RM, Gallivan JP, Culham JC, Gati JS, Menon RS, Everling S. 2012. Functional connectivity of the frontal eye fields in humans and macaque monkeys investigated with resting-state fMRI. *J Neurophysiol*. 107:2463–2474.
- Hutchison RM, Culham JC, Flanagan JR, Everling S, Gallivan JP. 2015. Functional subdivisions of medial parieto-occipital cortex in humans and nonhuman primates using resting-state fMRI. *Neuroimage*. 116:10–29.
- Hutchison RM, Everling S. 2012. Monkey in the middle: why non-human primates are needed to bridge the gap in resting-state investigations. *Front Neuroanat*. 6:1–19.
- Hutchison RM, Hutchison M, Manning KY, Menon RS, Everling S. 2014. Isoflurane induces dose-dependent alterations in the cortical connectivity profiles and dynamic properties of the brain's functional architecture. *Hum Brain Mapp*. 35(12): 5754–5775.
- Hutchison RM, Leung LS, Mirsattari SM, Gati JS, Menon RS, Everling S. 2011. Resting-state networks in the macaque at 7T. *Neuroimage*. 56(3):1546–1555.
- Hutchison RM, Womelsdorf T, Gati JS, Everling S, Menon RS. 2013. Resting-state networks show dynamic functional connectivity in awake humans and anaesthetized macaques. *Hum Brain Mapp*. 34(9):2154–2177.
- Jenkinson M, Peacock M, Smith S. 2005. BET2: MR-based estimation of brain, skull and scalp surfaces. In: *Eleventh Annual Meeting of the Organization for Human Brain Mapping*. http://ftp.nmr.mgh.harvard.edu/pub/dist/freesurfer/tutorial_packages/centos6/fsl_507/doc/wiki/BET.html
- Jung B, Taylor PA, Seidlitz J, Sponheim C, Perkins P, Ungerleider LG, Glen D, Messinger A. 2021. A comprehensive macaque fMRI pipeline and hierarchical atlas. *Neuroimage*. 235:117997.
- Koechlin E. 2003. The architecture of cognitive control in the human prefrontal cortex. *Science* (80-). 302(5648):1181–1185.
- Koechlin E, Summerfield C. 2007. An information theoretical approach to prefrontal executive function. *Trends Cogn Sci*. 11(6): 229–235.
- Li C, Zhang X. 2013. Isoflurane on resting cerebral blood flow and default mode network in macaque monkeys. *Neurosci Lett*. 541: 58–62.

- Loh KK, Hadj-Bouziane F, Petrides M, Procyk E, Amiez C. 2018. Rostro- Caudal organization of connectivity between cingulate motor areas and lateral frontal regions. *Front Neurosci.* 11:1–17.
- Lopez-Persem A, Roumazeilles L, Folloni D, Marche K, Fouragnan EF, Khalighinejad N, Rushworth MFS, Sallet J. 2020. Differential functional connectivity underlying asymmetric reward-related activity in human and nonhuman primates. *Proc Natl Acad Sci U S A.* 117(45):28452–28462.
- Luppino G, Rizzolatti G. 2000. The organization of the frontal motor cortex. *News Physiol Sci.* 15(5):219–224.
- Lv P, Xiao Y, Liu B, Wang Y, Zhang X, Sun H, Li F, Yao L, Zhang W, Liu L, et al. 2016. Dose-dependent effects of isoflurane on regional activity and neural network function: a resting-statefMRI study of 14 rhesus monkeys. *Neurosci Lett.* 611:116–122.
- Ma L, Liu W, Hudson AE. 2019. Propofol anaesthesia increases long- range frontoparietal corticocortical interaction in the oculomotor circuit in macaque monkeys. *Anesthesiology.* 130(4):560–571.
- Mantini D, Gerits A, Nelissen K, Durand J-B, Joly O, Simone L, Sawamura H, Wardak C, Orban GA, Buckner RL, et al. 2011. Default mode of brain function in Monkeys. *J Neurosci.* 31(36): 12954–12962.
- Mareyam A, Blau J, Polimeni J, Keil B, Farivar R, Benner T, Vanduffel W, Wald LL, Proceedings of the 19th Annual Meeting of ISMRM, Montreal, Canada. 2011. *Eight-channel arraycoil optimized for functional imaging of awake monkeys at 7T.* Montreal, Canada, p. 1823.
- Mars RB, Jbabdi S, Sallet J, O’Reilly JX, Croxson PL, Olivier E, Noonan MAP, Bergmann C, Mitchell AS, Baxter MG, et al. 2011. Diffusion-weighted imaging tractography-based parcellation of the human parietal cortex and comparison with human and macaque resting-state functional connectivity. *J Neurosci.* 31(11): 4087–4100.
- Mars RB, Neubert FX, Noonan MP, Sallet J, Toni I, Rushworth MFS. 2012. On the relationship between the “default mode network” and the “social brain”. *Front Hum Neurosci.* 6:1–9.
- Mars RB, Sallet J, Neubert FX, Rushworth MFS. 2013. Connectivity profiles reveal the relationship between brain areas for social cognition in human and monkey temporoparietal cortex. *Proc Natl Acad Sci U S A.* 110(26):10806–10811.
- Mars RB, Sotiropoulos SN, Passingham RE, Sallet J, Verhagen L, Khrapitchev AA, Sibson N, Jbabdi S. 2018. Whole brain comparative anatomy using connectivity blueprints. *Elife.* 7:e35237.
- Mars RB, Verhagen L, Gladwin TE, Neubert FX, Sallet J, Rushworth MFS. 2016. Comparing brains by matching connectivity profiles. *Neurosci Biobehav Rev.* 60:90–97.
- Mashour GA, Alkire MT. 2013. Consciousness, anaesthesia, and the thalamocortical system. *Anesthesiology.* 118(1):13–15.
- Matta BF, Heath KJ, Tipping K, Summors AC. 1999. Direct cerebral vasodilatory effects of sevoflurane and isoflurane. *Anesthesiology.* 91(3):677–680.
- Milham MP, Ai L, Koo B, Xu T, Amiez C, Balezeau F, Baxter MG, Blezer ELA, Brochier T, Chen A, et al. 2018. An open resource for non- human primate imaging. *Neuron.* 100(1):61–74.e2.

- Miranda-Dominguez O, Mills BD, Grayson D, Woodall A, Grant KA, Kroenke CD, Fair DA. 2014. Bridging the gap between the human and macaque connectome: a quantitative comparison of global interspecies structure-function relationships and network topology. *J Neurosci.* 34(16):5552–5563.
- Morecraft RJ, Stilwell-Morecraft KS, Cipolloni PB, Ge J, McNeal DW, Pandya DN. 2012. Cytoarchitecture and cortical connections of the anterior cingulate and adjacent somatomotor fields in the rhesus monkey. *Brain Res Bull.* 87(4–5):457–497.
- Murphy K, Birn RM, Handwerker DA, Jones TB, Bandettini PA. 2009. The impact of global signal regression on resting state correlations: are anti-correlated networks introduced? *Neuroimage.* 44(3): 893–905.
- Neubert FX, Mars RB, Thomas AG, Sallet J, Rushworth MFS. 2014. Comparison of human ventral frontal cortex areas for cognitive control and language with areas in monkey frontal cortex. *Neuron.* 81(3):700–713.
- Neubert F-X, Mars RB, Sallet J, Rushworth MFS. 2015. Connectivity reveals relationship of brain areas for reward-guided learning and decision making in human and monkey frontal cortex. *Proc Natl Acad Sci.* 112(20):E2695–E2704.
- Petrides M. 2005a. Lateral prefrontal cortex: architectonic and functional organization. *Philos Trans R Soc B Biol Sci.* 360(1456):781–795. Petrides M. 2005b. The rostral-caudal axis of cognitive control within the lateral frontal cortex. In: Dehaene S, Duhamel JR, Hauser MC, Rizzolatti G, editors. *From monkey brain to human brain. A Fyssen Foundation Symposium.* Cambridge (MA): The MIT Press, pp. 293–314.
- Petrides M, Pandya DN. 1994. Comparative architectonic analysis of the human and the macaque frontal cortex. In: Boller F, Grafman J, editors. *Handbook of neuropsychology.* Amsterdam (NL): Psychology Press, pp. 17–58.
- Picard N, Strick PL. 2001. Imaging the premotor areas. *Curr Opin Neurobiol.* 11(6):663–672.
- Power JD, Barnes KA, Snyder AZ, Schlaggar BL, Petersen SE. 2012. Spurious but systematic correlations in functional connectivity MRI networks arise from subject motion. *NeuroImage.* 59(3): 2142–2154.
- Power JD, Plitt M, Laumann TO, Martin A. 2017. Sources and implications of whole-brain fMRI signals in humans. *NeuroImage.* 146: 609–625.
- Procyk E, Wilson CRE, Stoll FM, Faraut MCM, Petrides M, Amiez C. 2016. Midcingulate motor map and feedback detection: converging data from humans and monkeys. *Cereb Cortex.* 26(2): 467–476.
- Quilodran R, Rothé M, Procyk E. 2008. Behavioral shifts and action valuation in the anterior cingulate cortex. *Neuron.* 57(2):314–325. Ramkiran S, Sharma A, Rao NP. 2019. Psychiatryresearch: neuroimaging resting-state anticorrelated networks in Schizophrenia. *Psychiatry Res Neuroimaging.* 284:1–8.
- Rao J-S, Liu Z, Zhao C, Wei R-H, Zhao W, Tian P-Y, Zhou X, Yang Z-Y, Li X-G. 2017. Ketamine changes the local resting-state functional properties of anaesthetized-monkey brain. *Magn Reson Imaging.* 43:144–150.
- Rothé M, Quilodran R, Sallet J, Procyk E. 2011. Coordination of high gamma activity in anterior cingulate and lateral prefrontal cortical areas during adaptation. *J Neurosci.* 31:11110–11117.

- Saad ZS, Gotts SJ, Murphy K, Chen G, Jo HJ, Martin A, Cox RW. 2012. Trouble at rest: how correlation patterns and group differences become distorted after global signal regression. *Brain Connect.* 2(1):25–32.
- Sallet J, Mars RB, Noonan MP, Neubert F-X, Jbabdi S, O'Reilly JX, Filippini N, Thomas AG, Rushworth MF. 2013. The organization of dorsal frontal cortex in humans and macaques. *J Neurosci.* 33(30): 12255–12274.
- Scharf MT, Kelz MB. 2013. Sleep and anaesthesia interactions: a pharmacological appraisal. *Curr Anesthesiol Rep.* 3(1):1–9.
- Schroeder KE, Irwin ZT, Gaidica M, Bentley JN, Patil PG, Mashour GA, Chestek CA. 2016. Disruption of corticocortical information transfer during ketamine anaesthesia in the primate brain. *Neuroimage.* 134:459–465.
- Seidlitz J, Sponheim C, Glen D, Ye FQ, Saleem KS, Leopold DA, Ungerleider L, Messinger A. 2018. A population MRI brain template and analysis tools for the macaque. *Neuroimage.* 170:121–131.
- Signorelli CM, Uhrig L, Kringelbach M, Jarraya B, Deco G. 2021. Hierarchical disruption in the cortex of anaesthetized monkeys as a new signature of consciousness loss. *Neuroimage.* 227:117618.
- Stoll FM, Fontanier V, Procyk E. 2016. Specific frontal neural dynamics contribute to decisions to check. *Nat Commun.* 7(1):11990.
- Straathof M, Sinke MRT, Dijkhuizen RM, Otte WM. 2019. A systematic review on the quantitative relationship between structural and functional network connectivity strength in mammalian brains. *J Cereb Blood Flow Metab.* 39(2):189–209.
- Thomas J, Sharma D, Mohanta S, Jain N. 2021. Resting-state functional networks of different topographic representations in the somatosensory cortex of macaque monkeys and humans. *Neuroimage.* 228:117694.
- Uhrig L, Sitt JD, Jacob A, Tasserie J, Barttfeld P, Dupont M, Dehaene S, Jarraya B. 2018. Resting-state dynamics as a cortical signature of anaesthesia in monkeys. *Anesthesiology.* 129(5):942–958.
- Van Essen DC, Donahue C, Dierker DL, Glasser MF. 2016. Parcellations and connectivity patterns in human and macaque cerebral cortex. In: Kennedy H, David C, Van Essen, Christen Y, editors. *Micro-, meso- and macro- connectomics of the brain.* Switzerland, pp. 89–106.
- Vincent JL, Patel GH, Fox MD, Snyder AZ, Baker JT, Van Essen DC, Zempel JM, Snyder LH, Corbetta M, Raichle ME. 2007. Intrinsic functional architecture in the anaesthetized monkey brain. *Nature.* 447(7140):83–86.
- White NS, Alkire MT. 2003. Impaired thalamocortical connectivity in humans during general-anaesthetic-induced unconsciousness. *Neuroimage.* 19(2):402–411.
- Wu TL, Mishra A, Wang F, Yang PF, Gore JC, Chen LM. 2016. Effects of isoflurane anaesthesia on resting-state fMRI signals and functional connectivity within primary somatosensory cortex of monkeys. *Brain Behav.* 6(12):1–12.
- Xu T, Falchier A, Sullivan EL, Colcombe S, Fair DA, Milham MP, Linn G, Ramirez JSB, Ross D, Feczko E, et al. 2018. Delineating the macroscale areal organization of the macaque cortex in vivo. *Cell Rep.* 23:429–441.

- Xu T, Sturgeon D, Ramirez JSB, Froudish-Walsh S, Margulies DS, Schroeder CE, Fair DA, Milham MP. 2019. Interindividual variability of functional connectivity in awake and anaesthetized rhesus macaque monkeys. *Biol Psychiatry Cogn Neurosci Neuroimaging*. 4(6):543–553.
- Yin D, Zhang Z, Zhiwei W, Zeljic K, Lv Q, Cai D, Wang Y, Zheng W. 2019. Brain map of intrinsic functional flexibility in anaesthetized monkeys and awake humans. *Front Neurosci*. 13(FEB):174.

communications biology

CHAPTER II. DIFFERENTIAL FUNCTIONAL ORGANIZATION OF AMYGDALA-MEDIAL PREFRONTAL CORTEX NETWORKS IN MACAQUE AND HUMAN

Camille Giacometti[†], Delphine Autran-Clavagnier, Laura Viñales, Franck Lambertson, Audrey Dureux, Emmanuel Procyk, Charles R.E. Wilson, Céline Amiez^{†}, Fadila Hadj-Bouziane^{†*}*

(in revision)

[†] **Corresponding authors:** **Camille Giacometti**, camille.giacometti@inserm.fr; **Fadila Hadj-Bouziane**, fadila.hadj-bouziane@inserm.fr; **Céline Amiez**. INSERM U1208, Stem Cell and Brain Research Institute, 69500 Bron, France. E-mail address: celine.amiez@inserm.fr.

ABSTRACT

Over the course of evolution, the amygdala (AMG) and medial frontal cortex (mPFC) network, involved in behavioral adaptation, underwent structural changes in the old-world monkey and human lineages. Yet, whether and how the functional organization of this network differs remains poorly understood. Using resting-state functional magnetic resonance imagery, we show that the functional connectivity (FC) between AMG nuclei and mPFC regions differs between humans and awake macaques. In humans, the AMG-mPFC FC displays U-shaped pattern along the corpus callosum: a positive FC with the ventromedial prefrontal (vmPFC) and anterior cingulate cortex (ACC), a negative FC with the anterior mid-cingulate cortex (MCC), and a positive FC with the posterior MCC. Conversely, in macaques, the negative FC shifted more ventrally at the junction between the vmPFC and the ACC. The functional organization divergence of AMG-mPFC network between humans and macaques might help understanding behavioral adaptation abilities differences in their respective socio-ecological niches.

INTRODUCTION

In the face of uncertain environments, one must quickly detect salient information and adapt in consequence. Animals constantly monitor their surroundings (peer interactions, resource availability, danger, etc.), while also considering information related to their own internal state (emotional, motivational and physiological)¹. A growing number of studies converge toward a critical role of the network formed by the medial prefrontal cortex (mPFC) and the amygdala (AMG) in behavioral adaptation ability²⁻⁸. Both regions are highly heterogeneous. The AMG is a complex structure composed of several interconnected nuclei^{2,9}. The lateral nucleus (LA) is the main entry of sensory inputs, the basolateral nucleus (BL) and the basomedial nucleus (BM) are gating information from higher cognitive processes regions (e.g., mPFC), and the central nucleus (CE), is tightly connected with the autonomous system¹⁰. Within the mPFC, the ventro-medial PFC (vmPFC) and the anterior cingulate cortex (ACC) are involved in environmental stimulus valuation in the light of current internal states, while the mid-cingulate cortex (both its anterior -aMCC- and posterior -pMCC- part) is involved in outcome- and action-based decision monitoring^{1,11-15}.

Although the regions composing this network find their homologues in macaques and humans, they present structural differences that might result from the influence of environmental and social factors relative to the respective ecological niche of each species. First, the AMG is 10 times larger in humans compared to macaques due in particular to a larger expansion of LA nucleus¹⁶⁻¹⁹. Second, although the macaque mPFC displays all the sulcal precursors of the human mPFC, the region interfacing with vmPFC and MCC (which contains ACC) expanded in humans²⁰. The present paper aims at identifying whether and how these structural changes affect the functional coupling within the AMG-mPFC network.

By means of resting state functional MRI, a powerful cross-species reproducible method²¹⁻²⁴, we compared the functional connectivity (FC) pattern between the various AMG nuclei and mPFC regions in both awake humans (n=20) and awake macaques (n=3) as we have shown that anaesthesia alters FC within the frontal cortex²⁵. Results show that, in humans, the AMG-mPFC FC displays a rostro-caudal U-shaped pattern along the corpus callosum: positive FC with vmPFC and ACC, negative FC with anterior MCC, and positive FC with posterior MCC. By contrast, although a U-shape FC organization is observed in macaques, the negative FC shifted

more ventrally between the AMG and the region located at the junction between vmPFC and ACC. We also show that this FC pattern is driven by all AMG nuclei in both species, with the exception of the CE in humans. Altogether, these results highlight an anatomo-functional organization of the AMG-mPFC network divergence in the cercopithecoid monkeys and human lineages.

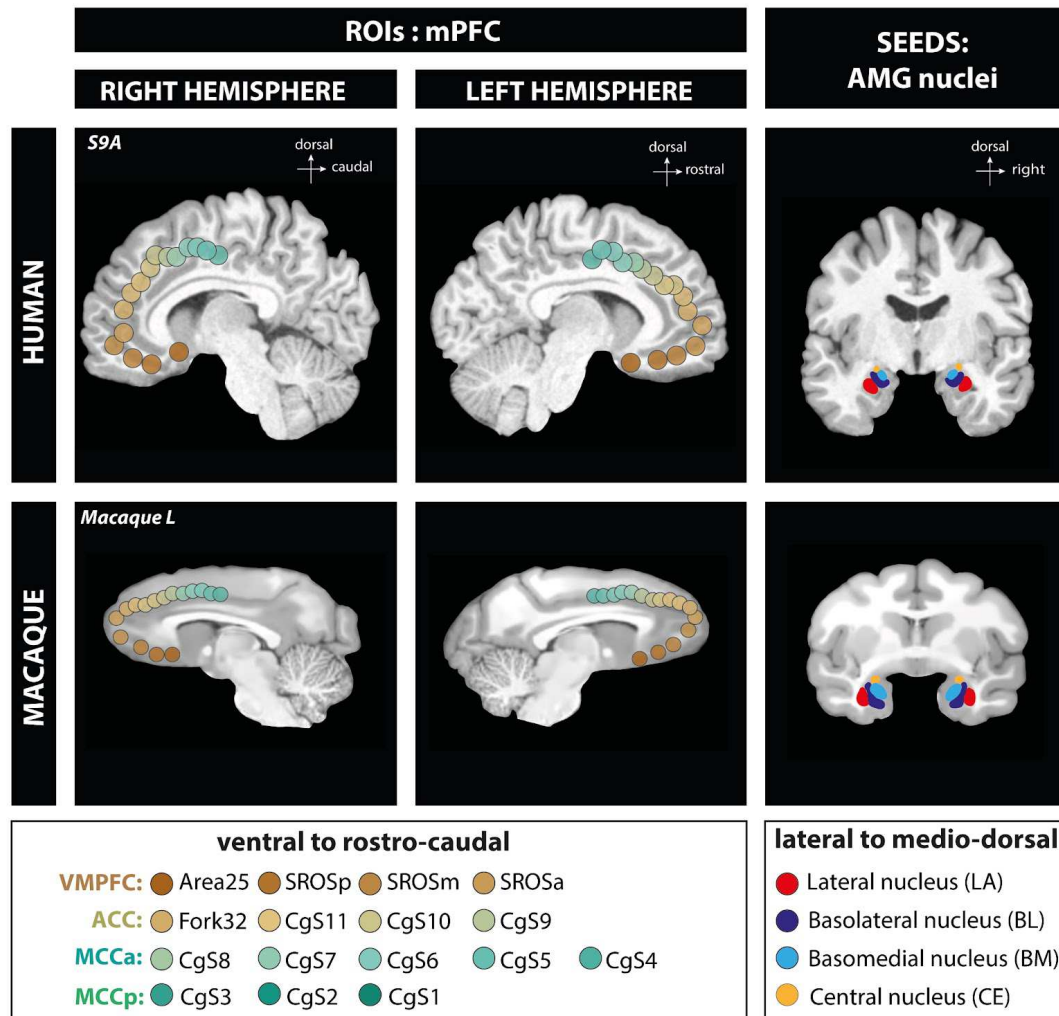


Figure 1. Amygdala nuclei Seeds and medial prefrontal cortex ROIs localization in human (top panel) and macaque (bottom panel) in the right and left hemispheres. *Left panel:* mPFC ROI localization on mid-sagittal brain sections in both hemispheres. The 16 ROIs are color-coded from brown to seagreen gradient in the ventro-dorsocaudal axis along the corpus callosum: vmPFC: Area25, SROSp, SROSm, SROSa; ACC: Fork32, CgS11, CgS10, CgS9; aMCC: CgS8, CgS7, CgS6, CgS5, CgS4; pMCC: CgS3, CgS2 and CgS1. *Right panel:* AMG 4 main nuclei, extracted from Tyszka an Pauli (2016) atlas for human and SARM atlas for macaque, illustrated on coronal sections. Lateral (LA) in red, basolateral (BL) in dark blue, basomedial (BM) in cyan and central (CE) in yellow.

RESULTS

In both humans and macaques, we assessed FC between 1) the atlas-based parcellation of the 4 main AMG nuclei (CE, BL, BM, and LA)^{26,27}, and 2) a fine-grained parcellation of the mPFC (16 ROIs) based on anatomical sulcal landmarks²⁰ (**Figure 1**). The mPFC ROIs were

spheres covering 1) the vmPFC (4 ROIs: subgenual Area 25, 3 ROIs in the Superior Rostral Sulcus, the posterior –SROSp–, medial –SROSm–, anterior –SROSa– part), 2) the ACC (4 ROIs on a rostrocaudal axis: Fork32 - part of cytoarchitectonic area 32 located just anterior to the fork formed by the suprarostal and the sus-orbitalis sulcus, CgS11, CgS10 and CgS9), 3) the aMCC (5 ROIs on a rostrocaudal axis in the cingulate sulcus: CgS8, CgS7, CgS6, CgS5, CgS4), and iv) the pMCC (3 ROIs on a rostrocaudal axis: CgS3, CgS2, CgS1). Note that results presented in the main text correspond to the AMG-mPFC FC pattern observed in the right hemisphere. The FC pattern observed in the left hemisphere is displayed in supplementary materials (**Figures S1 and S2**).

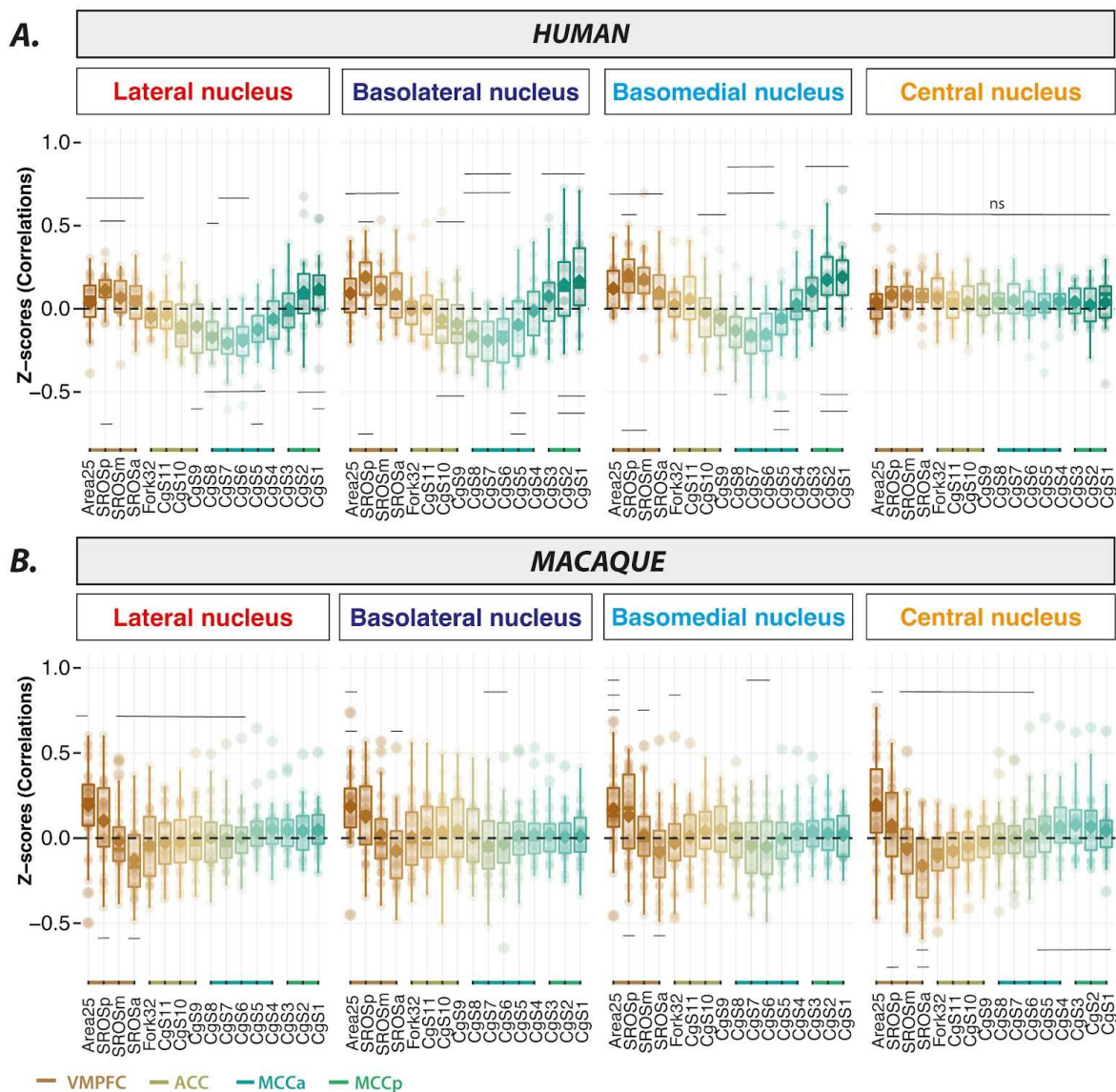


Figure 2. Functional connectivity pattern between AMG nuclei and mPFC ROIs in humans and macaques. A. Humans. Boxplots display correlation strength (z-scores) between each AMG nuclei (seed) and the mPFC ROIs across subjects. Results show a U-shape functional pattern for LA, BL and BM but not for CE: mPFC ventral seeds (vmPFC) present positive z-score values, then z-scores

decrease, reaching a negative peak in aMCC (ROIs CgS7-CgS6) and z-scores increase back to positive values in pMCC. GLMM: significant effect of SEEDS ($F=19.103$, $df=3$, $p=4.197e-12$), ROIs ($F=28.805$, $df=15$, $p<2.2e-16$) and their interactions ($F=2782$, $df=45$, $p=6.531e-09$). **B. *Macaques*.** The 4 AMG seeds present a similar functional pattern: more ventral vmPFC ROIs present positive z-scores, then z-scores decrease reaching a negative peak in dorsal vmPFC ROIs (ROI SROSa) and z-scores increase back towards positive value in MCC ROIs. GLMM: significant effect of ROIs ($F=22.57$, $df=15$, $p<2e-16$), no effect of Seeds ($F=0.837$, $df=3$, $p=0.4736$) and a trend for Seeds*ROIs interactions ($F=1.287$, $df=45$, $p=0.097$). In both species, black lines represent significant pairwise results within seeds associated with FDR corrections.

Functional connectivity within the AMG-mPFC network in humans.

The correlation strengths between AMG nuclei (LA, BL, BM and CE seeds) and mPFC ROIs are displayed on boxplots in **Figure 2.A**. Statistical analysis using General Linear Mixed Model -GLMM- with “Seeds” and “ROIs” as fixed factors (see Methods) revealed a significant main effect of Seeds ($F(3,1197)=19.103$, $p=4.197e-12$) and an interaction between Seeds and ROIs ($F(45,1197)=2.782$, $p=6.531e-09$) pointing toward a differential FC pattern between AMG nuclei and mPFC ROIs (see **Table S1** for a complete description of the statistical results). Specifically, the FC between CE and mPFC ROIs at rest is close to zero and does not present any specific pattern. By contrast, the BL, BM and LA seeds present a U-shaped FC pattern with the various ROIs of the mPFC along a ventro-dorsocaudal axis. They display positive correlations with vmPFC ROIs (*i.e.*, from Area25 to SROSa for LA and BL, and from Area25 to CgS11 for BM), negative correlations with ACC/aMCC ROIs (from Fork32 to CgS4/CgS3), and positive correlations with pMCC ROIs (CgS3, CgS2, CgS1). Importantly, the most negative FC in the U-shaped pattern is located within mPFC ROIs CgS6 to CgS8 -part of MCCa- for LA and BM and BL seeds with a peak at ROI CgS7 (pairwise post-hoc comparisons, $p<0.05$). These results are further confirmed by the SEED-ROI pairs correlation strength comparison to 0 significantly highlighting the negative curve along ROI peak CgS7 for LA, BL and BM ($p<0.01$) and the positive correlation within vmPFC ($p<0.05$; see also Supplemental **Figure S3**). Note that results in the left hemisphere are similar to those observed for the right hemisphere and are presented in supplemental material (**Figure S1, S2**, and **Table S1**). To confirm that these correlation profiles did not depend on physical distance between Seeds and ROIs, we calculated the Euclidean distances between the different Seeds and ROIs (**Figure S5**). Results confirmed that the z-scores (displayed in **Figure 2.A**) do not strictly vary as a function of distance (**Figure S7**).

Functional connectivity within AMG-mPFC networks in awake macaques.

Correlation strengths between AMG nuclei and mPFC ROIs are displayed on boxplots in **Figure 2B**. Contrary to humans, the GLMM analysis revealed no main effect of Seeds ($F(3,225)=0.837$, $p=0.4736$) nor any strict significant interaction between Seeds and ROIs ($F(45,2225)=1.287$, $p=0.097$; see Methods, Supplementary methods and **Table S1** for details), pointing toward a similar FC pattern between all AMG nuclei and mPFC ROIs. Two main differences in macaques compared to humans were identified: 1) the 4 AMG Seeds, including CE, display a U-shape FC pattern with mPFC ROIs, and 2) macaques present a different U-shape FC pattern in which the negative FC relationship between all AMG nuclei with mPFC ROIs extended from ROIs SROSp to Fork32 -part of vmPFC- with a negative peak located at the level of ROI SROSa (**Figure 2**, see also Supplemental **Figure S4** showing SEED-ROI pairs displaying a correlation strength significantly different from 0 using one sample T.test). Within vmPFC, the most ventro-caudal ROIs (*i.e.*, ROI Area25 and SROSp) present a high positive correlation strength with all AMG nuclei similar to the one observed in humans (**Figure 2.B** and **Figure S4**). In addition, in macaques, the FC between BM and BL AMG nuclei tends to display negative functional coupling with mPFC ROIs CgS6 to CgS7, *i.e.*, with the aMCC region, although not statistically significantly different from 0 (**Figure S4**). Note that results in the left hemisphere are slightly different in macaques (**Figure S1, S2** and **Table S1**) with significant effects of the factor “Seeds” and of the Seeds-ROIs interaction, mostly driven by CE. Finally, as in humans, this gradient did not depend on mere physical distance as assessed with the Euclidean distance between each AMG nuclei and mPFC ROIs pairs for each subject (**Figure S6** and **Figure S7**).

Of note, the FC pattern observed in awake macaque monkeys with rewarded ocular fixation (**Figure 2**) is similar to observed when monkeys do not perform ocular fixation and thus do not receive any rewards (**Figure S8**). Note also that the connectivity profile between mPFC and AMG nuclei in the awake state was greatly reduced under anaesthesia (Isoflurane 1-1.5%) for the same 3 monkeys (**Figure S9** and **Figure S10**).

An FC shift between macaques and humans: a species-specific pattern?

In humans, the most negative FC was observed between CgS7 (within aMCC) and LA (-0.21 ± 0.16), BL (-0.19 ± 0.16), and BM (-0.16 ± 0.18) nuclei. In macaques, the most negative FC was observed more anteriorly: between SROSa and LA (-0.13 ± 0.20), BL (-0.08 ± 0.21), BM (-0.08 ± 0.21), and CE (-0.16 ± 0.23) nuclei. Thus, the negative FC peak, which triggers the U-shape FC gradient, differs critically between the 2 species: whereas it is located in aMCC (CgS7) in humans, it is located in the anteriormost part of vmPFC (SROSa) in macaques (**Figure 3.A**). Note that this differential functional topography between macaque and human is supported by an additional analysis assessing the FC of the whole AMG with the mPFC (**see Figure S10**). Another main difference is the FC of CE that follows the same pattern as the other nuclei in macaques but not in humans (**Figure 3.A**).

To further characterize these differences, we computed mean differences of correlation strength between each human AMG seed with mPFC ROIs (ordered from ventral-to-dorso-caudal) compared to their macaque homologues (**Figure 3B**). Results showed significant mean differences between humans and macaques regarding 1) FC between the aMCC region (CgS8 to CgS6) and both LA and BL, 2) FC between the ACC/aMCC limit (CgS9 and CgS8), and BM, BL, and LA ($p < 0.05$, FDR-corrected tests). These results confirmed a differential FC organization between humans and macaques characterized by a shift of the negative FC curve from aMCC in humans to vmPFC/ACC in macaques. In addition, it confirms a differential pattern of FC of the CE AMG nuclei between humans and monkeys (**Figures 3A and 3B**).

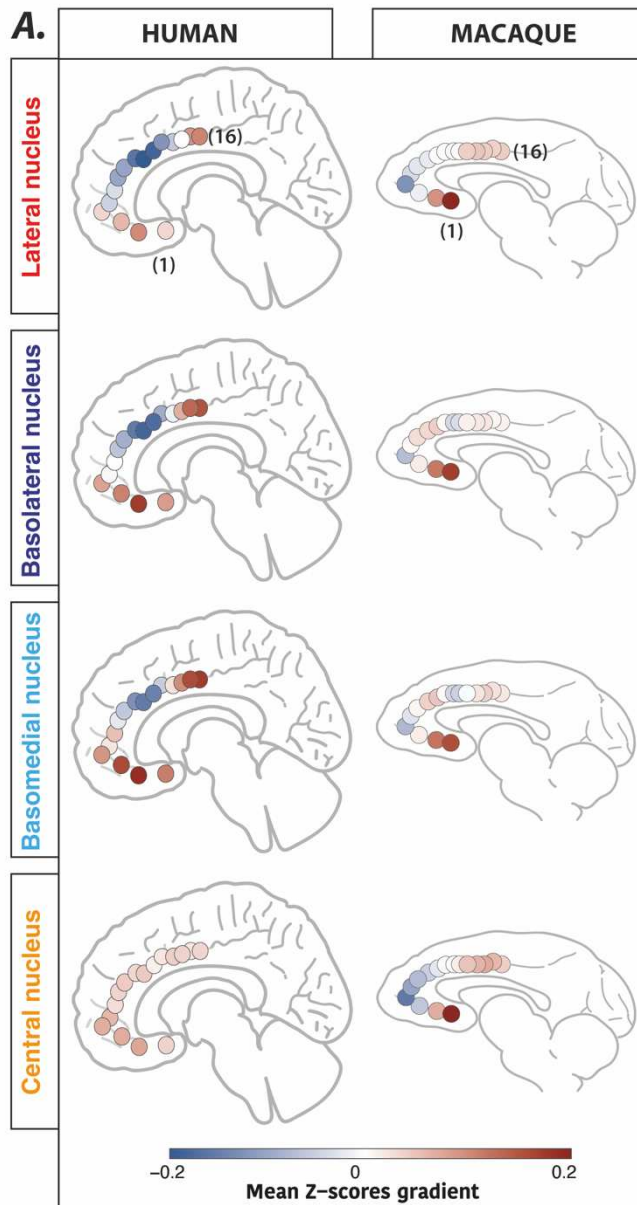
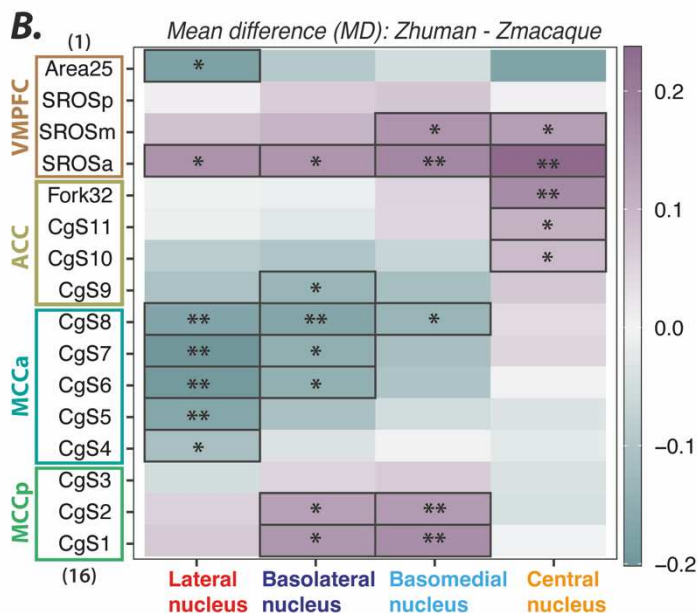


Figure 3. Comparison of functional connectivity between AMG nuclei and mPFC ROIs in macaque versus human. **A.** Mean functional FC (expressed as z-scores) for each seed with mPFC ROIs in humans (left part) and macaques (right part) on mid-sagittal views. Mean z-scores values are displayed as a positive-to-negative gradient color-coded from red-to-blue. **B.** Mean difference (MD) heatmap: $z\text{-scores}_{\text{human}} - z\text{-scores}_{\text{macaque}}$ for each seed-ROI pair. MD is color-coded from pastel cyan to purple corresponding to negative and positive differences respectively. Significant differences between species are highlighted: * for $p\text{-value} < 0.05$ and ** for $p\text{-value} < 0.01$. These results demonstrate two key differences between humans and monkeys: 1) a differential FC pattern of the CE nuclei with mPFC ROIs and 2) a differential functional coupling (positive versus negative) of mPFC ROIs with AMG nuclei, with a negative coupling in aMCC in humans and in vmPFC in macaques. These results suggest a ventral shift of the negative FC between macaques and humans.



DISCUSSION

The aim of this study was twofold: 1) to determine the functional connectivity pattern between AMG main nuclei (LA, BL, BM and CE) and mPFC regions, and 2) to identify whether and how this organization evolved between the cercopithecoid monkeys and human lineages since the split from their last common ancestor. By exploring intrinsic spontaneous low-frequency correlations in rs-fMRI signal, we show that whereas AMG activity is negatively correlated with aMCC activity in humans, it is negatively correlated with activity of the region located at the intersection between the vmPFC and the ACC in macaques. We also identified the contribution of all AMG nuclei in this pattern in both species, at the exception of the CE in humans (**Figure 2**). These data first refine our knowledge on the complex functional dialogue between AMG and mPFC in humans ^{28–32} by precisely seizing i) a FC silhouette with a positive-to-negative transition area within the aMCC and ii) the absence of contribution of the CE nucleus to this pattern. Second, it provides critical novel information of the AMG-mPFC dialogue in macaques by identifying i) a shift of the positive-to-negative transition area to the vmPFC/ACC intersection region and ii) the contribution of the CE nucleus to this pattern. Our study thus critically uncovers two key differences in the AMG-mPFC FC organization between humans and monkeys: an antero-posterior shift in the AMG dialogue with the mPFC from macaques to humans and a differential connectivity pattern of the CE nucleus, both suggesting a divergence between the two species.

Differential functional connectivity organization between AMG nuclei and mPFC and behavioral significance in humans and macaques.

To date, only a few studies have examined the functional interplay between AMG and mPFC in macaques using resting-state fMRI ^{33–35}. However, these studies did not capture the fine-grained organization of this interplay because of 2 main factors: 1) they considered the AMG as a whole and not the AMG nuclei separately, and 2) they have been carried out under anaesthesia, which has been shown to strongly affect frontal cortical FC ²⁵. However, the observed functional dialogue could be supported by the known structural connectivity in macaques ^{36–38}. Indeed, tract-tracing studies have shown that the most caudal part of vmPFC (Area25) and the MCC are densely connected to AMG nuclei, while the rostral part of vmPFC (SROSa) and the

ACC share lesser anatomical connections with AMG nuclei. The presence of a U-shape FC pattern, characterized by negative functional coupling with AMG nuclei uncovered in our study, may therefore reflect the specific known structural connectivity between these regions ³⁹, featuring the existence of a transitional zone in the rostral part of vmPFC (SROSa) in macaques.

By contrast, our results show that, in humans, this vmPFC region displays a positive functional coupling with 3 AMG nuclei (LA, BL and BM). This result may appear surprising given that MRI tractography studies have suggested that fiber tracts between the AMG and the mPFC seem to be preserved between humans and monkeys at the macroscopic level ^{40,41}. However, this latter finding should be taken cautiously ^{42,43}. Indeed, contrary to macaques, our knowledge of the detailed structural connectivity at the microscopic level in this network in humans is lacking, preventing direct comparisons between structural connectivity at the microscopic level and functional relationships.

Importantly, the differences between humans and macaques observed in the present study find support in the known structural differences both in the mPFC and the AMG. First, the assessment of the evolution of the sulcal organization of the mPFC in the primate order has revealed that the only mPFC region that displays a strong evolution is the transition between vmPFC/ACC region ²⁰. This is precisely where we identified the main difference between species. Second, the total volume of AMG and its nuclei evolved in the primate order ^{16–19,44}; the largest expansion was found in the LA nucleus, occupying the major portion of the AMG in humans, compared to great apes ¹⁷ and macaques ^{16,18} where the BL nucleus presents the largest volume ^{16,19}. It is thus reasonable to suggest that with an increasing volume and neuron number in humans, the AMG might display more intricate connections with mPFC regions, resulting in a differential functional interplay between AMG nuclei and mPFC ⁴⁵.

In human adults, the MCC is known to exert a strong top-down control onto the AMG ⁴⁶. Importantly, this top-down control is acquired during development. From childhood to adolescence and early adulthood, a shift from bottom-up (AMG to mPFC) to top-down regulatory processes has been described ^{47–50}. Indeed, AMG responses decrease concomitantly with the emergence of stronger top-down influences from mPFC during adolescence that further strengthen in adulthood compared to childhood in response to fearful faces ⁵⁰. This is in line with our findings in adult humans identifying negative FC between ACC/aMCC and AMG nuclei BM/LA/BL at rest (**Figures 2.A** and

3.A). In adult rhesus macaques, this negative FC pattern was shifted ventrally in the vmPFC/ACC (**Figure 2.B** and **Figure 3.A**) for the 4 AMG nuclei, including the CE nucleus. Based on these results, it is reasonable to hypothesize that the source of top-down control might be different in humans (*i.e.*, the aMCC) and in macaques (*i.e.*, the vmPFC/ACC limit), and this shift might reflect differential regulatory processes in adaptive behaviors. Adult macaques *rhesus* are characterized by specific behavioral traits such as aggressiveness and impulsivity⁵¹ that are greatly reduced following AMG lesions⁵²⁻⁵⁴. It is thus reasonable to hypothesize that, compared to humans, a reduced top-down regulatory control exerted onto the AMG leads to higher AMG reactivity associated with higher emotional responsiveness in macaques.

It is important to highlight that the identification of a differential fine-grained FC pattern in the AMG-mPFC network in macaques and humans could be unveiled thanks to the sulcal-based positioning of homologous mPFC ROIs in both species. Indeed, recent advances have revealed a remarkably similar sulcal mPFC organization in the macaque and human brains that allows the identification of homologous regions^{20,55}.

Differential contribution of the CE nucleus in the AMG-mPFC functional dialogue in humans and macaques.

In humans, contrary to macaques, the FC of the CE nucleus at rest was close to zero and did not present any specific pattern with mPFC regions. Based on anatomical evidence, a differential functional dialogue of the CE on one hand and of BL/BM/LA on the other hand would be expected. First, during ontogeny, the CE does not originate from the same structure as BL/BM/LA, opposing a pallial versus a subpallial origins^{26,56}. Second, these different developmental origins may thus explain their differential structural -and consequently functional- connections: contrary to BL/BM/LA, CE shares only very weak structural connections with the mPFC and is rather mostly connected to autonomic centers such as brainstem and hypothalamus¹⁰. Third, the CE nucleus is thought to be the mostpreserved AMG nucleus during evolution in terms of morphology (*i.e.*, volume, neuron numbers etc.)¹⁶.

However, the connectivity and function of the CE nucleus in the primate order may have evolved. Indeed, the CE nucleus is part of the extended amygdala, *i.e.*, one of the main substrates for defensive behavior (*i.e.*, avoidance-approach responses)⁵⁷. It has also been shown to be susceptible to stressful environmental influences during development⁵⁸ and involved in anxious and stress-related behaviors as its removal

reduced stressed/anxious responses in macaques ⁵³. Importantly, in their specific ecological niches, humans and macaques do not face the same environmental challenges (e.g., less food availability issues, lack of predators in humans compared to macaques, etc.). Accordingly, macaques are constantly on high alert, balancing predator vigilance, within-group vigilance, and the need to access food ⁵⁹. Consequently, we hypothesize that the CE-mPFC FC pattern observed in macaques -as opposed to humans- may be driven by stronger bottom-up excitatory inputs (AMG to mPFC) and reduced top-down regulation from mPFC onto the AMG, stemming in particular from the expansion of the vmPFC/ACC region. This functional divergence between macaques and humans may relate to the inherent characteristics of their respective ecological niches. As the CE does not display direct connections with the mPFC ¹⁰, its contribution to the AMG-mPFC FC in macaques may depend on its indirect functional connectivity, involving or not the autonomous centers.

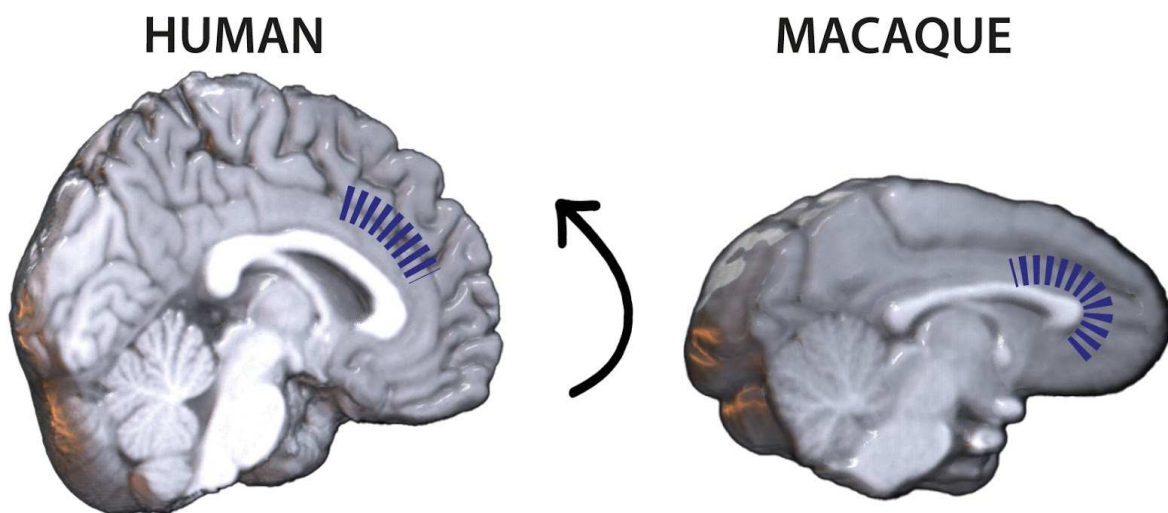


Figure 4. Schematical representation of the functional dialogue between AMG nuclei and mPFC regions in human and macaque. Blue dashed lines represent the extent of negative functional correlations between AMG nuclei and mPFC regions on structural brain images in human (right) and macaque (left). We identified a dorsal shift (represented by the arrow) in the functional gradient from vmPFC to aMCC from macaque to human, that might reflect structural differences governing bottom-up and top-down regulatory processes essential for flexible behavioral adaptation to the ecological niche.

Limitations

First, although our results display similar FC profiles in the AMG-mPFC network in macaques engaged in i) an ocular fixation task in which they received rewards or ii) not engaged in such a task (i.e., sleepy runs, see **Figures 2, 3 and S8**), humans were

by contrast engaged only in an ocular fixation task without receiving rewards. While our results in macaques suggest that the FC pattern in the AMG-mPFC network is not affected by the context of juice reward and ocular fixation, a final statement regarding any impact of the reward on this FC pattern would require the use of the exact same protocol in both humans and macaques (*i.e.*, adding reward in the human protocol or removing it in the macaque protocol).

Second, one may hypothesize that the lack of contribution of the CE nucleus to the U-shape FC in the AMG-mPFC network in humans could be attributed to the limited number of voxels of this nucleus and/or, more generally, to the different numbers of voxels included in the seeds versus the ROIs. While we cannot rule out this hypothesis, we deemed it unlikely. Indeed, in human brains, AMG seeds are smaller than the mPFC ROIs, but the 3 nuclei contributing equally to the U-shape FC pattern (LA, BL, BM) display different numbers of voxels. In addition, the number of voxels in the human CE nucleus is not significantly different from the BM nucleus (in the right hemisphere: 80mm³ vs. 110mm³, **Table S2**), the latest being extensively involved in the U-shape FC pattern. Furthermore, in macaque brains, with the exception of the CE nucleus, the volume and number of voxels in the AMG seeds are similar to those in the mPFC ROIs, strongly suggesting that voxel size does not significantly impact the FC pattern in the AMG-mPFC network (**Table S3**). Of note, the CE nucleus, *i.e.*, which displays the smallest number of voxels, is the nucleus exhibiting the strongest contribution to the U-shape FC pattern in macaques.

Conclusions

The present study identified a differential functional interplay between AMG nuclei and mPFC subregions between humans and macaques (see Summary in **Figure 4**) that may reflect structural differences governing bottom-up and top-down regulatory processes in response to changes in internal and external milieu, thus triggering differential adaptive behaviors appropriately to their respective socio-ecological niche. Future studies employing fine-grained effective connectivity in both species may help better understand the complex functional interplay within this network at the heart of behavioral adaptation ⁵⁰ and identify whether and how the connectivity of the CE nucleus have evolved differently in the old-world monkeys and human lineages.

METHODS

Participants

Humans. Twenty healthy subjects participated in the resting-state fMRI experiment (14 F and 6 M; age 25.6 ± 5.3) and received monetary compensation at the end of the session. The study was approved by a national ethics committee in biomedical research (Comité de Protection des Personnes (CPP) Sud-Est III, authorization ID: 2015-A00897-42 and 2018-A00405-50). It also received Clinical Trial Numbers (NCT03119909 and NCT03483233, see <https://clinicaltrials.gov>). Because the ventro-dorsal extent of the cingulate cortex in humans depends on the presence or not of a paracingulate sulcus (PCGS, presents in about 70% of subjects in at least one hemisphere ⁶⁰), we selected subjects based on this morphological feature in order to obtain a sample in which 50% of both left and right hemispheres presented a PCGS, and 50% did not.

Rhesus macaques. Three rhesus monkeys (*Macaca mulatta*) were included in the study (2 F: Monkeys C, 21 yo and N 9.5 yo and 1 M: Monkey L, 9.5 yo; weight 5 - 8 kg). Animals were maintained on a water and food regulation schedule, individually tailored to maintain a stable level of performance for each monkey. All procedures follow the guidelines of European Community on animal care (European Community Council, Directive No. 86–609, November 24, 1986) and were approved by French Animal Experimentation Ethics Committee #42 (CELYNE).

Rs-fMRI data acquisition

Scanning was performed on a 3T Siemens Magnetom Prisma MRI Scanner (Siemens Healthcare, Germany). Details of the procedure can be found in **Table 1** of the supplemental materials.

Humans. Rs-fMRI runs lasted 10min. Subjects were instructed to keep still and maintain fixation on a white cross presented at the center of the screen. Data were acquired with a T2* weighted multiband and multi-echo (ME) sequence: TR = 1500ms, TE1=16.4ms, TE2=37.59 ms, TE3=58.78 ms, voxel size = 2.5 mm³. We collected 1 runs of rs-fMRI (400 TRs) for each subject. An anatomical MRI was also obtained (see **Table 1**).

Rhesus macaques. Rs-fMRI runs lasted 13min. Subjects were trained to maintain fixation on a white cross presented on the center of the screen in order to receive a

liquid reward through the runs. Data were acquired with a T2* weighted gradient echo planar sequence: TR = 1800ms, TE=16.4ms, voxel size = 1.8 mm³. We collected 12 runs of rs-fMRI (400 TRs/run) for each subject (Table 1 for details). A high-resolution anatomical MRI was also acquired in a different session where macaques were maintained under anaesthesia with Isoflurane 1-1.5%. During this anaesthetized session, we also acquire 4 resting-state functional runs for the 3 macaque monkeys (see supplementary data, supplementary method section and **Figure S9 and S10**).

MRI Acquisition parameters		
Species	Human	Rhesus macaque
Sample	n=20	n=3
MRI Scanner	3T Siemens Magnetom Prisma	
<i>rs-fMRI sequence: T2*-weighted gradient echo planar EPI images</i>		
Slices	51	30
Spatial voxel resolution	2.5mm ³	1.8mm ³
Temporal resolution (TR)	1.5s	1.8s
Echo times (TE)	TE ₁ =16.4ms TE ₂ =37.59ms TE ₃ =58.78ms	TE=27ms
Volumes	400 vol/run	400 vol/run
Number of Runs	1/subject	12/subject
<i>T1 weighted MPRAGE sequence: anatomical scans</i>		
Slices	244	144
Spatial voxel resolution	0.8mm ³	0.5mm ³
Temporal resolution (TR)	3s	3s

Table 1. MRI acquisition parameters for humans and awake rhesus macaques. High-resolution anatomical scans were acquired in macaques under anaesthesia in a different session.

Awake macaque experimental setting

Briefly, macaque monkeys were first trained in a mock-scanner setting in an MRI compatible chair before the headpost surgery. After the surgery and recovery period,

they were trained head-fixed in the same condition before going to the MRI. These steps are further developed below.

Headpost surgical procedure. To limit head motion, macaque monkeys were head-fixed during MRI acquisition. They were first surgically implanted with a PEEK MR-compatible head post (Rogue Research, CA) under aseptic conditions. Animals were sedated prior to intubation (tiletamine and zolazepam, Zoletil 7mg/kg) and then maintained under gas anaesthesia with a mixture of O₂ and air (isoflurane 1-2%). After an incision of the skin along the skull midline, the head fixation device was positioned under stereotaxic guidance on the skull and maintained in place using ceramic sterile screws (Thomas RECORDING products) and acrylic dental cement (Palacos® Bone cements). Throughout the surgery, heart rate, respiration rate, blood pressure, expired CO₂, and body temperature were continuously monitored. Analgesic and antibiotic treatment were administered for 5 days postoperatively and a recovery period of at least 1 month was observed after the surgery.

Experimental setup. The setup is detailed in Giacometti et al. 2022²⁵. Shortly, before the scanning session, macaques were trained head-fixed in a mock scanner mimicking the actual MRI environment in an MRI compatible plastic chair (Rogue Research). They were trained to fixate a central cross for long periods of time using positive reinforcement learning (juice-reward). During the scanning sessions, eye position was monitored using an eye-tracking system (Eyelink, SR research). The calibration procedure involved a central point and 4 additional points (up, down, left, right, 5° eccentricity), presented sequentially in the same plane as the fixation cross. Throughout the rs-fMRI sessions, monkeys were required to fixate a central cross on the screen (4x4°) in order to receive liquid reward through a plastic tube placed in their mouth. In the reward schedule and to promote long periods of fixation, the frequency of reward delivery increased as the duration of fixation increased⁶¹. The mean time with eyes open across runs was, respectively, 69%, 69%, and 84% for Monkeys L, N, and C. Within this time, the percentage of fixation varied from 36% to 69%, 2% to 58%, and 5% to 98% for Monkeys L, N, and C, respectively.

During scanning sessions, we also collected several runs in which Monkey L (6 runs) and N (4 runs) did not perform ocular fixation (eyes close/sleepy, eyes wandering etc.) resulting in no rewards delivery. In our previous paper²⁵, we showed that the juice reward associated with ocular fixation did not impact the FC pattern of frontal cortical networks. We found similar results within the AMG-mPFC network, suggesting

stable FC within this network under different task conditions (**Figure S8**, supplemental data).

Seeds and ROIs selections

The main goal of the rs-fMRI analyses was to investigate the FC pattern between AMG nuclei and mPFC in humans and macaques. Our analysis focuses on the ipsilateral functional connectivity of the 4 main AMG nuclei, Central (CE), Basolateral (BL), Basomedial (BM), and Lateral (LA), chosen as our seed regions, and 16 mPFC regions chosen as our ROIs located in the vmPFC, ACC and MCC. Location of Seeds and ROIs are displayed on **Figure 1** for humans and macaque monkeys in both hemispheres. For both species, we also provide SEEDS and ROIs masks volume and number of voxels included in supplemental data (**Table S2** for humans and **Table S3** for macaques).

Amygdala seeds. The four main AMG nuclei masks were extracted from Tyszka and Pauli (2016)²⁷ atlas for humans and from the Subcortical Atlas of the Rhesus Macaque (SARM) atlas for macaques²⁶. **LA** is situated on the lateral part of the AMG complex and is ventrally and caudally bounded by the temporal horn of the lateral ventricle and laterally by temporal lobe white matter. **BL** is bounded laterally by LA. In humans, in the Tyszka and Pauli (2016) atlas²⁷, the BL nucleus mask comprises both BL and paralaminar nucleus. Therefore, we also combined these nuclei in macaques. **BM** is located medially to BL. **CE** lies dorsally and caudally within the AMG complex.

Medial Prefrontal Cortex ROIs. mPFC ROIs were precisely positioned based on local anatomical sulcal landmarks in both individual human and macaque subjects²⁰. Indeed, the sulcal pattern in the mPFC is preserved in the primate order and allows to infer homologies between primate species^{20,55}. Moreover, to account for differences in brain size across species, ROI dimensions were adjusted to a radius of 6mm and 2.5mm for humans and macaques, respectively (**Figure 1**). Indeed, the antero-posterior extent of the human brain in the MNI template is 175 mm (<https://www.bic.mni.mcgill.ca/ServicesAtlases/ICBM152NLin2009>) and of the macaque brain in the NMT template is 72 mm (https://afni.nimh.nih.gov/pub/dist/doc/html/doc/nonhuman/macaque_tempatl/template_nmtv2.html,⁶²). The radius of each mPFC ROIs being 6 mm in humans, we thus used a radius of 2.5 mm in macaques to conserve the proportions (*i.e.*, $6 \cdot 72 / 175 = 2.5$). Specifically, ROIs were positioned along the ventro-dorsocaudal axis of the

corpus callosum (CC). In the ventral portion of mPFC below the corpus callosum, the **vmPFC** includes 4 ROIs: Area25 (localized in the Brodman area 25), SROSp, SROSm, and SROSa. SROS ROIs are named after the Superior Rostral Sulcus. The prefix p, m and a, respectively corresponding to posterior, medial and anterior part of SROS. Rostrally to the genu of the corpus callosum, the **ACC** includes 4 ROIs. Fork 32 located just in front to the fork situated at the rostral end of CGS formed by the supra-rostral sulcus (SU-ROS) and the supra-orbital sulcus (SOS), presumably occupied by area 32. It also includes several ROIs within the cingulate sulcus (CgS): CgS11, CgS10, and CgS9. Posteriorly to the genu of the genu of corpus callosum, the **MCC** includes 8 ROIs: CgS8, CgS7, CgS6, CgS5, CgS4 in the **amMCC** and CgS3, CgS2, CgS1 in the **pMCC**. In humans, cingulate ROIs cover both banks of the cingulate sulcus and the paracingulate sulcus (PCGS) if present. While not present in the macaque brains, a PCGS is present in 70% of subjects in at least one hemisphere in humans^{20,55}. Note that when a PCGS was present, for a given ROI, two spheres were positioned on both CGS and PCGS and averaged to form one ROI (supplemental material **Figure S11**: PCGS ROIs localization in both hemispheres).

Data preprocessing

Data analysis was performed using SPM12, AFNI⁶³, FSL⁶⁴ and R.

Humans. The first 5 volumes of each run were removed to allow for T1 equilibrium effects. Slice timing correction for multiband sequences was then applied and TEDANA package 56 was used to combine the 3 echo time series and to perform motion correction. The combined data is decomposed via, first, a principal component analysis (PCA) and second, an independent component analysis (ICA). TE-dependent components are classified as BOLD signal, while TE-independent components are classified as non-BOLD signal, and are discarded. For more information, please check TEDANA community page: <https://zenodo.org/record/4509480#.YmEnNy8RqJ8>^{65–67}. Functional and anatomical images were then spatially normalized into standard MNI space.

Macaques. The first 5 volumes of each run were removed to allow for T1 equilibrium effects. First, we performed a slice timing correction using the time center of the volume as reference. The head motion correction was then applied using rigid body realignment. Then, images were skull-stripped using the bet tool from the FSL software (<https://fsl.fmrib.ox.ac.uk/fsl/fslwiki/BET>). Using the AFNI and FSL softwares

^{63,64}, the segmentation of each brain of each session was performed on skull-stripped brains. To ensure optimized inter-session and inter-subject comparisons, both anatomical and functional images were registered in the NMT v2 template space ⁶² to 1) ensure optimized inter-session and inter-subject comparisons and 2) use SARM atlas ²⁶ for AMG parcellation.

Note that for both species, the registration of individual macaque and human brains to their respective template has been carefully checked individually for each human and macaque monkey subject.

Functional connectivity pattern analysis in humans and macaques.

For both species, a temporal filtering was applied to extract the spontaneous slowly fluctuating brain activity (0.01–0.1Hz). Linear regression was used to remove nuisance variables (the six parameter estimates for head motion, the cerebrospinal fluid and white matter signal from brain segmentation). Finally, a spatial smoothing with a 6-mm and a 4-mm full-width half maximum (FWHM) Gaussian kernel, for humans and macaques respectively, was applied to the output of the regression.

For each subject in each run, each species, and each hemisphere, we computed the averaged correlation coefficient between the 4 AMG nuclei's activity and the activity of each of the 16 mPFC ROIs using Pearson correlation scores. Those correlation scores were then normalized using the Fisher r-to-z transform formula. In order to characterize the FC organization pattern for each seed and for each separately, we computed a global General Linear Mixed Model (GLMM, lsmeans package <https://cran.r-project.org/web/packages/lsmeans/lsmeans.pdf>). GLMM were built for each species and for each hemisphere separately with "SEEDS" and "ROIs" as main factor and "SUBJECT" as a random factor. In humans, "PCGS" factor was added as a random factor (1 | PCGS). In macaques, we added "RUN" as a random factor (1 | RUN). To account for inter-run variability for each subject, we added as random factor the effect of "RUN" within "SUBJECT": (1 | SUBJECT:RUN). Main GLMM effects are displayed for each species in **Table S1** (Supplementary data). GLMM were followed by post-hoc pairwise comparisons to assess for any differences/similarities in correlation strength between each Seed-ROIs pair. In addition, and to better characterize the functional peaks observed in the previous results, each SEED-ROI pair correlation strength was compared to 0 using a one sample Student test for each species and in each hemisphere (**Figure S3** and **S4**). All

p values were adjusted with False Discovery Rate (FDR) correction for multiple comparisons with an alpha level set to 0.05 for both humans and macaques.

We also analyze AMG FC connectivity with mPFC ROIs by merging and averaging the 4 AMG nuclei SEEDs for each species. Results are displayed in supplementary data in **Figure S10**. Note that we did not test for any inter-hemispheric differences given our small number of macaque subjects. Hence the statistics were carried out for each hemisphere separately in both humans and monkey to allow inter-species comparisons.

We calculated Euclidean distances (ED) as a measure of physical distance between each AMG seed and mPFC ROIs for both species. EDs were computed using the x, y and z coordinates for each subject in accordance with their local morphology (**Figure S5** for humans and **Figure S6** for macaques). We also expressed the Z-scores as a function of ED to examine possible correlation linking physical distance and FC. Results are displayed in supplemental data (**Figure S7**) and show that in both species the ED does not predict the Z-score values.

Inter-species comparison. We computed the mean z-score for each Seed-ROI pair and displayed it as color-coded heatmaps on brain schemas. The red-blue gradient corresponds to positive-to-negative z-score values, respectively (**Figure 3.A**). To compare the AMG-mPFC FC patterns in both species, we computed the statistical mean difference (MD) between humans and macaques for each Seed-ROI pair and compared them with two-sided student tests (**Figure 3.B**). Humans were used as the reference group.

Data availability

The authors declare that the data supporting the findings of this study are available within its supplementary information files (Datasets S1 and S2).

References

1. Juechems, K. *et al.* A Network for Computing Value Equilibrium in the Human Medial Prefrontal Cortex. *Neuron* **101**, 977-987.e3 (2019).
2. Gothard, K. M. Multidimensional processing in the amygdala. *Nat Rev Neurosci* **21**, 565–575 (2020).
3. Janak, P. H. & Tye, K. M. From circuits to behaviour in the amygdala. *Nature* **517**, 284–292 (2015).

4. Jiang, Y., Tian, Y. & Wang, Z. Causal Interactions in Human Amygdala Cortical Networks across the Lifespan. *Sci Rep* **9**, 1–11 (2019).
5. Morawetz, C., Bode, S., Baudewig, J. & Heekeren, H. R. Effective amygdala-prefrontal connectivity predicts individual differences in successful emotion regulation. *Soc Cogn Affect Neurosci* **12**, 569–585 (2017).
6. Murray, E. A. & Fellows, L. K. Prefrontal cortex interactions with the amygdala in primates. *Neuropsychopharmacology* 1–17 (2021) doi:10.1038/s41386-021-01128-w.
7. Saez, A., Rigotti, M., Ostojic, S., Fusi, S. & Salzman, C. D. Abstract Context Representations in Primate Amygdala and Prefrontal Cortex. *Neuron* **87**, 869–881 (2015).
8. Salzman, C. D. & Fusi, S. Emotion, cognition, and mental state representation in amygdala and prefrontal cortex. *Annu Rev Neurosci* **33**, 173–202 (2010).
9. Putnam, P. T. & Gothard, K. M. Multidimensional neural selectivity in the primate amygdala. *eNeuro* **6**, 1–13 (2019).
10. Aggleton, J. P. *The amygdala: a functional analysis*. (Oxford University Press, 2000).
11. Amiez, C., Joseph, J. P. & Procyk, E. Anterior cingulate error-related activity is modulated by predicted reward. *European Journal of Neuroscience* **21**, 3447–3452 (2005).
12. Amiez, C., Sallet, J., Procyk, E. & Petrides, M. Modulation of feedback related activity in the rostral anterior cingulate cortex during trial and error exploration. *Neuroimage* **63**, 1078–1090 (2012).
13. Quilodran, R., Rothé, M. & Procyk, E. Behavioral Shifts and Action Valuation in the Anterior Cingulate Cortex. *Neuron* **57**, 314–325 (2008).
14. Grabenhorst, F. & Rolls, E. T. Value, pleasure and choice in the ventral prefrontal cortex. *Trends Cogn Sci* **15**, 56–67 (2011).
15. Wittmann, M. K. *et al.* Predictive decision making driven by multiple time-linked reward representations in the anterior cingulate cortex. *Nat Commun* **7**, (2016).
16. Chareyron, L. J., Banta Lavenex, P., Amaral, D. G. & Lavenex, P. Stereological analysis of the rat and monkey amygdala. *J Comp Neurol* **519**, 3218–3239 (2011).
17. Barger, N. *et al.* Neuronal populations in the basolateral nuclei of the amygdala are differentially increased in humans compared with apes: A stereological study. *J Comp Neurol* **520**, 3035–3054 (2012).
18. Carlo, C. N., Stefanacci, L., Semendeferi, K. & Stevens, C. F. Comparative analyses of the neuron numbers and volumes of the amygdaloid complex in Old and New World primates. *J Comp Neurol* NA-NA (2009) doi:10.1002/cne.22264.
19. Barger, N., Stefanacci, L. & Semendeferi, K. A comparative volumetric analysis of the amygdaloid complex and basolateral division in the human and ape brain. *Am J Phys Anthropol* **134**, 392–403 (2007).
20. Amiez, C. *et al.* Sulcal organization in the medial frontal cortex provides insights into primate brain evolution. *Nat Commun* **10**, (2019).
21. Biswal, B., Zerrin Yetkin, F., Haughton, V. M. & Hyde, J. S. Functional connectivity in the motor cortex of resting human brain using echo-planar mri. *Magn Reson Med* **34**, 537–541 (1995).
22. Chen, L. M. *et al.* Biophysical and neural basis of resting state functional connectivity: Evidence from non-human primates. *Magn Reson Imaging* **39**, 71–81 (2017).
23. Barron, H. C., Mars, R. B., Dupret, D., Lerch, J. P. & Sampaio-Baptista, C. Cross-species neuroscience: closing the explanatory gap. *Philosophical Transactions of the Royal Society B: Biological Sciences* **376**, 20190633 (2021).

24. Friedrich, P. *et al.* Imaging evolution of the primate brain: the next frontier? *Neuroimage* **228**, 117685 (2021).
25. Giacometti, C. *et al.* Frontal cortical functional connectivity is impacted by anaesthesia in macaques. *Cerebral Cortex* **32**, 4050–4067 (2022).
26. Hartig, R. *et al.* The Subcortical Atlas of the Rhesus Macaque (SARM) for neuroimaging. *Neuroimage* **235**, 117996 (2021).
27. Tyszka, J. M. & Pauli, W. M. In vivo delineation of subdivisions of the human amygdaloid complex in a high-resolution group template. *Hum Brain Mapp* **37**, 3979–3998 (2016).
28. Amunts, K. *et al.* Cytoarchitectonic mapping of the human amygdala, hippocampal region and entorhinal cortex: intersubject variability and probability maps. *Anat Embryol (Berl)* **210**, 343–352 (2005).
29. Roy, A. K. *et al.* Functional connectivity of the human amygdala using resting state fMRI. *Neuroimage* **45**, 614–626 (2009).
30. Kerestes, R., Chase, H. W., Phillips, M. L., Ladouceur, C. D. & Eickhoff, S. B. Multimodal evaluation of the amygdala's functional connectivity. *Neuroimage* **148**, 219–229 (2017).
31. Zhang, X. *et al.* Individualized Functional Parcellation of the Human Amygdala Using a Semi-supervised Clustering Method: A 7T Resting State fMRI Study. *Front Neurosci* **12**, (2018).
32. Klein-Flügge, M. C. *et al.* Relationship between nuclei-specific amygdala connectivity and mental health dimensions in humans. *Nat Hum Behav* (2022) doi:10.1038/s41562-022-01434-3.
33. Neubert, F.-X., Mars, R. B., Sallet, J. & Rushworth, M. F. S. Connectivity reveals relationship of brain areas for reward-guided learning and decision making in human and monkey frontal cortex. *Proceedings of the National Academy of Sciences* **112**, E2695–E2704 (2015).
34. Folloni, D. *et al.* Manipulation of Subcortical and Deep Cortical Activity in the Primate Brain Using Transcranial Focused Ultrasound Stimulation. *Neuron* **101**, 1109–1116.e5 (2019).
35. Reding, K. M. *et al.* Effects of social subordination and oestradiol on resting-state amygdala functional connectivity in adult female rhesus monkeys. *J Neuroendocrinol* **32**, (2020).
36. Ghashghaei, H. T., Hilgetag, C. C. & Barbas, H. Sequence of information processing for emotions based on the anatomic dialogue between prefrontal cortex and amygdala. *Neuroimage* **34**, 905–923 (2007).
37. Ghashghaei, H. T. & Barbas, H. Pathways for emotion: Interactions of prefrontal and anterior temporal pathways in the amygdala of the rhesus monkey. *Neuroscience* **115**, 1261–1279 (2002).
38. Sharma, K. K., Kelly, E. A., Pfeifer, C. W. & Fudge, J. L. Translating Fear Circuitry: Amygdala Projections to Subgenual and Perigenual Anterior Cingulate in the Macaque. *Cerebral Cortex* **30**, 550–562 (2020).
39. Straathof, M., Sinke, M. R. T., Dijkhuizen, R. M. & Otte, W. M. A systematic review on the quantitative relationship between structural and functional network connectivity strength in mammalian brains. *Journal of Cerebral Blood Flow and Metabolism* **39**, 189–209 (2019).
40. Barrett, R. L. C. *et al.* Differences in frontal network anatomy across primate species. *Journal of Neuroscience* **40**, 2094–2107 (2020).

41. Thiebaut de Schotten, M., Dell'Acqua, F., Valabregue, R. & Catani, M. Monkey to human comparative anatomy of the frontal lobe association tracts. *Cortex* **48**, 82–96 (2012).
42. Sarwar, T., Ramamohanarao, K. & Zalesky, A. A critical review of connectome validation studies. *NMR in Biomedicine* vol. 34 Preprint at <https://doi.org/10.1002/nbm.4605> (2021).
43. Yendiki, A. *et al.* Post mortem mapping of connectional anatomy for the validation of diffusion MRI. *Neuroimage* **256**, (2022).
44. Stephan, H., Frahm, H. D. & Baron, G. Comparison of brain structure volumes in Insectivora and primates. VII. Amygdaloid components. *J Hirnforsch* **28**, 571–584 (1987).
45. Pryluk, R., Kfir, Y., Gelbard-Sagiv, H., Fried, I. & Paz, R. A Tradeoff in the Neural Code across Regions and Species. *Cell* **176**, 597-609.e18 (2019).
46. Constantinidis, C. & Luna, B. Neural Substrates of Inhibitory Control Maturation in Adolescence. *Trends Neurosci* **42**, 604–616 (2019).
47. Gee, D. G. *et al.* A developmental shift from positive to negative connectivity in human amygdala-prefrontal circuitry. *Journal of Neuroscience* **33**, 4584–4593 (2013).
48. Tottenham, N. Social scaffolding of human amygdala-mPFC circuit development. *Soc Neurosci* **10**, 489–499 (2015).
49. Silvers, J. A. *et al.* VIPFC-vmPFC-Amygdala Interactions Underlie Age-Related Differences in Cognitive Regulation of Emotion. *Cerebral Cortex* **27**, 3502–3514 (2017).
50. Gee, D. G. *et al.* Experimental evidence for a child-to-adolescent switch in human amygdala-prefrontal cortex communication: A cross-sectional pilot study. *Dev Sci* 1–16 (2022) doi:10.1111/desc.13238.
51. Thierry, B., Mewa, S. & Kaumanns, W. *Macaque societies: A model for study of Social Organization*. vol. 41 (Cambridge University Press, 2010).
52. Emery, N. J. *et al.* The effects of bilateral lesions of the amygdala on dyadic social interactions in rhesus monkeys (*Macaca mulatta*). *Behavioral Neuroscience* **115**, 515–544 (2001).
53. Kalin, N. H. The Role of the Central Nucleus of the Amygdala in Mediating Fear and Anxiety in the Primate. *Journal of Neuroscience* **24**, 5506–5515 (2004).
54. Elorette, C., Aguilar, B. L., Novak, V., Forcelli, P. A. & Malkova, L. Dysregulation of behavioral and autonomic responses to emotional and social stimuli following bidirectional pharmacological manipulation of the basolateral amygdala in macaques. *Neuropharmacology* **179**, 108275 (2020).
55. Amiez, C. *et al.* A revised perspective on the evolution of the lateral frontal cortex in primates. *Sci Adv* **9**, (2023).
56. Medina, L., Bupesh, M. & Abellán, A. Contribution of genoarchitecture to understanding forebrain evolution and development, with particular emphasis on the amygdala. *Brain Behav Evol* **78**, 216–236 (2011).
57. Holley, D. & Fox, A. S. The central extended amygdala guides survival-relevant tradeoffs: Implications for understanding common psychiatric disorders. *Neuroscience and Biobehavioral Reviews* vol. 142 Preprint at <https://doi.org/10.1016/j.neubiorev.2022.104879> (2022).
58. Fox, A. S. *et al.* Central amygdala nucleus (Ce) gene expression linked to increased trait-like Ce metabolism and anxious temperament in young primates. *Proc Natl Acad Sci U S A* **109**, 18108–18113 (2012).

59. Treves, A. Theory and method in studies of vigilance and aggregation. *Anim Behav* **60**, 711–722 (2000).
60. Amiez, C. *et al.* The location of feedback-related activity in the midcingulate cortex is predicted by local morphology. *Journal of Neuroscience* **33**, 2217–2228 (2013).
61. Hadj-Bouziane, F. *et al.* Amygdala lesions disrupt modulation of functional MRI activity evoked by facial expression in the monkey inferior temporal cortex. *Proc Natl Acad Sci U S A* **109**, E3640–E3648 (2012).
62. Jung, B. *et al.* A comprehensive macaque fMRI pipeline and hierarchical atlas. *Neuroimage* **235**, 117997 (2021).
63. Cox, R. W. AFNI: Software for analysis and visualization of functional magnetic resonance neuroimages. *Computers and Biomedical Research* **29**, 162–173 (1996).
64. Jenkinson, M., Beckmann, C. F., Behrens, T. E. J., Woolrich, M. W. & Smith, S. M. FSL - Review. *Neuroimage* **62**, 782–90 (2012).
65. DuPre, E. *et al.* TE-dependent analysis of multi-echo fMRI with tedana. *J Open Source Softw* **6**, 3669 (2021).
66. Kundu, P., Inati, S. J., Evans, J. W., Luh, W. M. & Bandettini, P. A. Differentiating BOLD and non-BOLD signals in fMRI time series using multi-echo EPI. *Neuroimage* **60**, 1759–1770 (2012).
67. Kundu, P. *et al.* Integrated strategy for improving functional connectivity mapping using multiecho fMRI. *Proc Natl Acad Sci U S A* **110**, 16187–16192 (2013).

Acknowledgments

This work was supported by the French National Research Agency (ANR-18-CE37-0012-01 to C.A, ANR-15-CE37-0003 to F.H.-B.). We thank Gislène Gardechaux for technical assistance in training awake macaques. We also thank Danielle Ibarrola for technical help in acquiring neuroimaging data in awake macaques and humans. C.A., E.P., and C.R.E. were also supported by Laboratoire d'excellence (LabEx) CORTEX ANR-11-LABX-0042 of Université de Lyon. Note that a CC-BY public copyright license has been applied by the authors to the present document and will be applied to all subsequent versions up to the Author Accepted Manuscript arising from this submission, in accordance with the grant's open access conditions. C.A., E.P., and F.H.-B. are employed by the Centre National de la Recherche Scientifique.

Author Contributions

C.A. and F.H.-B. organized the project. C.A. and L.V. designed the rs-fMRI task in humans. C.G and D.A.-C acquired neuroimaging data in humans. C.A., C.G., D.A.-C, F.H-B and F.L. analyzed human data. A.D., C.G., and D.A.-C. trained monkeys to perform ocular fixation in the MRI environment. A.D., C.A., C.G., and F.H-B. acquired

neuroimaging data in awake macaques. C.A., C.G and F.H.-B. analyzed data. C.G., C.A., and F.H-B. interpreted data and wrote the article.

Competing Interest Statement. The authors declare no competing interest.

CHAPTER III. THE FUNCTIONAL INTERPLAY OF THE FRONTO-AMYGDALA NETWORK DURING BEHAVIORAL ADAPTATION IN HUMAN

C. Giacometti, D. Autran-Clavagnier, L. Viñales, F. Lamberton, N. Clairis, C. Scarpa, S. Manickam, E. Procyk, F. Hadj-Bouziane and C. Amiez

(In preparation)

ABSTRACT

A hallmark of our survival in the real world is our ability to show behavioral adaptation (BA). In everyday life, BA can be necessary for a number of reasons, making the study of the process challenging. Two classes of events can signal a need for adaptation: those caused by one's own actions (FeedBack –FB), and those not linked to our actions (Action-Independent Events –AiDEs–). These two types of information will frequently occur concurrently and a critical and difficult part of adapting appropriately involves resolving the difference between the two. The aim of this study was to identify the respective networks involved in FB and AiDE processing in non-social and social contexts. We thus developed a new behavioral task in which subjects had to learn how to adapt when facing both FB and AiDEs. Results showed that FB analysis recruited the anterior and posterior parts of the midcingulate cortex (aMCC and pMCC), concomitantly with a deactivation of the amygdala (AMG). By contrast the understanding of how to adapt at the occurrence of unknown AiDEs recruited the AMG and was associated with a deactivation of the MCC. Once the appropriate adaptation to AiDEs was identified, the analysis of AiDEs was associated with increased activity in the pMCC. These main results were similar in both non-social and social contexts but learning social AiDE (i.e. happy/angry faces) meanings additionally recruited the temporal face network and the dorsomedial frontal cortex, compared to non-social AiDEs (i.e. sun/cloud drawings). Altogether, these results show that the networks underlying FB and AiDE processing are not identical, and that social contexts recruit additional brain regions.

INTRODUCTION

The ability to adapt to unexpected, negative and/or positive, or potentially hazardous events is essential for our survival in a complex and dynamic environment involving or not social information (i.e., related to our peers). Adaptation can be necessary for a number of reasons, making the study of the process challenging. Two classes of events can signal a need for adaptation: 1) events caused by one's own actions and specifically FeedBack –FB– from those actions (e.g. we adapt our strategy after an erroneous choice), and 2) events not temporally- and causally- linked to our actions, named Action-Independent Events (AiDEs; e.g., we adapt our strategy after an event independent of one's action occurred, e.g. a change of rule, someone cheated, etc.). An AiDE is thus an unknown event, not related to our own behavior, that might have an impact on FB processing and on the selection of the appropriate behavioral adaptation but that does not necessarily indicate what response to select (e.g., shift or stay on the current choice). These two types of information, FB and AiDEs, will frequently occur concurrently, and a critical and difficult part of adapting appropriately involves understanding and resolving the difference between these two. It is therefore not a sensory event that does not impact on us (e.g. a plane passing overhead). It is not a conditional cue because AiDEs do not instruct what action must be performed. Indeed, a conditional cue relies on If/then relationships and is associated with a specific response (e.g. If cue A, B, C, D, then select response W, X, Y, Z, respectively)(Amiez et al., 2006, 2012; Loh et al., 2020). It is not a switching cue because an AiDE does not necessarily indicate a need to switch response or strategy (e.g. as in the Wisconsin Card Sorting Task (e.g. Hyafil et al., 2009). In everyday life, these two types of information – FB and AiDEs – will frequently occur concurrently, and a critical and difficult part of adapting appropriately involves resolving the difference between these two. So, for example an incorrect FB can occur because we made an error, or because something unexpected in the environment has changed – the rule switched, etc. We must work out which it is, as they will frequently require different behavioral adaptations. Our task is made even more complex by the fact that the dynamics of evidence accumulation after FB vs AiDEs are very different. FB has a direct temporal and causal link to an executed action, which means that we are certain to derive information about a given action from a given FB. In contrast, AiDEs have no such contiguity and no initial relation to our actions, which means that we

must accumulate evidence to identify the appropriate adaptation to AiDEs. So, the crucial dilemma is this: after an unwanted outcome, should we adapt as if we made an error and received a negative FB, or should we continue to accumulate evidence as if there has been an AiDE to which we need to know how to adapt. Furthermore, evidence to accumulate must come from different contexts (social or non-social). Primates in general and humans in particular are able to resolve this credit assignment problem, as evidenced by their ability to appropriately adapt their behavior in various contexts. The goal of this study is to shed light on the neural basis of this process, which remains misunderstood largely because FB and AiDEs processing have been assessed separately so far.

A large amount of evidence has shown that the key role of the midcingulate cortex (MCC) in FB processing in exploratory behavior both in non-social and social contexts and both in both humans and non-human primates (Amiez et al., 2005, 2006, 2012, 2013; Amiez & Petrides, 2014; Loh et al., 2020; Pelliccia et al., 2023; Procyk et al., 2016; Quilodran et al., 2008; Rothé et al., 2011). By contrast, the neural basis of AiDEs processing received little attention. Learning how to adapt at the occurrence of AiDEs would reasonably recruit AMG, the ventro-medial prefrontal cortex (vmPFC), and the anterior cingulate cortex (ACC) as they are known as being involved in the valuation of the environment (Boorman et al., 2013; Behrens et al., 2007; Gangopadhyay et al., 2021; Gläscher et al., 2012; Grabenhorst & Rolls, 2011; Juechems et al., 2019; Murray & Fellows, 2021; Pelliccia et al., 2023; Saez et al., 2015; Vassena et al., 2014). Specifically, the AMG is a key structure in environmental monitoring, contributing to the detection of salient information (Cunningham & Brosch, 2012; Ousdal et al., 2008; Pessoa & Adolphs, 2010; Santos et al., 2011), participating in vigilance mechanisms and in novelty detection (Blackford et al., 2010; Pedersen et al., 2017). Once the adaptive significance of AiDEs learnt, we then hypothesize that the MCC will take over. We recently demonstrated that the activity of MCC and AMG in humans are anti-correlated, strongly suggesting that when the MCC is activated, the AMG is deactivated, and the other way around (Giacometti et al. 2023b, in revision, see also Klein-Flügge et al., 2022). We thus hypothesize that this dynamic will also be reflected during behavioral adaptation: FB and learnt AiDEs processing should recruit the MCC and deactivate the AMG, whereas learning AiDEs processing should recruit the AMG and deactivate the MCC. We also hypothesize that processing FB and AiDEs

to adequately adapt in a social context would induce increased activity in the AMG and thus modulate the activity in the AMG-MCC network.

Here, we conducted a functional magnetic resonance imaging (fMRI) on a group of 42 human subjects while they performed a novel behavioral adaptation task involving both FB and AiDEs in non-social and social contexts. Results confirmed our hypothesis showing that 1) AMG and MCC display reversed dynamic activities, 2) the AMG is critical to evaluate the meaning of AiDEs at their first occurrence, 3) the pMCC is critical to process FB and learnt AiDEs when they are associated with a need to behaviorally adapt in the next trial, 4) the aMCC is critical for FB processing only. The context in which the task is performed appears to recruit the same AMG-MCC network but learning AiDEs recruits a differential additional network: VMPFC versus DMPFC/Face network for the non-social as compared to the social context.

MATERIALS AND METHODS

Participants

Two groups of 21 healthy right-handed subjects (first group: 10F and 11M, age 25.8 ± 2.5 , second group: 11F and 10M, age 25.1 ± 3.1) were included in 2 fMRI experiments, with either non-social or social context, see below). Note that 7 subjects were additionally scanned but were excluded because of 1) the fortuit discovery of brain anatomical anomalies, or 2) poor performances in the tasks, or 3) the presence of large head movements that could not be corrected (see below). All subjects received monetary compensation for their participation. The study was approved by a national ethics committee in biomedical research (Comité de Protection des Personnes (CPP) Sud-Est III, authorization ID: 2018-A00405-50). It also received Clinical Trial Numbers (NCT03119909, see <https://clinicaltrials.gov>).

MRI experimental paradigm

Subjects performed a deterministic problem-solving task (PST) where FB and AiDEs were both present. Four gray circle stimuli were presented on a black background in a diamond configuration to mimic the position of the button on the MRI-compatible response remote (FIU 904, Current Designs®, Philadelphia, United States). Subjects had to complete problems composed each of an exploration and an exploitation period. During the exploration period, 4 stimuli were presented to the subjects (stimulus presentation, Fig 1) who had to identify by trial and error in

successive trials which one of them was associated with a positive feedback -FB- (i.e., a green checkmark), the other ones being associated with a negative FB (i.e. a red cross, FBneg). At the occurrence of the first positive feedback (FBco1), subjects had to stop the exploration period and start the exploitation period in which they selected the correct stimulus and thus obtained the positive FB (FBcor) in 2 successive trials. Then, a signal-to-change stimulus (SC, abstract symbol) was presented to the subject to indicate that a new problem will have to be resolved in the next trial. Thus, at the next occurrence of the stimuli, all four stimuli had to be explored again to find the correct one. Stimuli were presented during 2s and subjects had to provide a response during that time. All FB were presented during 1s. Delays between stimuli and feedbacks and inter-trial intervals (ITI, between FB and stimuli presentation in the next trial, and before and after the presentation of SC) were jittered: between 500 to 6000ms (exponential distribution with mean=2000ms) and between 500 to 8000ms (mean 3000ms), respectively. During delays and ITIs, subjects had to fixate the central cross presented in the center of the screen. Importantly, subjects were trained for 10 min only on this version of the PST task that includes only FB, and no AiDEs, i.e., called “No AiDE” condition (**Figure 1.A**). They thus remained naive to AiDEs when they started the fMRI experiment.

During scanning, subjects performed the PST task without AiDEs in 25% of problems. In the remaining 75% of the problems, AiDEs were presented only once in the exploration period of a problem after either FBinc or FBco1 (**Figure 1.B**). AiDEs were represented by 3 types of images: neutral (i.e., an abstract symbol in both social and non-social groups), positively (i.e. sun drawing and happy masculine face in the non-social and social contexts of the task, respectively), and negatively (i.e. cloud drawing and angry masculine face in the non-social and social contexts of the task, respectively) emotionally valenced. Note that faces were selected from the Radboud Faces Databases (**Figure 1.C**; Langner et al., 2010). Subjects had to learn in successive functional runs composed of 16 problems that the neutral AiDEs were meaningless (i.e. the adaptation was driven by the latest FB only), whereas both negative and positive AiDEs equally invalidated the FB and thus required to adapt appropriately. Specifically, a negative or positive AiDE presented after FBinc both indicated that the stimulus selected was in fact correct, the correct adaptive response in the next trial (“correct response post AiDEs”) thus being to keep selecting this stimulus to get a positive feedback and finish up the exploration period of the task.

Similarly, a negative or positive AiDEs presented after FBco1 both indicated that the stimulus selected was in fact incorrect, the correct adaptive response in the next trial thus being to keep continuing exploring the other stimulus to identify the correct one and finish up the exploration period of the task. Thus, 6 conditions can occur in the exploration period of the PST with AiDEs: FBinc or FBco1 followed by AiDE neutral, or positive AiDE, or negative AiDE (**Figure 1.C**). Note that we contrast in the rest of the present paper non-significant AiDEs (neutral) and significant AiDEs (positive and negative). During each functional run, 16 problems were presented to the subjects: 4 without AiDE, 4 with a positive AiDE, 4 with a negative AiDE, and 4 with the neutral AiDE.

Importantly, we identified 2 phases during the fMRI experiment: the learning phase composed of several functional runs (see results) in which subjects learn whether and how to adapt to the 3 AiDEs, and a post-learning phase composed of 2 successive runs in which subject systematically adapt appropriately to the different AiDEs.

The task was developed and ran through MATLAB with Psychtoolbox (<http://psychtoolbox.org>) and was projected on a white screen positioned at the back of the MRI tunnel with a projector (LX501, Christie®, California, United States). Subjects visualized the task thanks to a reverse mirror, EyeLink compatible, positioned on top of the head-coil. An eye calibration was performed before every functional task run of the session by presenting 9 points (i.e., top/center/bottom left/middle/right positions of the screen) thanks to the EyeLink system (EyeLink1000 Plus, SR-Research®, Ottawa, Canada). In addition, eye position was monitored throughout the fMRI experiment. Heart rate and respiration were also monitored via the MP150 Biopac system (Biopac Systems Inc.®, California, United States). Task events, eyes and physiological parameters were synchronized to fMRI data acquisition and recorded throughout the fMRI session.

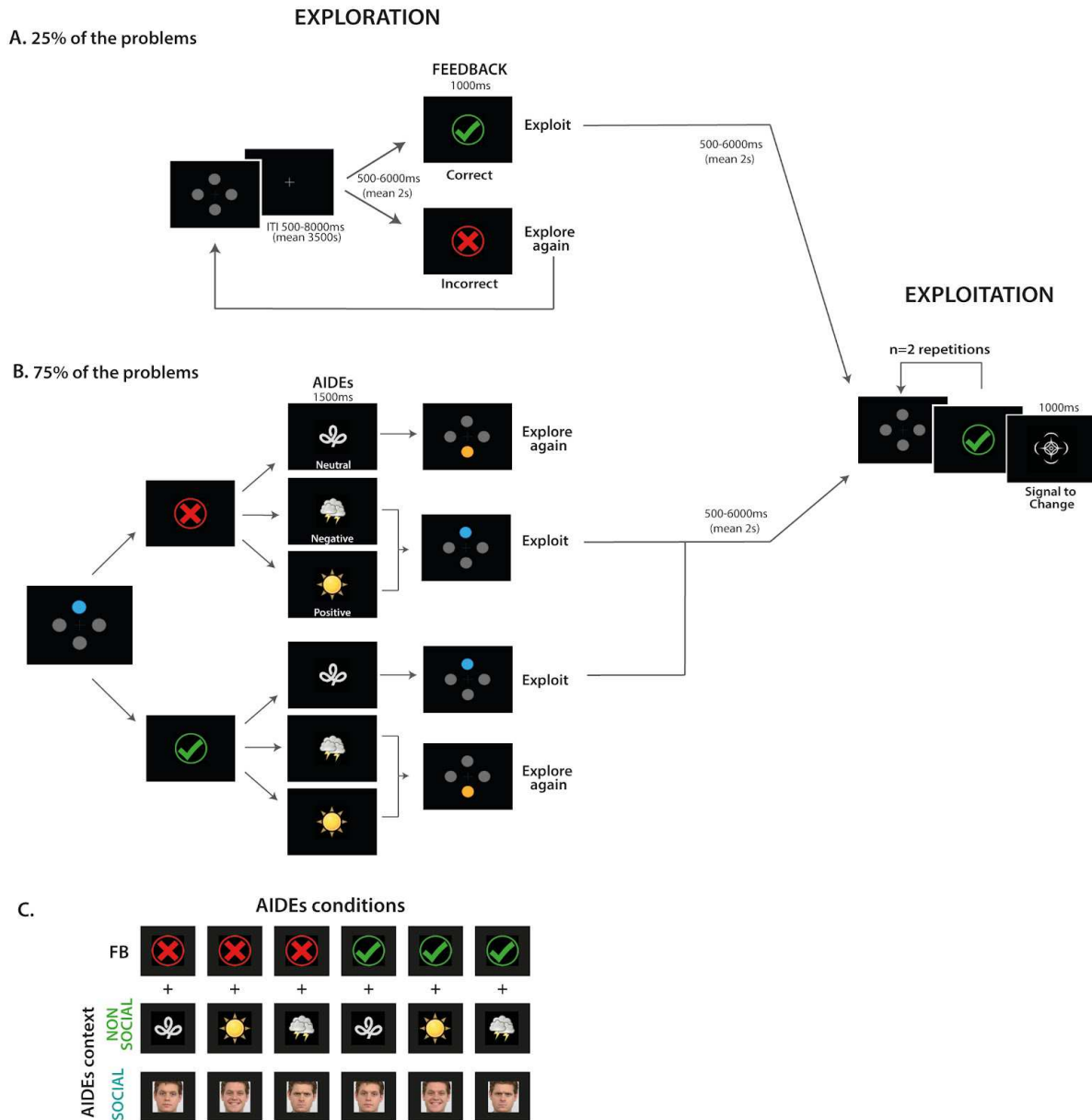


Figure 1. Experimental design of the behavioral adaptation task. During scanning, subjects performed the PST task without (Action-Independent Events) AiDEs in 25% of problems and with AiDEs in the remaining 75% of the problems. **A.** PST task without AiDEs. A problem is composed of an exploration period followed by an exploitation period. During the exploration period, 4 visual stimuli were presented to the subjects and they had to identify, by trial and error in successive trials the visual stimulus associated with a positive feedback (FBcor; green checkmark). At the occurrence of the first positive feedback (FBco1), subjects had to stop the exploration period and start the exploitation period in which they selected the correct stimulus and thus obtained the positive FB (FBcor) in 2 successive trials. Then, a signal-to-change stimulus (SC, abstract symbol) indicated that a new problem will start in the next trial. An error was signaled by an incorrect FB (FBinc; circled red cross). After a FBinc, subjects have to explore again for the correct stimulus and complete the exploitation period. **B.** PST task with AiDEs, presented only once in the exploration period of a given problem after either FBinc or FBco1. AiDEs could have neutral (i.e. an abstract symbol in both social and non-social groups), positively (i.e. sun drawing and happy masculine face in the non-social and social contexts of the task, respectively), or negatively (i.e. cloud drawing and angry masculine face in the non-social and social contexts of the task, respectively) emotionally valenced. Subjects had to learn across runs that the neutral AiDE did not require any change in BA whereas both negative and positive AiDEs invalidated

the FB and thus required to adapt appropriately. Specifically, a negative or positive AiDE presented after FBinc both indicated that the stimulus selected was in fact correct, the correct adaptive response in the next trial thus being to keep selecting this stimulus to get a positive feedback and move to the exploitation period. Similarly, a negative or positive AiDE presented after FBco1 both indicated that the stimulus selected was in fact incorrect, the correct adaptive response in the next trial thus being to keep continuing exploring the other stimulus to identify the correct one and move to the exploitation period.

C. Table representing the condition types in problems with AiDEs for the two contexts: non-social (green) and social (blue). 6 conditions were presented during the exploration period of the PST with AiDEs: FBinc or FBco1 followed by AiDE neutral, or positive AiDE, or negative AiDE. During each functional run, 16 problems were presented to the subjects: 4 without AiDE, 4 with a positive AiDE, 4 with a negative AiDE, and 4 with the neutral AiDE.

fMRI data acquisition

Scanning was performed on a 3T Siemens Magnetom Prisma MRI Scanner (Siemens Healthcare, Germany). To minimize movements during the tasks, the subjects' heads were tightly cushioned throughout the acquisition. The main experimental protocol consisted of two MRI sessions (from 90 to 120 min). In the first session, subjects performed 6-7 runs of the task and an anatomical scan was obtained. In the second session, subjects who did not reach the criteria for the post-learning phase during the first session performed additional runs (maximum 4). In addition, resting-state and localizer motor task scans were performed during the second session (Loh et al., 2018). Each run lasted on average 10.1 and 10.2 mins in, respectively, the non-social and social context of the task. In each run, the task was initiated at the 5th TTL pulse from the MRI scanner. Task and resting-state runs were acquired with a T2* weighted multiband and multi-echo (ME) sequence: TR = 1500ms, TE1=16.4ms, TE2=37.59 ms, TE3=58.78 ms, voxel size = 2.5 mm³. A high resolution T1-weighted anatomical MRI was also obtained during the first session (MPRAGE, TR=3s, voxel size= 0.8 mm³, 244 slices).

Behavioral data analysis

We identified in each problem with AiDEs in each run and each subject whether and how the subjects adapted to the trials following the occurrence of AiDEs. Briefly, a neutral AiDE indicated no change in BA whereas a significant (positive or negative) AiDE indicated a change in BA (after a FBinc, the subject had to keep selecting the previous stimulus in the next trial to find the correct one while after a FBco1, the subject had to select another stimulus until he found the correct one). Once the subjects adapted appropriately in 100% of the 1st trials post-AiDEs in all conditions and in 2 successive functional runs, these runs were categorized as belonging to the post-

learning phase and indicated that the learning criteria was reached. All runs before to reach this criteria were categorized as belonging to the learning phase.

Note that in the present paper, to capture networks involved in the early learning phase versus in the post-learning phase, we focused on the comparison in the 1st learning run versus in the post-learning runs.

Problems completed. For each subject, run and condition, we identified the number of problems completed, i.e. composed of both an exploration and an exploitation period, for which the learning criterion defined above was reached. We computed the averaged problems completed across subjects. Note that the following analyses were exclusively performed on problems completed.

Number of trials in the exploration period. In each condition, run, and subject, we obtained the number of trials composing the exploration period of each problem, i.e. the number of trials required to reach the exploitation period. As we focused on the comparison between behavior and fMRI results in the 1st learning run versus in the post-learning runs, we then calculated the average number of trials composing the exploration period of each problem in the first run of the learning phase versus in the post-learning phase.

Number of runs in the learning phase. For each subject, run and condition, we computed the averaged number of runs in the learning phase across subjects (i.e. runs before to reach the learning criteria defined above).

The percentage of correct responses and Reaction Time in the learning and post learning phase. The percentage of correct responses and Reaction times (RT in seconds) to select a given stimulus in the trial following the occurrence of the various AiDEs were computed for each condition, subject, and context of the task in the first learning run and in the post-learning runs. They were then averaged across subjects.

Statistical Analysis.

To identify whether the condition (i.e. 6 conditions with AiDEs and 1 with No AiDEs) and the context of the task (social and non-social) had an impact of the number of trials composing the exploration period of each problem in the 1st learning run versus in the post-learning runs, we fitted a General Linear Mixed Model (GLMM; <https://cran.r-project.org/web/packages/lme4/index.html>) following a Poisson

distribution (i.e., count data) with “Conditions” and “Contexts” as main effects (conditions comprising the 7 conditions: 6 AiDEs and 1 No AiDEs).

To identify whether the response to AiDEs was learnt before the 1st learning run and the post-learning runs, we fitted a GLMM following a binomial distribution with main effects of “Conditions”, “Contexts” and “Phases” (with Phases including only the 1st learning run and the post-learning runs). Note that this analysis was performed only in the PST with AiDEs (i.e. including 6 conditions) Finally, to identify whether a given AiDE impacted RTs in the trials following its presentation, we fitted a GLMM with the main effect of “Conditions”, “Versions” and “Phases” (with Phases including only the 1st learning run and the post-learning runs). Note that this analysis was performed only in the PST with AiDEs (i.e. including 6 conditions).

In all GLMM, we also included the random factor Subject (i.e. 1 | Subject) and the random factor Contexts within subjects (i.e. 1 + Contexts | Subject) to account for the subjects variability across the 2 contexts. GLMM were tested for main effect significance and followed by post-hoc pairwise analysis (Tukey Test; <https://cran.r-project.org/web/packages/emmeans/index.html>). All pairwise comparison p.values were adjusted with False Discovery Rate (FDR) correction.

fMRI data analysis

Preprocessing. Preprocessing was performed using SPM12 (Wellcome Department of Cognitive Neurology, University of College London, London, UK; <http://www.fil.ion.ucl.ac.uk/spm>) and AFNI (Cox, 1996) softwares. The first 5 volumes of each run were removed to allow for T1 equilibrium effects. Slice timing correction for multiband sequences was then applied using AFNI software. TEDANA package⁵⁶ was used to combine the 3 echo time series and to perform motion correction. The combined data is decomposed by, first, a principal component analysis (PCA) and second, an independent component analysis (ICA). TE-dependent components are classified as BOLD signal, while TE-independent components are classified as non-BOLD signal, and are discarded. For more information, please check TEDANA community page: <https://zenodo.org/record/4509480#.YEnNy8Rq8> (DuPre et al., 2021; Kundu et al., 2012, 2013; The tedana Community; et al., 2021). Note that the 6 motion parameters were saved in a separate file as covariates to model potential nonlinear head motion artifacts in subsequent statistical analyses. Using SPM12, functional and anatomical images were then spatially normalized into standard MNI

space. Finally, functional images were smoothed using a 6-mm full-width half-maximum Gaussian kernel.

fMRI analysis. The following analyses were used using SPM12 and performed for each context group (non-social and social) separately. At the first level, we identified: (1) the blood oxygenation-level dependent (BOLD) signal at the occurrence of FB in the exploration (i.e. including FBinc and FBco1) versus in the exploitation (i.e. FBpos) periods of each problem. (2) The BOLD signal at the occurrence of the various AiDEs in the 1st learning run versus in post-learning runs. Both contrasts were computed in the non-social and in the social context of the task. Note that we separate this contrast for neutral AiDE and significant AiDEs which includes both negative and positive AiDEs. These regressors were then convolved with the canonical hemodynamic response function and entered into a general linear model of each subject fMRI data. The 6 motion parameters were also included in the general linear model as additional regressors to account for residual effects of movement. Both contrasts were then examined for each context at the group level and at the subject-by-subject level.

Subject-by-subject approach. We identified the coordinates and t-values of the maxima of increased activities in our regions of interest (AMG and MCC) for each subject and in each context. As it has been shown that the functional organization in the cingulate cortex depends on the sulcal morphology (Amiez et al., 2013, 2016; Loh et al., 2020), we performed subject-by-subject analysis to identify whether activity located in the MCC was located in the paracingulate sulcus, a sulcus present in 70% of subjects in at least one hemisphere (Amiez et al., 2013), or not.

Group and individual subject analysis. The resulting t statistic images were thresholded using the minimum given by a Bonferroni correction and random field theory to account for multiple comparisons. Statistical significance for the group analyses was assessed based on peak thresholds in exploratory and directed search, and the spatial extent of consecutive voxels. For a single voxel in a directed search, involving all peaks within an estimated grey matter of 600 cm³ covered by the slices, the threshold for significance ($p < 0.05$) was set at $t = 5.39$. For a single voxel in an exploratory search, involving all peaks within an estimated grey matter of 600 cm³ covered by the slices, the threshold for reporting a peak as significant ($p < 0.05$) was $t = 6.47$ (Worsley et al. 1996). A predicted cluster of voxels with a volume extent >69.32

mm³, with a t-value > 3 was significant ($p < 0.05$) corrected for multiple comparisons (Worsley et al., 1996). Concerning the individual subject analysis, we conducted a region of interest (ROI) analysis to identify individual increased activity in AMG. It has been shown that the cortex within the AMG presents an average volume of 1285 mm³ (Giacometti et al., 2023). In this volume, a predicted cluster of voxels with a t value > 2 and with a volume extent > 184.46 mm³ was significant ($p < 0.05$), corrected for multiple comparisons using the method of Friston et al. (1995) (Friston et al., 1995).

RESULTS

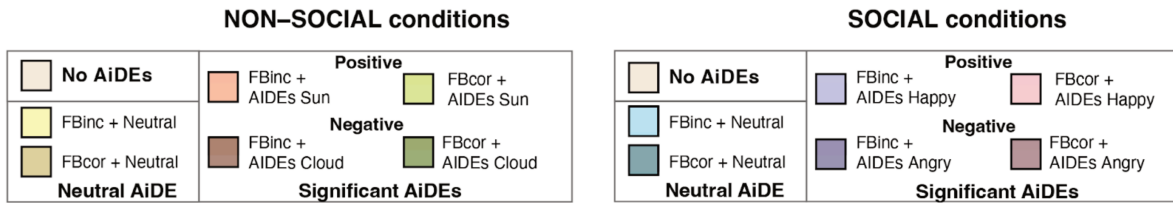
Behavior

General impacts of AiDEs on exploration.

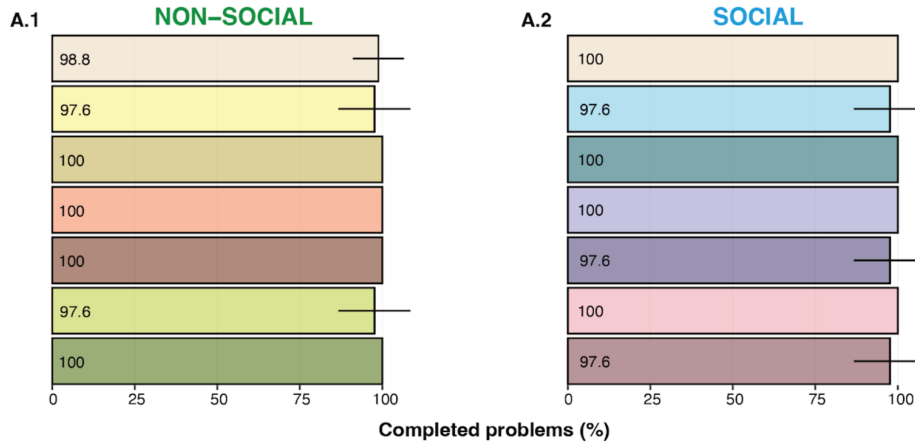
We first identified the percentage of problems completed for both contexts in each of the 7 conditions on the first run. Results revealed that in both contexts the % of completed problems was slightly impacted in the first learning run (i.e. 3/16 problems were not completed in each context, **Figure 2.A**). These runs were excluded from subsequent analysis.

Second, results indicated that the presence of AiDEs significantly impacts the exploration phase when compared to the No AiDEs conditions in both contexts (non-social and social). Statistical analysis showed a main significant effect of Conditions (GLMM, $\chi^2(6, n=42)=880.201, p < 2e-16$) and no effect of Context ($\chi^2(1, n=41)=0.103, p=0.748$). Specifically, the presence of AiDEs lead to an increased number of trials composing the exploration period across subjects, in particular with significant (positive and negative) AiDEs compared to no AiDEs or neutral AiDEs (post-hoc analysis on Conditions, $p < 0.05$, **Figure 2.B**), demonstrating that the first occurrences of AiDEs impacted the exploration period. This impact was particularly exacerbated in conditions in which significant AiDEs followed an incorrect FB.

Finally, the exploration period in problems with AiDEs was decreased in post-learning phase compared to the first run of the learning phase, showing that once the significance of AiDE learnt, the exploration period was optimized. Importantly, no difference was observed in the non-social and social contexts.



A. Problems completed



B. Number of trials in exploration period

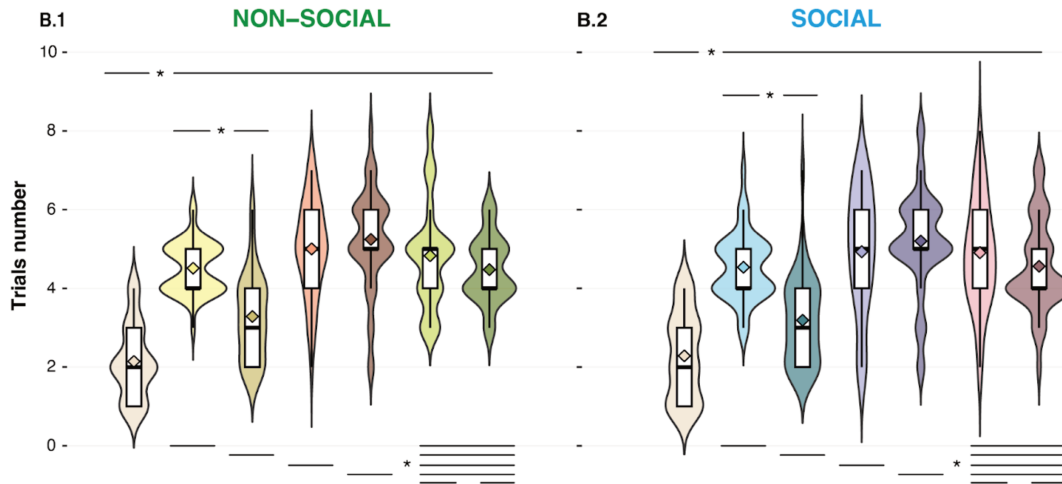


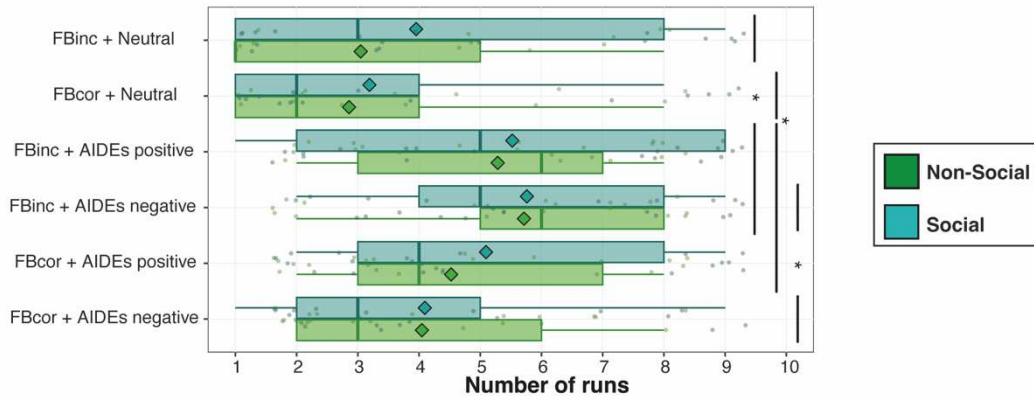
Figure 3. Learning the significance of the AiDEs in the non-social and social context. **A.** Boxplot representing the number of runs in the learning period for both non-social (blue) and social (green): mean (diamond) and median (vertical bar) are displayed. GLMM shows a main effect of conditions ($X^2(5, n=42)=54.404, p<1.731e-10$) and no effect of Context ($X^2(1, n=42)=0.199, p=0.656$). Post-hoc shows differences between the 2 neutral AiDEs conditions and FBneg + AiDEs significant, between FBcor + Neutral and FBcor + AiDEs positive ($p<0.05$, FDR corrected). Within significant AiDEs, differences between the 2 AiDEs negative conditions ($p<0.05$, FDR corrected). **B.** Boxrange plots displaying the mean (diamond) and standard deviation (box bar extremities) of the percentage of appropriate action selection following up AiDEs presentation. GLMM show a main effect of phase ($X^2(1, n=42)=132.893, p<2e-16$) and Conditions ($X^2(5, n=42)=120.574, p<2e-16$) and no effect of context ($X^2(1, n=42)=0.890, p=0.345$). Post-hoc results show a significant effect of Learnt compared to 1st Occurrence for all conditions ($p<0.05$, FDR corrected). An effect for the 1st Occurrence performance in Neutral AiDEs conditions compared to significant AiDEs conditions (#, $p<0.05$, FDR corrected). Also, an effect during 1st Occurrence for both AiDEs negative conditions. **C.** Rangepoint plot displaying the mean (square) and standard deviation (vertical bar) of the RT in the trial after AiDEs occurrence. GLMM shows main effects of Phase ($F(1, 949.85)=74.702, p<2e-16$) no effect of Conditions ($F(5,$

949.77)=0.414, $p=0.839$) and Context ($F(2, 39.81)=0.594$, $p=0.446$). Post-hoc comparisons show a significant difference between RT after AiDEs in the 1st Occurrence compared to Learnt phase for all conditions and in both contexts ($p<0.05$, FDR corrected).

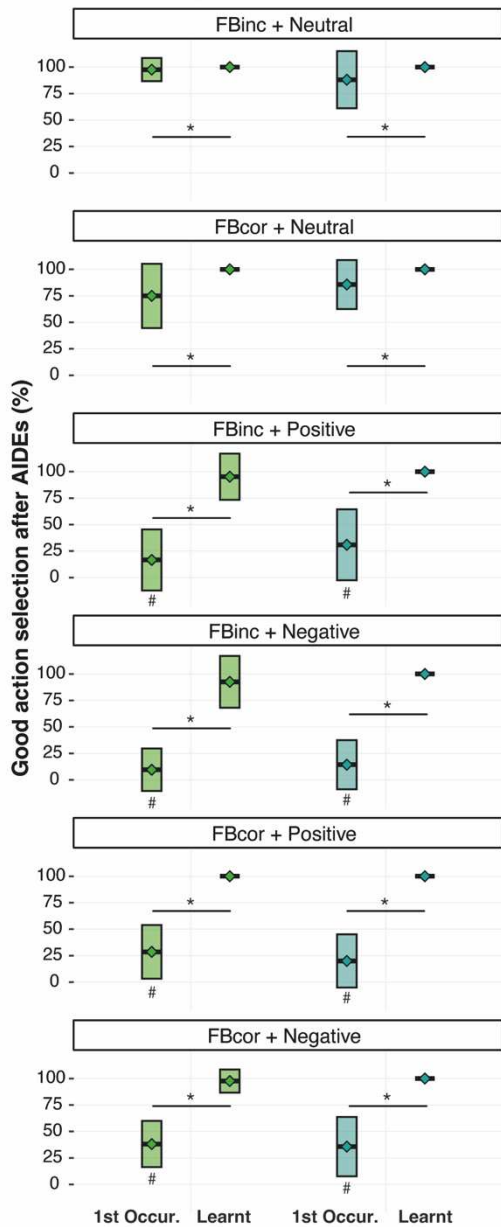
Learning AiDEs' meanings

We identified whether subjects have learnt the meaning of the various AiDEs at the completion of the fMRI experiments. First, we examined the number of runs composing the learning phase for each AiDE type and each context (**Figure 3.A**). GLMM analysis showed a significant effect of Conditions ($X^2(5,n=42)=54.404$, $p<1.731e-10$) and no effect of Context ($X^2(1,n=42)=0.199$, $p=0.656$) on the number of runs required to learn the behavioral significance of AiDEs. Post-hoc analysis (Tukey test) revealed that significant AiDEs (positive and negative) required 4.89 ± 2.35 and 5.12 ± 2.80 runs on average in the non-social and social context (median 5 and 4 runs respectively). By contrast, the neutral AiDE were understood almost immediately (average of 2.95 ± 2.56 and 3.57 ± 3.14 , median of 1 and 2 runs). These findings suggest that the initial presentation of AiDEs was perceived as irrelevant for the PST task performance. The adaptation occurred only in subsequent trials when AiDE was associated with a deviation in the expected response-feedback relationship. Note that for significant AiDEs conditions following a FBinc tend to require more runs to be learn than FBcor ones, especially for the negative AiDEs (Tukey test, $p<0.05$, FDR corrected). Second, we compared the success/failure of appropriate action selection in the post-AiDE trial in the first learning compared to post-learning runs in the 2 contexts. Results are displayed as a percentage of correct action selection (**Figure 3.B**). GLMM results showed a main effect of Phase ($X^2(1,n=42)=132.893$, $p<2e-16$) and Conditions ($X^2(5,n=42)=120.574$, $p<2e-16$) and no effect of Context ($X^2(1,n=42)=0.891$, $p=0.345$). Post-hoc results (Tukey test, $p<0.05$, FDR corrected) revealed that, in both contexts, the success of correct responses in the trial following the presentation of a significant AiDE (positive and negative) was low in the first learning run and reached the learning criteria in the post-learning phase. In accordance with our previous observation, the initial performance in AiDEs neutral conditions is significantly higher compared to AiDEs significant conditions ($p < 0.05$, FDR corrected). Finally, RTs after AiDEs in the first learning versus in the post-learning runs were shortened in both contexts (**Figure 3.C**). Indeed, GLMM shows main effects of Phase ($F(1,949.85)=16.881$, $p<2e-16$), but no effect of Conditions ($F(5, 949.77)=0.414$, $p=0.839$) and Context ($F(2, 35.55)=0.594$, $p=0.446$).

A. Number of runs in the learning phase



B. Correct response selection after AiDEs



C. Reaction Time after AiDEs

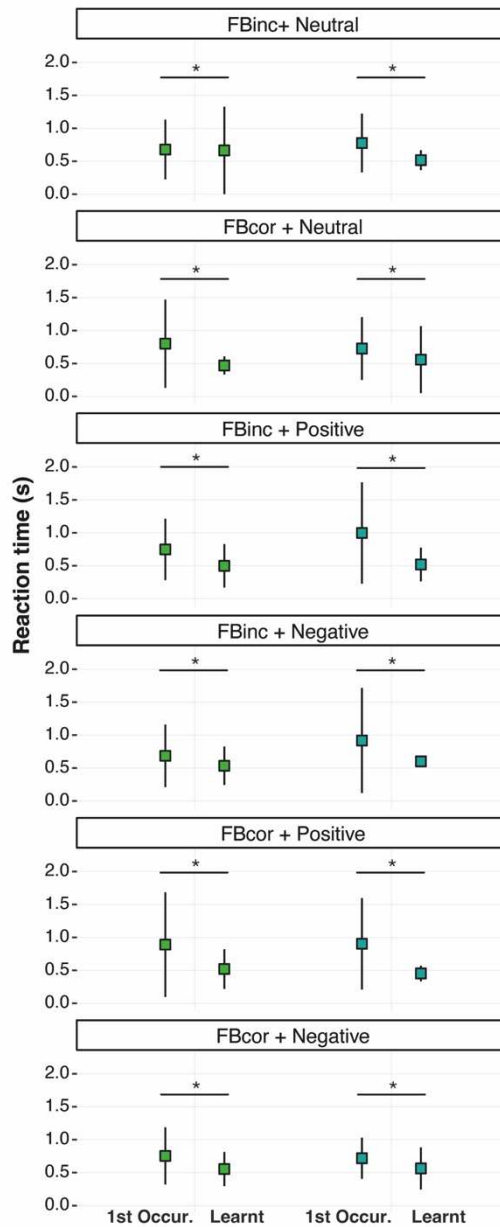


Figure 3. Learning the significance of the AiDEs in the non-social and social context. A. Boxplot representing the number of runs in the learning period for both non-social (blue) and social (green):

mean (diamond) and median (vertical bar) are displayed. GLMM shows a main effect of conditions ($X^2(5, n=42)=54.404, p<1.731e-10$) and no effect of Context ($X^2(1, n=42)=0.199, p=0.656$). Post-hoc shows differences between the 2 neutral AiDEs conditions and FBneg + AiDEs significant, between FBcor + Neutral and FBcor + AiDEs positive ($p<0.05$, FDR corrected). Within significant AiDEs, differences between the 2 AiDEs negative conditions ($p<0.05$, FDR corrected). **B.** Boxrange plots displaying the mean (diamond) and standard deviation (box bar extremities) of the percentage of correct response selection following AiDEs presentation. GLMM show a main effect of phase ($X^2(1, n=42)=132.893, p<2e-16$) and Conditions ($X^2(5, n=42)=120.574, p<2e-16$) and no effect of context ($X^2(1, n=42)=0.890, p=0.345$). Post-hoc results show a significant effect of Learnt compared to 1st Occurrence for all conditions ($p<0.05$, FDR corrected). An effect for the 1st Occurrence performance in Neutral AiDEs conditions compared to significant AiDEs conditions (#, $p<0.05$, FDR corrected). Also, an effect during 1st Occurrence for both AiDEs negative conditions. **C.** Rangepoint plot displaying the mean (square) and standard deviation (vertical bar) of the RT in the trial after AiDEs occurrence. GLMM shows main effects of Phase ($F(1, 949.85)=74.702, p<2e-16$) no effect of Conditions ($F(5, 949.77)=0.414, p=0.839$) and Context ($F(2, 39.81)=0.594, p=0.446$). Post-hoc comparisons show a significant difference between RT after AiDEs in the 1st Occurrence compared to Learnt phase for all conditions and in both contexts ($p<0.05$, FDR corrected).

fMRI results

Network involved in feedback processing in the exploration period of problems with no AiDE in non-social and social contexts

To identify the network involved in the analysis of FB in exploratory behaviors in both non-social and social contexts, we compared the BOLD signal at the occurrence of FB in the exploration period (i.e. both FBinc and FBco1) compared to the exploitation period (i.e. FBcor) in problems with no AiDE. This analysis confirmed previous results (Amiez et al., 2005, 2006, 2012, 2013; Amiez & Petrides, 2014; Loh et al., 2020; Procyk, Amiez, et al., 2016; Procyk, Wilson, et al., 2016; Quilodran et al., 2008; Rothé et al., 2011) and showed increased activity in the aMCC, pMCC, dIPFC (i.e. areas 9/46 and 46), prefrontal extent of the frontal operculum, the inferior frontal junction, and the caudate nucleus in both contexts (Figure 4. A.B, Table S1). Additional activity increases were observed in the parietal cortex as previously shown, but their description is beyond the scope of the present paper. Importantly, no activity increase was observed in the temporal cortex, including the amygdala. We then performed a conjunction analysis and identified that the MCC regions involved in the analysis of behavioral feedback in exploration versus exploitation periods were similar in non-social and social contexts of the task (**Figure 4.C**). Note that, by contrast, the analysis of FB during the following exploitation period as compared to the exploration period (i.e. FBcor) was associated with increased activity in the AMG, vmPFC and ACC in both contexts, regions not present in exploration (Data not shown).

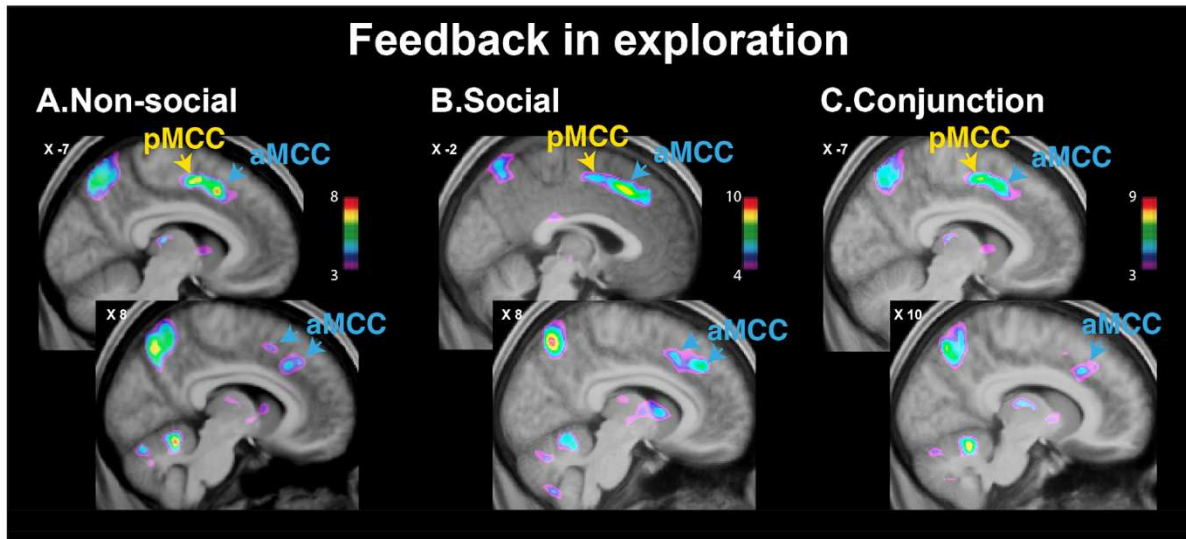


Figure 4. Feedback processing during the exploration period in No AiDEs condition. Group BOLD signal in the non-social (A), social (B) and a conjunction analysis with both contexts (C) for FB occurrence during exploration (contrast FB exploration - FB exploitation) on sagittal brain sections. The color bar displays the range of the t-values. All peaks are significant at $p < 0.05$ corrected for multiple comparisons. Results show significant activations in the aMCC (blue) in both hemispheres and pMCC (yellow) in the left hemisphere in the same location for both contexts.

Finally, a subject-by-subject analysis identified that a PCGS was present in both groups of subjects involved in the social and non-social context of the task (**Table S2**). Importantly, as observed previously (Amiez et al. 2013, 2016, Loh et al. 2020), results revealed that the MCC increased activity related to visual feedback processing in exploratory situations is systematically located in the PCGS if present, and in the CGS if the PCGS is absent.

Networks involved in learning AiDEs significance in non-social versus social contexts

The identification of networks involved in the analysis of AiDE in learning versus post-learning phases was based on 2 contrasts: 1) the difference between the BOLD signal at the occurrence of significant AiDEs in the first run of the learning period versus in the post-learning period (when subjects adapt appropriately to the occurrence of AiDE), and 2) the reverse contrast.

The first contrast revealed that, in both contexts of the tasks, the first occurrences of significant AiDE (positive and negative) during the first learning run was associated with increased activity in the AMG, the vmPFC, the ACC, and the accumbens nucleus (NAC), but not in the MCC (**Table S3** and **Figure 5.A, Figure 6**). Note that the identification of the meaning of social (face) AiDEs recruited additionally

the face perception network (i.e. OFA, FFA). Importantly, the subject-by-subject analysis revealed that the AMG displayed increased activity in this contrast in 86% and 81% of subjects, respectively in the social and non-social context of the task (18 and 17 subjects out of 21).

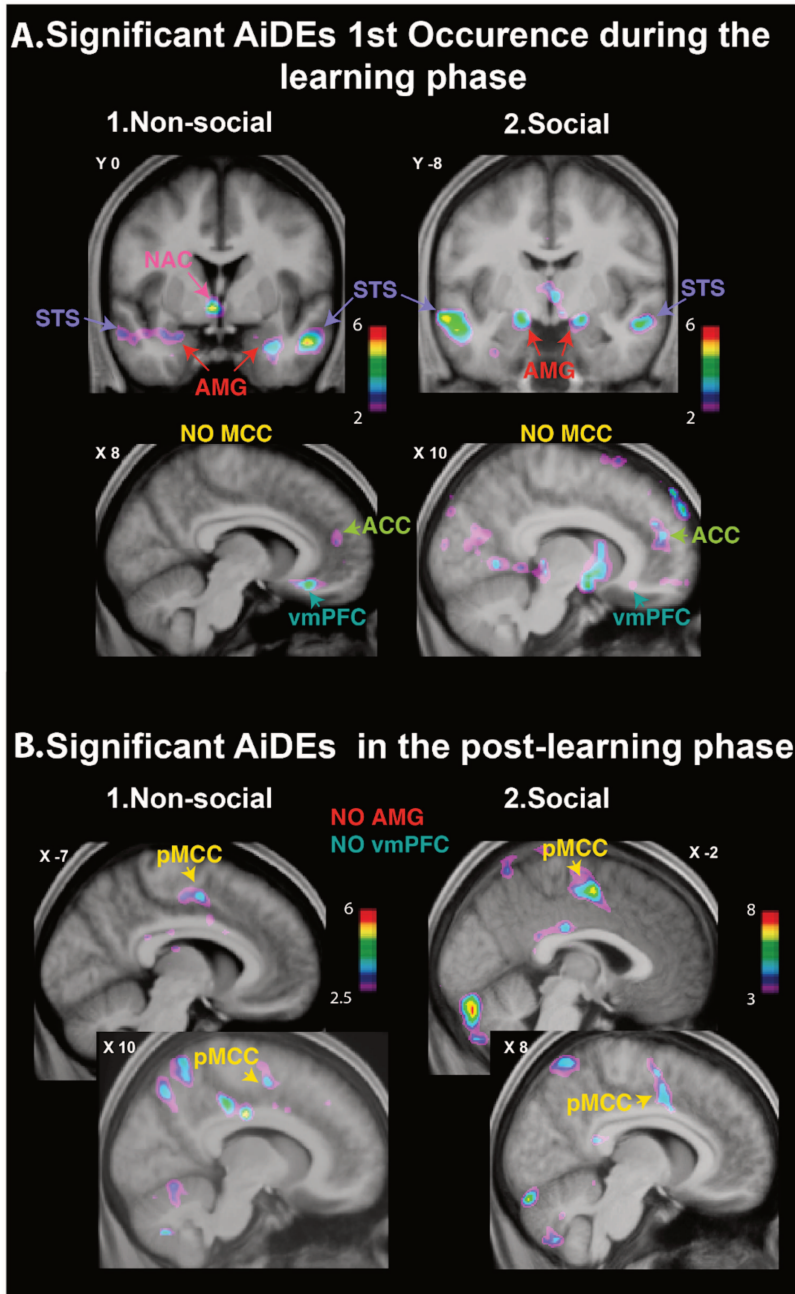


Figure 5. AiDEs adaptive significance learning process: opposite activation of AMG and pMCC for AiDEs 1st occurrence and AiDEs significance learnt. Representation of the MRI BOLD signals at the 1st Occurrence of significant AiDEs (A) and during one post learning run (B) in both the non-social (1) and social (2) contexts (contrast: AiDEs 1st Occurrence - AiDEs occurrence in one post-learning run). The color bar displays the range of the t-values. All peaks are significant at $p < 0.05$ corrected for multiple comparisons. **A.** On a coronal brain section, we observed an activation of the AMG (red), STS (purple) and NAC (pink) bilaterally during significant AiDEs first occurrence. **B.** On a mid-sagittal brain section we observed an activation of the pMCC (yellow) in both hemispheres and for both contexts.

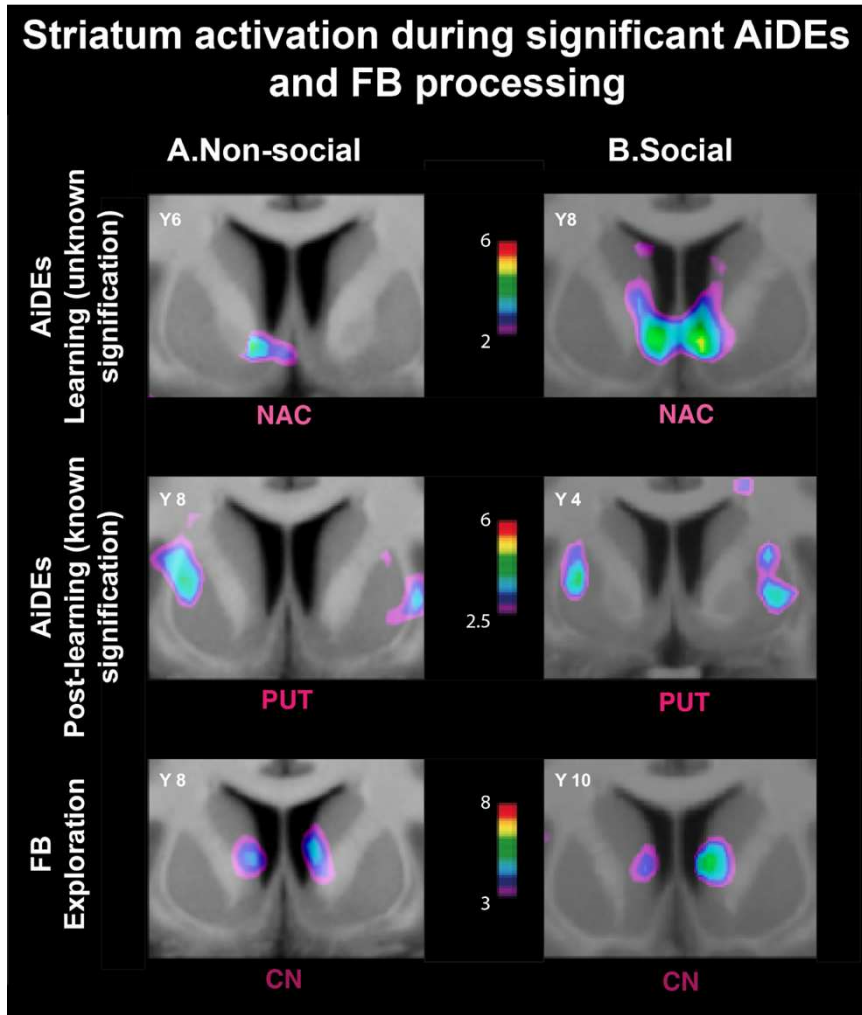


Figure 6. Differential involvement of the striatum in learning AiDE, in processing learnt AiDE, and in FB processing. BOLD signal activation is presented on coronal brain sections centered on the striatum area in both hemispheres. Results are presented for both the non-social (A) and social (B) contexts. The initial learning of AiDE meaning recruited the NAC, whereas adapting from learnt AiDEs and FB recruited, respectively the putamen (PUT) and the head of the caudate nucleus (CN).

The reverse contrast aimed at identifying the network involved in AiDEs processing during the post-learning phase, revealed that in both contexts of the task, once AiDEs adaptive meaning was learnt, the occurrence of significant AiDEs was associated with increased activity in the MCC and the putamen but not in the AMG (**Table S4, Figure 5.B, Figure 6**). Importantly, while FB occurrence in the exploration period induced an activation of both aMCC and pMCC, only the pMCC displayed increased activity when a learnt significant AiDE occurred. The subject-by-subject analysis revealed that the pMCC activation was observed in 67% and 71% of the subjects, respectively in the social and non-social contexts (14 and 15 out of 21). Importantly, FB processing also recruited the head caudate nucleus (Figure 6), and thus a different striatal region than learnt AiDE processing. Note that, in neutral AiDEs conditions, the same network was observed for both phases (Data not shown).

DISCUSSION

This study aimed at identifying the commonalities and differences between networks involved in learning how to adapt from FB and AiDEs in exploratory situations in various contexts. At the behavioral level, results indicate that the presence of AiDEs, when subjects are naïve (i.e., 1st Occurrence), significantly increased the exploration period of the problems when compared to the No AiDEs conditions in both contexts (non-social and social). Next, when comparing two precise points of AiDEs learning timeline, subjects show similar learning patterns for all conditions with AiDEs in both contexts, as evidenced by the performance improvement between the first occurrence and the learnt phase. Although, significant AiDEs generally require more time to be learnt than neutral AiDEs conditions. Indeed, in a first intention, subjects tend to adapt based on what they already know, no AiDEs condition, and ignore AiDEs presence. It is important to note that subjects seem to be more impacted when significant AiDEs occur after an incorrect FB: more time spent to explore in the learning period. It suggests that they encounter greater difficulty in choosing the same stimulus again when this stimulus has been previously associated with an incorrect response. Similar performance reduction is observed in learning in situations where there is response-FB conflict, i.e, an incongruent FB following a choice (e.g., visual correct FB for incorrect choices; Hammerstrom et al., 2021). The visual of FBinc associated with the response might create a reluctance to repeat the same error.

At the neural level, results revealed that the learning process required to adapt from AiDEs is underlied by a particular dynamic in the AMG-MCC network, the AMG being involved in the first learning step and the MCC in the post-learning step. Importantly, the MCC region involved in AiDE processing (i.e. pMCC) corresponded only to the posterior part of the MCC region involved in FB processing (i.e. pMCC and aMCC), strongly suggesting that adapting from FB and from AiDE recruit, at least in part, differential networks. Finally, learning how to adapt from non-social and social AiDEs recruit the same AMG-MCC network. Altogether, these results strongly suggest that FB and AiDE processing recruit differential networks to some extent but that these networks subserve this function in a generic manner across contexts.

The dynamic interplay between AMG and MCC during AiDEs learning process.

A critical finding of the present study is the AMG-pMCC dynamic in the learning process of AiDE meanings. Specifically, whereas the first occurrences of unknown

AiDE was associated with a bilateral increased activity in the AMG and deactivation in the pMCC, the reverse pattern was observed once the AiDE meaning was learnt. In other words, once the AiDE is understood as an event requiring a specific adaptation, the pMCC is involved. Importantly, the additional involvement of the vmPFC was observed in the early learning step of AiDE meaning.

This is in line with the known connectivity pattern in the AMG-vmPFC network. Indeed, these regions share high density structural connections (Aggleton, 2000; Calderazzo et al., 2021; Ghashghaei et al., 2007; Sharma et al., 2020) and strong positive functional connectivity as measured with resting-state functional MRI (rs-fMRI; Giacometti et al. 2023b, in revision; Klein-Flügge et al., 2022). They also both partake in the contextual/emotional valuation of the environment and choices in regard of internal state demands (e.g. Bechara et al., 1999, 2000, 2003; Behrens et al., 2007; Cunningham & Brosch, 2012; Grabenhorst & Rolls, 2011; Gupta et al., 2011; Hampton et al., 2007; Mehta et al., 2019; Ousdal et al., 2008; Pessoa & Adolphs, 2010; Santos et al., 2011; Schneider & Koenigs, 2017; Yizhar & Klavir, 2018; Zangemeister et al., 2020), a critical step required in decision-making. AMG has also been demonstrated to be involved in attention, vigilance mechanisms (Gothard et al., 2020; Pederson et al., 2017), and in general contextual novelty detection alongside the hippocampus (also displaying increased activity in the present study at the first occurrence of AiDEs, see **Table S3**; Blackford et al., 2010). The additional involvement of NAC (also called the ventral striatum) is supported by its known involvement in stimuli evaluation (Basile et al., 2021; Costa et al., 2016; Ousdal et al., 2012), and its strong connections with the AMG, the vmPFC, and the hippocampus (Basile et al., 2021; Di Martino et al., 2008).

As subjects are naïve at the 1st occurrence of AiDEs, these events are thus processed as potential salient stimuli in the environment, as revealed by strong increased activity of the AMG-vmPFC-hippocampus-NAC network, but behavioral adaptation is processed only if a deviation in the stimulus-response relationship occurred, as revealed by behavioral results (only with significant AiDEs). Thus, in a first intention, the AMG-vmPFC-hippocampus-NAC network is recruited to detect and evaluate AiDEs. Note that social AiDEs additionally recruit the dmPFC and the temporal face processing network, consistently with the literature (e.g. Bernstein et al., 2018). Then, once AiDEs adaptive meaning is learnt, the AMG-vmPFC network is deactivated, concomitantly with the involvement of the pMCC-dIPFC network (**Figure**

5.B). This is in line with a large literature showing that this latter network is involved in performance monitoring (Amiez et al., 2005, 2006, 2012, 2013; Amiez & Petrides, 2014; Loh et al., 2020; Procyk, Amiez, et al., 2016; Procyk, Wilson, et al., 2016; Quilodran et al., 2008; Rothé et al., 2011).

Altogether, these results suggest that learning how to adapt from events not related to our action requires first the AMG to detect salient information from the environment and to constantly inform the MCC through a bottom-up pathway. When the MCC then identifies that a particular event requires behavioral adaptation, it exerts a top-down control onto AMG and interacts with the dlPFC to select the most appropriate behavioral response and to control the exploration-exploitation tradeoff required in the task (Rothé et al., 2011; Sallet et al., 2013; Smith et al., 2015).

To identify the precise dynamic of the AMG-MCC network in learning AiDE meaning, and particularly whether the deactivation of the AMG and the activation of the MCC that takes place at the end of the learning process is an abrupt or linear phenomenon, and whether it is modulated by the context and the valence of the AiDE (negative/positive), model-based analysis on a trial by trial basis, employing mixed models combining coordinated working memory and reinforcement learning (Viejo et al., 2015) will be required in future studies.

Distinct MCC subregions involved in FB and learnt AiDES processing

An unexpected but critical result is the differential involvement of the pMCC and the aMCC in FB and AiDEs processing. Specifically, whereas FB processing recruits the aMCC and the pMCC to a less extent, as suggested by a large number of studies (Amiez et al., 2005, 2006, 2012, 2013, 2016; Procyk et al., 2016; Quilodran et al., 2008; Rothé et al., 2011; Loh et al., 2020), AiDE processing during the post-learning period recruits only the pMCC. Whereas both aMCC and pMCC appear to correspond to Cingulate Motor Area (CMA), both containing somatotopic motor representations (Amiez & Petrides, 2014; Dum & Strick, 1991; Loh et al., 2018), the aMCC, but not the pMCC, displays strong functional connectivity with the lateral prefrontal cortex (Giacometti et al., 2022; Loh et al., 2018) Altogether, these results strongly suggest main functional differences between the two regions. One hypothesis is that learning from FB from our own actions requires a higher level of integration between motor and cognition aspects than learning from AiDEs. Indeed, learning from FB specifically requires retrieving the history of action-FB relations, a process known

as critically involving the aMCC (Amiez, Joseph, et al., 2006; Rushworth et al., 2004, 2011; Scholl et al., 2015; Wittmann et al., 2016). This conclusion is also supported by two additional lines of evidence. First, the present study revealed that FB processing recruit the head of the caudate nucleus, a region involved in learning action-feedback contingencies, whereas learnt AiDE processing recruit the putamen, a region known as involved in successful learning (Amiez et al., 2012; Seger & Cincotta, 2005). Second, it has been shown that the aMCC and pMCC display differential functional connectivity with the basolateral AMG in humans, i.e. a negative versus a positive correlation strength, respectively (Giacometti et al., 2023b, *in revision*). Third, it has been shown that the aMCC and pMCC display stronger functional connectivity with, respectively, the anterior vs. whole insula, suggesting again that the aMCC is involved in higher cognitive control of motor processes than the pMCC (Taylor et al., 2009).

MCC region involved in FB and learnt AiDES processing

The subject-by-subject analysis revealed that the aMCC and the pMCC regions recruited for visual FB and AiDES processing was systematically located in the PCGS when present and in the CGS when the PCGS was absent. The pMCC was located at the intersection between the preparacental sulcus (PREPACS) and the CGS or PCGS, whereas the aMCC was located at the intersection between the posterior vertical paracingulate sulcus (P-VPCGS) and the CGS or PCGS, as previously shown using juice, visual, and auditory FB in similar problem-solving tasks without AiDE (Amiez et al., 2013, 2016; Loh et al., 2020). These regions reasonably correspond to the location of the face/eye cingulate motor areas as they follow the exact same relationships with sulcal pattern, suggesting that visual FB and AiDE are embodied in CMA of corresponding modalities (Procyk et al. 2016).

Conclusion

To effectively adapt to the demands of our environment, two critical aspects come into play: 1) the need to be aware of the outcomes of our own actions in the immediate environment (i.e, feedback) and 2) the need to remain vigilant to unexpected events unrelated to our actions, such as AiDEs. While learning from FB is quasi-immediate, AiDEs significance learning is more progressive as we must first decipher whether they are behavioral relevant, i.e., trigger or not an adaptive response. In that line of research, Mushtaq et al., (2011) suggested that decision-

making under uncertainty requires first a monitoring stage recruiting a network of brain areas thought to be involved in detection of contextual cues signaling the need for cognitive control, i.e., AMG, OFC, ACC, MCC, and in the utilization of this information to bias behavior. Resolving behavioral uncertainty would require regions involved in cognitive control such as the dlPFC (Mushtaq et al., 2011). Our results further complete this hypothesis by demonstrating that decision-making in behavioral adaptation precisely relies on the dynamic functional interplay of activation and deactivation between distinct brain networks: a network involved in environment evaluation, the AMG-vmPFC network, and a network involved in detecting events requiring an adaptation, the MCC-dlPFC network. Importantly, this network generically processes information from various contexts.

Acknowledgments

This work was funded by the French National Research Agency (ANR-18-CE37-0012-01 to C.A.). We also thank D. Ibarrola for technical help in acquiring neuroimaging data and G. Martin for help during the study pilote acquisition. C.A., F.H.-B. and E.P are employed by the Centre National de la Recherche Scientifique. Note that a CC-BY public copyright license has been applied by the authors to the present document and will be applied to all subsequent versions up to the Author Accepted Manuscript arising from this submission, in accordance with the grant's open access conditions. *Conflict of Interest:* None declared.

Author contributions

C.G: data acquisition, investigation, analyze both behavioral and fMRI, writing and reviewing the paper. **D.A-C:** data acquisition and pre-analyse of the fMRI data. **L.V:** fMRI task development. **F.L:** development of the pre-analyse of the fMRI data. **N.C,** **C.S:** participate in the pre-task developpement. **S.M:** Data acquisition. **E.P:** conceptualization and reviewing & editing the paper. **F.H-B:** conceptualization, investigation, writing, reviewing & editing the paper. **C.A:** funding, conceptualization, analysis and investigation of the fMRI data, writing, reviewing & editing the paper.

References

Aggleton, J. P. (2000). *The amygdala: a functional analysis* (J. P. Aggleton, Ed.; 2nd ed). Oxford University Press. <https://global.oup.com/academic/product/the-amygdala-9780198505013?cc=us&lang=en&>

- Amiez, C., Joseph, J. P., & Procyk, E. (2005). Anterior cingulate error-related activity is modulated by predicted reward. *European Journal of Neuroscience*, *21*(12), 3447–3452. <https://doi.org/10.1111/j.1460-9568.2005.04170.x>
- Amiez, C., Joseph, J. P., & Procyk, E. (2006). Reward encoding in the monkey anterior cingulate cortex. *Cerebral Cortex*, *16*(7), 1040–1055. <https://doi.org/10.1093/cercor/bhj046>
- Amiez, C., Kostopoulos, P., Champod, A. S., & Petrides, M. (2006). Local morphology predicts functional organization of the dorsal premotor region in the human brain. *Journal of Neuroscience*, *26*(10), 2724–2731. <https://doi.org/10.1523/JNEUROSCI.4739-05.2006>
- Amiez, C., Neveu, R., Warrot, D., Petrides, M., Knoblauch, K., & Procyk, E. (2013). The location of feedback-related activity in the midcingulate cortex is predicted by local morphology. *Journal of Neuroscience*, *33*(5), 2217–2228. <https://doi.org/10.1523/JNEUROSCI.2779-12.2013>
- Amiez, C., & Petrides, M. (2014). Neuroimaging evidence of the anatomo-functional organization of the human cingulate motor areas. *Cerebral Cortex*, *24*(3), 563–578. <https://doi.org/10.1093/cercor/bhs329>
- Amiez, C., Sallet, J., Procyk, E., & Petrides, M. (2012). Modulation of feedback related activity in the rostral anterior cingulate cortex during trial and error exploration. *NeuroImage*, *63*(3), 1078–1090. <https://doi.org/10.1016/j.neuroimage.2012.06.023>
- Amiez, C., Wutte, M. G., Faillenot, I., Petrides, M., Burle, B., & Procyk, E. (2016). Single subject analyses reveal consistent recruitment of frontal operculum in performance monitoring. *NeuroImage*, *133*, 266–278. <https://doi.org/10.1016/j.neuroimage.2016.03.003>
- Basile, G. A., Bertino, S., Bramanti, A., Ciurleo, R., Anastasi, G. P., Milardi, D., & Cacciola, A. (2021). Striatal topographical organization: Bridging the gap between molecules, connectivity and behavior. In *European Journal of Histochemistry* (Vol. 65, Issue s1).
- Bechara, A., Damasio, H., & Damasio, A. R. (2003). Role of the amygdala in decision-making. *Annals of the New York Academy of Sciences*, *985*, 356–369. <https://doi.org/10.1111/j.1749-6632.2003.tb07094.x>
- Bechara, A., Damasio, H., Damasio, A. R., & Lee, G. P. (1999). Different contributions of the human amygdala and ventromedial prefrontal cortex to decision-making. *Journal of Neuroscience*, *19*(13), 5473–5481. <https://doi.org/10.1523/jneurosci.19-13-05473.1999>
- Bechara, A., Tranel, D., & Damasio, H. (2000). Characterization of the decision-making deficit of patients with ventromedial prefrontal cortex lesions. In *Brain* (Vol. 123).
- Behrens, T. E. J., Woolrich, M. W., Walton, M. E., & Rushworth, M. F. S. (2007). Learning the value of information in an uncertain world. *Nature Neuroscience*, *10*(9), 1214–1221. <https://doi.org/10.1038/nn1954>
- Bernstein, M., Erez, Y., Blank, I., & Yovel, G. (2018). An Integrated Neural Framework for Dynamic and Static Face Processing. *Scientific Reports*, *8*(1). <https://doi.org/10.1038/s41598-018-25405-9>
- Blackford, J. U., Buckholz, J. W., Avery, S. N., & Zald, D. H. (2010). A unique role for the human amygdala in novelty detection. *NeuroImage*, *50*(3), 1188–1193. <https://doi.org/10.1016/j.neuroimage.2009.12.083>
- Boorman, E. D., Rushworth, M. F., & Behrens, T. E. (2013). Ventromedial prefrontal and anterior cingulate cortex adopt choice and default reference frames during sequential multi-

- alternative choice. *Journal of Neuroscience*, 33(6), 2242–2253. <https://doi.org/10.1523/JNEUROSCI.3022-12.2013>
- Calderazzo, S. M., Busch, S. E., Moore, T. L., Rosene, D. L., & Medalla, M. (2021). Distribution and overlap of entorhinal, premotor, and amygdalar connections in the monkey anterior cingulate cortex. *Journal of Comparative Neurology*, 529(4), 885–904. <https://doi.org/10.1002/cne.24986>
- Costa, V. D., Dal Monte, O., Lucas, D. R., Murray, E. A., & Averbeck, B. B. (2016). Amygdala and Ventral Striatum Make Distinct Contributions to Reinforcement Learning. *Neuron*, 92(2), 505–517. <https://doi.org/10.1016/j.neuron.2016.09.025>
- Cox, R. W. (1996). AFNI: Software for analysis and visualization of functional magnetic resonance neuroimages. *Computers and Biomedical Research*, 29(3), 162–173. <https://doi.org/10.1006/cbmr.1996.0014>
- Cunningham, W. A., & Brosch, T. (2012). Motivational salience: Amygdala tuning from traits, needs, values, and goals. *Current Directions in Psychological Science*, 21(1), 54–59. <https://doi.org/10.1177/0963721411430832>
- Di Martino, A., Scheres, A., Margulies, D. S., Kelly, A. M. C., Uddin, L. Q., Shehzad, Z., Biswal, B., Walters, J. R., Castellanos, F. X., & Milham, M. P. (2008). Functional connectivity of human striatum: A resting state fMRI study. *Cerebral Cortex*, 18(12), 2735–2747. <https://doi.org/10.1093/cercor/bhn041>
- Dum, R. P., & Strick, P. L. (1991). The origin of corticospinal projections from the premotor areas in the frontal lobe. *Journal of Neuroscience*, 11(3), 667–689. <https://doi.org/10.1523/jneurosci.11-03-00667.1991>
- DuPre, E., Salo, T., Ahmed, Z., Bandettini, P., Bottenhorn, K., Caballero-Gaudes, C., Dowdle, L., Gonzalez-Castillo, J., Heunis, S., Kundu, P., Laird, A., Markello, R., Markiewicz, C., Moia, S., Staden, I., Teves, J., Uruñuela, E., Vaziri-Pashkam, M., Whitaker, K., & Handwerker, D. (2021). TE-dependent analysis of multi-echo fMRI with tedana. *Journal of Open Source Software*, 6(66), 3669. <https://doi.org/10.21105/joss.03669>
- Friston, K. J., Holmes, A. P., Poline, J.-B., Grasby, P. J., Williams, S. C. R., Frackowiak, R. S. J., & Turner, R. (1995). Analysis of fMRI Time-Series Revisited. *NeuroImage*, 2(1), 45–53. <https://doi.org/10.1006/nimg.1995.1007>
- Gangopadhyay, P., Chawla, M., Dal Monte, O., & Chang, S. W. C. (2021). Prefrontal–amygdala circuits in social decision-making. In *Nature Neuroscience* (Vol. 24, Issue 1, pp. 5–18). Nature Research. <https://doi.org/10.1038/s41593-020-00738-9>
- Ghashghaei, H. T., Hilgetag, C. C., & Barbas, H. (2007). Sequence of information processing for emotions based on the anatomic dialogue between prefrontal cortex and amygdala. *NeuroImage*, 34(3), 905–923. <https://doi.org/10.1016/j.neuroimage.2006.09.046>
- Giacometti, C., Amiez, C., & Hadj-Bouziane, F. (2023). Multiple routes of communication within the amygdala-mPFC network: A comparative approach in humans and macaques. *Current Research in Neurobiology*, 100103. <https://doi.org/10.1016/j.crneur.2023.100103>
- Giacometti, C., Dureux, A., Autran-Clavagnier, D., Wilson, C. R. E., Sallet, J., Dirheimer, M., Procyk, E., Hadj-Bouziane, F., & Amiez, C. (2022). Frontal cortical functional connectivity is impacted by anaesthesia in macaques. *Cerebral Cortex*, 32(18), 4050–4067. <https://doi.org/10.1093/cercor/bhab465>

- Gläscher, J., Adolphs, R., Damasio, H., Bechara, A., Rudrauf, D., Calamia, M., Paul, L. K., & Tranel, D. (2012). Lesion mapping of cognitive control and value-based decision making in the prefrontal cortex. *Proceedings of the National Academy of Sciences of the United States of America*, *109*(36), 14681–14686. <https://doi.org/10.1073/pnas.1206608109>
- Gothard, K. M. (2020). Multidimensional processing in the amygdala. *Nature Reviews Neuroscience*, *21*(10), 565–575. <https://doi.org/10.1038/s41583-020-0350-y>
- Grabenhorst, F., & Rolls, E. T. (2011). Value, pleasure and choice in the ventral prefrontal cortex. *Trends in Cognitive Sciences*, *15*(2), 56–67. <https://doi.org/10.1016/j.tics.2010.12.004>
- Gupta, R., Koscik, T. R., Bechara, A., & Tranel, D. (2011). The amygdala and decision-making. *Neuropsychologia*, *49*(4), 760–766. <https://doi.org/10.1016/j.neuropsychologia.2010.09.029>
- Hammerstrom, M. R., Ferguson, T. D., Williams, C. C., & Krigolson, O. E. (2021). What happens when right means wrong? The impact of conflict arising from competing feedback responses. *Brain Research*, *1761*. <https://doi.org/10.1016/j.brainres.2021.147393>
- Hampton, A. N., Adolphs, R., Tyszka, M. J., & O'Doherty, J. P. (2007). Contributions of the Amygdala to Reward Expectancy and Choice Signals in Human Prefrontal Cortex. *Neuron*, *55*(4), 545–555. <https://doi.org/10.1016/j.neuron.2007.07.022>
- Hyafil, A., Summerfield, C., & Koehlin, E. (2009). Two mechanisms for task switching in the prefrontal cortex. *Journal of Neuroscience*, *29*(16), 5135–5142. <https://doi.org/10.1523/JNEUROSCI.2828-08.2009>
- Juechems, K., Balaguer, J., Hecce Castañón, S., Ruz, M., O'Reilly, J. X., & Summerfield, C. (2019). A Network for Computing Value Equilibrium in the Human Medial Prefrontal Cortex. *Neuron*, *101*(5), 977–987.e3. <https://doi.org/10.1016/j.neuron.2018.12.029>
- Klein-Flügge, M. C., Jensen, D. E. A., Takagi, Y., Priestley, L., Verhagen, L., Smith, S. M., & Rushworth, M. F. S. (2022). Relationship between nuclei-specific amygdala connectivity and mental health dimensions in humans. *Nature Human Behaviour*. <https://doi.org/10.1038/s41562-022-01434-3>
- Kundu, P., Brenowitz, N. D., Voon, V., Worbe, Y., Vértes, P. E., Inati, S. J., Saad, Z. S., Bandettini, P. A., & Bullmore, E. T. (2013). Integrated strategy for improving functional connectivity mapping using multiecho fMRI. *Proceedings of the National Academy of Sciences of the United States of America*, *110*(40), 16187–16192. <https://doi.org/10.1073/pnas.1301725110>
- Kundu, P., Inati, S. J., Evans, J. W., Luh, W. M., & Bandettini, P. A. (2012). Differentiating BOLD and non-BOLD signals in fMRI time series using multi-echo EPI. *NeuroImage*, *60*(3), 1759–1770. <https://doi.org/10.1016/j.neuroimage.2011.12.028>
- Langner, O., Dotsch, R., Bijlstra, G., Wigboldus, D. H. J., Hawk, S. T., & van Knippenberg, A. (2010). Presentation and validation of the Radboud Faces Database. *Cognition & Emotion*, *24*(8), 1377–1388. <https://doi.org/10.1080/02699930903485076>
- Loh, K. K., Hadj-Bouziane, F., Petrides, M., Procyk, E., & Amiez, C. (2018). Rostro-Caudal organization of connectivity between cingulate motor areas and lateral frontal regions. *Frontiers in Neuroscience*, *11*(JAN). <https://doi.org/10.3389/fnins.2017.00753>
- Loh, K. K., Procyk, E., Neveu, R., Lambertson, F., Hopkins, W. D., Petrides, M., & Amiez, C. (2020). Cognitive control of orofacial motor and vocal responses in the ventrolateral and

- dorsomedial human frontal cortex. *Proceedings of the National Academy of Sciences*, 117(9), 4994–5005. <https://doi.org/10.1073/pnas.1916459117>
- Mehta, P. S., Tu, J. C., LoConte, G. A., Pesce, M. C., & Hayden, B. Y. (2019). Ventromedial prefrontal cortex tracks multiple environmental variables during search. *Journal of Neuroscience*, 39(27), 5336–5350. <https://doi.org/10.1523/JNEUROSCI.2365-18.2019>
- Murray, E. A., & Fellows, L. K. (2021). Prefrontal cortex interactions with the amygdala in primates. *Neuropsychopharmacology*, July, 1–17. <https://doi.org/10.1038/s41386-021-01128-w>
- Mushtaq, F., Bland, A. R., & Schaefer, A. (2011). Uncertainty and cognitive control. *Frontiers in Psychology*, 2(SEP). <https://doi.org/10.3389/fpsyg.2011.00249>
- Ousdal, O. T., Jensen, J., Server, A., Hariri, A. R., Nakstad, P. H., & Andreassen, O. A. (2008). The human amygdala is involved in general behavioral relevance detection: Evidence from an event-related functional magnetic resonance imaging Go-NoGo task. *Neuroscience*, 156(3), 450–455. <https://doi.org/10.1016/j.neuroscience.2008.07.066>
- Ousdal, O. T., Reckless, G. E., Server, A., Andreassen, O. A., & Jensen, J. (2012). Effect of relevance on amygdala activation and association with the ventral striatum. *NeuroImage*, 62(1), 95–101. <https://doi.org/10.1016/j.neuroimage.2012.04.035>
- Pedersen, W. S., Balderston, N. L., Miskovich, T. A., Belleau, E. L., Helmstetter, F. J., & Larson, C. L. (2017). The effects of stimulus novelty and negativity on BOLD activity in the amygdala, hippocampus, and bed nucleus of the stria terminalis. *Social Cognitive and Affective Neuroscience*, 12(5), 748–757. <https://doi.org/10.1093/scan/nsw178>
- Pelliccia, V., Del Vecchio, M., Avanzini, P., Revay, M., Sartori, I., & Caruana, F. (2023). 70 Years of Human Cingulate Cortex Stimulation. Functions and Dysfunctions Through the Lens of Electrical Stimulation. *Journal of Clinical Neurophysiology*. <https://doi.org/10.1097/WNP.0000000000000961>
- Pessoa, L., & Adolphs, R. (2010). Emotion processing and the amygdala: From a “low road” to “many roads” of evaluating biological significance. In *Nature Reviews Neuroscience* (Vol. 11, Issue 11, pp. 773–782). <https://doi.org/10.1038/nrn2920>
- Procyk, E., Amiez, C., Fontanier, V., & Stoll, F. (2016). Frontal neural dynamics during performance monitoring and decisions to explore. *International Journal of Psychophysiology*, 108, 11. <https://doi.org/10.1016/j.ijpsycho.2016.07.039>
- Procyk, E., Wilson, C. R. E., Stoll, F. M., Faraut, M. C. M., Petrides, M., & Amiez, C. (2016). Midcingulate Motor Map and Feedback Detection: Converging Data from Humans and Monkeys. *Cerebral Cortex*, 26(2), 467–476. <https://doi.org/10.1093/cercor/bhu213>
- Quilodran, R., Rothé, M., & Procyk, E. (2008). Behavioral Shifts and Action Valuation in the Anterior Cingulate Cortex. *Neuron*, 57(2), 314–325. <https://doi.org/10.1016/j.neuron.2007.11.031>
- Rothé, M., Quilodran, R., Sallet, J., & Procyk, E. (2011). Coordination of high gamma activity in anterior cingulate and lateral prefrontal cortical areas during adaptation. *Journal of Neuroscience*, 31(31), 11110–11117. <https://doi.org/10.1523/JNEUROSCI.1016-11.2011>
- Rushworth, M. F. S., Noonan, M. A. P., Boorman, E. D., Walton, M. E., & Behrens, T. E. (2011). Frontal Cortex and Reward-Guided Learning and Decision-Making. In *Neuron* (Vol. 70, Issue 6, pp. 1054–1069). <https://doi.org/10.1016/j.neuron.2011.05.014>

- Rushworth, M. F. S., Walton, M. E., Kennerley, S. W., & Bannerman, D. M. (2004). Action sets and decisions in the medial frontal cortex. In *Trends in Cognitive Sciences* (Vol. 8, Issue 9, pp. 410–417). <https://doi.org/10.1016/j.tics.2004.07.009>
- Saez, A., Rigotti, M., Ostojic, S., Fusi, S., & Salzman, C. D. (2015). Abstract Context Representations in Primate Amygdala and Prefrontal Cortex. *Neuron*, *87*(4), 869–881. <https://doi.org/10.1016/j.neuron.2015.07.024>
- Sallet, J., Camille, N., & Procyk, E. (2013). Modulation of feedback-related negativity during trial-and-error exploration and encoding of behavioral shifts. *Frontiers in Neuroscience*, *7* NOV. <https://doi.org/10.3389/fnins.2013.00209>
- Santos, A., Mier, D., Kirsch, P., & Meyer-Lindenberg, A. (2011). Evidence for a general face salience signal in human amygdala. *NeuroImage*, *54*(4), 3111–3116. <https://doi.org/10.1016/j.neuroimage.2010.11.024>
- Schneider, B., & Koenigs, M. (2017). Human lesion studies of ventromedial prefrontal cortex. *Neuropsychologia*, *107*(July), 84–93. <https://doi.org/10.1016/j.neuropsychologia.2017.09.035>
- Scholl, J., Kolling, N., Nelissen, N., Wittmann, M. K., Harmer, C. J., & Rushworth, M. F. S. (2015). The good, the bad, and the irrelevant: Neural mechanisms of learning real and hypothetical rewards and effort. *Journal of Neuroscience*, *35*(32), 11233–11251. <https://doi.org/10.1523/JNEUROSCI.0396-15.2015>
- Seger, C. A., & Cincotta, C. M. (2005). The Roles of the Caudate Nucleus in Human Classification Learning. *The Journal of Neuroscience*, *25*(11), 2941–2951. <https://doi.org/10.1523/JNEUROSCI.3401-04.2005>
- Sharma, K. K., Kelly, E. A., Pfeifer, C. W., & Fudge, J. L. (2020). Translating Fear Circuitry: Amygdala Projections to Subgenual and Perigenual Anterior Cingulate in the Macaque. *Cerebral Cortex*, *30*(2), 550–562. <https://doi.org/10.1093/cercor/bhz106>
- Smith, E. H., Banks, G. P., Mikell, C. B., Cash, S. S., Patel, S. R., Eskandar, E. N., & Sheth, S. A. (2015). Frequency-dependent representation of reinforcement-related information in the human medial and lateral prefrontal cortex. *Journal of Neuroscience*, *35*(48), 15827–15836. <https://doi.org/10.1523/JNEUROSCI.1864-15.2015>
- Taylor, K. S., Seminowicz, D. A., & Davis, K. D. (2009). Two systems of resting state connectivity between the insula and cingulate cortex. *Human Brain Mapping*, *30*(9), 2731–2745. <https://doi.org/10.1002/hbm.20705>
- The tedana Community; Ahmed, Z., Bandettini, P. A. ;, Bottenhorn, K. L. ;, Caballero-Gaudes, C., Dowdle, L. T. ;, DuPre, E., Handwerker, D., Heunis, S., Kundu, P., Laird, A. R. ;, Markello, R., Markiewicz, C. J. ;, Maullin-Sapey, T., Moia, S., Salo, T., Staden, I., Teves, J., Uruñuela, E., ... Whitaker, K. (2021). *ME-ICA/tedana: 0.0.9*. <https://doi.org/https://doi.org/10.5281/zenodo.4509480>
- Vassena, E., Krebs, R. M., Silvetti, M., Fias, W., & Verguts, T. (2014). Dissociating contributions of ACC and vmPFC in reward prediction, outcome, and choice. *Neuropsychologia*, *59*, 112–123. <https://doi.org/10.1016/j.neuropsychologia.2014.04.019>
- Viejo, G., Khamassi, M., Brovelli, A., & Girard, B. (2015). Modeling choice and reaction time during arbitrary visuomotor learning through the coordination of adaptive working memory and reinforcement learning. *Frontiers in Behavioral Neuroscience*, *9*(AUGUST). <https://doi.org/10.3389/fnbeh.2015.00225>

- Wittmann, M. K., Kolling, N., Akaishi, R., Chau, B. K. H., Brown, J. W., Nelissen, N., & Rushworth, M. F. S. (2016). Predictive decision making driven by multiple time-linked reward representations in the anterior cingulate cortex. *Nature Communications*, 7(1). <https://doi.org/10.1038/ncomms12327>
- Worsley, K. J., Marrett, S., Neelin, P., Vandal, A. C., Friston, K. J., Evans, A. C., & Brain, M. (1996). A Unified Statistical Approach for Determining Significant Signals in Images of Cerebral Activation + +. In *Human Brain Mapping*.
- Yizhar, O., & Klavir, O. (2018). Reciprocal amygdala–prefrontal interactions in learning. *Current Opinion in Neurobiology*, 52, 149–155. <https://doi.org/10.1016/j.conb.2018.06.006>
- Zangemeister, L., Grabenhorst, F., & Schultz, W. (2020). Neural activity in human ventromedial prefrontal cortex reflecting the intention to save reward. *Social Cognitive and Affective Neuroscience*, 14(12), 1255–1261. <https://doi.org/10.1093/scan/nsaa013>

Tables

Table S1. Maxima of activity increases observed at the occurrence of FB in Search versus Repetition periods of the problems displaying no AiDE in non-social and social contexts.

	Non-social				Social			
	x	y	z	t-value	x	y	z	t-value
Left hemisphere								
pMCC	-8	8	54	7.07	-8	0	52	7.87
aMCC	-8	14	46	7.37	-2	20	46	8.69
OFC	-24	48	-12	3.97	-22	50	-14	3.43
Area 46	-24	48	4	5.35	-34	52	0	5.61
Area 9/46	-42	28	28	5.73	-44	30	28	6.31
PFOp	-28	20	-2	7.13	-32	18	-4	8.14
IFJ	-52	6	32	5.45	-56	3	36	8.51
Caudate nucleus	-8	8	4	3.38	-6	10	4	4.12
AMG	-	-	-	-	-	-	-	-
Right hemisphere								
aMCC	10	24	34	5.11	8	18	44	6.27
					8	38	36	7.28
dlPFC:								
Area 46	48	46	28	3.66	34	50	-4	6.12
Area 9/46	40	44	24	3.61	-44	30	28	6.31
PFOp	30	22	-2	6.33	30	20	0	7.36
IFJ	58	10	28	4.43	56	4	30	3.12
Caudate nucleus	8	8	8	3.94	10	10	4	5.71
AMG	-	-	-	-	-	-	-	-

Table S2. Distribution of subjects displaying a PCGS in the left hemisphere only (LH only), in the right hemisphere only (RH only), in both hemispheres, or not.

PCGS patterns	Social	Non-social
LH only	7	4
RH only	2	4
Both Hem	6	6
Absent	6	7

Table S3. Maxima of activity increases are observed at the occurrence of AiDE in the first run of the learning period compared to the post-learning period in non-social and social contexts.

	Non-social				Social			
	x	y	z	t-value	x	y	z	t-value
Left hemisphere								
Amygdala	-24	0	-22	3.04	-16	-8	-16	4.42
NAC	-6	2	-6	4.61	4	6	-6	7.38
VMPFC	-2	24	-10	4.25	-4	28	-10	3.11
ACC	-	-	-	-	-12	50	10	4.18
DMPFC (9m)	-	-	-	-	-2	54	21	3.76
VLPFC	-42	30	-6	3.84	-36	30	-8	4.04
Temporal pole	-40	5	-34	4.19	-42	18	-34	5.66
STS	-52	-6	-20	3.81	-52	-2	-20	5.12
OFA	-	-	-	-	-30	-80	-8	6.99
FFA	-	-	-	-	-40	-48	-18	5.56
MCC	-	-	-	-	-	-	-	-
Right hemisphere								
Amygdala	22	-4	-22	3.43	18	-8	-14	4.05
NAC	-	-	-	-	4	6	-6	7.38
VMPFC	8	30	-16	4.22	-	-	-	-
ACC	-	-	-	-	30	20	0	7.36
DMPFC (9m)	-	-	-	-	56	4	30	3.12
VLPFC	8	8	8	3.94	48	28	-2	5.41
Temporal pole	32	6	-34	4.44	50	18	-22	5.25
STS	52	0	-24	5.56	52	-8	-18	4.25
OFA	-	-	-	-	26	-80	-8	7.22
FFA	-	-	-	-	40	-44	-16	4.3
MCC	-	-	-	-	-	-	-	-

Table S4. Maxima of activity increases are observed at the occurrence of AiDE in the post-learning period compared to the first run of the learning period in non-social and social contexts.

	Non-social				Social			
	x	y	z	t-value	x	y	z	t-value
Left hemisphere								
pMCC	-7	-4	50	3.97	-2	-4	52	6.82
OFC	-34	48	-16	3.66	-	-	-	-
Area 9/46	-	-	-	-	-34	38	24	3.43
PFOp	-28	16	10	3.95	-	-	-	-
Putamen	-26	6	6	3.7	-24	4	6	5.3
AMG	-	-	-	-	-	-	-	-
Right hemisphere								
pMCC	10	-4	52	3.22	8	2	42	4.66
OFC	26	46	-10	3.95	24	44	-16	3.26
dIPFC:								
Area 46	44	46	18	3.26	44	52	5	5.68
Area 9/46	30	36	28	3.54	30	38	20	4.42
PFOp	28	24	12	4.89	30	16	10	3.69
Putamen	22	4	10	3.13	26	4	0	5.92
AMG	-	-	-	-	-	-	-	-

GENERAL DISCUSSION

CHAPTER I. FINDINGS OVERVIEW

The central objective of my thesis was to uncover: 1) the intricate organization of the anatomo-functional dialogue between the amygdala (AMG) and the prefrontal cortex/medial prefrontal cortex (PFC/mPFC) in primates, and 2) whether and how it evolved across species. Through this research, I shedded light on how this dialogue contributes to specific aspects of behavioral adaptation. More specifically, I identified how the dynamic interplay within the AMG-mPFC network dynamic interplay unfolds when we learn to adapt to unexpected behaviorally relevant information from our immediate environment (*i.e.*, action independent events, AiDEs). In the introduction review (Giacometti et al., 2023; **Chapter III of the Introduction**), I hypothesized that two routes within the AMG-mPFC network might support distinct temporal dynamics of integration necessary for behavioral adaptation, the former dealing with long-term contextual adaptation (vmPFC-LB) and the latter dealing with online monitoring of actions (LB-aMCCa and CM-aMCC). My results demonstrated that the two routes engage in a complementary dynamic interplay of positive/negative correlations of activity in rs-fMRI and activation/deactivation during a task requiring behavioral adaptation.

In **Chapter I**, I explored the effect of the anaesthesia in the cingulo-frontal network by comparing the FC at rest in the same group of macaques in an awake and anaesthetized state. I pinpointed two important results. First, in a comparative view, I observed that the most rostral cingulate regions were more functionally correlated with the most rostral lateral prefrontal regions (*i.e.*, areas 10, 46, and 9/46) compared with frontolateral motor regions. Inversely, caudal cingulate regions were more functionally correlated with frontal lateral motor regions (*i.e.*, M1 Face and M1 Hand) compared with rostrolateral prefrontal regions. This functional gradient organization in macaques is highly similar to the one that has been previously described in humans by Loh et al. (2018). Second, my results revealed that this functional gradient can be tackled only when macaques are in the awake state, anesthesia causing an overall reduction of the correlation strength between the activity of the regions.

Building on these results, in **Chapter II**, based on a precise methodology that accounts for regions complexity and morphological variabilities and rs-fMRI, I

investigated the functional connectivity between the AMG main nuclei and the whole extent of the mPFC in both humans and awake macaques. Results unravel their complex functional interplay and especially how it manifests and diverges across species. In humans, the laterobasal AMG (LA, BL and BM nuclei) shows a U-shaped functional connectivity pattern with the mPFC along the corpus callosum, featuring a negative correlation peak in the aMCC. By contrast, in macaques, the negative functional connectivity peak shifts more ventrally to the junction between the vmPFC and the ACC and involves the entire AMG (including CE). This study offers new insights into the nuanced interplay within the AMG-mPFC network and their possible contribution to behavioral adaptation.

Finally, in the last chapter of the experimental part of my thesis, **Chapter III**, I examined how the functional interplay within the AMG-mPFC network uncovered at rest would be reflected during behavioral adaptation in humans. More specifically, I identified how the brain learns how to adapt to Action InDependant Events (AiDE) versus to behavioral feedback (FB). Indeed, these two events can frequently occur concurrently and demand distinct behavioral adjustments. Importantly, adapting from FB and AiDE requires resolving their dynamic differences (*i.e.*, causality and temporality): while FB directly links to our actions, AiDE lacks such causal relationship, necessitating evidence accumulation for proper adaptation. The neural basis of this credit assignment problem remains unknown and particularly the contribution of the AMG-PFC network. Using fMRI associated with a novel behavioral task combining both FB and AiDEs and in accordance with our humans rs-fMRI results, I revealed a differential involvement of the AMG-vmPFC-ACC and the MCC-dIPFC networks in learning AiDEs adaptive meaning: the former is recruited in the early AiDEs occurrence stage whereas the latter is recruited once the adaptive relevance is integrated. Importantly, FB and learnt AiDEs processing recruit distinct MCC regions (aMCC and pMCC, respectively), shedding new lights on how the brain adapts from distinct events and on the anatomo-functional distinction between aMCC and pMCC.

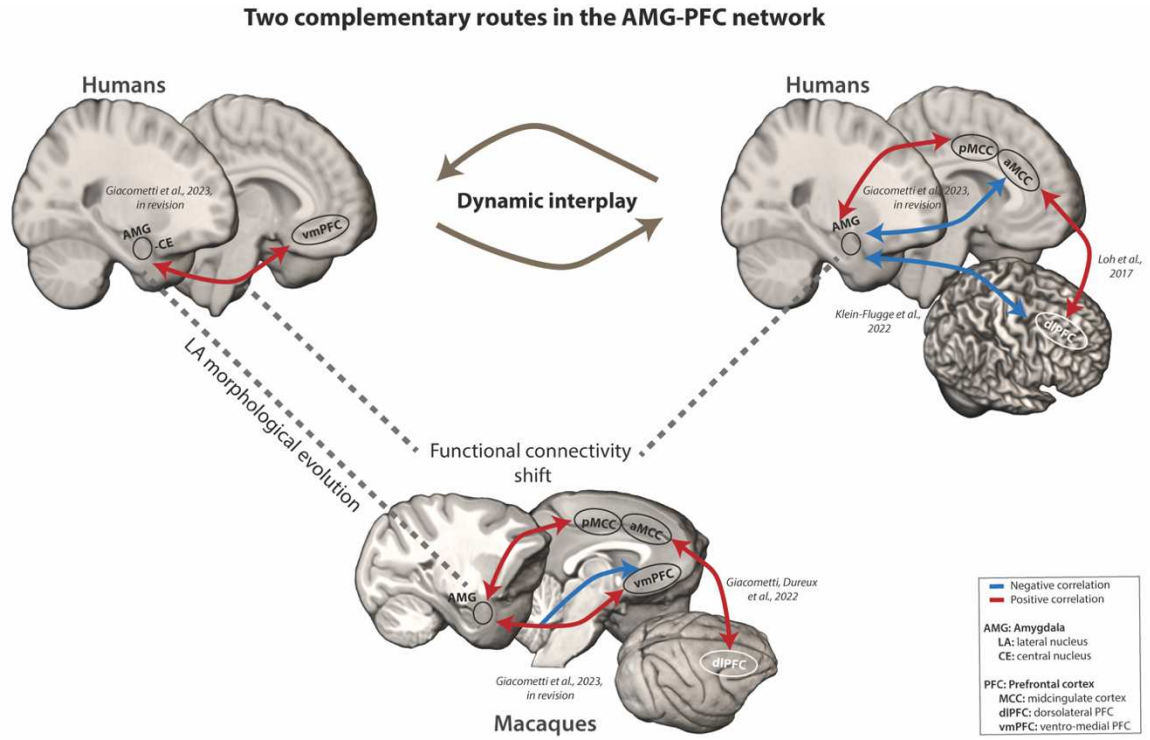


Figure1. A schematic representation of the key findings of this thesis.

CHAPTER II. AMG-PFC ANATOMO-FUNCTIONAL INTERPLAY

CONTRIBUTION TO BEHAVIORAL ADAPTATION IN HUMANS

For behavioral adaptation, decision-making in an uncertain environment is rather complex. Several events can trigger a need for adaptive response. Learning the adaptive significance of these events can be straightforward (e.g., actions-FB) or require accumulating evidence, especially when facing novel and uncertain events (e.g., FB-AiDE). In my introduction review (Giacometti et al., 2023; **Chapter III of the Introduction**), I highlighted two dynamic routes within the AMG-mPFC network with complementary temporal dynamics of integration: long-term contextual evaluation and short-term behavioral adaptation via an online monitoring of actions. Accordingly, my results revealed a dynamic interplay of positive/negative correlation at rest (**Chapter II of Experimental part**) that is further translated into an engagement/disengagement dynamic that sustained specific timeline of behavioral adaptation features in humans (**Chapter III of the Experimental part**).

1. DETECTION AND CONTEXTUAL EVALUATION OF SALIENT EVENTS: AMG-vmPFC

The former route articulated around AMG-vmPFC interactions. In the **Chapter II of the Experimental part**, I revealed a progressive and dynamic positive-negative u-shape functional connectivity pattern between the laterobasal AMG (include LA, BL and BM nuclei, minus CE) and mPFC in humans. More precisely, I showed strong positive correlation between the laterobasal AMG and the functionally defined extent of the vmPFC (Lopez-Persem et al., 2019). Along the corpus callosum, positive correlations start to decrease towards negativity at the level of the vmPFC/ACC limit (sulci fork, Amiez et al., 2019). ACC is viewed as a transition zone between AMG-vmPFC and AMG-aMCC where correlation strengths are globally weaker (i.e., weak positive and weak negative). Negative correlation reached its highest negative correlation peak in the aMCC at the level of the VPCGS-a sulcus and, correlation progressively returned to positive correlation for the whole extent of the pMCC. Coherently, in the **Chapter III of the Experimental part**, I further demonstrated that

the AMG and the vmPFC were conjointly recruited during significant AiDEs first occurrence while the MCC was deactivated. The ACC was also recruited with the AMG and the vmPFC and did not co-activate with the MCC later on (*i.e.*, when subjects were naïve and thus faced unexpected and uncertain stimuli; significant AiDEs present a certain emotional salience: sun/clouds in the non-social context and happy/angry faces in the social context). To note, although eliciting a ventral striatum activation, neutral AiDE did not trigger AMG nor vmPFC activation especially for the non-social context (Data not shown). This first route is necessary for learning behavioral significance for relevant events such as AiDEs due to their complementary and conjoint involvement in 3 specific functions guiding behavioral decisions to adapt where the MCC-dIPFC network takes over.

The initial step in comprehending the significance of events like significant AiDEs is quite straightforward: their immediate detection. When individuals were naïve to these events, they first considered them as unexpected, uncertain but however salient events (*i.e.*, significant AiDEs were positively and negatively valenced). Although not yet possible with MRI data due to poor temporal resolution, if I was to describe a timeline, prior to vmPFC I would expect an activation of the AMG. As demonstrated by a wide amount of studies in fear conditioning, during dangerous situations, AMG is on the first line and acts as the body radar and alarm to detect possible threats (see for review Kang et al., 2022; Liddell et al., 2005; Öhman, 2005). However, AMG detecting abilities extend beyond threat assessment. Davis and Whalen (2001) have suggested a model in which the AMG is responsible for increasing levels of vigilance in response to uncertain stimuli or situations (Davis & Whalen, 2001). In line with that idea, further neuroimaging studies suggested that the AMG plays a crucial role in detecting novel and salient informations (Blackford et al., 2010; Jacobs et al., 2012; Mason et al., 2006; Pedersen et al., 2017; Santos et al., 2011) as well as mediating vigilance, redirecting and guiding attention towards relevant cues of the environment (Belova et al., 2008; Domínguez-Borràs et al., 2020; Herry et al., 2007; Jacobs et al., 2012; Ousdal et al., 2008, 2014; Paton et al., 2006; Pessoa & Adolphs, 2010; Tazumi et al., 2010).

Subsequently, the evaluation phases ensue in which both the AMG and the vmPFC partake. After salient features of the stimulus have been processed, we are able to assign a value based on its emotional (*i.e.*, trigger an emotional state) and behavioral relevance (*i.e.*, ignore or not). This value, reflecting the perceived and

subjective significance of the stimulus, is integrated with individual current goals and motivation. In decision-making processes, the value is learnt through the association between a stimulus and/or available options and its outcome (*i.e.*, rewards or not). In humans, individuals with lesions in both the vmPFC and the AMG regions demonstrated the capacity to make decisions; however, their decision-making processes were characterized by inconsistency and increased risk-taking due to their diminished ability to thoroughly evaluate their options and failure to induce an emotional/somatic state (*i.e.*, also refers to an arousal state; Anderson & Phelps, 2001; Bechara et al., 1999, 2000, 2003; Davis & Whalen, 2001; Fellows & Farah, 2007). Both the AMG and the vmPFC are involved in the creation of this somatic/emotional state towards a stimulus. However, the AMG is more seen as an inducer while the vmPFC has been proposed as a modulator, tuning-down the arousal when needed (Andrewes & Jenkins, 2019; Bechara et al., 1999, 2000, 2003; Morawetz et al., 2017; Motzkin et al., 2015; Nicholson et al., 2015; Watanabe et al., 2019). Not only, the AMG-vmPFC network has the ability to encode the value representation of a current stimuli/option but also, keep track of the value of previous ones and thus create value expectations towards novel ones (Belova et al., 2008; Boorman et al., 2013; Costa et al., 2019; Cunningham & Brosch, 2012; Kolling et al., 2012; Leathers & Olson, 2017; Meder et al., 2017; Ousdal et al., 2014; Paton et al., 2006; Rushworth et al., 2011; A. Saez et al., 2015; R. A. Saez et al., 2017; Scholl et al., 2015; Vassena et al., 2014; Zangemeister et al., 2016, 2020; W. Zhang et al., 2013). Additionally, and coherently with their value representation and attribution function, the AMG and the vmPFC regions are important components of associative learning (Esber et al., 2015; Li et al., 2011; Spalding et al., 2018). Although, in my study, I did not particularly assess this specific feature yet, I would expect to see their complementary activation of these two regions in learning the association the AiDEs to the FB and concomitant the choice during the first phases.

On a wider scale, the complementary roles of the AMG and the vmPFC in environmental monitoring, involving the detection and evaluation of stimuli, require also the recruitment of additional brain regions. Notably, the nucleus accumbens (NAC), a part of the ventral striatum known for its robust anatomical and functional connections with both the AMG and vmPFC (Basile et al., 2021; Di Martino et al., 2008). NAC has been shown to co-activate with with the AMG-vmPFC network during relevance detection, associative learning, value representation and emotional

evaluation (Antzoulatos & Miller, 2011; Basile et al., 2021; Cardinal et al., 2002; Costa et al., 2016; Doré et al., 2017; Esber et al., 2015; Li et al., 2011; Niznikiewicz & Delgado, 2011; Ousdal et al., 2012; Pasupathy & Miller, 2005; Pujara et al., 2016; van Holstein et al., 2020). In line with these findings, my study also revealed concurrent activation of the NAC alongside the AMG and the vmPFC during the initial occurrence of significant AiDEs. Furthermore, an essential aspect of the whole conceptualization process is the ability to maintain and store information. It implicates brain regions associated with complex and abstract context processing and memorization including structures of temporal lobe including the hippocampus, entorhinal cortex, temporal pole, STS, among others. These structures exhibit robust structural and functional connections with both the AMG and the vmPFC (Aggleton et al., 1980; Ghashghaei & Barbas, 2002; Herzog & Van Hoesen, 1976; Joyce & Barbas, 2018; Suzuki, 1996; Wang et al., 2021; Wang & Barbas, 2018). Accordingly, I also found activations of these regions during AiDEs first Occurrence phase.

Collectively, the complementarity activation of these brain regions with the AMG-vmPFC network created a larger brain-scale network that play an essential role in AiDEs conceptualization and learning, notably maintaining the accumulating perceptual evidence of AiDEs' meanings, by associating their value with FB and future choices thereby guiding behavioral decisions more accurately.

2. DETECTION OF LEARNT BEHAVIORALLY SIGNIFICANT EVENTS: MCC-DLPFC

Upon learning the behavioral and adaptive relevance of a stimulus, such as AiDEs, the second route, the MCC-dIPFC network, was recruited. Interestingly, while the MCC-dIPFC network was activated for both FB in exploration and learnt AiDEs processing, the AMG-vmPFC network disengaged. To note, the AMG-vmPFC network was recruited for FB in the exploration period during the task (Data not shown), when no need of adaptive response was needed and individuals were fully rewarded for their appropriate choices (*i.e.*, positive FB reinforcement; Costa et al., 2016; Watanabe et al., 2019). These align with the widely accepted role of MCC-dIPFC in online monitoring of actions and behavioral shift (Amiez et al., 2005, 2006, 2012, 2013; Amiez & Petrides, 2014; Kolling et al., 2012; Loh et al., 2020; Procyk, Amiez, et al., 2016; Procyk, Wilson, et al., 2016; Quilodran et al., 2008; Rothé et al., 2011; Wittmann et

al., 2016). However, our results further envisioned the MCC-dIPFC network as an important network in, not only monitoring our own actions outcomes or behavioral shift, but also salient events that specifically signal a need to adjust our behavioral responses: a need to adapt. It is also coherent with our rs-fMRI results in **Chapter II and Chapter III of the Experimental part**, where 1) MCC-dIPFC shares strong functional connections and with a great emphasis aMCC-dIPFC compare to pMCC-dIPFC that shares weaker ones (Giacometti et al., 2022; Loh et al., 2018) and 2) the laterobasal AMG displayed a strong anticorrelation pattern with the aMCC. More precisely, negative correlation starts from the ACC, peaked in the aMCC and diminished towards positive correlation for the pMCC (Giacometti et al., 2023, *in revision*). In agreement with the anticorrelated AMG-aMCC and disengagement of the AMG in task, the AMG and the dIPFC have been shown to also be negatively correlated in rs-fMRI (Klein-Flügge, Jensen, et al., 2022). Altogether, this suggests a dynamic interplay of correlation/anticorrelation at rest translated into an activation/deactivation process between both networks when known adaptive events are detected (*i.e.*, both FB and AiDEs trigger a shift-or-stay type of responses), possibly to avoid any interferences. I further hypothesized that the MCC-DIPFC network would exhibit a top-down cognitive control towards the AMG and by echo would also affect vmPFC (Dixon, 2015; Gee et al., 2022). However, this interpretation needs to be a bit nuanced. Hare et al., (2011), demonstrated via a combination of DCM analysis and fMRI showed that activity in the MCC exhibited increased functional coupling at the time of decision (*i.e.*, choices) with vmPFC (Hare et al., 2011). Hare's team further suggested that the dIPFC and the vmPFC engaged further at the time of the decisions. While the vmPFC computes the value of options by first assessing their various attributes (*i.e.*, the AMG-vmPFC network), the dIPFC online-monitors the vmPFC activity for a more optimal decision-making process: development of a certain self-control over the valued options (*i.e.*, modulatory change in effective connectivity; (Baumgartner et al., 2011; Hare et al., 2009, 2011, 2014; Rudolf & Hare, 2014).

During decision-making, once an adaptive event has been previously detected by the MCC-dIPFC network, they further use value signals from the vmPFC (and possibly AMG) as inputs to guide and optimally adjust future behavior by playing moderator roles. An electrophysiological study in monkey demonstrated that, a delay in response latency is observed between the MCC and the dIPFC during FB processing (Rothé et al., 2011). Given the crucial role of the dIPFC in behavioral shifts

and cognitive control, this suggests that the MCC first detects the adaptive event, and then the dlPFC selects the appropriate behavioral response (Pochon, 2001; Rothé et al., 2011; Sallet, Camille, et al., 2013; E. H. Smith et al., 2015).

In the **Chapter III of the Experimental part**, I further highlighted MCC and Striatum variabilities in their inherent activation during adaptive FB processing and AiDEs learning processing: the aMCC/pMCC and the Caudate Nucleus (CN, located in dorsomedial part of the striatum) and were recruited for FB in exploration while pMCC and the Putamen (PUT, located in the dorsolateral part of the striatum) were recruited for learnt AiDEs. *What could be a reasonable explanation?* As Loh et al. (2018) and I previously demonstrated, the pMCC is more densely connected to motor regions than the aMCC while the aMCC is more functionally connected to higher cognitive regions such as the dlPFC or Broca area (Giacometti et al., 2022; Loh et al., 2018). For the striatum, based on functional connectivity profile, Choi et al. (2012) showed that motor-related connectivity (SMA, motor regions) is localized in the putamen, limbic-related connectivity in the ventral striatum (*i.e.*, NAC see previous section) and associations cortices both in a part of the putamen and caudate (Choi et al., 2012). Interestingly, monkey tracer studies and rs-fMRI functional have revealed that the connection of the striatum ventral are highly similar to those of the AMG, notably with more ventral mPFC regions (vmPFC; to nuance, the vmPFC connections with the striatum also include the CN part of the dorsal striatum) while the dorsal striatum is more connected to dorsal cingulate regions including the MCC and its CMAs (Beckmann et al., 2009; Haber et al., 2006; Kunishio & Haber, 1994). Although, very few functional differentiations are proposed for the pMCC and the aMCC, for the striatum several studies in animal models (rodents and macaques) and humans have proposed two differential behavioral routes: habitual behavioral responses recruit the dorsolateral striatum (*i.e.*, PUT) whereas goal-oriented behavioral responses recruit the dorsomedial striatum (*i.e.*, CN) (see for review (BALLEINE, 2005; Balleine & O'Doherty, 2010; Miyachi et al., 1997, 2002; Redgrave et al., 2010; Tricomi et al., 2009; van Steenbergen et al., 2017). Altogether, I hypothesized that while CN and NAC together with the dlPFC-MCC (including aMCC and pMCC) and the AMG-vmPFC networks respectively are oriented towards goal-directed decision-making, the pMCC together with the PUT nuanced its role also towards the detection of habitual adaptive events. Therefore, once the behavioral relevance of significant AiDEs is learnt and applied to the decision, AiDEs are still viewed as adaptive events -unrelated to our

own actions- that however became part of a routine (i.e., repetition). The process of adaptation and adjusting its behavioral response is faster and almost immediate (i.e, highly and directly connected to motor regions) as shown also by the significant decreases in reaction time facing learnt AiDEs.

CHAPTER III. HUMANS AND MACAQUES SIMILARITY AND DIVERGENCE WITHIN THE AMG-MPFC NETWORK, A POSSIBLE BEHAVIORAL EXPLANATION?

1. MORPHOLOGICAL EVOLUTION: LA EXPANSION, A HUMAN FEATURE

Over the course of the evolution, the AMG has not remained static in terms of morphological changes. Or, at least, some of its components were more affected by these changes than others, indicating that AMG did not evolve as a single unit. One of the first study exploring this subject was conducted by Stephan et al., in 1987, across 88 species including 18 species of prosimians and 26 species of simians, they show a tendency of increasing size of the cortico-basolateral subdivision compared to the centromedial subdivision that tended to stay constant (Stephan et al., 1987). More recently, Równiak et al., (2020) conducted a similar study with 5 mammalian species (not including simians groups) and further demonstrated that AMG different components evolved independently and differently: a size progression of the basolateral division (= laterobasal), a size regression of the corticomedial division, whereas the central nucleus size remains stable (Równiak & Bogus-Nowakowska, 2020). To note, these distinct evolutive paths might be due to their different ontogenetic origins (see **Chapter II of the Introduction part**, The Amygdala section; Medina et al., 2011).

In that line of AMG volumetric research, Barger et al. (2007, 2012) specifically compare humans and great apes, Carlo et al., (2020) compared Old-World and New-World monkeys, Chareyron et al. (2011) compared the most used animal model used in neurosciences, rats and macaques rhesus, and humans and, Stimpson et al. (2016) compared two different Great Apes species (Barger et al., 2007, 2012; Carlo et al., 2010; Chareyron et al., 2011; Stimpson et al., 2016). In light of my review (Giacometti et al., 2023; **Chapter III of the introduction**) regrouping these studies, I highlighted that the particular volume increases of the basolateral subdivisions is relatively pronounced in primates (chimpanzee and macaques) while the specific increases of the LA nucleus, component of this division, is human specific. In primates, volume

increase is correlated with an increase in neuron numbers (Barger et al., 2012; Chareyron et al., 2011; Schumann & Amaral, 2005). Chareyron et al., (2011) further showed that macaques and especially humans present a larger neuropil volume most likely associated with a greater complexity in dendritic and axonal arborization of individual AMG neurons (Chareyron et al., 2011). Accordingly, the increases of the basolateral subdivision, and exclusively this subdivision, is correlated with a significant increase of the neocortical volumes (Barton, 1996; Barton et al., 2003). Altogether, these data suggest that primates basolateral subdivision and humans' LA nucleus have a greater capacity to integrate sensory and more complex information coming from extended cortical regions.

The LA nucleus is recognized for its extensive connections with both unimodal and polymodal sensory and association cortices including regions within the temporal lobe such as the insula, inferior temporal areas TE and TEO, and the superior temporal gyrus/sulcus (Aggleton, 2000; Stefanacci & Amaral, 2000). Due to these connections, the LA is often regarded as the sensory gateway of the AMG. In light of the previous hypothesis, LA expansion might be related to a larger expansion of these mentioned association cortices. Semendeferi and Damasio (2000) have shown human presents an expansion of the temporal lobes and the insula compared to Great Apes (Semendeferi & Damasio, 2000). Thus, the LA nucleus might have further progressed in humans compared to the other nuclei with a greater complexity that could contribute to an enhanced connectivity: inputs' integration and outputs connection. A recent study employing electrical stimulation in epileptic human patients demonstrated that stimulating the LA nucleus prompted an earlier response in ACC/aMCC compared to BL or BM nucleus stimulation (Sawada et al., 2022). While in macaques, LA only shares very few to none direct projections with mPFC compared to AB and B, it remains to be determined whether the LA nucleus significant large expansion in humans might impact the organization of its anatomical projections towards mPFC in humans leading to a higher density of connections between LA and mPFC. Reciprocally, the hypothetical increase of structural connections sent towards LA by cortical regions leading to an increase in neuron proportions in humans might also drive its drastic expansion. As of today, the hypothetical question of causality between the two, particularly in humans, still remains to be clarified.

The LA morphological shift after the human lineage split from the last shared common ancestor with great apes, is most probably due to the influx, nature, and

complexity increases of information received from the external world including more complex social interactions with our peers (Barger et al., 2012, 2014; Zalla & Sperduti, 2013). Several neuroimaging studies reported an increase in the entire AMG volume related to the size and complexity of social networks (Bickart et al., 2012; Dziura & Thompson, 2014; Kanai et al., 2012; Sallet et al., 2011). To note, LA nucleus morphological impairments are notably reported in a large number of neuropsychiatric diseases characterized by exaggerated, reduced or even absence of behavioral responses (Asami et al., 2018; Berretta et al., 2007; Bezchlibnyk et al., 2007; Kreczmanski et al., 2007; Lew et al., 2018; Rubinow et al., 2016; Schumann et al., 2011; Schumann & Amaral, 2006).

2. RESTING-STATE INTERACTIONS: A FUNCTIONAL CONNECTIVITY SHIFT IN THE AMG-MPFC NETWORK

In the *Chapter I of the Experimental part*, I showed that awake macaque monkeys and humans presented a similar gradient of connectivity within the cingulo-fronto lateral network (Giacometti et al., 2022; Loh et al., 2018). Of interest, both species displayed a strong correlation between MCC, stronger for aMCC, with dIPFC (area 46 and 9/46), in line with macaques tract-tracer structural evidence (Morecraft et al., 2004, 2012; Petrides, 2005). *In Chapter II*, I showed that humans and macaques presented some similarities and divergences of functional connectivity within the AMG-mPFC network. Both species presented strong and intricate functional connectivity patterns characterized by a u-shape along the corpus callosum, similarly marked by strong positive correlation strength with vmPFC area 25 and also with the whole extent of the pMCC, a with slight variation depending on nuclei in both species (*i.e.*, include the dorsal extreme part of aMCC). In both species, vmPFC functional connectivity with the laterobasal AMG match the structural connections gradient observed in macaques in tracer studies (Giacometti et al., 2023). Altogether, these results indicated a relatively preserved interplay in the two-route involved in behavioral adaptation (the vmPFC-AMG and MCC-dIPFC networks).

However, it can be nuanced as I have also revealed some divergences, especially regarding the AMG and the MCC interactions. First, the presence of a shift in the functional pattern: while for humans the decrease of the correlation strength started at the limit of the vmPFC/ACC (fork shape sulci formation; Amiez et al., 2019)

to peak within the aMCC, in macaques it started to decrease within the vmPFC itself in between the posterior and anterior part of superior rostral sulcus (SROS) and peaks in its anterior part. Right after these peaks, correlations started to increase again toward positive correlations (pMCC), and while the whole extent of the aMCC was negative in humans, the aMCC of macaques was rather mixed with weaker correlation strength. These particular point of divergences within the vmPFC might be caused by high interindividual structural variabilities in this specific region (Crosson et al., 2018; Lopez-Persem et al., 2019) and also, by the sulcal morphological divergences observed at the limit of vmPFC/ACC across Hominidae and Old-World monkeys. Indeed, the shape and orientation of these folds of the sulci forks are highly variable between species: in humans and chimpanzees the fork is pointing downwards while in macaques the fork is pointing forwards in the majority of cases. This has been suggested to reflect the extension of the mPFC in *Hominidae* (Amiez et al., 2019). Second, importantly, this pattern is fully conserved across nuclei in macaques including LA, BL, BM and CE while in humans CE presents rather weak correlation strength with the whole extent of the mPFC. These two main divergences might also highlight and reflect differential degree of behavioral modulation across primates species (see next section).

3. HUMANS AND MACAQUES: DIFFERENCES IN BEHAVIORAL EXPRESSION?

During development, AMG-PFC circuitry matures slowly, reaching maturity in adulthood. In accordance with a large part of the neurodevelopment field (see for review Tottenham, 2015), a recent neuroimaging study (Gee et al., 2022) during a Stroop and face presentations mixed tasks revealed an age-related shift in functional connectivity from dominant AMG-to-mPFC in childhood to mPFC-to-AMG in adolescence. This suggests a change from bottom-up reactivity to top-down regulatory connectivity during development. This made of the AMG-mPFC a network highly malleable and sensitive to external influences such as stress (Tottenham & Galván, 2016).

In their specific ecological niches, humans and macaques do not face the same environmental challenges (e.g., less food availability issues, lack of predators in humans compared to macaques, etc.). Macaques must maintain a constant state of vigilance, balancing predator awareness, within-group vigilance, and the need for food

access (Treves, 2000). Considering the AMG's role in detecting salient events and mediating vigilance, it is conceivable that macaques may exhibit heightened AMG activation due to these factors, resulting in increased reactivity within the AMG-mPFC network. This hypothesis aligns with the observation that the CE plays a significant role in macaque AMG-mPFC functional connectivity (and not in humans), despite lacking direct connections with the mPFC. CE contribution to the AMG-mPFC FC in macaques may depend on its indirect functional connectivity through AMG microcircuitry or also autonomous centers (as brainstem and hypothalamus; Aggleton, 2000; Liddell et al., 2005). The CE nucleus is part of the extended amygdala, *i.e.*, one of the main substrates for defensive behavior (*i.e.*, avoidance-approach responses; Holley & Fox, 2022). The CE is also susceptible to environmental stress during development and is linked to anxious and stress-related behaviors, as evidenced by reduced stress/anxiety responses following its removal in macaques (Elouette et al., 2020; Kalin, 2004). Considering the shift from bottom-up to top-down regulation within the AMG-mPFC circuit during development, it is plausible that macaque monkeys exhibit a different degree of top-down modulation induced by the mPFC over emotional reactions, resulting in a more raw and primitive emotional/arousal state trigger by the whole AMG. This aligns with observations that 1) adult macaque rhesus display traits like aggressiveness and impulsivity that are significantly reduced following AMG lesions (Demaria & Thierry, 2001; Elouette et al., 2020; Emery et al., 2001; Kalin, 2004; Thierry, 2015; Thierry et al., 2010) and 2) the functional divergence that we observed in our resting-state results specifically target two important center of modulation and/or regulation of the AMG (vmPFC and MCC; Gee et al., 2022; Tottenham, 2015). Compared to humans, macaques might experience a differential top-down modulation of the AMG, potentially leading to higher emotional responsiveness, as humans tend to exert greater self-control over their emotions. This perspective suggests that the increase in information flow through the AMG, such as LA expansion, may have reinforced top-down modulation in humans.

One last behavioral hypothesis is sustained by a specific neurochemistry pathway driven by the serotonin. Serotonin, a neurotransmitter synthesized primarily in serotonergic neurons located in the brainstem (*i.e.*, mainly in the raphe nucleus), has been demonstrated to be a key modulator of various physiological processes and particularly in mood regulation, emotional processing, and social behavior. Although debated (Duke et al., 2013), a low serotonin concentration level has been highly

associated with aggressive and impulsive behaviors (Çetin et al., 2017; Keele, 2005; Klasen et al., 2019; Seo et al., 2008). The serotonin system has been shown to heavily innervate the AMG (Lew et al., 2019; Man et al., 2012; Stimpson et al., 2016). Across primate's species, comparative postmortem studies have shed light on intriguing disparities in serotonergic innervation within the AMG (Lew et al., 2019; Stimpson et al., 2016). Bonobos, recognized for their enhanced social tolerance and diminished aggression compared to chimpanzees, exhibit significantly greater absolute serotonergic innervation in the AMG (Stimpson et al., 2016). Phenomenon that may contribute to the behavioral contrasts between these two Pan species. Recent findings also unveil a similar trend in humans, wherein AMG serotonergic innervation surpasses that of chimpanzees especially for the CE, BM, and BL nuclei (Lew et al., 2019). As briefly mentioned above, behavioral analyses conducted across populations of macaque species, revealed that *rhesus* macaques are characterized by higher despotic traits: most rigid dominance hierarchies, infrequent conflict resolution, elevated aggression and impulsivity behaviors (Adams et al., 2015; Balasubramaniam et al., 2012; de Waal & Luttrell, 1985; Demaria & Thierry, 2001; Petit et al., 1997; Thierry, 2015; Thierry et al., 2010). For example, rhesus macaques, show increased aggression, species-specific threat, and submissive behaviors, while less despotic species such as Tonkean macaques display higher rates of affiliative behaviors (Demaria & Thierry, 2001; Petit et al., 1997; Thierry, 2015). Serotonin concentrations are inversely correlated with aggression levels among macaque species: *rhesus* macaques tend to have lower concentrations than less despotic species (pigtailed macaques; Westergaard et al., 1999, 2003). To note, lower levels of serotonin shaped choice towards riskier options in macaques (Long et al., 2009). Thus, it is very likely that lower levels of serotonin levels might contribute to regulating aggression and dominance relationships across populations (*i.e.*, macaques see for review for more details (Weinberg-Wolf & Chang, 2019) and especially across different primates' species. Although no evidence has directly compared the level of serotonergic innervation between humans and macaques *rhesus*, one can further hypothesize that, serotonin level is associated to more negative emotional trait (*i.e.*, aggression/tolerance) in macaques and that change of AMG innervations in great apes, great apes and humans, serotonergic innervation of the AMG might differ in macaques compare to humans, and particularly macaque species, *i.e.*, *rhesus*, would present lower level of serotonergic connections in the AMG.

The hypothesis of variation of serotonergic innervation of the AMG across species would further lead to the heightened emotional reactivity (aggression and impulsiveness) that characterize macaques species triggered by a differential modulation of AMG reactivity (see previous paragraph). Yet, whether these serotonergic potential changes would participate in the functional connectivity divergences that I observed between humans and macaques (CE involvement in macaques and the functional connectivity shift within the AMG-mPFC) still remain to be demonstrated.

CONCLUSION

In conclusion, my research shed lights on the intricate amygdala-frontal anatomo-functional connections that underlie specific processes guiding behavioral adaptations. It has also revealed significant evolutionary differences among primate species, which in turn might explain variations in their behavioral expressions within their respective ecological niches. In regards to previous works, my thesis aimed to highlight the critical importance of deciphering and understanding the connections between different brain regions to gain a more comprehensive understanding of their integrated functions. In my opinion, while it is tempting to attribute specific functions to individual brain regions, it is crucial to recognize that a region role is not solely determined by its isolated function but influenced by its intricate connections with other brain regions and its integration within one or multiple networks. To fully comprehend the dynamics of these interactions, I believe it is essential to explore future research directions that involve causally manipulating the complex connections within the amygdala-frontal networks. This approach holds the potential to provide deeper insights into understanding their dynamic interplay and also might procure further insight to humans and macaque divergences.

CHAPTER IV. FUTURE PERSPECTIVES

This chapter has the objective to address future perspectives regarding my thesis works with a specific focus on 1) exploring individual AMG nuclei connectivity at a larger scale and 2) the causal manipulation within the AMG-PFC networks in both macaques and humans.

1. BEYOND THE AMG-MPFC NETWORK, WHOLE BRAIN CONNECTIVITY

Examining dynamic interactions across the entire brain can offer a more comprehensive and nuanced understanding of a particular cognitive function or process. By investigating these interactions on a larger scale, we gain insights into the complexity and intricacies of neural processes, which can lead to more robust and accurate interpretations of brain function.

In the work I carried throughout my thesis, I focused specifically on the AMG-mPFC network. In the *Chapter II of the Experimental part*, I used a rs-fMRI seed/ROIs-based approach using predefined SEEDs and ROIs. This approach had the great advantage to tackle the intricate functional connectivity pattern within our network of interest and also revealed similarities and differences between species. While seed-based approach has the great advantage of precisely tackling the functional connectivity subtle variation within my networks of interest, it also constrains the connectivity within specific selected ROIs/SEEDs couples, constraints the activity to the size of the selected ROIs/SEEDs where voxels are not totally homogeneous (Lv et al., 2018; Song et al., 2016). Thus, as future and complementary perspectives, I have started to use an rs-fMRI data-driven approach that will allow me to explore AMG connectivity on a broader scale to tackle AMG nuclei connection specificities. In humans, previous data-driven AMG parcellation studies have been realized. On the base of the model of 3 parcels of the AMG (Amunts et al., 2005), several studies have parcellate the AMG in 2/3 differently connected clusters using rs-fMRI, task-based fMRI and even DTI (Avecillas-Chasin et al., 2023; Bickart et al., 2012; Bielski et al., 2021; Bzdok et al., 2013; Elvira et al., 2022; Kerestes et al., 2017; Mishra et al., 2014; Rausch et al., 2018; Solano-Castiella et al., 2010, 2011; Sylvester et al., 2020; Wen et al., 2017; X. Zhang et al., 2018). While another a more recent study using ultra field

MRI (e.g., 7T MRI, Human Connectome Project Dataset) manage to parcellate the AMG into 7 reliable clusters (Klein-Flügge, Jensen, et al., 2022). In light of these previous work in humans and using my own rs-fMRI data, I am planning to use a similar strategy in humans and more importantly, assessed it accordingly in awake macaques' monkeys. Indeed, the main objective is to compare humans and awake macaques using the same individual-base data-driven approach to create probabilistic AMG parcellation (to account for the subject interindividual variability). Once parcels created for each species, I will further assess their specific and respective functional connectivity profile at the whole-brain level and compared them across species.

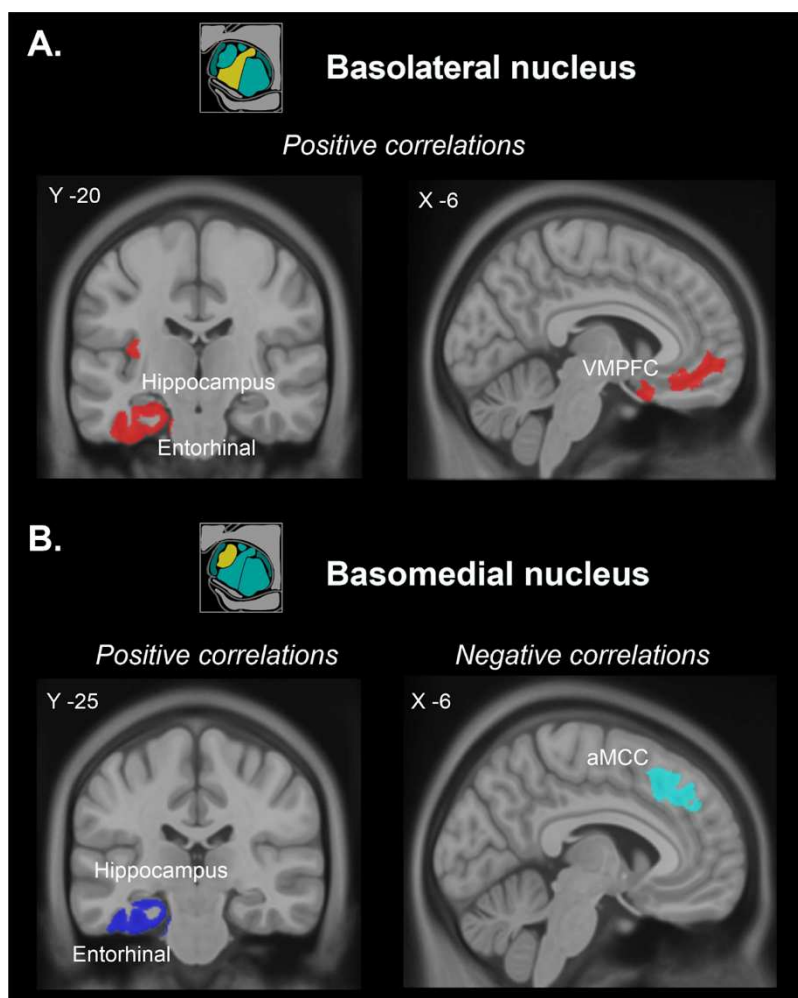


Figure 1. Differential basolateral and basomedial nuclei functional connectivity at the whole brain level. Positive and negative correlation map for BL (A, highlighted in yellow) and BM (B, highlighted in yellow) clusters across 55 human subjects. Clusters are obtained using a resting-state fMRI data-driven clustering method based on the correlation strength of each voxel within the whole AMG mask with whole brain gray-matter voxel. Each AMG cluster's correlation strength is then computed with the whole brain Glasser atlas (Glasser et al., 2016).

Therefore, I first conducted a preliminary study using an rs-fMRI data-driven approach in humans. This method allowed me to 1) parcellate the AMG of 55 human participants in 4 parcels based on the correlation profile of each voxel of the AMG mask with each voxel of the whole-brain gray matter mask, 2) compute the z-score

between each one of these 4 AMG subregions and each of the 180 regions of the Glasser atlas ipsilaterally in individual subjects (Glasser et al. 2016), 3) compute across the 55 subjects the mean z-score between each one of the 4 AMG subregions and each ROI of the atlas (see details of the method in Appendix). Across subjects, parcellation algorithms provide 4 clusters that correspond, at the individual level, to the known spatial organization of the LA, BL, BM, and CE nucleus. Preliminary functional connectivity results are presented in **Figure 1** exclusively for the clusters corresponding to BL and BM (**Figure 1.A** and **1.B** respectively).

In my literature review on tract-tracing studies in macaques, I specifically highlight the preferential projection route connecting AMG nuclei (BM and BL) with distinct mPFC regions in macaques' histological studies (Giacometti et al., 2023); **Chapter III of the Introduction**). Specifically, BL nucleus projects more towards rostral and dorsal mPFC areas (ACC and aMCC), while BM nucleus shows denser projections to vmPFC than aMCC/ACC cingulate regions. This pattern is reciprocally mirrored in the efferences from mPFC to AMG nuclei, with ACC and MCC preferentially targeting BL nucleus and vmPFC projecting to both BM and BL nuclei. I notably proposed that these meaningful preferential routes might support different and complementary levels of integration during behavioral adaptation. Nonetheless, my rs-fMRI findings in both human and macaque participants did not reveal particular variabilities among AMG nuclei and notably clear-cut functional connectivity variation between the BL and BM nuclei with the mPFC (**Chapter II of the Experimental part**). A possible explanation is that rs-fMRI does not possess the necessary resolution to tackle these microscopic intricate connectivity distinctions of BL/BM with mPFC regions. One alternative explanation could be the seed-based method used is not able to specifically highlight these differences with the hypothesis that this AMG nuclei distinction is not only restricted to the mPFC. Thus, I explored the functional connectivity of the parcels identify as BL and BM with the atlas regions of mPFC. Result show that BL exhibits a significant preferential positive correlation with vmPFC whereas BM does not show such a preference. However, in macaques, structural tract studies demonstrated that BM has stronger structural connections with vmPFC, while BL has a more balanced distribution between vmPFC and ACC/MCC. To address this discrepancy, an interesting future perspective would involve further exploration of the functional connectivity of AMG by using the rs-fMRI data-driven approach in awake macaque rhesus. First, to examine the unique functional connectivity patterns of each

of the AMG parcels at the whole brain level in macaques. Secondly, compare the specific functional connectivity of each AMG cluster, with a special emphasis put on LA identified-parcel (*i.e.*, expansion in humans), in both humans and awake macaques. This approach could yield more valuable information explaining AMG evolution between these two primate species and further insights into their respective behavior as well as behavioral regulation/control capacities within their respective environment.

The second result indicate that both BL and BM are highly positively correlated with hippocampus and entorhinal cortex. Both hippocampus and entorhinal cortex are recruited during long-term memory processes, thus, this result further emphasizes the involvement of both BL and BM in a more long-term contextual behavioral adaptation. This is to put in light of our results in ***the Chapter III of the Experimental part***, where I also showed several others and important activation in the brain during the two timelines of behavioral adaptation (*i.e.*, temporal cortices, striatum ventral and dorsal, etc.). Regions that are coherently and complementary activated with the AMG-vmPFC and MCC-dIPFC networks, highlighting a more complex and intricate process involving several other brain regions within these two routes. Further digging into this specific co-activation and especially 1) how these regions are functionally interconnected with our network of interest and 2) what are their dynamically interplay within these two distinct and complementary routes (*i.e.*, striatum dorsal and ventral specific activation/deactivation within these two routes), will also be the next objective of this analysis. Importantly, the same questioning will be applied for macaque rhesus and thus I will further compare these two species to assess whether and how these larger scales routes evolved from the last common ancestor of humans and old-world monkeys to humans.

2. TOWARDS CAUSALLY IDENTIFYING AMG-PFC FUNCTIONAL INTERACTION

In neurosciences, the purpose of doing causal perturbations of the brain structure is to investigate its specific p.value in a function, within a defined network and at the overall brain level. By modifying, disrupting or removing the activity of a particular brain region and/or structure, we can come closer to understanding brain functions. In accordance to the scientific question and also to the ethical regulation, several techniques can be used to causality manipulate brain regions, each one of them coming with some advantages and inconvenients. Surgical or excitotoxic lesion and/or ablation of a brain region and/or structure (e.g., white matter fibers) was one of the first, if not the first, approach to understand the function and also how this region is structurally connected to others. For instance, five decades ago lesions and/or ablation of the whole AMG in macaque monkeys unveiled its structural connectivity with other brain regions (NAUTA, 1961) and offered initial glimpses into its functional significance (Schwartzbaum, 1960, 1964). Subsequent research involved both surgical (Emery et al., 2001; Mason et al., 2006) and neurotoxic lesions (Bauman et al., 2004, 2006; Dal Monte et al., 2015; Hadj-Bouziane et al., 2012; Machado, Emery, et al., 2008; Machado, Snyder, et al., 2008; Málková et al., 1997; Rudebeck et al., 2013; Taswell et al., 2021; Taubert et al., 2018) as well as pharmacological manipulation (Elorette et al., 2020; Gothard, 2020; Wellman et al., 2016) to explore the amygdala's roles in emotion, fear processing, decision-making, attention, social processing, and stimulus valuation. Human lesion studies following patient disease-caused AMG lesions also contributed to understanding its roles in value-based decision-making, fear processing, and emotion (Anderson & Phelps, 2001; Bechara et al., 1999; Domínguez-Borràs et al., 2020; Feinstein et al., 2011; Paul et al., 2010). Collectively, all of these -non-exhaustive listed- studies provided vital insights into the AMG's involvement in complex cognitive processes, positioning it as a pivotal brain hub (Gothard, 2020).

However, lesion studies of these types are invasive causing irreversible lesions and can also damage surrounding AMG regions as well as passing white fibers. Thus, several other techniques have been developed. Here are a few noteworthy techniques. In animal model, we can find optogenetics manipulation, a method to turn on/off neurons that express light-sensitive proteins using light, is widely used in rodent

studies and to a lesser extent and still under proper implantation in monkeys (El-Shamayleh & Horwitz, 2019; Vanduffel & Li, 2020). In humans, Transcranial magnetic stimulation (TMS), a noninvasive form of brain stimulation in which a changing magnetic field is used to induce an electric current at a specific area of the brain through electromagnetic induction. Although being first tested in animal models, this technique is now mostly used for treatments in humans (*i.e.*, depression, Alzheimer or even Parkinson symptoms). The main limit of this technique is that it is not able to target deep brain structures such as the AMG (see for review Klomjai et al., 2015; note that deep brain stimulation (DBS) does exist but is exclusively conducted for clinical purpose).

In the case of my present objective, I will use not use the aforementioned techniques but rather two emerging complementary and novel techniques: 1) transcranial ultrasound stimulation (TUS) both in macaques and humans and 2) Designer Receptor Exclusively Activated by Designer Drugs (DREADDs) combine with neuroimaging acquisition (rs-fMRI and task-based MRI). These techniques have the great advantages to be reversible, target deep brain structure and use both offline and online during experiments. The significant advantage of each lies in their ability to target distinct functional connectivity scales – macroscopic for the former and microscopic for the latter – making their combination complementary. I will further discuss their specificities and how they would specifically tackle my objective.

Macroscopic-scale

The first of the objective is to establish the causal role of the important nodes within the AMG-PFC network and at the global cerebral level. I will use one emerging non-invasive neurostimulation technique: pulse Transcranial Ultrasound Stimulation (TUS). It consists in sending a repetition of multiple ultrasound waves throughout the skull of an individual accounting for diverse parameters (*i.e.*, frequency, amplitude, deepness of the region, thickness of the skull, etc.) that allow to specifically target a define target. The mechanistic effect of TUS is still under intensive research and as of today one explanation emerges. The mechanical interaction between ultrasound and neuronal membranes can modify the membrane gating kinetics through the action on mechanosensitive voltage-gated ion channels or neurotransmitter receptors and thus affect its activity (see for review Di Biase et al., 2019).

Unlike other Non-Invasive Brain Stimulation (NIBS) methods, TUS has the great advantages to be reversible (effect lasts up to 2h after stimulation), to have a great spatial resolution as it is able to target deep brain structures, be combined with neuroimaging and behavioral studies and be realized either online or offline. TUS also offers the advantage to allow for different targets to be stimulated in the same subject bilaterally (*i.e.*, both AMG and MCC) within a short delay period. Previous studies have shown the compatibility of the TUS and rs-fMRI approach to manipulate brain circuits in the macaque monkeys (Folloni et al., 2019; Verhagen et al., 2019).

**Bilateral Transcranial Ultrasound Stimulation of the Amygdala
Anaesthetized macaques (n=5)**

Conditions : ■ SHAM ■ TUSAMG

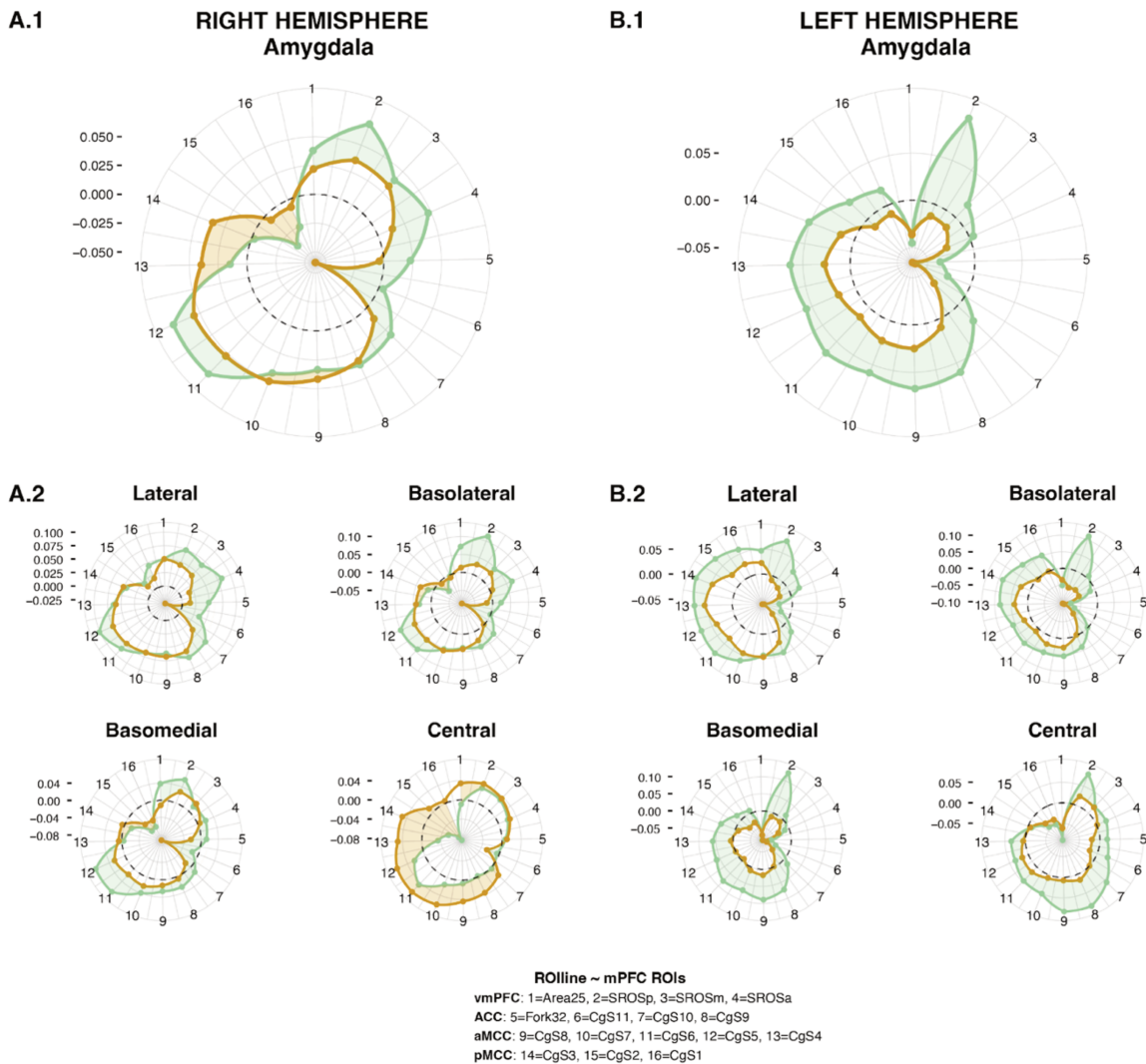


Figure 2. Pilot study: Effect of the Transcranial Ultrasound Stimulation (TUS) of the bilateral Amygdala in anaesthetized macaques. Spider plots displaying the correlation strength between AMG and 16 mPFC ROIs in TUS (brown) and SHAM (green) conditions. Results are averaged across 5

anaesthetized macaque monkeys. Right (A) and left (B) AMG with (1) the whole AMG and (2) AMG 4 main nuclei: LA, BL, BM and CE. **1.** General linear mixed models (GLMM) with ROIs, Conditions and Hemisphere as main factor and Run within subjects as random factor shows significant effect of Conditions ($F(1,279.93)=7.926$, $p=0.005$), ROIs ($F(15,453.18)=3.544$, $p=8.311e-06$) and Hemisphere ($F(1,453.18)=7.262$, $p=0.007$). **2.** Same GLMM model with the addition of SEEDs AMG as main factor. Significant effect of Conditions ($F(1,1338.6)=21.144$, $p=4.662e-06$), SEEDs ($F(3,1887.1)=11.294$, $p=2.416e-07$), ROIs ($F(15,1887.1)=10.015$, $p<2.2e-16$), Hemisphere ($F(1,1887.1)=20.521$, $p=6.268e-06$) and the interaction between SEEDs and Conditions ($F(3,1887.1)=4.644$, $p=0.003$).

On the model of Folloni et al. (2019), that manipulate both the ACC and the AMG in anaesthetized macaque monkeys and demonstrated functional connectivity perturbations at the global level, I recently tested out the bilateral AMG TUS perturbation effect within my network of interest in 5 anaesthetized macaque monkeys (see Appendix for further details on the method). For each of the monkeys, I acquired rs-fMRI data in a SHAM session (*i.e.*, absence of perturbations) and 2 TUS sessions. Preliminary results of this pilot study are presented on **Figure 2** for the entire AMG functional connectivity with the 16 mPFC ROIs and for its 4 main nuclei LA, BL, BM and CE in the left and right hemisphere (respectively **Figure 2.A** and **2.B**). Similarly, to Folloni et al. (2019) results for the whole AMG, I observed a significant decrease of the functional connectivity after TUS perturbations of the AMG, with slightly stronger effect for the left than the right hemisphere. The lateralization difference might be due to an absence of effect in the CE of the right hemisphere. TUS perturbations did not appear to change the pattern of connectivity but rather shrink its overall correlation strength: positive correlations are less positive and negative correlations are more negative.

Following the validation of the TUS effect on my network of interest, the subsequent step involves applying the same procedure to awake macaque monkeys, given the known influence of anaesthesia on prefrontal functional connectivity as demonstrated in my previous work (**Chapter I of the Experimental part**; Giacometti et al., 2022). This approach will integrate both in rs-fMRI seed-based and data-driven parcellation methods along with TUS perturbations the AMG and mPFC, including the MCC and vmPFC. To note, it is also possible to combine TUS perturbations and behavior assessment in monkeys. It can either be realized online with a behavioral task (*i.e.*, perturbate while the monkey is performing the task; Deffieux et al., 2013) or offline in a behavioral task associated with neuroimaging (*i.e.*, perturbate before as TUS materials). In the context of this project, an optimal strategy might involve associating TUS perturbations of the AMG and MCC with monkeys performing a

behavioral adaptation task combining AiDEs and FB. This would enable an evaluation of whether TUS perturbations impact the learning process related to the behavioral significance of AiDEs.

Importantly, one of the major advantages of this method lies in its applicability to healthy human participants as well whether during behavioral tasks, task-based neuroimaging, or rs-fMRI studies (Attali et al., 2023; Yaakub et al., 2023). This approach holds immense promise for comparative neuroscience. Indeed, the ability to apply TUS perturbations in both humans and macaques, using similar protocols and experimental designs, offers a unique opportunity for direct cross-species comparison. This will not only enhance our understanding on anatomo-functional dynamic interplay and mechanism in large brain networks underlying complex cognitive processes but also provides a means to directly investigate the shared and divergent aspects of brain function and connectivity across species.

Microscopic scale

A comprehensive and full understanding of the AMG-PFC circuitry and its dynamics, however, also requires to know how the interaction itself is functioning, and specifically to identify the directionality of the anatomo-functional interplay. To address this, the initial focus will specifically target the top-down MCC-AMG pathway (*i.e.*, structurally in macaques, mPFC and especially MCC sends more projections to AMG than it receives, Ghashghaei et al., 2007). The objective is to assess whether specifically disrupting this pathway in this one direction leads to perturbation of the functional connectivity in the network involved in behavioral adaptation. In order to achieve this, I plan to use a complementary innovative tool to investigate causality, DREADD (Designer Receptor Exclusively Activated by Designer Drugs) and rs-fMRI in awake macaques *rhesus* (Campbell & Marchant, 2018; Cushnie et al., 2023; Roth, 2016). To note, Grayson et al. (2016) conducted the first DREADD perturbation of the whole AMG in monkeys associated with rs-fMRI recordings and demonstrated that the perturbation did affect AMG functional connectivity whole-brain wise (Grayson et al., 2016). However, here the aim is not to perturbate one region but to impair the specific structural connection between two regions. Indeed, DREADD technology also offers the unique possibility to transiently disrupt activity within a specifically targeted pathway: a double viral vector strategy to express ‘designer’ receptors specifically in

cells that originate in MCC and project to AMG. The DREADD receptors in question are ‘designer’ in the sense that they have been modified to provide experimental control of their activity, and therefore the activity of the cells in which they are expressed. By injecting the animal with a specific receptor ligand (Deschloroclozapine, DCZ; Cushnie et al., 2023), it is possible to suppress the activity of those cells in a reversible manner for 2-4 hours. This pathway-specific DREADD approach will be coupled with rs-fMRI recordings to evaluate the impact of the specific disruption of the AMG-MCC pathway on the functional connectivity within the network involved in behavioral adaptation that I have previously identified. Because of the imbalanced anatomical projections between AMG and MCC described above, I hypothesize that the perturbation of the MCC->AMG pathway would induce a stronger inversion of the functional interplay than the perturbation of the AMG->MCC pathway.

Combining fine-grained interventional approaches based on the complementarity of TUS and DREADDs in macaque (and possibly in humans for TUS) is a promising avenue for future research. This combined approach holds the potential to offer causal insights into the intricate functional dynamics of the AMG-mPFC network crucial for behavioral adaptation. By selectively perturbing specific nodes and meticulously disrupting key structural pathways, this approach could provide a deeper understanding of the network's dynamics and its role in adaptive behaviors.

BIBLIOGRAPHY

- Adams, M. J., Majolo, B., Ostner, J., Schülke, O., De Marco, A., Thierry, B., Engelhardt, A., Widdig, A., Gerald, M. S., & Weiss, A. (2015). Personality structure and social style in macaques. *Journal of Personality and Social Psychology*, *109*(2), 338–353. <https://doi.org/10.1037/pspp0000041>
- Aggleton, J. P. (2000). *The amygdala: a functional analysis* (J. P. Aggleton, Ed.; 2nd ed). Oxford University Press. <https://global.oup.com/academic/product/the-amygdala-9780198505013?cc=us&lang=en&>
- Aggleton, J. P., Burton, M. J., & Passingham, R. E. (1980). Cortical and subcortical afferents to the amygdala of the rhesus monkey (*Macaca mulatta*). *Brain Research*, *190*(2), 347–368. [https://doi.org/10.1016/0006-8993\(80\)90279-6](https://doi.org/10.1016/0006-8993(80)90279-6)
- Amiez, C., Joseph, J. P., & Procyk, E. (2005). Anterior cingulate error-related activity is modulated by predicted reward. *European Journal of Neuroscience*, *21*(12), 3447–3452. <https://doi.org/10.1111/j.1460-9568.2005.04170.x>
- Amiez, C., Joseph, J. P., & Procyk, E. (2006). Reward encoding in the monkey anterior cingulate cortex. *Cerebral Cortex*, *16*(7), 1040–1055. <https://doi.org/10.1093/cercor/bhj046>
- Amiez, C., Neveu, R., Warrot, D., Petrides, M., Knoblauch, K., & Procyk, E. (2013). The location of feedback-related activity in the midcingulate cortex is predicted by local morphology. *Journal of Neuroscience*, *33*(5), 2217–2228. <https://doi.org/10.1523/JNEUROSCI.2779-12.2013>
- Amiez, C., & Petrides, M. (2014). Neuroimaging evidence of the anatomo-functional organization of the human cingulate motor areas. *Cerebral Cortex*, *24*(3), 563–578. <https://doi.org/10.1093/cercor/bhs329>
- Amiez, C., & Procyk, E. (2019). Midcingulate somatomotor and autonomic functions. In *Handbook of Clinical Neurology* (Vol. 166, pp. 53–71). <https://doi.org/10.1016/B978-0-444-64196-0.00004-2>
- Amiez, C., Sallet, J., Giacometti, C., Verstraete, C., Gandaux, C., Morel-Latour, V., Meguerditchian, A., Hadj-Bouziane, F., Ben Hamed, S., Hopkins, W. D., Procyk, E., Wilson, C. R. E., & Petrides, M. (2023). A revised perspective on the evolution of the lateral frontal cortex in primates. *Science Advances*, *9*(20). <https://doi.org/10.1126/sciadv.adf9445>
- Amiez, C., Sallet, J., Hopkins, W. D., Meguerditchian, A., Hadj-Bouziane, F., Ben Hamed, S., Wilson, C. R. E., Procyk, E., & Petrides, M. (2019). Sulcal organization in the medial frontal cortex provides insights into primate brain evolution. *Nature Communications*, *10*(1). <https://doi.org/10.1038/s41467-019-11347-x>
- Amiez, C., Sallet, J., Novek, J., Hadj-Bouziane, F., Giacometti, C., Andersson, J., Hopkins, W. D., & Petrides, M. (2021). Chimpanzee histology and functional brain imaging show that the paracingulate sulcus is not human-specific. *Communications Biology*, *4*(1), 1–12. <https://doi.org/10.1038/s42003-020-01571-3>
- Amiez, C., Sallet, J., Procyk, E., & Petrides, M. (2012). Modulation of feedback related activity in the rostral anterior cingulate cortex during trial and error exploration. *NeuroImage*, *63*(3), 1078–1090. <https://doi.org/10.1016/j.neuroimage.2012.06.023>

- Amir, A., Lee, S. C., Headley, D. B., Herzallah, M. M., & Pare, D. (2015). Amygdala signaling during foraging in a hazardous environment. *Journal of Neuroscience*, *35*(38), 12994–13005. <https://doi.org/10.1523/JNEUROSCI.0407-15.2015>
- Amunts, K., Kedo, O., Kindler, M., Pieperhoff, P., Mohlberg, H., Shah, N. J., Habel, U., Schneider, F., & Zilles, K. (2005). Cytoarchitectonic mapping of the human amygdala, hippocampal region and entorhinal cortex: intersubject variability and probability maps. *Anatomy and Embryology*, *210*(5–6), 343–352. <https://doi.org/10.1007/s00429-005-0025-5>
- Anderson, A. K., & Phelps, E. A. (2001). Lesions of the human amygdala impair enhanced perception of emotionally salient events. *Nature*, *411*(6835), 305–309. <https://doi.org/10.1038/35077083>
- Andrewes, D. G., & Jenkins, L. M. (2019). The Role of the Amygdala and the Ventromedial Prefrontal Cortex in Emotional Regulation: Implications for Post-traumatic Stress Disorder. *Neuropsychology Review*, *29*(2), 220–243. <https://doi.org/10.1007/s11065-019-09398-4>
- Antzoulatos, E. G., & Miller, E. K. (2011). Differences between Neural Activity in Prefrontal Cortex and Striatum during Learning of Novel Abstract Categories. *Neuron*, *71*(2), 243–249. <https://doi.org/10.1016/j.neuron.2011.05.040>
- Apps, M. A. J., Rushworth, M. F. S., & Chang, S. W. C. (2016). The Anterior Cingulate Gyrus and Social Cognition: Tracking the Motivation of Others. In *Neuron* (Vol. 90, Issue 4, pp. 692–707). Cell Press. <https://doi.org/10.1016/j.neuron.2016.04.018>
- Asami, T., Nakamura, R., Takaishi, M., Yoshida, H., Yoshimi, A., Whitford, T. J., & Hirayasu, Y. (2018). Smaller volumes in the lateral and basal nuclei of the amygdala in patients with panic disorder. *PLoS ONE*, *13*(11), e0207163. <https://doi.org/10.1371/journal.pone.0207163>
- Attali, D., Tiennot, T., Schafer, M., Fouragnan, E., Sallet, J., Caskey, C. F., Chen, R., Darmani, G., Bublick, E. J., Butler, C., Stagg, C. J., Klein-Flügge, M., Verhagen, L., Yoo, S. S., Pauly, K. B., & Aubry, J. F. (2023). Three-layer model with absorption for conservative estimation of the maximum acoustic transmission coefficient through the human skull for transcranial ultrasound stimulation. *Brain Stimulation*, *16*(1), 48–55. <https://doi.org/10.1016/j.brs.2022.12.005>
- Avecillas-Chasin, J. M., Levinson, S., Kuhn, T., Omidbeigi, M., Langevin, J. P., Pouratian, N., & Bari, A. (2023). Connectivity-based parcellation of the amygdala and identification of its main white matter connections. *Scientific Reports*, *13*(1). <https://doi.org/10.1038/s41598-023-28100-6>
- Baddeley, A. (2003). Working memory: looking back and looking forward. *Nature Reviews Neuroscience*, *4*(10), 829–839. <https://doi.org/10.1038/nrn1201>
- Balasubramaniam, K. N., Dittmar, K., Berman, C. M., Butovskaya, M., Cooper, M. A., Majolo, B., Ogawa, H., Schino, G., Thierry, B., & De Waal, F. B. M. (2012). Hierarchical Steepness, Counter-Aggression, and Macaque Social Style Scale. *American Journal of Primatology*, *74*(10), 915–925. <https://doi.org/10.1002/ajp.22044>
- BALLEINE, B. (2005). Neural bases of food-seeking: Affect, arousal and reward in corticostriatolimbic circuits☆. *Physiology & Behavior*, *86*(5), 717–730. <https://doi.org/10.1016/j.physbeh.2005.08.061>
- Balleine, B. W., & O'Doherty, J. P. (2010). Human and Rodent Homologies in Action Control: Corticostriatal Determinants of Goal-Directed and Habitual Action. *Neuropsychopharmacology*, *35*(1), 48–69. <https://doi.org/10.1038/npp.2009.131>

- Barbas, H., & de Olmos, J. (1990). Projections from the amygdala to basoventral and mediodorsal prefrontal regions in the rhesus monkey. *The Journal of Comparative Neurology*, 300(4), 549–571. <https://doi.org/10.1002/cne.903000409>
- Barbas, H., & Pandya, D. N. (1989). Architecture and intrinsic connections of the prefrontal cortex in the rhesus monkey. *The Journal of Comparative Neurology*, 286(3), 353–375. <https://doi.org/10.1002/cne.902860306>
- Barger, N., Hanson, K. L., Teffer, K., Schenker-Ahmed, N. M., & Semendeferi, K. (2014). Evidence for evolutionary specialization in human limbic structures. *Frontiers in Human Neuroscience*, 8(MAY). <https://doi.org/10.3389/fnhum.2014.00277>
- Barger, N., Stefanacci, L., Schumann, C. M., Sherwood, C. C., Annese, J., Allman, J. M., Buckwalter, J. A., Hof, P. R., & Semendeferi, K. (2012). Neuronal populations in the basolateral nuclei of the amygdala are differentially increased in humans compared with apes: A stereological study. *The Journal of Comparative Neurology*, 520(13), 3035–3054. <https://doi.org/10.1002/cne.23118>
- Barger, N., Stefanacci, L., & Semendeferi, K. (2007). A comparative volumetric analysis of the amygdaloid complex and basolateral division in the human and ape brain. *American Journal of Physical Anthropology*, 134(3), 392–403. <https://doi.org/10.1002/ajpa.20684>
- Barron, H. C., Mars, R. B., Dupret, D., Lerch, J. P., & Sampaio-Baptista, C. (2021). Cross-species neuroscience: closing the explanatory gap. *Philosophical Transactions of the Royal Society B: Biological Sciences*, 376(1815), 20190633. <https://doi.org/10.1098/rstb.2019.0633>
- Barton, R. A. (1996). Neocortex size and behavioural ecology in primates. *Proceedings of the Royal Society B: Biological Sciences*, 263(1367), 173–177. <https://doi.org/10.1098/rspb.1996.0028>
- Barton, R. A., Aggleton, J. P., & Grenyer, R. (2003). Evolutionary coherence of the mammalian amygdala. *Proceedings of the Royal Society of London. Series B: Biological Sciences*, 270(1514), 539–543. <https://doi.org/10.1098/rspb.2002.2276>
- Basile, G. A., Bertino, S., Bramanti, A., Ciurleo, R., Anastasi, G. P., Milardi, D., & Cacciola, A. (2021). Striatal topographical organization: Bridging the gap between molecules, connectivity and behavior. In *European Journal of Histochemistry* (Vol. 65, Issue s1).
- Bauman, M. D., Lavenex, P., Mason, W. A., Capitanio, J. P., & Amaral, D. G. (2004). The Development of Social Behavior Following Neonatal Amygdala Lesions in Rhesus Monkeys. *Journal of Cognitive Neuroscience*, 16(8), 1388–1411. <https://doi.org/10.1162/0898929042304741>
- Bauman, M. D., Toscano, J. E., Mason, W. A., Lavenex, P., & Amaral, D. G. (2006). The expression of social dominance following neonatal lesions of the amygdala or hippocampus in rhesus monkeys (*Macaca mulatta*). *Behavioral Neuroscience*, 120(4), 749–760. <https://doi.org/10.1037/0735-7044.120.4.749>
- Baumgartner, T., Knoch, D., Hotz, P., Eisenegger, C., & Fehr, E. (2011). Dorsolateral and ventromedial prefrontal cortex orchestrate normative choice. *Nature Neuroscience*, 14(11), 1468–1474. <https://doi.org/10.1038/nn.2933>
- Bechara, A., Damasio, H., & Damasio, A. R. (2003). Role of the amygdala in decision-making. *Annals of the New York Academy of Sciences*, 985, 356–369. <https://doi.org/10.1111/j.1749-6632.2003.tb07094.x>
- Bechara, A., Damasio, H., Damasio, A. R., & Lee, G. P. (1999). Different contributions of the human amygdala and ventromedial prefrontal cortex to decision-making. *Journal of Neuroscience*, 19(13), 5473–5481. <https://doi.org/10.1523/jneurosci.19-13-05473.1999>

- Bechara, A., Tranel, D., & Damasio, H. (2000). Characterization of the decision-making deficit of patients with ventromedial prefrontal cortex lesions. In *Brain* (Vol. 123).
- Beckmann, M., Johansen-Berg, H., & Rushworth, M. F. S. (2009). Connectivity-Based Parcellation of Human Cingulate Cortex and Its Relation to Functional Specialization. *Journal of Neuroscience*, 29(4), 1175–1190. <https://doi.org/10.1523/JNEUROSCI.3328-08.2009>
- Behrens, T. E. J., Woolrich, M. W., Walton, M. E., & Rushworth, M. F. S. (2007). Learning the value of information in an uncertain world. *Nature Neuroscience*, 10(9), 1214–1221. <https://doi.org/10.1038/nn1954>
- Belova, M. A., Paton, J. J., & Salzman, C. D. (2008). Moment-to-moment tracking of state value in the amygdala. *Journal of Neuroscience*, 28(40), 10023–10030. <https://doi.org/10.1523/JNEUROSCI.1400-08.2008>
- Bermudez, M. A., & Schultz, W. (2010). Reward magnitude coding in primate amygdala neurons. *Journal of Neurophysiology*, 104(6), 3424–3432. <https://doi.org/10.1152/jn.00540.2010>
- Berretta, S., Pantazopoulos, H., & Lange, N. (2007). Neuron Numbers and Volume of the Amygdala in Subjects Diagnosed with Bipolar Disorder or Schizophrenia. *Biological Psychiatry*, 62(8), 884–893. <https://doi.org/10.1016/j.biopsych.2007.04.023>
- Bezchlibnyk, Y. B., Sun, X., Wang, J.-F., MacQueen, G. M., McEwen, B. S., & Young, L. T. (2007). Neuron somal size is decreased in the lateral amygdalar nucleus of subjects with bipolar disorder. *Journal of Psychiatry & Neuroscience: JPN*, 32(3), 203–210. <http://www.ncbi.nlm.nih.gov/pubmed/17476367>
- Bickart, K. C., Dickerson, B. C., & Barrett, L. F. (2014). The amygdala as a hub in brain networks that support social life. *Neuropsychologia*, 63, 235–248. <https://doi.org/10.1016/j.neuropsychologia.2014.08.013>
- Bickart, K. C., Hollenbeck, M. C., Barrett, L. F., & Dickerson, B. C. (2012). Intrinsic amygdala-cortical functional connectivity predicts social network size in humans. *Journal of Neuroscience*, 32(42), 14729–14741. <https://doi.org/10.1523/JNEUROSCI.1599-12.2012>
- Bielski, K., Adamus, S., Kolada, E., Rączaszek – Leonardi, J., & Szatkowska, I. (2021). Parcellation of the human amygdala using recurrence quantification analysis. *NeuroImage*, 227. <https://doi.org/10.1016/j.neuroimage.2020.117644>
- Blackford, J. U., Buckholz, J. W., Avery, S. N., & Zald, D. H. (2010). A unique role for the human amygdala in novelty detection. *NeuroImage*, 50(3), 1188–1193. <https://doi.org/10.1016/j.neuroimage.2009.12.083>
- Blumensath, T., Jbabdi, S., Glasser, M. F., Van Essen, D. C., Ugurbil, K., Behrens, T. E. J., & Smith, S. M. (2013). Spatially constrained hierarchical parcellation of the brain with resting-state fMRI. *NeuroImage*, 76, 313–324. <https://doi.org/10.1016/j.neuroimage.2013.03.024>
- Boorman, E. D., Rushworth, M. F., & Behrens, T. E. (2013). Ventromedial prefrontal and anterior cingulate cortex adopt choice and default reference frames during sequential multi-alternative choice. *Journal of Neuroscience*, 33(6), 2242–2253. <https://doi.org/10.1523/JNEUROSCI.3022-12.2013>
- Borra, E., Ferroni, C. G., Gerbella, M., Giorgetti, V., Mangiaracina, C., Rozzi, S., & Luppino, G. (2019). Rostro-caudal Connectional Heterogeneity of the Dorsal Part of the Macaque Prefrontal Area 46. *Cerebral Cortex*, 29(2), 485–504. <https://doi.org/10.1093/cercor/bhx332>

- Brett, M., Markiewicz, C., Hanke, M., Côté, M.-A., Cipollini, B., McCarthy, P., Cheng, C., Halchenko, Y., Ghosh, S., Larson, E., Wassermann, D., Gerhard, S., Markello, R., & et al. (2019). *nipy/nibabel: 2.5.1*. Zenodo.
- Brodmann, K. (1909). *Vergleichende Lokalisationslehre der Grosshirnrinde in ihren Prinzipien dargestellt auf Grund des Zellenbaues* (J. A. Barth, Ed.).
- Brosch, T., & Sander, D. (2013). Neurocognitive mechanisms underlying value-based decision-making: From core values to economic value. *Frontiers in Human Neuroscience*, *JUL*. <https://doi.org/10.3389/fnhum.2013.00398>
- Bzdok, D., Laird, A. R., Zilles, K., Fox, P. T., & Eickhoff, S. B. (2013). An investigation of the structural, connectional, and functional subspecialization in the human amygdala. *Human Brain Mapping*, *34*(12), 3247–3266. <https://doi.org/10.1002/hbm.22138>
- Calderazzo, S. M., Busch, S. E., Moore, T. L., Rosene, D. L., & Medalla, M. (2021). Distribution and overlap of entorhinal, premotor, and amygdalar connections in the monkey anterior cingulate cortex. *Journal of Comparative Neurology*, *529*(4), 885–904. <https://doi.org/10.1002/cne.24986>
- Campbell, E. J., & Marchant, N. J. (2018). The use of chemogenetics in behavioural neuroscience: receptor variants, targeting approaches and caveats. In *British Journal of Pharmacology* (Vol. 175, Issue 7, pp. 994–1003). John Wiley and Sons Inc. <https://doi.org/10.1111/bph.14146>
- Cardinal, R. N., Parkinson, J. A., Hall, J., & Everitt, B. J. (2002). Emotion and motivation: the role of the amygdala, ventral striatum, and prefrontal cortex. *Neuroscience & Biobehavioral Reviews*, *26*(3), 321–352. [https://doi.org/10.1016/S0149-7634\(02\)00007-6](https://doi.org/10.1016/S0149-7634(02)00007-6)
- Carlo, C. N., Stefanacci, L., Semendeferi, K., & Stevens, C. F. (2010). Comparative analyses of the neuron numbers and volumes of the amygdaloid complex in old and new world primates. *Journal of Comparative Neurology*, *518*(8), 1176–1198. <https://doi.org/10.1002/cne.22264>
- Carmichael, S. T., & Price, J. L. (1995). Limbic connections of the orbital and medial prefrontal cortex in macaque monkeys. *The Journal of Comparative Neurology*, *363*(4), 615–641. <https://doi.org/10.1002/cne.903630408>
- Çetin, F. H., Torun, Y. T., & Güney, E. (2017). The Role of Serotonin in Aggression and Impulsiveness. In *Serotonin - A Chemical Messenger Between All Types of Living Cells*. InTech. <https://doi.org/10.5772/intechopen.68918>
- Chareyron, L. J., Banta Lavenex, P., Amaral, D. G., & Lavenex, P. (2011). Stereological analysis of the rat and monkey amygdala. *The Journal of Comparative Neurology*, *519*(16), 3218–3239. <https://doi.org/10.1002/cne.22677>
- Cheng, L., Zhang, Y., Li, G., Wang, J., Sherwood, C., Gong, G., Fan, L., & Jiang, T. (2021). Connectional asymmetry of the inferior parietal lobule shapes hemispheric specialization in humans, chimpanzees, and rhesus macaques. *ELife*, *10*. <https://doi.org/10.7554/eLife.67600>
- Chiba, T., Kayahara, T., & Nakano, K. (2001). Efferent projections of infralimbic and prelimbic areas of the medial prefrontal cortex in the Japanese monkey, *Macaca fuscata*. *Brain Research*, *888*(1), 83–101. [https://doi.org/10.1016/S0006-8993\(00\)03013-4](https://doi.org/10.1016/S0006-8993(00)03013-4)
- Choi, E. Y., Thomas Yeo, B. T., & Buckner, R. L. (2012). The organization of the human striatum estimated by intrinsic functional connectivity. *Journal of Neurophysiology*, *108*(8), 2242–2263. <https://doi.org/10.1152/jn.00270.2012>

- Chong, T. T. J., Bonnelle, V., & Husain, M. (2016). Quantifying motivation with effort-based decision-making paradigms in health and disease. In *Progress in Brain Research* (Vol. 229, pp. 71–100). Elsevier B.V. <https://doi.org/10.1016/bs.pbr.2016.05.002>
- Clark, L., Bechara, A., Damasio, H., Aitken, M. R. F., Sahakian, B. J., & Robbins, T. W. (2008). Differential effects of insular and ventromedial prefrontal cortex lesions on risky decision-making. *Brain*, *131*(5), 1311–1322. <https://doi.org/10.1093/brain/awn066>
- Costa, V. D., Dal Monte, O., Lucas, D. R., Murray, E. A., & Averbeck, B. B. (2016). Amygdala and Ventral Striatum Make Distinct Contributions to Reinforcement Learning. *Neuron*, *92*(2), 505–517. <https://doi.org/10.1016/j.neuron.2016.09.025>
- Costa, V. D., Mitz, A. R., & Averbeck, B. B. (2019). Subcortical Substrates of Explore-Exploit Decisions in Primates. *Neuron*, *103*(3), 533-545.e5. <https://doi.org/10.1016/j.neuron.2019.05.017>
- Cox, R. W. (1996). AFNI: Software for analysis and visualization of functional magnetic resonance neuroimages. *Computers and Biomedical Research*, *29*(3), 162–173. <https://doi.org/10.1006/cbmr.1996.0014>
- Croxson, P. L., Forkel, S. J., Cerliani, L., & Thiebaut De Schotten, M. (2018). Structural Variability Across the Primate Brain: A Cross-Species Comparison. *Cerebral Cortex*, *28*(11), 3829–3841. <https://doi.org/10.1093/cercor/bhx244>
- Cunningham, W. A., & Brosch, T. (2012). Motivational salience: Amygdala tuning from traits, needs, values, and goals. *Current Directions in Psychological Science*, *21*(1), 54–59. <https://doi.org/10.1177/0963721411430832>
- Cushnie, A. K., Bullock, D. N., Manea, A. M. G., Tang, W., Zimmermann, J., & Heilbronner, S. R. (2023). The use of chemogenetic actuator ligands in nonhuman primate DREADDs-fMRI. *Current Research in Neurobiology*, *4*, 100072. <https://doi.org/10.1016/j.crneur.2022.100072>
- Dal Monte, O., Costa, V. D., Noble, P. L., Murray, E. A., & Averbeck, B. B. (2015). Amygdala lesions in rhesus macaques decrease attention to threat. *Nature Communications*, *6*. <https://doi.org/10.1038/ncomms10161>
- Dal Monte, O., Fan, S., Fagan, N. A., Chu, C.-C. J., Zhou, M. B., Putnam, P. T., Nair, A. R., & Chang, S. W. C. (2022). Widespread implementations of interactive social gaze neurons in the primate prefrontal-amygdala networks. *Neuron*, *110*(13), 2183-2197.e7. <https://doi.org/10.1016/j.neuron.2022.04.013>
- Dang, T. P., Mattan, B. D., Kubota, J. T., & Cloutier, J. (2019). The ventromedial prefrontal cortex is particularly responsive to social evaluations requiring the use of person-knowledge. *Scientific Reports*, *9*(1). <https://doi.org/10.1038/s41598-019-41544-z>
- Davidson, J. D., & El Hady, A. (2019). Foraging as an evidence accumulation process. *PLoS Computational Biology*, *15*(7). <https://doi.org/10.1371/journal.pcbi.1007060>
- Davis, M., & Whalen, P. J. (2001). The amygdala: vigilance and emotion. In *Molecular Psychiatry* (Vol. 6). www.nature.com/mp
- de Waal, F. B. M., & Luttrell, L. M. (1985). The formal hierarchy of rhesus macaques: An investigation of the bared-teeth display. *American Journal of Primatology*, *9*(2), 73–85. <https://doi.org/10.1002/ajp.1350090202>
- Deffieux, T., Younan, Y., Wattiez, N., Tanter, M., Pouget, P., & Aubry, J. F. (2013). Low-intensity focused ultrasound modulates monkey visuomotor behavior. *Current Biology*, *23*(23), 2430–2433. <https://doi.org/10.1016/j.cub.2013.10.029>
- Demaria, C., & Thierry, B. (2001). A comparative study of reconciliation in rhesus and Tonkean macaques. *Behaviour*, *138*(3), 397–410. <https://doi.org/10.1163/15685390152032514>

- Di Biase, L., Falato, E., & Di Lazzaro, V. (2019). Transcranial Focused Ultrasound (tFUS) and Transcranial Unfocused Ultrasound (tUS) neuromodulation: From theoretical principles to stimulation practices. *Frontiers in Neurology*, *10*(JUN). <https://doi.org/10.3389/fneur.2019.00549>
- Di Martino, A., Scheres, A., Margulies, D. S., Kelly, A. M. C., Uddin, L. Q., Shehzad, Z., Biswal, B., Walters, J. R., Castellanos, F. X., & Milham, M. P. (2008). Functional connectivity of human striatum: A resting state fMRI study. *Cerebral Cortex*, *18*(12), 2735–2747. <https://doi.org/10.1093/cercor/bhn041>
- Dixon, M. L. (2015). Cognitive control, emotional value, and the lateral prefrontal cortex. In *Frontiers in Psychology* (Vol. 6, Issue JUN). Frontiers Media S.A. <https://doi.org/10.3389/fpsyg.2015.00758>
- Domenech, P., & Koechlin, E. (2015). Executive control and decision-making in the prefrontal cortex. *Current Opinion in Behavioral Sciences*, *1*, 101–106. <https://doi.org/10.1016/j.cobeha.2014.10.007>
- Domínguez-Borràs, J., Moyne, M., Saj, A., Guex, R., & Vuilleumier, P. (2020). Impaired emotional biases in visual attention after bilateral amygdala lesion. *Neuropsychologia*, *137*. <https://doi.org/10.1016/j.neuropsychologia.2019.107292>
- Doré, B. P., Boccagno, C., Burr, D., Hubbard, A., Long, K., Weber, J., Stern, Y., & Ochsner, K. N. (2017). Finding positive meaning in negative experiences engages ventral striatal and ventromedial prefrontal regions associated with reward valuation. *Journal of Cognitive Neuroscience*, *29*(2), 235–244. https://doi.org/10.1162/jocn_a_01041
- Duke, A. A., Bègue, L., Bell, R., & Eisenlohr-Moul, T. (2013). Revisiting the serotonin-aggression relation in humans: A meta-analysis. *Psychological Bulletin*, *139*(5), 1148–1172. <https://doi.org/10.1037/a0031544>
- Dum, R. P., & Strick, P. L. (1991). The origin of corticospinal projections from the premotor areas in the frontal lobe. *Journal of Neuroscience*, *11*(3), 667–689. <https://doi.org/10.1523/jneurosci.11-03-00667.1991>
- Dum, R. P., & Strick, P. L. (1992). Medial wall motor areas and skeletomotor control. *Current Opinion in Neurobiology*, *2*(6), 836–839. [https://doi.org/10.1016/0959-4388\(92\)90142-8](https://doi.org/10.1016/0959-4388(92)90142-8)
- Dum, R. P., & Strick, P. L. (2002). Motor areas in the frontal lobe of the primate. *Physiology & Behavior*, *77*, 677–682.
- DuPre, E., Salo, T., Ahmed, Z., Bandettini, P., Bottenhorn, K., Caballero-Gaudes, C., Dowdle, L., Gonzalez-Castillo, J., Heunis, S., Kundu, P., Laird, A., Markello, R., Markiewicz, C., Moia, S., Staden, I., Teves, J., Uruñuela, E., Vaziri-Pashkam, M., Whitaker, K., & Handwerker, D. (2021). TE-dependent analysis of multi-echo fMRI with tedana. *Journal of Open Source Software*, *6*(66), 3669. <https://doi.org/10.21105/joss.03669>
- Dziura, S. L., & Thompson, J. C. (2014). Social-Network Complexity in Humans Is Associated With the Neural Response to Social Information. *Psychological Science*, *25*(11), 2095–2101. <https://doi.org/10.1177/0956797614549209>
- Elorette, C., Aguilar, B. L., Novak, V., Forcelli, P. A., & Malkova, L. (2020). Dysregulation of behavioral and autonomic responses to emotional and social stimuli following bidirectional pharmacological manipulation of the basolateral amygdala in macaques. *Neuropharmacology*, *179*(July), 108275. <https://doi.org/10.1016/j.neuropharm.2020.108275>
- El-Shamayleh, Y., & Horwitz, G. D. (2019). Primate optogenetics: Progress and prognosis. *Proceedings of the National Academy of Sciences*, *116*(52), 26195–26203. <https://doi.org/10.1073/pnas.1902284116>

- Elvira, U. K. A., Seoane, S., Janssen, J., & Janssen, N. (2022). Contributions of human amygdala nuclei to resting-state networks. *PLoS ONE*, *17*(12 December). <https://doi.org/10.1371/journal.pone.0278962>
- Emery, N. J., Capitano, J. P., Mason, W. A., Machado, C. J., Mendoza, S. P., & Amaral, D. G. (2001). The effects of bilateral lesions of the amygdala on dyadic social interactions in rhesus monkeys (*Macaca mulatta*). *Behavioral Neuroscience*, *115*(3), 515–544. <https://doi.org/10.1037/0735-7044.115.3.515>
- Esber, G. R., Torres-Tristani, K., & Holland, P. C. (2015). Amygdalo-striatal interaction in the enhancement of stimulus salience in associative learning. *Behavioral Neuroscience*, *129*(2), 87–95. <https://doi.org/10.1037/bne0000041>
- Etkin, A., Egner, T., & Kalisch, R. (2011). Emotional processing in anterior cingulate and medial prefrontal cortex. *Trends in Cognitive Sciences*, *15*(2), 85–93. <https://doi.org/10.1016/j.tics.2010.11.004>
- Feinstein, J. S., Adolphs, R., Damasio, A., & Tranel, D. (2011). The Human Amygdala and the Induction and Experience of Fear. *Current Biology*, *21*(1), 34–38. <https://doi.org/10.1016/j.cub.2010.11.042>
- Fellows, L. K. (2004). The cognitive neuroscience of human decision making: a review and conceptual framework. In *Behavioral and cognitive neuroscience reviews* (Vol. 3, Issue 3, pp. 159–172). <https://doi.org/10.1177/1534582304273251>
- Fellows, L. K., & Farah, M. J. (2007). The role of ventromedial prefrontal cortex in decision making: Judgment under uncertainty or judgment per se? *Cerebral Cortex*, *17*(11), 2669–2674. <https://doi.org/10.1093/cercor/bhl176>
- Fisher, R. A. (1915). Frequency Distribution of the Values of the Correlation Coefficient in Samples from an Indefinitely Large Population. *Biometrika*, *10*(4), 507. <https://doi.org/10.2307/2331838>
- Folloni, D., Verhagen, L., Mars, R. B., Fouragnan, E., Constans, C., Aubry, J.-F., Rushworth, M. F. S., & Sallet, J. (2019). Manipulation of Subcortical and Deep Cortical Activity in the Primate Brain Using Transcranial Focused Ultrasound Stimulation. *Neuron*, *101*(6), 1109–1116.e5. <https://doi.org/10.1016/j.neuron.2019.01.019>
- Fuster, J. M. (1991). Chapter 10 The prefrontal cortex and its relation to behavior. In *Progress in Brain Research* (Vol. 87, pp. 201–211). [https://doi.org/10.1016/S0079-6123\(08\)63053-8](https://doi.org/10.1016/S0079-6123(08)63053-8)
- Fuster, J. M. (2001). The prefrontal cortex - An update: Time is of the essence. *Neuron*, *30*(2), 319–333. [https://doi.org/10.1016/S0896-6273\(01\)00285-9](https://doi.org/10.1016/S0896-6273(01)00285-9)
- Gangopadhyay, P., Chawla, M., Dal Monte, O., & Chang, S. W. C. (2021). Prefrontal–amygdala circuits in social decision-making. In *Nature Neuroscience* (Vol. 24, Issue 1, pp. 5–18). Nature Research. <https://doi.org/10.1038/s41593-020-00738-9>
- Gee, D. G., Hanson, C., Caglar, L. R., Fareri, D. S., Gabard-Durnam, L. J., Mills-Finnerty, C., Goff, B., Caldera, C. J., Lumian, D. S., Flannery, J., Hanson, S. J., & Tottenham, N. (2022). Experimental evidence for a child-to-adolescent switch in human amygdala-prefrontal cortex communication: A cross-sectional pilot study. *Developmental Science*, *January*, 1–16. <https://doi.org/10.1111/desc.13238>
- Gerbella, M., Borra, E., Tonelli, S., Rozzi, S., & Luppino, G. (2013). Connectional Heterogeneity of the Ventral Part of the Macaque Area 46. *Cerebral Cortex*, *23*(4), 967–987. <https://doi.org/10.1093/cercor/bhs096>
- Ghashghaei, H. T., & Barbas, H. (2002). Pathways for emotion: Interactions of prefrontal and anterior temporal pathways in the amygdala of the rhesus monkey. *Neuroscience*, *115*(4), 1261–1279. [https://doi.org/10.1016/S0306-4522\(02\)00446-3](https://doi.org/10.1016/S0306-4522(02)00446-3)

- Ghashghaei, H. T., Hilgetag, C. C., & Barbas, H. (2007). Sequence of information processing for emotions based on the anatomic dialogue between prefrontal cortex and amygdala. *NeuroImage*, 34(3), 905–923. <https://doi.org/10.1016/j.neuroimage.2006.09.046>
- Giacometti, C., Amiez, C., & Hadj-Bouziane, F. (2023). Multiple routes of communication within the amygdala-mPFC network: A comparative approach in humans and macaques. *Current Research in Neurobiology*, 5, 100103. <https://doi.org/10.1016/j.crneur.2023.100103>
- Giacometti, C., Dureux, A., Autran-Clavagnier, D., Wilson, C. R. E., Sallet, J., Dirheimer, M., Procyk, E., Hadj-Bouziane, F., & Amiez, C. (2022). Frontal cortical functional connectivity is impacted by anaesthesia in macaques. *Cerebral Cortex*, 32(18), 4050–4067. <https://doi.org/10.1093/cercor/bhab465>
- Gläscher, J., Adolphs, R., Damasio, H., Bechara, A., Rudrauf, D., Calamia, M., Paul, L. K., & Tranel, D. (2012). Lesion mapping of cognitive control and value-based decision making in the prefrontal cortex. *Proceedings of the National Academy of Sciences of the United States of America*, 109(36), 14681–14686. <https://doi.org/10.1073/pnas.1206608109>
- Glasser, M. F., Coalson, T. S., Robinson, E. C., Hacker, C. D., Harwell, J., Yacoub, E., Ugurbil, K., Andersson, J., Beckmann, C. F., Jenkinson, M., Smith, S. M., & Van Essen, D. C. (2016). A multi-modal parcellation of human cerebral cortex. *Nature*, 536(7615), 171–178. <https://doi.org/10.1038/nature18933>
- Gothard, K. M. (2020). Multidimensional processing in the amygdala. *Nature Reviews Neuroscience*, 21(10), 565–575. <https://doi.org/10.1038/s41583-020-0350-y>
- Grabenhorst, F., Báez-Mendoza, R., Genest, W., Deco, G., & Schultz, W. (2019). Primate Amygdala Neurons Simulate Decision Processes of Social Partners. *Cell*, 177(4), 986–998.e15. <https://doi.org/10.1016/j.cell.2019.02.042>
- Grabenhorst, F., & Rolls, E. T. (2011). Value, pleasure and choice in the ventral prefrontal cortex. *Trends in Cognitive Sciences*, 15(2), 56–67. <https://doi.org/10.1016/j.tics.2010.12.004>
- Grabenhorst, F., & Schultz, W. (2021). Functions of primate amygdala neurons in economic decisions and social decision simulation. *Behavioural Brain Research*, 409. <https://doi.org/10.1016/j.bbr.2021.113318>
- Grayson, D. S., Bliss-Moreau, E., Machado, C. J., Bennett, J., Shen, K., Grant, K. A., Fair, D. A., & Amaral, D. G. (2016). The Rhesus Monkey Connectome Predicts Disrupted Functional Networks Resulting from Pharmacogenetic Inactivation of the Amygdala. *Neuron*, 91(2), 453–466. <https://doi.org/10.1016/j.neuron.2016.06.005>
- Haber, S. N., Kim, K.-S., Mally, P., & Calzavara, R. (2006). Reward-Related Cortical Inputs Define a Large Striatal Region in Primates That Interface with Associative Cortical Connections, Providing a Substrate for Incentive-Based Learning. *The Journal of Neuroscience*, 26(32), 8368–8376. <https://doi.org/10.1523/JNEUROSCI.0271-06.2006>
- Hadj-Bouziane, F., Liu, N., Bell, A. H., Gothard, K. M., Luh, W. M., Tootell, R. B. H., Murray, E. A., & Ungerleider, L. G. (2012). Amygdala lesions disrupt modulation of functional MRI activity evoked by facial expression in the monkey inferior temporal cortex. *Proceedings of the National Academy of Sciences of the United States of America*, 109(52), E3640–E3648. <https://doi.org/10.1073/pnas.1218406109>
- Hampton, A. N., Adolphs, R., Tyszka, M. J., & O'Doherty, J. P. (2007). Contributions of the Amygdala to Reward Expectancy and Choice Signals in Human Prefrontal Cortex. *Neuron*, 55(4), 545–555. <https://doi.org/10.1016/j.neuron.2007.07.022>

- Hare, T. A., Camerer, C. F., & Rangel, A. (2009). Self-Control in Decision-Making Involves Modulation of the vmPFC Valuation System. *Science*, 324(5927), 646–648. <https://doi.org/10.1126/science.1168450>
- Hare, T. A., Hakimi, S., & Rangel, A. (2014). Activity in dlPFC and its effective connectivity to vmPFC are associated with temporal discounting. *Frontiers in Neuroscience*, 8 MAR. <https://doi.org/10.3389/fnins.2014.00050>
- Hare, T. A., Schultz, W., Camerer, C. F., O'Doherty, J. P., & Rangel, A. (2011). Transformation of stimulus value signals into motor commands during simple choice. *Proceedings of the National Academy of Sciences of the United States of America*, 108(44), 18120–18125. <https://doi.org/10.1073/pnas.1109322108>
- Harris, A., Adolphs, R., Camerer, C., & Rangel, A. (2011). Dynamic Construction of Stimulus Values in the Ventromedial Prefrontal Cortex. *PLoS ONE*, 6(6), e21074. <https://doi.org/10.1371/journal.pone.0021074>
- Harris, C. R., Millman, K. J., van der Walt, S. J., Gommers, R., Virtanen, P., Cournapeau, D., Wieser, E., Taylor, J., Berg, S., Smith, N. J., Kern, R., Picus, M., Hoyer, S., van Kerkwijk, M. H., Brett, M., Haldane, A., del Río, J. F., Wiebe, M., Peterson, P., ... Oliphant, T. E. (2020). Array programming with NumPy. In *Nature* (Vol. 585, Issue 7825, pp. 357–362). Nature Research. <https://doi.org/10.1038/s41586-020-2649-2>
- Haskell, R. E. (2004). Transfer of Learning. In *Encyclopedia of Applied Psychology* (pp. 575–586). Elsevier. <https://doi.org/10.1016/B0-12-657410-3/00834-5>
- He, S., Dum, R., & Strick, P. (1995a). Topographic organization of corticospinal projections from the frontal lobe: motor areas on the medial surface of the hemisphere. *The Journal of Neuroscience*, 15(5), 3284–3306. <https://doi.org/10.1523/JNEUROSCI.15-05-03284.1995>
- He, S., Dum, R., & Strick, P. (1995b). Topographic organization of corticospinal projections from the frontal lobe: motor areas on the medial surface of the hemisphere. *The Journal of Neuroscience*, 15(5), 3284–3306. <https://doi.org/10.1523/JNEUROSCI.15-05-03284.1995>
- Herry, C., Bach, D. R., Esposito, F., Di Salle, F., Perrig, W. J., Scheffler, K., Lüthi, A., & Seifritz, E. (2007). Processing of temporal unpredictability in human and animal amygdala. *Journal of Neuroscience*, 27(22), 5958–5966. <https://doi.org/10.1523/JNEUROSCI.5218-06.2007>
- Hertrich, I., Dietrich, S., Blum, C., & Ackermann, H. (2021). The Role of the Dorsolateral Prefrontal Cortex for Speech and Language Processing. In *Frontiers in Human Neuroscience* (Vol. 15). Frontiers Media S.A. <https://doi.org/10.3389/fnhum.2021.645209>
- Herzog, A. G., & Van Hoesen, G. W. (1976). Temporal neocortical afferent connections to the amygdala in the rhesus monkey. *Brain Research*, 115(1), 57–69. [https://doi.org/10.1016/0006-8993\(76\)90822-2](https://doi.org/10.1016/0006-8993(76)90822-2)
- Hiser, J., & Koenigs, M. (2017). *The multifaceted role of ventromedial prefrontal cortex in emotion, decision-making, social cognition, and psychopathology*.
- Holley, D., & Fox, A. S. (2022). The central extended amygdala guides survival-relevant tradeoffs: Implications for understanding common psychiatric disorders. In *Neuroscience and Biobehavioral Reviews* (Vol. 142). Elsevier Ltd. <https://doi.org/10.1016/j.neubiorev.2022.104879>
- Humphrey, T. (1968). The development of the human amygdala during early embryonic life. *The Journal of Comparative Neurology*, 132(1), 135–165. <https://doi.org/10.1002/cne.901320108>

- Hutchison, R. M., Hutchison, M., Manning, K. Y., Menon, R. S., & Everling, S. (2014). Isoflurane induces dose-dependent alterations in the cortical connectivity profiles and dynamic properties of the brain's functional architecture. *Human Brain Mapping*, 35(12), 5754–5775. <https://doi.org/10.1002/hbm.22583>
- Jacobs, R. H. A. H., Renken, R., Aleman, A., & Cornelissen, F. W. (2012). The amygdala, top-down effects, and selective attention to features. In *Neuroscience and Biobehavioral Reviews* (Vol. 36, Issue 9, pp. 2069–2084). <https://doi.org/10.1016/j.neubiorev.2012.05.011>
- Jenkinson, M., Beckmann, C. F., Behrens, T. E. J., Woolrich, M. W., & Smith, S. M. (2012). FSL - Review. *NeuroImage*, 62(2), 782–790. <https://doi.org/10.1016/j.neuroimage.2011.09.015>
- Jiang, X., Zhang, T., Zhang, S., Kendrick, K. M., & Liu, T. (2021). Fundamental functional differences between gyri and sulci: implications for brain function, cognition, and behavior. *Psychoradiology*, 1(1), 23–41. <https://doi.org/10.1093/psyrad/kkab002>
- Johansen-Berg, H., Gutman, D. A., Behrens, T. E. J., Matthews, P. M., Rushworth, M. F. S., Katz, E., Lozano, A. M., & Mayberg, H. S. (2008). Anatomical connectivity of the subgenual cingulate region targeted with deep brain stimulation for treatment-resistant depression. *Cerebral Cortex*, 18(6), 1374–1383. <https://doi.org/10.1093/cercor/bhm167>
- Joyce, M. K. P., & Barbas, H. (2018). Cortical connections position primate area 25 as a keystone for interoception, emotion, and memory. *Journal of Neuroscience*, 38(7), 1677–1698. <https://doi.org/10.1523/JNEUROSCI.2363-17.2017>
- Juechems, K., Balaguer, J., Herce Castañón, S., Ruz, M., O'Reilly, J. X., & Summerfield, C. (2019). A Network for Computing Value Equilibrium in the Human Medial Prefrontal Cortex. *Neuron*, 101(5), 977–987.e3. <https://doi.org/10.1016/j.neuron.2018.12.029>
- Kalin, N. H. (2004). The Role of the Central Nucleus of the Amygdala in Mediating Fear and Anxiety in the Primate. *Journal of Neuroscience*, 24(24), 5506–5515. <https://doi.org/10.1523/JNEUROSCI.0292-04.2004>
- Kanai, R., Bahrami, B., Roylance, R., & Rees, G. (2012). Online social network size is reflected in human brain structure. *Proceedings of the Royal Society B: Biological Sciences*, 279(1732), 1327–1334. <https://doi.org/10.1098/rspb.2011.1959>
- Kang, S. J., Liu, S., Ye, M., Kim, D. II, Pao, G. M., Copits, B. A., Roberts, B. Z., Lee, K. F., Bruchas, M. R., & Han, S. (2022). A central alarm system that gates multi-sensory innate threat cues to the amygdala. *Cell Reports*, 40(7). <https://doi.org/10.1016/j.celrep.2022.111222>
- Keele, N. B. (2005). The role of serotonin in impulsive and aggressive behaviors associated with epilepsy-like neuronal hyperexcitability in the amygdala. *Epilepsy & Behavior*, 7(3), 325–335. <https://doi.org/10.1016/j.yebeh.2005.06.014>
- Kerestes, R., Chase, H. W., Phillips, M. L., Ladouceur, C. D., & Eickhoff, S. B. (2017). Multimodal evaluation of the amygdala's functional connectivity. *NeuroImage*, 148, 219–229. <https://doi.org/10.1016/j.neuroimage.2016.12.023>
- Klasen, M., Wolf, D., Eisner, P. D., Eggermann, T., Zerres, K., Zepf, F. D., Weber, R., & Mathiak, K. (2019). Serotonergic contributions to human brain aggression networks. *Frontiers in Neuroscience*, 13(FEB). <https://doi.org/10.3389/fnins.2019.00042>
- Klein-Flügge, M. C., Bongioanni, A., & Rushworth, M. F. S. (2022). Medial and orbital frontal cortex in decision-making and flexible behavior. In *Neuron* (Vol. 110, Issue 17, pp. 2743–2770). Cell Press. <https://doi.org/10.1016/j.neuron.2022.05.022>
- Klein-Flügge, M. C., Jensen, D. E. A., Takagi, Y., Priestley, L., Verhagen, L., Smith, S. M., & Rushworth, M. F. S. (2022). Relationship between nuclei-specific amygdala connectivity

- and mental health dimensions in humans. *Nature Human Behaviour*.
<https://doi.org/10.1038/s41562-022-01434-3>
- Klomjai, W., Katz, R., & Lackmy-Vallée, A. (2015). Basic principles of transcranial magnetic stimulation (TMS) and repetitive TMS (rTMS). *Annals of Physical and Rehabilitation Medicine*, 58(4), 208–213. <https://doi.org/10.1016/j.rehab.2015.05.005>
- Kolling, N., Behrens, T. E. J., Mars, R. B., & Rushworth, M. F. S. (2012). Neural mechanisms of foraging. *Science*, 335(6077), 95–98. <https://doi.org/10.1126/science.1216930>
- Kondo, H., Saleem, K. S., & Price, J. L. (2005). Differential connections of the perirhinal and parahippocampal cortex with the orbital and medial prefrontal networks in macaque monkeys. *Journal of Comparative Neurology*, 493(4), 479–509. <https://doi.org/10.1002/cne.20796>
- Kreczmanski, P., Heinsen, H., Mantua, V., Woltersdorf, F., Masson, T., Ulfing, N., Schmidt-Kastner, R., Korr, H., Steinbusch, H. W. M., Hof, P. R., & Schmitz, C. (2007). Volume, neuron density and total neuron number in five subcortical regions in schizophrenia. *Brain*, 130(3), 678–692. <https://doi.org/10.1093/brain/awl386>
- Kundu, P., Brenowitz, N. D., Voon, V., Worbe, Y., Vértes, P. E., Inati, S. J., Saad, Z. S., Bandettini, P. A., & Bullmore, E. T. (2013). Integrated strategy for improving functional connectivity mapping using multiecho fMRI. *Proceedings of the National Academy of Sciences of the United States of America*, 110(40), 16187–16192. <https://doi.org/10.1073/pnas.1301725110>
- Kundu, P., Inati, S. J., Evans, J. W., Luh, W. M., & Bandettini, P. A. (2012). Differentiating BOLD and non-BOLD signals in fMRI time series using multi-echo EPI. *NeuroImage*, 60(3), 1759–1770. <https://doi.org/10.1016/j.neuroimage.2011.12.028>
- Kunishio, K., & Haber, S. N. (1994). Primate cingulostriatal projection: Limbic striatal versus sensorimotor striatal input. *The Journal of Comparative Neurology*, 350(3), 337–356. <https://doi.org/10.1002/cne.903500302>
- Leathers, M. L., & Olson, C. R. (2017). In monkeys making value-based decisions, amygdala neurons are sensitive to cue value as distinct from cue salience. *J Neurophysiol*, 117, 1499–1511. <https://doi.org/10.1152/jn.00564.2016.-Neurons>
- Lee, D. (2006). Best to go with what you know? *Nature*, 441(7095), 822–823. <https://doi.org/10.1038/441822a>
- Lew, C. H., Groeniger, K. M., Bellugi, U., Stefanacci, L., Schumann, C. M., & Semendeferi, K. (2018). A postmortem stereological study of the amygdala in Williams syndrome. *Brain Structure and Function*, 223(4), 1897–1907. <https://doi.org/10.1007/s00429-017-1592-y>
- Lew, C. H., Hanson, K. L., Groeniger, K. M., Greiner, D., Cuevas, D., Hrvoj-Mihic, B., Schumann, C. M., & Semendeferi, K. (2019). Serotonergic innervation of the human amygdala and evolutionary implications. *American Journal of Physical Anthropology*, 170(3), 351–360. <https://doi.org/10.1002/ajpa.23896>
- Li, J., Schiller, D., Schoenbaum, G., Phelps, E. A., & Daw, N. D. (2011). Differential roles of human striatum and amygdala in associative learning. *Nature Neuroscience*, 14(10), 1250–1252. <https://doi.org/10.1038/nn.2904>
- Liddell, B. J., Brown, K. J., Kemp, A. H., Barton, M. J., Das, P., Peduto, A., Gordon, E., & Williams, L. M. (2005). A direct brainstem–amygdala–cortical ‘alarm’ system for subliminal signals of fear. *NeuroImage*, 24(1), 235–243. <https://doi.org/10.1016/j.neuroimage.2004.08.016>
- Loh, K. K., Hadj-Bouziane, F., Petrides, M., Procyk, E., & Amiez, C. (2018). Rostro-Caudal organization of connectivity between cingulate motor areas and lateral frontal regions. *Frontiers in Neuroscience*, 11(JAN), 1–17. <https://doi.org/10.3389/fnins.2017.00753>

- Loh, K. K., Procyk, E., Neveu, R., Lamberton, F., Hopkins, W. D., Petrides, M., & Amiez, C. (2020). Cognitive control of orofacial motor and vocal responses in the ventrolateral and dorsomedial human frontal cortex. *Proceedings of the National Academy of Sciences*, *117*(9), 4994–5005. <https://doi.org/10.1073/pnas.1916459117>
- Long, A. B., Kuhn, C. M., & Platt, M. L. (2009). Serotonin shapes risky decision making in monkeys. *Social Cognitive and Affective Neuroscience*, *4*(4), 346–356. <https://doi.org/10.1093/scan/nsp020>
- Lopez-Persem, A., Verhagen, L., Amiez, C., Petrides, M., & Sallet, J. (2019). The Human Ventromedial Prefrontal Cortex: Sulcal Morphology and Its Influence on Functional Organization. *The Journal of Neuroscience*, *39*(19), 3627–3639. <https://doi.org/10.1523/JNEUROSCI.2060-18.2019>
- Lunenburg, F. C. (2010). THE DECISION MAKING PROCESS. In *NATIONAL FORUM OF EDUCATIONAL ADMINISTRATION AND SUPERVISION JOURNAL* (Vol. 27).
- Luppino, G., Matelli, M., Camarda, R. M., Gallese, V., & Rizzolatti, G. (1991). Multiple representations of body movements in mesial area 6 and the adjacent cingulate cortex: An intracortical microstimulation study in the macaque monkey. *The Journal of Comparative Neurology*, *311*(4), 463–482. <https://doi.org/10.1002/cne.903110403>
- Luppino, G., Matelli, M., Camarda, R., & Rizzolatti, G. (1993). Corticocortical connections of area F3 (SMA-proper) and area F6 (pre-SMA) in the macaque monkey. *The Journal of Comparative Neurology*, *338*(1), 114–140. <https://doi.org/10.1002/cne.903380109>
- Lv, H., Wang, Z., Tong, E., Williams, L. M., Zaharchuk, G., Zeineh, M., Goldstein-Piekarski, A. N., Ball, T. M., Liao, C., & Wintermark, M. (2018). Resting-State Functional MRI: Everything That Nonexperts Have Always Wanted to Know. *American Journal of Neuroradiology*, *39*(8), 1390–1399. <https://doi.org/10.3174/ajnr.A5527>
- MacDonald, A. W., Cohen, J. D., Andrew Stenger, V., & Carter, C. S. (2000). Dissociating the role of the dorsolateral prefrontal and anterior cingulate cortex in cognitive control. *Science*, *288*(5472), 1835–1838. <https://doi.org/10.1126/science.288.5472.1835>
- Machado, C. J., Emery, N. J., Capitanio, J. P., Mason, W. A., Mendoza, S. P., & Amaral, D. G. (2008). Bilateral Neurotoxic Amygdala Lesions in Rhesus Monkeys (*Macaca mulatta*): Consistent Pattern of Behavior Across Different Social Contexts. *Behavioral Neuroscience*, *122*(2), 251–266. <https://doi.org/10.1037/0735-7044.122.2.251>
- Machado, C. J., Snyder, A. Z., Cherry, S. R., Lavenex, P., & Amaral, D. G. (2008). Effects of neonatal amygdala or hippocampus lesions on resting brain metabolism in the macaque monkey: A microPET imaging study. *NeuroImage*, *39*(2), 832–846. <https://doi.org/10.1016/j.neuroimage.2007.09.029>
- Mackey, S., & Petrides, M. (2010). Quantitative demonstration of comparable architectonic areas within the ventromedial and lateral orbital frontal cortex in the human and the macaque monkey brains. *European Journal of Neuroscience*, *32*(11), 1940–1950. <https://doi.org/10.1111/j.1460-9568.2010.07465.x>
- Mackey, S., & Petrides, M. (2014). Architecture and morphology of the human ventromedial prefrontal cortex. *European Journal of Neuroscience*, *40*(5), 2777–2796. <https://doi.org/10.1111/ejn.12654>
- Málková, L., Gaffan, D., & Murray, E. A. (1997). Excitotoxic lesions of the amygdala fail to produce impairment in visual learning for auditory secondary reinforcement but interfere with reinforcer devaluation effects in rhesus monkeys. *Journal of Neuroscience*, *17*(15), 6011–6020. <https://doi.org/10.1523/jneurosci.17-15-06011.1997>
- Man, M. S., Mikheenko, Y., Braesicke, K., Cockcroft, G., & Roberts, A. C. (2012). Serotonin at the level of the amygdala and orbitofrontal cortex modulates distinct aspects of positive

- emotion in primates. *International Journal of Neuropsychopharmacology*, 15(1), 91–105. <https://doi.org/10.1017/S1461145711000587>
- Margulies, D. S., Kelly, A. M. C., Uddin, L. Q., Biswal, B. B., Castellanos, F. X., & Milham, M. P. (2007). Mapping the functional connectivity of anterior cingulate cortex. *NeuroImage*, 37(2), 579–588. <https://doi.org/10.1016/j.neuroimage.2007.05.019>
- Mars, R. B., Sotiropoulos, S. N., Passingham, R. E., Sallet, J., Verhagen, L., Khrapitchev, A. A., Sibson, N., & Jbabdi, S. (2018). Whole brain comparative anatomy using connectivity blueprints. *ELife*, 7. <https://doi.org/10.7554/eLife.35237>
- Mars, R. B., Verhagen, L., Gladwin, T. E., Neubert, F. X., Sallet, J., & Rushworth, M. F. S. (2016). Comparing brains by matching connectivity profiles. *Neuroscience and Biobehavioral Reviews*, 60, 90–97. <https://doi.org/10.1016/j.neubiorev.2015.10.008>
- Mason, W. A., Capitanio, J. P., Machado, C. J., Mendoza, S. P., & Amaral, D. G. (2006). Amygdectomy and responsiveness to novelty in rhesus monkeys (*Macaca mulatta*): Generality and individual consistency of effects. *Emotion*, 6(1), 73–81. <https://doi.org/10.1037/1528-3542.6.1.73>
- Matthew Hutchison, R., & Everling, S. (2012). Monkey in the middle: Why non-human primates are needed to bridge the gap in resting-state investigations. In *Frontiers in Neuroanatomy* (Vol. 6, Issue JULY 2012). Front Neuroanat. <https://doi.org/10.3389/fnana.2012.00029>
- Mckinney, W. (2010). *Data Structures for Statistical Computing in Python*.
- Meder, D., Kolling, N., Verhagen, L., Wittmann, M. K., Scholl, J., Madsen, K. H., Hulme, O. J., Behrens, T. E. J., & Rushworth, M. F. S. (2017). Simultaneous representation of a spectrum of dynamically changing value estimates during decision making. *Nature Communications*, 8(1). <https://doi.org/10.1038/s41467-017-02169-w>
- Medina, L., Bupesh, M., & Abellán, A. (2011). Contribution of genoarchitecture to understanding forebrain evolution and development, with particular emphasis on the amygdala. *Brain, Behavior and Evolution*, 78(3), 216–236. <https://doi.org/10.1159/000330056>
- Mehta, P. S., Tu, J. C., LoConte, G. A., Pesce, M. C., & Hayden, B. Y. (2019). Ventromedial prefrontal cortex tracks multiple environmental variables during search. *Journal of Neuroscience*, 39(27), 5336–5350. <https://doi.org/10.1523/JNEUROSCI.2365-18.2019>
- Miller, E. N., Hof, P. R., Sherwood, C. C., & Hopkins, W. D. (2021). The Paracingulate Sulcus Is a Unique Feature of the Medial Frontal Cortex Shared by Great Apes and Humans. *Brain, Behavior and Evolution*, 96(1), 26–36. <https://doi.org/10.1159/000517293>
- Miranda-Dominguez, O., Mills, B. D., Grayson, D., Woodall, A., Grant, K. A., Kroenke, C. D., & Fair, D. A. (2014). Bridging the gap between the human and macaque connectome: A quantitative comparison of global interspecies structure-function relationships and network topology. *Journal of Neuroscience*, 34(16), 5552–5563. <https://doi.org/10.1523/JNEUROSCI.4229-13.2014>
- Mishra, A., Rogers, B. P., Chen, L. M., & Gore, J. C. (2014). Functional connectivity-based parcellation of amygdala using self-organized mapping: A data driven approach. *Human Brain Mapping*, 35(4), 1247–1260. <https://doi.org/10.1002/hbm.22249>
- Miyachi, S., Hikosaka, O., & Lu, X. (2002). Differential activation of monkey striatal neurons in the early and late stages of procedural learning. *Experimental Brain Research*, 146(1), 122–126. <https://doi.org/10.1007/s00221-002-1213-7>
- Miyachi, S., Hikosaka, O., Miyashita, K., Kárádi, Z., & Rand, M. K. (1997). Differential roles of monkey striatum in learning of sequential hand movement. *Experimental Brain Research*, 115(1), 1–5. <https://doi.org/10.1007/PL00005669>

- Morawetz, C., Bode, S., Baudewig, J., & Heekeren, H. R. (2017). Effective amygdala-prefrontal connectivity predicts individual differences in successful emotion regulation. *Social Cognitive and Affective Neuroscience*, 12(4), 569–585. <https://doi.org/10.1093/scan/nsw169>
- Morecraft, R. J., Cipolloni, P. B., Stilwell-Morecraft, K. S., Gedney, M. T., & Pandya, D. N. (2004). Cytoarchitecture and cortical connections of the posterior cingulate and adjacent somatosensory fields in the rhesus monkey. *The Journal of Comparative Neurology*, 469(1), 37–69. <https://doi.org/10.1002/cne.10980>
- Morecraft, R. J., Mcneal, D. W., Stilwell-Morecraft, K. S., Gedney, M., Ge, J., Schroeder, C. M., & Van Hoesen, G. W. (2007). Amygdala interconnections with the cingulate motor cortex in the rhesus monkey. *Journal of Comparative Neurology*, 500(1), 134–165. <https://doi.org/10.1002/cne.21165>
- Morecraft, R. J., Schroeder, C. M., & Keifer, J. (1996). Organization of face representation in the cingulate cortex of the rhesus monkey. *NeuroReport*, 7(8), 1343–1348. <https://doi.org/10.1097/00001756-199605310-00002>
- Morecraft, R. J., Stilwell-Morecraft, K. S., Cipolloni, P. B., Ge, J., McNeal, D. W., & Pandya, D. N. (2012). Cytoarchitecture and cortical connections of the anterior cingulate and adjacent somatomotor fields in the rhesus monkey. *Brain Research Bulletin*, 87(4–5), 457–497. <https://doi.org/10.1016/j.brainresbull.2011.12.005>
- Morrison, S. E., & Daniel Salzman, C. (2010). Re-valuing the amygdala. *Current Opinion in Neurobiology*, 20, 221–230. <https://doi.org/10.1016/j.conb.2010.02.007>
- Morrow, J., Mosher, C., & Gothard, K. (2019). Multisensory neurons in the primate amygdala. *Journal of Neuroscience*, 39(19), 3663–3675. <https://doi.org/10.1523/JNEUROSCI.2903-18.2019>
- Motzkin, J. C., Philippi, C. L., Wolf, R. C., Baskaya, M. K., & Koenigs, M. (2015). Ventromedial prefrontal cortex is critical for the regulation of amygdala activity in humans. *Biological Psychiatry*, 77(3), 276–284. <https://doi.org/10.1016/j.biopsych.2014.02.014>
- Murray, E. A., & Fellows, L. K. (2021). Prefrontal cortex interactions with the amygdala in primates. *Neuropsychopharmacology*, July, 1–17. <https://doi.org/10.1038/s41386-021-01128-w>
- NAUTA, W. J. (1961). Fibre degeneration following lesions of the amygdaloid complex in the monkey. *Journal of Anatomy*, 95(Pt 4), 515–531. <http://www.ncbi.nlm.nih.gov/pubmed/14478601>
- Neubert, F.-X., Mars, R. B., Sallet, J., & Rushworth, M. F. S. (2015). Connectivity reveals relationship of brain areas for reward-guided learning and decision making in human and monkey frontal cortex. *Proceedings of the National Academy of Sciences*, 112(20), E2695–E2704. <https://doi.org/10.1073/pnas.1410767112>
- Neubert, F.-X., Mars, R. B., Thomas, A. G., Sallet, J., & Rushworth, M. F. S. (2014). Comparison of Human Ventral Frontal Cortex Areas for Cognitive Control and Language with Areas in Monkey Frontal Cortex. *Neuron*, 81(3), 700–713. <https://doi.org/10.1016/j.neuron.2013.11.012>
- Nicholson, A. A., Densmore, M., Frewen, P. A., Théberge, J., Neufeld, R. W., McKinnon, M. C., & Lanius, R. A. (2015). The Dissociative Subtype of Posttraumatic Stress Disorder: Unique Resting-State Functional Connectivity of Basolateral and Centromedial Amygdala Complexes. *Neuropsychopharmacology*, 40(10), 2317–2326. <https://doi.org/10.1038/npp.2015.79>

- Niznikiewicz, M. A., & Delgado, M. R. (2011). Two sides of the same coin: Learning via positive and negative reinforcers in the human striatum. *Developmental Cognitive Neuroscience*, 1(4), 494–505. <https://doi.org/10.1016/j.dcn.2011.07.006>
- Novek, J., Sprung-Much, T., Nolan, E., & Petrides, M. (2023). Optimal blocking of the cerebral cortex for cytoarchitectonic examination: a neuronavigation-based approach. *Cerebral Cortex (New York, N.Y. : 1991)*, 33(6), 2704–2714. <https://doi.org/10.1093/cercor/bhac236>
- Öhman, A. (2005). The role of the amygdala in human fear: Automatic detection of threat. *Psychoneuroendocrinology*, 30(10), 953–958. <https://doi.org/10.1016/j.psyneuen.2005.03.019>
- Okano, H., Hirano, T., & Balaban, E. (2000). Learning and memory. *Proceedings of the National Academy of Sciences*, 97(23), 12403–12404. <https://doi.org/10.1073/pnas.210381897>
- Olsson, A., Knapska, E., & Lindström, B. (2020). The neural and computational systems of social learning. In *Nature Reviews Neuroscience* (Vol. 21, Issue 4, pp. 197–212). Nature Research. <https://doi.org/10.1038/s41583-020-0276-4>
- O'Reilly, J. X. (2013). Making predictions in a changing world—inference, uncertainty, and learning. *Frontiers in Neuroscience*, 7 JUN. <https://doi.org/10.3389/fnins.2013.00105>
- Ousdal, O. T., Jensen, J., Server, A., Hariri, A. R., Nakstad, P. H., & Andreassen, O. A. (2008). The human amygdala is involved in general behavioral relevance detection: Evidence from an event-related functional magnetic resonance imaging Go-NoGo task. *Neuroscience*, 156(3), 450–455. <https://doi.org/10.1016/j.neuroscience.2008.07.066>
- Ousdal, O. T., Reckless, G. E., Server, A., Andreassen, O. A., & Jensen, J. (2012). Effect of relevance on amygdala activation and association with the ventral striatum. *NeuroImage*, 62(1), 95–101. <https://doi.org/10.1016/j.neuroimage.2012.04.035>
- Ousdal, O. T., Specht, K., Server, A., Andreassen, O. A., Dolan, R. J., & Jensen, J. (2014). The human amygdala encodes value and space during decision making. *NeuroImage*, 101, 712–719. <https://doi.org/10.1016/j.neuroimage.2014.07.055>
- Palomero-Gallagher, N., Eickhoff, S. B., Hoffstaedter, F., Schleicher, A., Mohlberg, H., Vogt, B. A., Amunts, K., & Zilles, K. (2015). Functional organization of human subgenual cortical areas: Relationship between architectonical segregation and connectional heterogeneity. *NeuroImage*, 115, 177–190. <https://doi.org/10.1016/j.neuroimage.2015.04.053>
- Palomero-Gallagher, N., Mohlberg, H., Zilles, K., & Vogt, B. (2008). Cytology and receptor architecture of human anterior cingulate cortex. *The Journal of Comparative Neurology*, 508(6), 906–926. <https://doi.org/10.1002/cne.21684>
- Palomero-Gallagher, N., Vogt, B. A., Schleicher, A., Mayberg, H. S., & Zilles, K. (2009). Receptor architecture of human cingulate cortex: Evaluation of the four-region neurobiological model. *Human Brain Mapping*, 30(8), 2336–2355. <https://doi.org/10.1002/hbm.20667>
- Panikratova, Y. R., Vlasova, R. M., Akhutina, T. V., Korneev, A. A., Sinitsyn, V. E., & Pechenkova, E. V. (2020). Functional connectivity of the dorsolateral prefrontal cortex contributes to different components of executive functions. *International Journal of Psychophysiology*, 151, 70–79. <https://doi.org/10.1016/j.ijpsycho.2020.02.013>
- Passingham, R. E. (2021). *Understanding the Prefrontal Cortex*. Oxford University Press. <https://doi.org/10.1093/oso/9780198844570.001.0001>

- Pasupathy, A., & Miller, E. K. (2005). Different time courses of learning-related activity in the prefrontal cortex and striatum. *Nature*, 433(7028), 873–876. <https://doi.org/10.1038/nature03287>
- Paton, J. J., Belova, M. A., Morrison, S. E., & Salzman, C. D. (2006). The primate amygdala represents the positive and negative value of visual stimuli during learning. *Nature*, 439(7078), 865–870. <https://doi.org/10.1038/nature04490>
- Paul, L. K., Corsello, C., Tranel, D., & Adolphs, R. (2010). Does bilateral damage to the human amygdala produce autistic symptoms? *Journal of Neurodevelopmental Disorders*, 2(3), 165–173. <https://doi.org/10.1007/s11689-010-9056-1>
- Pearce, J. M., & Bouton, M. E. (2000). *THEORIES OF ASSOCIATIVE LEARNING IN ANIMALS*. www.annualreviews.org
- Pedersen, W. S., Balderston, N. L., Miskovich, T. A., Belleau, E. L., Helmstetter, F. J., & Larson, C. L. (2017). The effects of stimulus novelty and negativity on BOLD activity in the amygdala, hippocampus, and bed nucleus of the stria terminalis. *Social Cognitive and Affective Neuroscience*, 12(5), 748–757. <https://doi.org/10.1093/scan/nsw178>
- Pedregosa, F., Michel, V., Grisel, O., Blondel, M., Prettenhofer, P., Weiss, R., Vanderplas, J., Cournapeau, D., Pedregosa, F., Varoquaux, G., Gramfort, A., Thirion, B., Grisel, O., Dubourg, V., Passos, A., Brucher, M., Perrot, M., & Duchesnay, É. (2011). Scikit-learn: Machine Learning in Python. In *Journal of Machine Learning Research* (Vol. 12). <http://scikit-learn.sourceforge.net>.
- Pelliccia, V., Del Vecchio, M., Avanzini, P., Revay, M., Sartori, I., & Caruana, F. (2023). 70 Years of Human Cingulate Cortex Stimulation. Functions and Dysfunctions Through the Lens of Electrical Stimulation. *Journal of Clinical Neurophysiology*. <https://doi.org/10.1097/WNP.0000000000000961>
- Pessoa, L., & Adolphs, R. (2010). Emotion processing and the amygdala: From a “low road” to “many roads” of evaluating biological significance. In *Nature Reviews Neuroscience* (Vol. 11, Issue 11, pp. 773–782). <https://doi.org/10.1038/nrn2920>
- Petit, O., Abegg, C., & Thierry, B. (1997). A Comparative Study of Aggression and Conciliation in Three Cercopithecine Monkeys (*Macaca Fuscata*, *Macaca Nigra*, *Papio Papio*). *Behaviour*, 134(5–6), 415–432. <https://doi.org/10.1163/156853997X00610>
- Petrides, M. (2000). The role of the mid-dorsolateral prefrontal cortex in working memory. In *Experimental Brain Research* (Vol. 133, Issue 1, pp. 44–54). Springer Verlag. <https://doi.org/10.1007/s002210000399>
- Petrides, M. (2005). Lateral prefrontal cortex: Architectonic and functional organization. *Philosophical Transactions of the Royal Society B: Biological Sciences*, 360(1456), 781–795. <https://doi.org/10.1098/rstb.2005.1631>
- Petrides, M., & Pandya, D. N. (1994). *Comparative architectonic analysis of the human and the macaque frontal cortex* (F. Boller & J. Grafman, Eds.; Elsevier, Vol. 9). Handbook of Neuropsychology.
- Petrides, M., & Pandya, D. N. (1999). Dorsolateral prefrontal cortex: Comparative cytoarchitectonic analysis in the human and the macaque brain and corticocortical connection patterns. *European Journal of Neuroscience*, 11(3), 1011–1036. <https://doi.org/10.1046/j.1460-9568.1999.00518.x>
- Petrides, M., & Pandya, D. N. (2002). Comparative cytoarchitectonic analysis of the human and the macaque ventrolateral prefrontal cortex and corticocortical connection patterns in the monkey. *European Journal of Neuroscience*, 16(2), 291–310. <https://doi.org/10.1046/j.1460-9568.2001.02090.x>

- Petrides, M., & Pandya, D. N. (2006). Efferent association pathways originating in the caudal prefrontal cortex in the macaque monkey. *The Journal of Comparative Neurology*, 498(2), 227–251. <https://doi.org/10.1002/cne.21048>
- Picard, N., & Strick, P. L. (2001). Imaging the premotor areas. *Current Opinion in Neurobiology*, 11(6), 663–672. [https://doi.org/10.1016/S0959-4388\(01\)00266-5](https://doi.org/10.1016/S0959-4388(01)00266-5)
- Pochon, J.-B. (2001). The Role of Dorsolateral Prefrontal Cortex in the Preparation of Forthcoming Actions: an fMRI Study. *Cerebral Cortex*, 11(3), 260–266. <https://doi.org/10.1093/cercor/11.3.260>
- Powers, W. T. (1973). Feedback: Beyond Behaviorism Stimulus-response laws are wholly predictable within a control-system model of behavioral organization. *Science*, 179(4071), 351–356.
- Procyk, E., Amiez, C., Fontanier, V., & Stoll, F. (2016). Frontal neural dynamics during performance monitoring and decisions to explore. *International Journal of Psychophysiology*, 108, 11. <https://doi.org/10.1016/j.ijpsycho.2016.07.039>
- Procyk, E., Wilson, C. R. E., Stoll, F. M., Faraut, M. C. M., Petrides, M., & Amiez, C. (2016). Midcingulate Motor Map and Feedback Detection: Converging Data from Humans and Monkeys. *Cerebral Cortex*, 26(2), 467–476. <https://doi.org/10.1093/cercor/bhu213>
- Puelles, L., & Ferran, J. L. (2012). Concept of neural genoarchitecture and its genomic fundament. *Frontiers in Neuroanatomy*, NOV, 1–8. <https://doi.org/10.3389/fnana.2012.00047>
- Pujara, M. S., Philippi, C. L., Motzkin, J. C., Baskaya, M. K., & Koenigs, M. (2016). Ventromedial prefrontal cortex damage is associated with decreased ventral striatum volume and response to reward. *Journal of Neuroscience*, 36(18), 5047–5054. <https://doi.org/10.1523/JNEUROSCI.4236-15.2016>
- Putnam, P. T., & Chang, S. W. C. (2021). Toward a holistic view of value and social processing in the amygdala: Insights from primate behavioral neurophysiology. *Behavioural Brain Research*, 411(May), 113356. <https://doi.org/10.1016/j.bbr.2021.113356>
- Quilodran, R., Rothé, M., & Procyk, E. (2008). Behavioral Shifts and Action Valuation in the Anterior Cingulate Cortex. *Neuron*, 57(2), 314–325. <https://doi.org/10.1016/j.neuron.2007.11.031>
- Rausch, A., Zhang, W., Beckmann, C. F., Buitelaar, J. K., Groen, W. B., & Haak, K. V. (2018). Connectivity-Based Parcellation of the Amygdala Predicts Social Skills in Adolescents with Autism Spectrum Disorder. *Journal of Autism and Developmental Disorders*, 48(2), 572–582. <https://doi.org/10.1007/s10803-017-3370-3>
- Redgrave, P., Rodriguez, M., Smith, Y., Rodriguez-Oroz, M. C., Lehericy, S., Bergman, H., Agid, Y., DeLong, M. R., & Obeso, J. A. (2010). Goal-directed and habitual control in the basal ganglia: Implications for Parkinson's disease. In *Nature Reviews Neuroscience* (Vol. 11, Issue 11, pp. 760–772). <https://doi.org/10.1038/nrn2915>
- Roth, B. L. (2016). DREADDs for Neuroscientists. In *Neuron* (Vol. 89, Issue 4, pp. 683–694). Cell Press. <https://doi.org/10.1016/j.neuron.2016.01.040>
- Rothé, M., Quilodran, R., Sallet, J., & Procyk, E. (2011). Coordination of high gamma activity in anterior cingulate and lateral prefrontal cortical areas during adaptation. *Journal of Neuroscience*, 31(31), 11110–11117. <https://doi.org/10.1523/JNEUROSCI.1016-11.2011>
- Rousseeuw, P. J. (1987). Silhouettes: A graphical aid to the interpretation and validation of cluster analysis. *Journal of Computational and Applied Mathematics*, 20, 53–65. [https://doi.org/10.1016/0377-0427\(87\)90125-7](https://doi.org/10.1016/0377-0427(87)90125-7)

- Równiak, M., & Bogus-Nowakowska, K. (2020). The amygdala of the common shrew, guinea pig, rabbit, fox and pig: five flavours of the mammalian amygdala as a consequence of clade-specific mosaic-like evolution. *Journal of Anatomy*, 236(5), 891–905. <https://doi.org/10.1111/joa.13148>
- Royer, S., Martina, M., & Paré, D. (1999). An Inhibitory Interface Gates Impulse Traffic between the Input and Output Stations of the Amygdala. *The Journal of Neuroscience*, 19(23), 10575–10583. <https://doi.org/10.1523/JNEUROSCI.19-23-10575.1999>
- Rubinow, M. J., Mahajan, G., May, W., Overholser, J. C., Jurjus, G. J., Dieter, L., Herbst, N., Steffens, D. C., Miguel-Hidalgo, J. J., Rajkowska, G., & Stockmeier, C. A. (2016). Basolateral amygdala volume and cell numbers in major depressive disorder: a postmortem stereological study. *Brain Structure and Function*, 221(1), 171–184. <https://doi.org/10.1007/s00429-014-0900-z>
- Rudebeck, P. H., Mitz, A. R., Chacko, R. V., & Murray, E. A. (2013). Effects of Amygdala Lesions on Reward-Value Coding in Orbital and Medial Prefrontal Cortex. *Neuron*, 80(6), 1519–1531. <https://doi.org/10.1016/j.neuron.2013.09.036>
- Rudebeck, P. H., Ripple, J. A., Mitz, A. R., Averbeck, B. B., & Murray, E. A. (2017). Amygdala contributions to stimulus–reward encoding in the macaque medial and orbital frontal cortex during learning. *Journal of Neuroscience*, 37(8), 2186–2202. <https://doi.org/10.1523/JNEUROSCI.0933-16.2017>
- Rudorf, S., & Hare, T. A. (2014). Interactions between dorsolateral and ventromedial prefrontal cortex underlie context-dependent stimulus valuation in goal-directed choice. *Journal of Neuroscience*, 34(48), 15988–15996. <https://doi.org/10.1523/JNEUROSCI.3192-14.2014>
- Rushworth, M. F. S., Noonan, M. A. P., Boorman, E. D., Walton, M. E., & Behrens, T. E. (2011). Frontal Cortex and Reward-Guided Learning and Decision-Making. In *Neuron* (Vol. 70, Issue 6, pp. 1054–1069). <https://doi.org/10.1016/j.neuron.2011.05.014>
- Rushworth, M. F. S., Walton, M. E., Kennerley, S. W., & Bannerman, D. M. (2004). Action sets and decisions in the medial frontal cortex. In *Trends in Cognitive Sciences* (Vol. 8, Issue 9, pp. 410–417). <https://doi.org/10.1016/j.tics.2004.07.009>
- Saez, A., Rigotti, M., Ostojic, S., Fusi, S., & Salzman, C. D. (2015). Abstract Context Representations in Primate Amygdala and Prefrontal Cortex. *Neuron*, 87(4), 869–881. <https://doi.org/10.1016/j.neuron.2015.07.024>
- Saez, R. A., Saez, A., Paton, J. J., Lau, B., & Salzman, C. D. (2017). Distinct Roles for the Amygdala and Orbitofrontal Cortex in Representing the Relative Amount of Expected Reward. *Neuron*, 95(1), 70-77.e3. <https://doi.org/10.1016/j.neuron.2017.06.012>
- Sah, P., Faber, E. S. L., De Armentia, M. L., & Power, J. (2003). The amygdaloid complex: Anatomy and physiology. *Physiological Reviews*, 83(3), 803–834. <https://doi.org/10.1152/physrev.00002.2003>
- Sallet, J., Camille, N., & Procyk, E. (2013). Modulation of feedback-related negativity during trial-and-error exploration and encoding of behavioral shifts. *Frontiers in Neuroscience*, 7 NOV. <https://doi.org/10.3389/fnins.2013.00209>
- Sallet, J., Mars, R. B., Noonan, M. P., Andersson, J. L., O'Reilly, J. X., Jbabdi, S., Croxson, P. L., Jenkinson, M., Miller, K. L., & Rushworth, M. F. S. (2011). Social Network Size Affects Neural Circuits in Macaques. *Science*, 334(6056), 697–700. <https://doi.org/10.1126/science.1210027>
- Sallet, J., Mars, R. B., Noonan, M. P., Neubert, F. X., Jbabdi, S., O'Reilly, J. X., Filippini, N., Thomas, A. G., & Rushworth, M. F. (2013). The organization of dorsal frontal cortex in

- humans and macaques. *Journal of Neuroscience*, 33(30), 12255–12274. <https://doi.org/10.1523/JNEUROSCI.5108-12.2013>
- Santos, A., Mier, D., Kirsch, P., & Meyer-Lindenberg, A. (2011). Evidence for a general face salience signal in human amygdala. *NeuroImage*, 54(4), 3111–3116. <https://doi.org/10.1016/j.neuroimage.2010.11.024>
- Sawada, M., Adolphs, R., Dlouhy, B. J., Jenison, R. L., Rhone, A. E., Kovach, C. K., Greenlee, J. D. W., Howard III, M. A., & Oya, H. (2022). Mapping effective connectivity of human amygdala subdivisions with intracranial stimulation. *Nature Communications*, 13(1). <https://doi.org/10.1038/s41467-022-32644-y>
- Schneider, B., & Koenigs, M. (2017). Human lesion studies of ventromedial prefrontal cortex. *Neuropsychologia*, 107(July), 84–93. <https://doi.org/10.1016/j.neuropsychologia.2017.09.035>
- Scholl, J., Kolling, N., Nelissen, N., Wittmann, M. K., Harmer, C. J., & Rushworth, M. F. S. (2015). The good, the bad, and the irrelevant: Neural mechanisms of learning real and hypothetical rewards and effort. *Journal of Neuroscience*, 35(32), 11233–11251. <https://doi.org/10.1523/JNEUROSCI.0396-15.2015>
- Schumann, C. M., & Amaral, D. G. (2005). Stereological estimation of the number of neurons in the human amygdaloid complex. *Journal of Comparative Neurology*, 491(4), 320–329. <https://doi.org/10.1002/cne.20704>
- Schumann, C. M., & Amaral, D. G. (2006). Stereological Analysis of Amygdala Neuron Number in Autism. *Journal of Neuroscience*, 26(29), 7674–7679. <https://doi.org/10.1523/JNEUROSCI.1285-06.2006>
- Schumann, C. M., Bauman, M. D., & Amaral, D. G. (2011). Abnormal structure or function of the amygdala is a common component of neurodevelopmental disorders. *Neuropsychologia*, 49(4), 745–759. <https://doi.org/10.1016/j.neuropsychologia.2010.09.028>
- Schwartzbaum, J. S. (1960). Changes in reinforcing properties of stimuli following ablation of the amygdaloid complex in monkeys. *Journal of Comparative and Physiological Psychology*, 53(4), 388–395. <https://doi.org/10.1037/h0049187>
- Schwartzbaum, J. S. (1964). Visually reinforced behavior following ablation of the amygdaloid complex in monkeys. *Journal of Comparative and Physiological Psychology*, 57(3), 340–347. <https://doi.org/10.1037/h0042795>
- Semendeferi, K., & Damasio, H. (2000). The brain and its main anatomical subdivisions in living hominoids using magnetic resonance imaging. *Journal of Human Evolution*, 38(2), 317–332. <https://doi.org/10.1006/jhev.1999.0381>
- Semendeferi, K., Damasio, H., Frank, R., & Van Hoesen, G. W. (1997). The evolution of the frontal lobes: a volumetric analysis based on three-dimensional reconstructions of magnetic resonance scans of human and ape brains. In *Journal of Human Evolution* (Vol. 32). Academic Press.
- Seo, D., Patrick, C. J., & Kennealy, P. J. (2008). Role of serotonin and dopamine system interactions in the neurobiology of impulsive aggression and its comorbidity with other clinical disorders. In *Aggression and Violent Behavior* (Vol. 13, Issue 5, pp. 383–395). <https://doi.org/10.1016/j.avb.2008.06.003>
- Seymour, B., & Dolan, R. (2008). Emotion, Decision Making, and the Amygdala. *Neuron*, 58(5), 662–671. <https://doi.org/10.1016/j.neuron.2008.05.020>
- Shadlen, M. N., & Kiani, R. (2013). Decision making as a window on cognition. In *Neuron* (Vol. 80, Issue 3, pp. 791–806). <https://doi.org/10.1016/j.neuron.2013.10.047>

- Shen, Y., Cai, H., Mo, F., Yao, S., Yu, Y., & Zhu, J. (2023). Functional connectivity gradients of the cingulate cortex. *Communications Biology*, 6(1). <https://doi.org/10.1038/s42003-023-05029-0>
- Silvetti, M., Seurinck, R., & Verguts, T. (2013). Value and prediction error estimation account for volatility effects in ACC: A model-based fMRI study. *Cortex*, 49(6), 1627–1635. <https://doi.org/10.1016/j.cortex.2012.05.008>
- Šimić, G., Tkalčić, M., Vukić, V., Mulc, D., Španić, E., Šagud, M., Olucha-Bordonau, F. E., Vukšić, M., & Hof, P. R. (2021). Understanding emotions: Origins and roles of the amygdala. In *Biomolecules* (Vol. 11, Issue 6). MDPI AG. <https://doi.org/10.3390/biom11060823>
- Smaers, J. B. (2013). How humans stand out in frontal lobe scaling. *Proceedings of the National Academy of Sciences of the United States of America*, 110(39). <https://doi.org/10.1073/pnas.1308850110>
- Smaers, J. B., Gómez-Robles, A., Parks, A. N., & Sherwood, C. C. (2017). Exceptional Evolutionary Expansion of Prefrontal Cortex in Great Apes and Humans. *Current Biology*, 27(5), 714–720. <https://doi.org/10.1016/j.cub.2017.01.020>
- Smaers, J. B., Steele, J., Case, C. R., Cowper, A., Amunts, K., & Zilles, K. (2011). Primate Prefrontal Cortex Evolution: Human Brains Are the Extreme of a Lateralized Ape Trend. *Brain, Behavior and Evolution*, 77(2), 67–78. <https://doi.org/10.1159/000323671>
- Smith, E. H., Banks, G. P., Mikell, C. B., Cash, S. S., Patel, S. R., Eskandar, E. N., & Sheth, S. A. (2015). Frequency-dependent representation of reinforcement-related information in the human medial and lateral prefrontal cortex. *Journal of Neuroscience*, 35(48), 15827–15836. <https://doi.org/10.1523/JNEUROSCI.1864-15.2015>
- Smith, S. M., Jenkinson, M., Woolrich, M. W., Beckmann, C. F., Behrens, T. E. J., Johansen-Berg, H., Bannister, P. R., De Luca, M., Drobnjak, I., Flitney, D. E., Niazy, R. K., Saunders, J., Vickers, J., Zhang, Y., De Stefano, N., Brady, J. M., & Matthews, P. M. (2004). Advances in functional and structural MR image analysis and implementation as FSL. *NeuroImage*, 23, S208–S219. <https://doi.org/10.1016/j.neuroimage.2004.07.051>
- Solano-Castiella, E., Anwender, A., Lohmann, G., Weiss, M., Docherty, C., Geyer, S., Reimer, E., Friederici, A. D., & Turner, R. (2010). Diffusion tensor imaging segments the human amygdala in vivo. *NeuroImage*, 49(4), 2958–2965. <https://doi.org/10.1016/j.neuroimage.2009.11.027>
- Solano-Castiella, E., Schäfer, A., Reimer, E., Türke, E., Pröger, T., Lohmann, G., Trampel, R., & Turner, R. (2011). Parcellation of human amygdala in vivo using ultra high field structural MRI. *NeuroImage*, 58(3), 741–748. <https://doi.org/10.1016/j.neuroimage.2011.06.047>
- Soltani, A., & Izquierdo, A. (2019). Adaptive learning under expected and unexpected uncertainty. In *Nature Reviews Neuroscience* (Vol. 20, Issue 10, pp. 635–644). Nature Publishing Group. <https://doi.org/10.1038/s41583-019-0180-y>
- Song, X., Panych, L. P., & Chen, N. K. (2016). Data-Driven and Predefined ROI-Based Quantification of Long-Term Resting-State fMRI Reproducibility. *Brain Connectivity*, 6(2), 136–151. <https://doi.org/10.1089/brain.2015.0349>
- Spalding, K. N., Schlichting, M. L., Zeithamova, D., Preston, A. R., Tranel, D., Duff, M. C., & Warren, D. E. (2018). Ventromedial prefrontal cortex is necessary for normal associative inference and memory integration. *Journal of Neuroscience*, 38(15), 3767–3775. <https://doi.org/10.1523/JNEUROSCI.2501-17.2018>
- Staddon, J. E. R. (2016). *Adaptive Behavior and Learning*. Cambridge University Press. <https://doi.org/10.1017/CBO9781139998369>

- Stefanacci, L., & Amaral, D. G. (2000). Topographic Organization of Cortical Inputs to the Lateral Nucleus of the Macaque Monkey Amygdala: A Retrograde Tracing Study. In *J. Comp. Neurol* (Vol. 421).
- Stephan, H., Frahm, H. D., & Baron, G. (1987). Comparison of brain structure volumes in Insectivora and primates. VII. Amygdaloid components. *Journal Für Hirnforschung*, 28(5), 571–584. <http://www.ncbi.nlm.nih.gov/pubmed/3693895>
- Stimpson, C. D., Barger, N., Tagliabata, J. P., Gendron-Fitzpatrick, A., Hof, P. R., Hopkins, W. D., & Sherwood, C. C. (2016). Differential serotonergic innervation of the amygdala in bonobos and chimpanzees. *Social Cognitive and Affective Neuroscience*, 11(3), 413–422. <https://doi.org/10.1093/scan/nsv128>
- Suzuki, W. A. (1996). Neuroanatomy of the monkey entorhinal, perirhinal and parahippocampal cortices: Organization of cortical inputs and interconnections with amygdala and striatum. *Seminars in Neuroscience*, 8(1), 3–12. <https://doi.org/10.1006/smns.1996.0002>
- Swanson, L. W., & Petrovich, G. D. (1998). What is the amygdala? *Trends in Neurosciences*, 21(8), 323–331. [https://doi.org/10.1016/S0166-2236\(98\)01265-X](https://doi.org/10.1016/S0166-2236(98)01265-X)
- Sylvester, C. M., Yu, Q., Benjamin Srivastava, A., Marek, S., Zheng, A., Alexopoulos, D., Smyser, C. D., Shimony, J. S., Ortega, M., Dierker, D. L., Patel, G. H., Nelson, S. M., Gilmore, A. W., McDermott, K. B., Berg, J. J., Drysdale, A. T., Perino, M. T., Snyder, A. Z., Raut, R. V., ... Dosenbach, N. U. F. (2020). Individual-specific functional connectivity of the amygdala: A substrate for precision psychiatry. *Proceedings of the National Academy of Sciences of the United States of America*, 117(7), 3808–3818. <https://doi.org/10.1073/pnas.1910842117>
- Tanji, J., & Hoshi, E. (2008). Role of the Lateral Prefrontal Cortex in Executive Behavioral Control. *Physiological Reviews*, 88(1), 37–57. <https://doi.org/10.1152/physrev.00014.2007>
- Taswell, C. A., Costa, V. D., Basile, B. M., Pujara, M. S., Jones, B., Manem, N., Murray, E. A., & Averbeck, B. B. (2021). Effects of Amygdala Lesions on Object-Based Versus Action-Based Learning in Macaques. *Cerebral Cortex*, 31(1), 529–546. <https://doi.org/10.1093/cercor/bhaa241>
- Taubert, J., Flessert, M., Wardle, S. G., Basile, B. M., Murphy, A. P., Murray, E. A., & Ungerleider, L. G. (2018). Amygdala lesions eliminate viewing preferences for faces in rhesus monkeys. *Proceedings of the National Academy of Sciences of the United States of America*, 115(31), 8043–8048. <https://doi.org/10.1073/pnas.1807245115>
- Tazumi, T., Hori, E., Maior, R. S., Ono, T., & Nishijo, H. (2010). Neural correlates to seen gaze-direction and head orientation in the macaque monkey amygdala. *Neuroscience*, 169(1), 287–301. <https://doi.org/10.1016/j.neuroscience.2010.04.028>
- Teffer, K., & Semendeferi, K. (2012). Human prefrontal cortex. Evolution, development, and pathology. In *Progress in Brain Research* (1st ed., Vol. 195). Elsevier B.V. <https://doi.org/10.1016/B978-0-444-53860-4.00009-X>
- Thierry, B. (2015). Covariation of conflict management patterns across macaque species. *Natural Conflict Resolution, November*, 106–128.
- Thierry, B., Mewa, S., & Kaumanns, W. (2010). *Macaque societies: A model for study of Social Organization* (B. Thierry, S. Mewa, & W. Kaumanns, Eds.; Vol. 41). Cambridge University Press.
- Tottenham, N. (2015). Social scaffolding of human amygdala-mPFC circuit development. *Social Neuroscience*, 10(5), 489–499. <https://doi.org/10.1080/17470919.2015.1087424>

- Tottenham, N., & Galván, A. (2016). Stress and the adolescent brain: Amygdala-prefrontal cortex circuitry and ventral striatum as developmental targets. In *Neuroscience and Biobehavioral Reviews* (Vol. 70, pp. 217–227). Elsevier Ltd. <https://doi.org/10.1016/j.neubiorev.2016.07.030>
- Treves, A. (2000). Theory and method in studies of vigilance and aggregation. *Animal Behaviour*, 60(6), 711–722. <https://doi.org/10.1006/anbe.2000.1528>
- Tricomi, E., Balleine, B. W., & O'Doherty, J. P. (2009). A specific role for posterior dorsolateral striatum in human habit learning. *European Journal of Neuroscience*, 29(11), 2225–2232. <https://doi.org/10.1111/j.1460-9568.2009.06796.x>
- Trudel, N., Scholl, J., Klein-Flügge, M. C., Fouragnan, E., Tankelevitch, L., Wittmann, M. K., & Rushworth, M. F. S. (2021). Polarity of uncertainty representation during exploration and exploitation in ventromedial prefrontal cortex. *Nature Human Behaviour*, 5(1), 83–98. <https://doi.org/10.1038/s41562-020-0929-3>
- Tyszka, J. M., & Pauli, W. M. (2016). In vivo delineation of subdivisions of the human amygdaloid complex in a high-resolution group template. *Human Brain Mapping*, 37(11), 3979–3998. <https://doi.org/10.1002/hbm.23289>
- Uhrig, L., Sitt, J. D., Jacob, A., Tasserie, J., Barttfeld, P., Dupont, M., Dehaene, S., & Jarraya, B. (2018). Resting-state Dynamics as a Cortical Signature of Anesthesia in Monkeys. *Anesthesiology*, 129(5), 942–958. <https://doi.org/10.1097/ALN.0000000000002336>
- Usher, M., Tsetsos, K., Yu, E. C., & Lagnado, D. A. (2013). Dynamics of decision-making: From evidence accumulation to preference and belief. In *Frontiers in Psychology* (Vol. 4, Issue OCT). Frontiers Research Foundation. <https://doi.org/10.3389/fpsyg.2013.00758>
- Van Den Bos, W., & Güroğlu, B. (2009). The role of the ventral medial prefrontal cortex in social decision making. In *Journal of Neuroscience* (Vol. 29, Issue 24, pp. 7631–7632). <https://doi.org/10.1523/JNEUROSCI.1821-09.2009>
- van Holstein, M., MacLeod, P. E., & Floresco, S. B. (2020). Basolateral amygdala – nucleus accumbens circuitry regulates optimal cue-guided risk/reward decision making. *Progress in Neuro-Psychopharmacology and Biological Psychiatry*, 98(August 2019), 109830. <https://doi.org/10.1016/j.pnpbp.2019.109830>
- van Steenbergen, H., Watson, P., Wiers, R. W., Hommel, B., & de Wit, S. (2017). Dissociable corticostriatal circuits underlie goal-directed vs. cue-elicited habitual food seeking after satiation: evidence from a multimodal MRI study. *European Journal of Neuroscience*, 46(2), 1815–1827. <https://doi.org/10.1111/ejn.13586>
- Vanduffel, W., & Li, X. (2020). Exciting inhibition in primates. *eLife*, 9. <https://doi.org/10.7554/eLife.59381>
- Vassena, E., Krebs, R. M., Silvetti, M., Fias, W., & Verguts, T. (2014). Dissociating contributions of ACC and vmPFC in reward prediction, outcome, and choice. *Neuropsychologia*, 59, 112–123. <https://doi.org/10.1016/j.neuropsychologia.2014.04.019>
- Vergani, F., Martino, J., Morris, C., Attems, J., Ashkan, K., & Dell'Acqua, F. (2016). Anatomic Connections of the Subgenual Cingulate Region. *Neurosurgery*, 79(3), 465–472. <https://doi.org/10.1227/NEU.0000000000001315>
- Verhagen, L., Gallea, C., Folloni, D., Constans, C., Jensen, D. E., Ahnine, H., Roumazeilles, L., Santin, M., Ahmed, B., Lehericy, S., Klein-Flügge, M. C., Krug, K., Mars, R. B., Rushworth, M. F., Pouget, P., Aubry, J.-F., & Sallet, J. (2019). *Offline impact of transcranial focused ultrasound on cortical activation in primates*. <https://doi.org/10.7554/eLife.40541.001>

- Vogt, B. A. (2009). Regions and Subregions of the Cingulate Cortex. In B. A. Vogt (Ed.), *Cingulate Neurobiology and Disease* (pp. 3–30). Oxford University Press.
- Vogt, B. A. (2016). Midcingulate cortex: Structure, connections, homologies, functions and diseases. *Journal of Chemical Neuroanatomy*, *74*, 28–46. <https://doi.org/10.1016/j.jchemneu.2016.01.010>
- Vogt, B. A., Berger, G. R., & Derbyshire, S. W. G. (2003). Structural and functional dichotomy of human midcingulate cortex. *European Journal of Neuroscience*, *18*(11), 3134–3144. <https://doi.org/10.1111/j.1460-9568.2003.03034.x>
- Vogt, B. A., Nimchinsky, E. A., Vogt, L. J., & Hof, P. R. (1995). Human cingulate cortex: Surface features, flat maps, and cytoarchitecture. *The Journal of Comparative Neurology*, *359*(3), 490–506. <https://doi.org/10.1002/cne.903590310>
- Vogt, B. A., & Palomero-Gallagher, N. (2012). Cingulate Cortex. In *The Human Nervous System, Third Edition* (pp. 943–987). Elsevier. <https://doi.org/10.1016/B978-0-12-374236-0.10025-2>
- Vogt, B. A., & Pandya, D. N. (1987). Cingulate cortex of the rhesus monkey: II. Cortical afferents. *The Journal of Comparative Neurology*, *262*(2), 271–289. <https://doi.org/10.1002/cne.902620208>
- Vogt, B. A., Vogt, L., Farber, N. B., & Bush, G. (2005). Architecture and neurocytology of monkey cingulate gyrus. *The Journal of Comparative Neurology*, *485*(3), 218–239. <https://doi.org/10.1002/cne.20512>
- von Luxburg, U. (2007). A tutorial on spectral clustering. *Statistics and Computing*, *17*(4), 395–416. <https://doi.org/10.1007/s11222-007-9033-z>
- Wallis, J. D., & Rich, E. L. (2011). Challenges of Interpreting Frontal Neurons during Value-Based Decision-Making. *Frontiers in Neuroscience*, *5*. <https://doi.org/10.3389/fnins.2011.00124>
- Wang, J., & Barbas, H. (2018). Specificity of primate amygdalar pathways to hippocampus. *Journal of Neuroscience*, *38*(47), 10019–10041. <https://doi.org/10.1523/JNEUROSCI.1267-18.2018>
- Wang, J., John, Y., & Barbas, H. (2021). Pathways for contextual memory: The primate hippocampal pathway to anterior cingulate cortex. *Cerebral Cortex*, *31*(3), 1807–1826. <https://doi.org/10.1093/cercor/bhaa333>
- Wasserman, E. A., & Miller, R. R. (1997). WHAT'S ELEMENTARY ABOUT ASSOCIATIVE LEARNING? In *Annu. Rev. Psychol* (Vol. 48). www.annualreviews.org
- Wassum, K. M., & Izquierdo, A. (2015). The basolateral amygdala in reward learning and addiction. *Neuroscience and Biobehavioral Reviews*, *57*, 271–283. <https://doi.org/10.1016/j.neubiorev.2015.08.017>
- Watanabe, N., Bhanji, J. P., Tanabe, H. C., & Delgado, M. R. (2019). Ventromedial prefrontal cortex contributes to performance success by controlling reward-driven arousal representation in amygdala. *NeuroImage*, *202*. <https://doi.org/10.1016/j.neuroimage.2019.116136>
- Weinberg-Wolf, H., & Chang, S. W. C. (2019). Differences in how macaques monitor others: Does serotonin play a central role? *Wiley Interdisciplinary Reviews: Cognitive Science*, *10*(4). <https://doi.org/10.1002/wcs.1494>
- Wellman, L. L., Forcelli, P. A., Aguilar, B. L., & Malkova, L. (2016). Bidirectional Control of Social Behavior by Activity within Basolateral and Central Amygdala of Primates. *The Journal of Neuroscience*, *36*(33), 8746–8756. <https://doi.org/10.1523/JNEUROSCI.0333-16.2016>

- Wen, Q., Stirling, B. D., Sha, L., Shen, L., Whalen, P. J., & Wu, Y. C. (2017). Parcellation of human amygdala subfields using orientation distribution function and spectral k-means clustering. In *Mathematics and Visualization* (pp. 123–132). Springer Heidelberg. https://doi.org/10.1007/978-3-319-54130-3_10
- Wittmann, M. K., Kolling, N., Akaishi, R., Chau, B. K. H., Brown, J. W., Nelissen, N., & Rushworth, M. F. S. (2016). Predictive decision making driven by multiple time-linked reward representations in the anterior cingulate cortex. *Nature Communications*, 7(1). <https://doi.org/10.1038/ncomms12327>
- Woolrich, M. W., Jbabdi, S., Patenaude, B., Chappell, M., Makni, S., Behrens, T., Beckmann, C., Jenkinson, M., & Smith, S. M. (2009). Bayesian analysis of neuroimaging data in FSL. *NeuroImage*, 45(1), S173–S186. <https://doi.org/10.1016/j.neuroimage.2008.10.055>
- Yaakub, S. N., White, T. A., Roberts, J., Martin, E., Verhagen, L., Stagg, C. J., Hall, S., & Fouragnan, E. F. (2023). Transcranial focused ultrasound-mediated neurochemical and functional connectivity changes in deep cortical regions in humans. *Nature Communications*, 14(1), 5318. <https://doi.org/10.1038/s41467-023-40998-0>
- Yeterian, E. H., Pandya, D. N., Tomaiuolo, F., & Petrides, M. (2012). The cortical connectivity of the prefrontal cortex in the monkey brain. *Cortex*, 48(1), 58–81. <https://doi.org/10.1016/j.cortex.2011.03.004>
- Zalla, T., & Sperduti, M. (2013). The amygdala and the relevance detection theory of autism: An evolutionary perspective. In *Frontiers in Human Neuroscience* (Vol. 7, Issue DEC). Frontiers Media S. A. <https://doi.org/10.3389/fnhum.2013.00894>
- Zangemeister, L., Grabenhorst, F., & Schultz, W. (2016). Neural Basis for Economic Saving Strategies in Human Amygdala-Prefrontal Reward Circuits. *Current Biology*, 26(22), 3004–3013. <https://doi.org/10.1016/j.cub.2016.09.016>
- Zangemeister, L., Grabenhorst, F., & Schultz, W. (2020). Neural activity in human ventromedial prefrontal cortex reflecting the intention to save reward. *Social Cognitive and Affective Neuroscience*, 14(12), 1255–1261. <https://doi.org/10.1093/scan/nsaa013>
- Zhang, W., Schneider, D. M., Belova, M. A., Morrison, S. E., Paton, J. J., & Salzman, C. D. (2013). Functional circuits and anatomical distribution of response properties in the primate amygdala. *Journal of Neuroscience*, 33(2), 722–733. <https://doi.org/10.1523/JNEUROSCI.2970-12.2013>
- Zhang, X., Cheng, H., Zuo, Z., Zhou, K., Cong, F., Wang, B., Zhuo, Y., Chen, L., Xue, R., & Fan, Y. (2018). Individualized functional parcellation of the human amygdala using a semi-supervised clustering method: A 7T resting state fMRI study. *Frontiers in Neuroscience*, 12(APR), 1–17. <https://doi.org/10.3389/fnins.2018.00270>

APPENDIX

SUPPLEMENTARY METHODS

1. WHOLE BRAIN AMG PARCELLATION AND CONNECTIVITY USING A RS-FMRI DATA DRIVEN PARCELLATION

Subjects

Fifty-five healthy human subjects participated in the rsfMRI experiment. The study was carried out in accordance with the recommendations of the Code de la Santé Publique and was approved by the “Agence Nationale de Sécurité des médicaments et des produits de santé (ANSM)” and the “Comité de Protection des Personnes (CPP) Sud-Est III” (N° EudraCT: 2015-A00897-42 and 2018A00405-50). It also received a Clinical Trial Number (NCT03119909 and NCT03483233, see <https://clinicaltrials.gov>). All subjects gave written informed consent.

fMRI data acquisition and preprocessing

Scanning was performed on a 3T Siemens Magnetom Prisma MRI Scanner (Siemens Healthcare, Erlangen, Germany). During rs-fMRI acquisition, subjects were instructed to maintain ocular fixation on a white cross presented on the center of the black screen for 10 minutes. We used a T2* weighted multiband and multi-echo (ME) sequence with the following parameters: TR = 1500ms, TE1=16.4ms, TE2=37.59 ms, TE3=58.78 ms, FOV = 704 × 672 mm, voxel size = 2.5 mm isotropic and 51 slices. We obtained a total of 400 volumes per subject. Functional imaging acquisition was preceded by a T1-weighted high-resolution anatomical scan with a MPRAGE sequence (TR = 3000ms, TE=2.93ms, Flip angle 8°, FOV = 280 × 320 mm, voxel size = 0.8 mm isotropic). All the scans were performed before this work after a decision task based on fMRI protocol.

Preprocessing steps were realized using MATLAB toolbox SPM12 (<https://www.fil.ion.ucl.ac.uk/spm/doc/intro/>), AFNI software (Analysis of Functional NeuroImages; Cox, 1996) and FSL software (FMRIB Software Library; Jenkinson et al., 2012; Smith et al., 2004; Woolrich et al., 2009). The first 5 volumes of each run were removed to allow for T1 equilibrium effects. Slice timing correction for multiband sequences was then applied using AFNI pipeline. TEDANA package (<https://tedana.readthedocs.io/en/latest/>; DuPre et al., 2021; Kundu et al., 2012, 2013) was used to preprocess the multi-echo fMRI sequence. TEDANA pipeline works by

taking together the time series from all the collected TEs to combine them. The combined data is decomposed via, first, a principal component analysis (PCA) and second, an independent component analysis (ICA). Resulting components are then analyzed to determine whether they are TE-dependent or TE-independent. TE-dependent components are classified as BOLD, while TE-independent components are classified as non-BOLD, and are discarded as part of data cleaning. Finally, fMRI images and anatomical images were spatially linearly registered into standard MNI space.

All subsequent rs-fMRI processing steps were realized with AFNI software. A temporal filtering was applied to extract the spontaneous slowly fluctuating brain activity (0.01–0.1Hz). Linear regression was used to remove nuisance variables (the six parameter estimates for head motion, the cerebrospinal fluid and white matter signals from the segmentation). Finally, a spatial smoothing with a 4-mm full-width half maximum (FWHM) Gaussian kernel was then applied to the output of the regression.

Data-driven clustering of the AMG

1. Selection of AMG seeds.

We masked out the whole AMG in individual subjects using the mask provided by Tyszka and Pauli (2016) (<https://identifiers.org/neurovault.image:24479>; Tyszka & Pauli, 2016). Visualization and drawing were performed with AFNI software.

2. Correlation matrix voxel-based.

Each resulting AMG mask was resampled from anatomical (voxel size = 0.8mm³) to functional dimensions (voxel size = 2.5mm³). We then extracted in each subject, for each voxel of the AMG mask, a 4d-matrix ($x \times y \times z \times t$) with the coordinates of each voxel (x, y, z) and the time-course (t) of the BOLD signal of each voxel. We then computed, in each subject, Pearson's correlation (r) between the time course of each voxel of the AMG mask and the time course of each voxel composing the grey matter of the whole left hemisphere. These r values were then transformed in z-score (Fisher, 1915). The output was, for each subject, n 3D-matrix with n the number of voxels in the AMG mask. Finally, each 3D-matrix was flattened to reach a n by m 2D-matrix representing z-scores between each voxel of the AMG mask (n rows) and each voxel of the rest of the grey matter of the left hemisphere (m columns). The resulting matrix is represented in **Figure S1**.

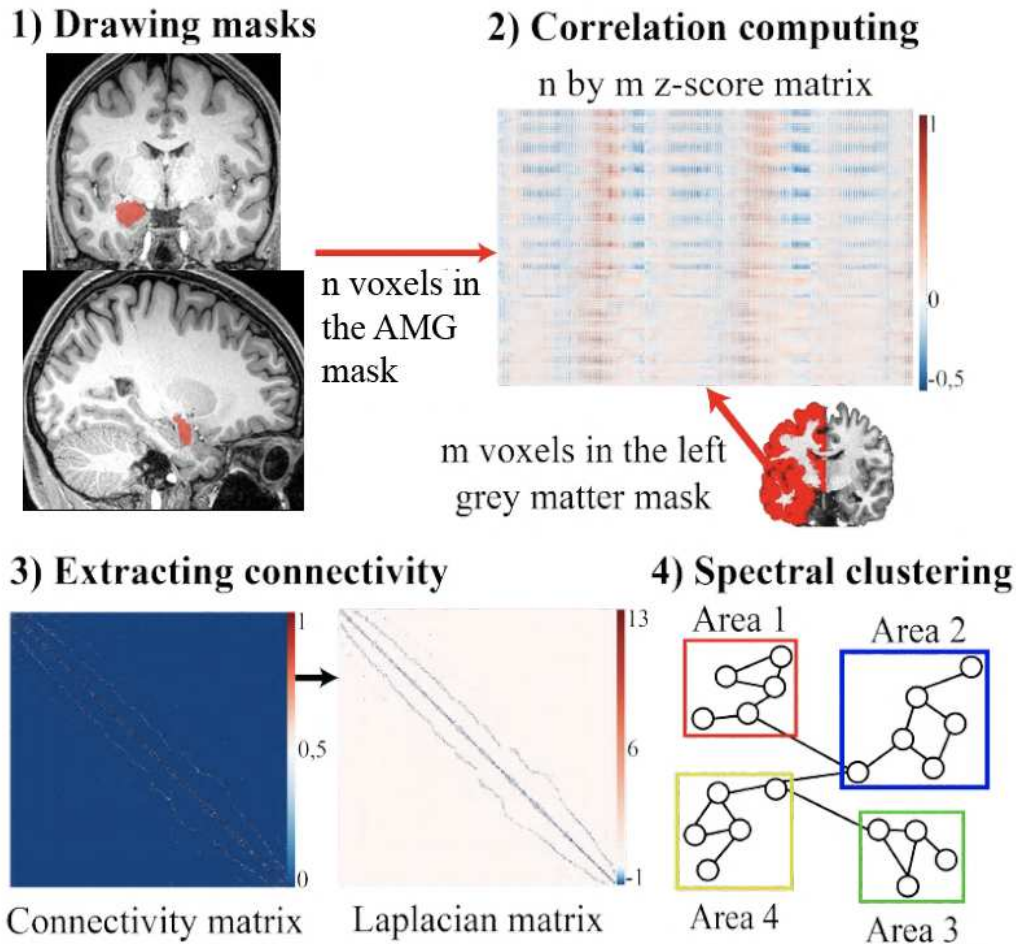


Figure S1. Connectivity-based brain parcellation steps: 1) generate AMG mask in a typical subject, 2) compute the z-scores between each voxel of the AMG mask and the voxels of the whole brain gray matter to obtain a 2D-matrix, 3) apply the k-neighbors algorithm to extract the connectivity between voxels and build the graph and then compute the Laplacian matrix. and 4) apply a spectral decomposition on this matrix and k-means algorithm to extract clusters.

3. Clustering method for parcellation

The main goal of this work was to identify subregions composing AMG, using a data driven approach based on their connectivity with the rest of the left brain. Based on previous work (Blumensath et al., 2013; Neubert et al., 2014), we applied a clustering algorithm to classify voxels depending on their z-scores profile with voxels composing the grey matter of the entire left hemisphere. Clustering algorithms aim at joining elements displaying the same features into the same group, elements with dissimilarities being included into other groups. Therefore, we expected that voxels of the AMG mask displaying similar connectivity profiles would be clustered together and would correspond to a particular AMG subregion associated to a particular whole-brain connectivity profile. We applied spectral clustering algorithms because it relies on

graph theory which is known to nicely reflect brain connectivity (Cheng et al., 2021). Then we computed the Laplacian matrix of the resulting graph. Finally, to extract particular features, eigenvalues and eigenvectors were computed from the Laplacian matrix, and a K-means algorithm was used to classify this decomposition (von Luxburg, 2007). Results were that nodes highly connected were grouped together and frontiers were chosen depending on the number of connections. All the clustering procedure was built with Python 3.8.10 and following libraries: scikit-learn (Pedregosa et al., 2011) for all the clustering part, pandas (McKinney, 2010) for the data management, numpy (Harris et al., 2020) for calculation and matrix building and operation, and nibabel (Brett et al., 2019) for NiFti file management.

4. *Identification of the best number of AMG subregions using a data-driven approach.*

We used Silhouette Index scores (Rousseeuw, 1987) to identify the optimal number of clusters composing our AMG mask across the 55 subjects. This score measures the ratio of the sum of between-clusters and within-cluster dispersions for all clusters (where dispersion is defined as the sum of distances squared) and is higher when clusters are dense and well separated.

Ipsilateral cortical connectivity of each AMG subregions

Whole brain regions: Glasser Atlas.

The last step of this analysis was to identify the connectivity profile between each AMG subregion resulting from the data-driven parcellation and the rest of the ipsilateral brain in individual subjects. In that goal, we used the independent multimodal Glasser's atlas (Glasser et al., 2016).

Connectivity extraction.

We computed the average time course of each AMG subregion extracted from the data-driven parcellation, and also the average time course of each region of the Glasser atlas. We then computed the z-score map for each one of these 4 AMG subregions with the 180 regions of the atlas in individual subjects. We finally averaged these maps across subjects.

2. TRANSCRANIAL ULTRASOUND STIMULATION APPROACH ON THE WHOLE AMG IN MACAQUES

Macaques rhesus

Five rhesus monkeys (*macaca mulatta*) were included in the study (1M and 4F, ages ranged between 11-22 years-old and weighed between 6-8.5kg). All procedures followed the guidelines of European Community on animal care (European Community Council, Directive No. 86–609, November 24, 1986) and were approved by French Animal Experimentation Ethics Committee #42 (CELYNE).

fMRI Data acquisition and experimental setup

Prior to anaesthesia, monkeys were injected with glycopyrrolate, an anticholinergic agent that decreases salivary secretion (Robinul; 0.06 mg/kg). Twenty minutes after, anaesthesia was induced with an intramuscular injection of tiletamine and zolazepam (Zoletil; 7 mg/kg). The animals were then intubated and ventilated with oxygen enriched air and 1% Isoflurane throughout the duration of the scan. An MRI-compatible stereotaxic frame (Kopf) was used to secure the head and reduce variability in the measure. Monkeys were placed in a sphinx position with their head facing the back of the scanner. Breathing volume and frequency were set based on the animal weight. During the scan, physiological parameters including heart rate and ventilation parameters (spO₂ and CO₂) were monitored. Body temperature was also measured and maintained using warm- air circulating blankets. The anaesthetized resting-state acquisitions were performed about 2h after anaesthesia induction (i.e. to exclude known confounds induced by Zoletil on functional connectivity) and at least 1h after first inhalation of isoflurane.

Scanning was performed on a 3T Siemens Magnetom Prisma MRI Scanner with 8 channels Rogue Research coils. fMRI experiments were divided in two sessions: a control (SHAM) and a TUS session. Note that the SHAM session was also used to position the fiducials markers on the animal head with the use of custom-made helmet to identify and precisely locate the TUS target with the neuronavigation system BRAINSIGHT. Structural image (MPRAGE, T1-weighted, 0.5 mm³ voxel size) and functional resting-state runs (T2*-weighted gradient echo planar, TR=1.7s, TE=30ms, 1.7mm³ voxel size, 25 slices). In the SHAM session 1 run was acquired and 2 runs in the TUS session, runs are composed of 2400 volumes (exception with 2000

volumes: monkey C for the SHAM session run and monkey L for the first run of the TUS session).

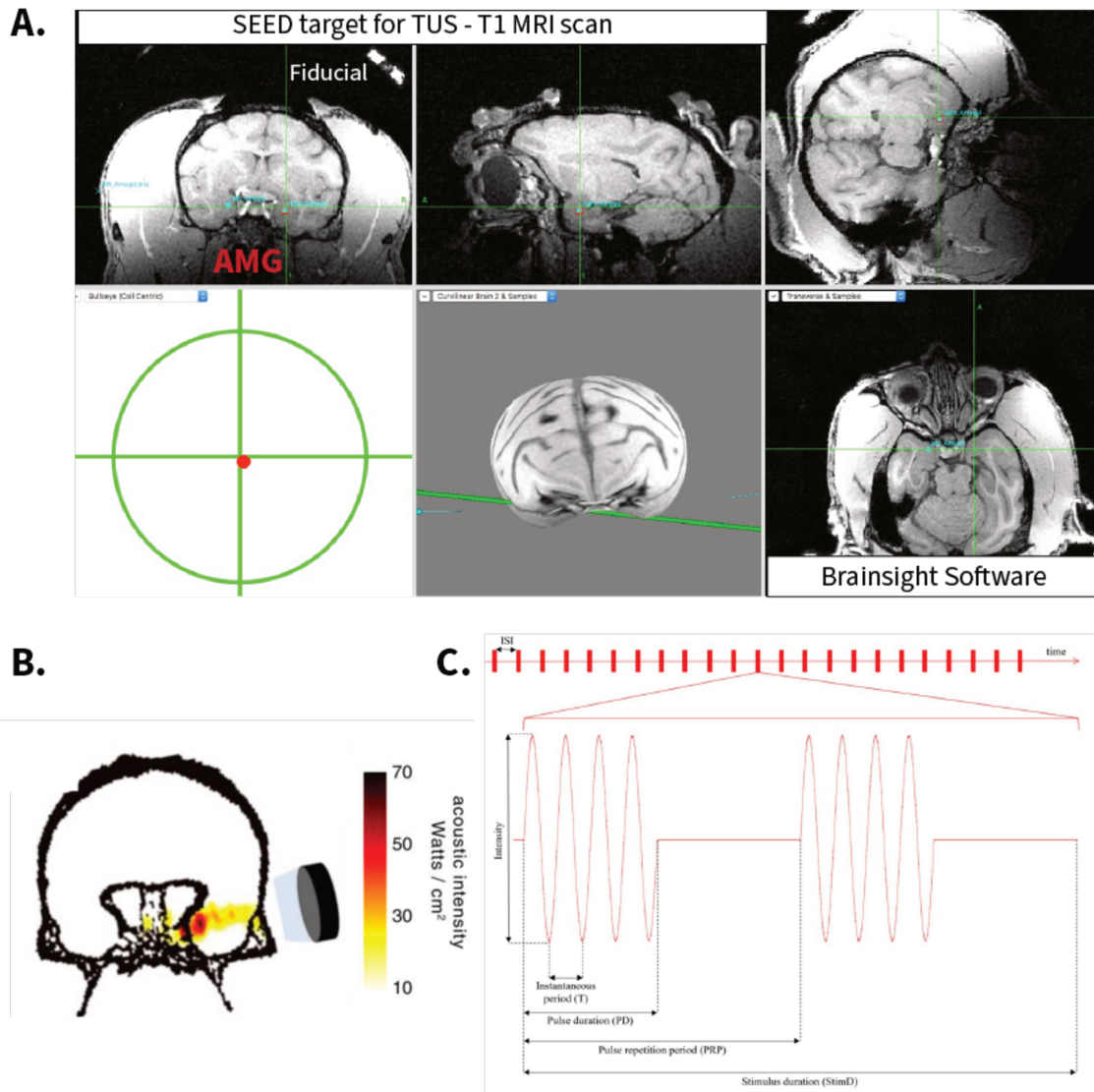
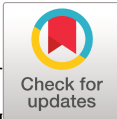


Figure S2. Transcranial ultrasound stimulation experimental setup. **A.** Brainsight Software interface during online target localization just before TUS perturbations. Target can be localized thanks to a previously acquired MPRAGE structural sequence with the presence of fiducial markers on monkeys heads. Before TUS, the fiducial markers are positioned back on the monkey head in the exact same position as during the structural scan. To precisely locate the targeted brain region the monkey head and TUS materials (transducer) are calibrated based on several positioned reference points in the space around the monkey (i.e., fiducial markers position and thus monkey brain position compared to the referential points). TUS occurs once the target position is secure. **B.** Extracted from *Folloni et al., 2019*. It represents a simulation of the acoustic intensity delivered through the skull. The highest acoustic intensity being located at the target point (AMG). **C.** Extracted from *Di Biase et al., 2019*. It is a schematic representation of a sonification with a pulse/repetition protocol and showed the different TUS metrics: intensity of stimulation, instantaneous period (T), pulse duration (PD), pulse repetition period (PRP), stimulus duration (StimD).

Transcranial ultrasound stimulation (TUS) of the AMG

Perturbation was guided by the prior identification of the target region and notably facilitated by the acquisition of a high-resolution structural scan during the SHAM session in which 4-6 fiducial markers were placed around the monkey's head (**Figure 1.A**). To ensure accurate positioning, BRAINSIGHT software (Rogue Research) was then used. Fiducial markers are positioned in the exact same position on the monkey head as during the structural. Both the monkey head and the transducer material are then calibrated based on precise reference points markers, recognized by the software, positioned in the space around the monkey. Once the head position and target region is secure TUS is then applied. In each TUS session, a 40-second train of pulsed ultrasound (250 kHz) consisting of 30-millisecond bursts of ultrasound every 100 milliseconds was directed towards the AMG using a single-element transducer alongside a region-specific coupling cone filled with degassed water (Folloni et al., 2019). To note, left and right AMG were sonicated one after the others. To control for any confounds resulting from concomitant ultrasound stimulation and neural signal recording, recordings of neural activity only began approximately 20-30 min after the end of TUS application.

PUBLICATIONS



NEUROSCIENCE

A revised perspective on the evolution of the lateral frontal cortex in primates

Céline Amiez^{1*†}, Jérôme Sallet^{1,2†}, Camille Giacometti¹, Charles Verstraete¹, Clémence Gandaux¹, Valentine Morel-Latour¹, Adrien Meguerditchian^{3,4,5}, Fadila Hadj-Bouziane⁶, Suliann Ben Hamed⁷, William D. Hopkins⁸, Emmanuel Procyk^{1†}, Charles R. E. Wilson^{1†}, Michael Petrides⁹

Detailed neuroscientific data from macaque monkeys have been essential in advancing understanding of human frontal cortex function, particularly for regions of frontal cortex without homologs in other model species. However, precise transfer of this knowledge for direct use in human applications requires an understanding of monkey to hominid homologies, particularly whether and how sulci and cytoarchitectonic regions in the frontal cortex of macaques relate to those in hominids. We combine sulcal pattern analysis with resting-state functional magnetic resonance imaging and cytoarchitectonic analysis to show that old-world monkey brains have the same principles of organization as hominid brains, with the notable exception of sulci in the frontopolar cortex. This essential comparative framework provides insights into primate brain evolution and a key tool to drive translation from invasive research in monkeys to human applications.

INTRODUCTION

The pattern and specific intersections of sulci in the cerebral cortex of the brain are reliable determinants of the anatomo-functional organization. For example, in the frontal cortex, the sulcal pattern indicates the positioning of different functional and cytoarchitectonic areas (1–10). Thus, the sulcus-determined functional anatomy is essential for interpreting neuroscientific data and for assessing clinical options in single individuals based on their specific sulcal anatomy (11). In many cases, interpreting group averaged functional activation data projected onto a template brain is blurred by the individual anatomical variations (2, 3). For example, we have shown that the presence or absence of a paracingulate sulcus on the medial wall in human subjects has an impact on the localization of functional foci in that region of the cortex (2).

Much of our detailed understanding of frontal cortical function comes from invasive studies carried out in macaque monkeys. Given the importance of sulcal anatomy, it becomes critical to determine whether and how the sulci in the frontal cortex of old-world primates (macaques and baboons) compare to those of hominids (great apes and humans), yet, to date, we lack understanding of this relationship (see fig. S1 for the position in the phylogenetic tree of the study species). Describing it will provide critical

information about the evolution of the anatomo-functional organization of the brain (12), but it is also essential if we are to use properly the plethora of neurophysiological, neuroanatomical, and neuropsychological data obtained in the past century in macaques to understand the human frontal cortex. We developed a methodology to examine morphological characteristics and variability of sulci across primates that has shed new light on the evolution of the anatomo-functional organization of the medial frontal cortex (12). In this comparative endeavor, the lateral portion of the prefrontal cortex has particular importance, given that its granular part is thought to be without homolog in nonprimate species (13–15). We therefore applied our methodology to provide clear identification of whether and how lateral frontal cortex from the central sulcus to the frontal pole varies across the primate order and to what extent direct cross-species homologies can be drawn. We show that old-world monkeys and hominids share key and previously unreported principles of frontal sulcal pattern organization.

The current view of the sulcal organization of primate lateral frontal cortex is that it is characterized by 13 sulci in the human brain (Fig. 1A) (16); that it is restricted to five large sulci in chimpanzees (Fig. 1B) (17, 18); and that, in old-world primates monkeys, it is defined by two major sulci (arcuate and principal sulcus) with up to four dimples located around these main sulci (Fig. 1, C and D) (19). By combining sulcal pattern analysis based on anatomical magnetic resonance imaging (MRI) (12) with resting-state functional MRI (rs-fMRI) and cytoarchitectonic analyses, we demonstrate that, despite apparent discrepancies, old-world monkeys share similar principles of organization to those of the chimpanzee and the human brains, with the exception of sulci associated with the rostral-most part of the frontopolar cortex that displays a similar organization only in great apes and humans. Thus, the sulci in the lateral frontal cortex of old-world monkeys can be directly understood in relation to those observed in the human frontal lobe, generating a revised framework to drive direct comparison of macaque monkey and human frontal cortical organization (Fig. 1D and Tables 1 and 2).

¹Univ Lyon, Université Lyon 1, Inserm, Stem Cell and Brain Research Institute U1208, 69500 Bron, France. ²Wellcome Integrative Neuroimaging Centre, Department of Experimental Psychology, University of Oxford, Oxford OX1 3SR, UK. ³Laboratoire de Psychologie Cognitive, UMR7290, Université Aix-Marseille, CNRS, 13331 Marseille, France. ⁴Station de Primatologie CNRS, UPS846, 13790 Rousset, France. ⁵Brain and Language Research Institute, Université Aix-Marseille, CNRS, 13604 Aix-en-Provence, France. ⁶Integrative Multisensory Perception Action and Cognition Team (ImpAct), INSERM U1028, CNRS UMR5292, Lyon Neuroscience Research Center (CRNL), Lyon, France; University of Lyon 1, Lyon, France. ⁷Institut des Sciences Cognitives Marc Jeannerod, UMR5229, CNRS-Université Claude Bernard Lyon I, Bron, France. ⁸Department of Comparative Medicine, University of Texas MD Anderson Cancer Center, Bastrop, TX, 78602, USA. ⁹Department of Neurology and Neurosurgery and Department of Psychology, Montreal Neurological Institute, McGill University, Montreal, QC, Canada.

*Corresponding author. Email: celine.amiez@inserm.fr

†These authors contributed equally to this work.

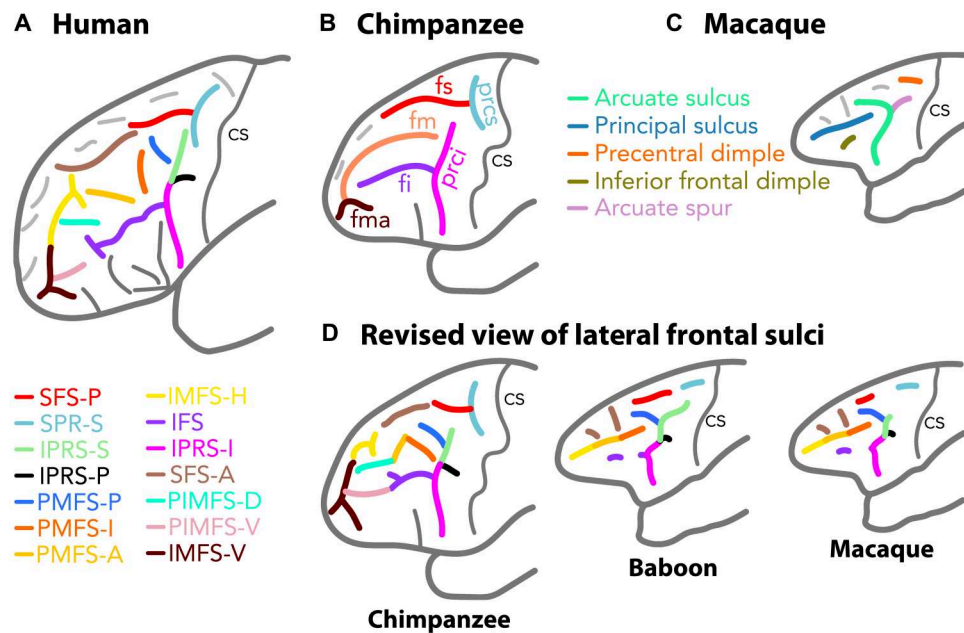


Fig. 1. Known and revised view of the sulcal organization in the lateral frontal cortex in human, chimpanzee, baboon, and macaque brains. Known sulcal organization in the lateral frontal cortex of humans (A), chimpanzees (B), and macaques (C). (D) Revised view of the human homologs of the frontal cortical sulcal organization in the chimpanzee and old-world monkey brains. The color coding of the sulci in (D) corresponds to the sulci identified in the human brain. All sulci observed in the lateral frontal lobe of the human brain have clear homologs in chimpanzees, and only the sulci in the most anterior part of the frontopolar cortex do not have their homologs in old-world monkeys. fs and fi, superior and inferior frontal sulcus; prcs and ipcs, superior and inferior precentral sulcus; fm, middle frontal sulcus; fma, frontomarginal sulcus; SFS-P and SFS-A, posterior and anterior superior frontal sulcus; IFS, inferior frontal sulcus; SPR-S, superior precentral sulcus; IPRS-S, IPRS-P, and IPRS-I, superior, posterior, and inferior segments of the inferior precentral sulcus; PMFS-P, PMFS-I, and PMFS-A, posterior, intermediate, and anterior posteromedial frontal sulcus; IMFS-H and IMFS-V, horizontal and vertical rami of the intermediate frontal sulcus; PIMFS-D and PIMFS-V, dorsal and ventral paraintermediate frontal sulcus; cs, central sulcus. The dark gray sulci represent sulci that are located in the ventrolateral prefrontal cortex and are excluded from this analysis. The light gray sulci represent sulci that have not been named yet.

RESULTS

Hominid correspondence of the arcuate sulcus in old-world monkeys

The present research reveals the complex morphology of the arcuate sulcus in old-world monkeys (Fig. 1A). We demonstrate that the field should stop considering the arcuate sulcus as a single linear sulcus as previously thought (Fig. 2A) (17, 18) but rather as a complex of sulcal elements that relate to specific sulci in hominid brains (Tables 1 and 2).

First, in old-world monkeys, below the genu of the arcuate sulcus—and the arcuate spur if present—we consistently observed the presence of an additional spur or dimple deep within this sulcal complex that had not been described previously (Fig. 2B; see typical examples and frequency of occurrence in fig. S2). The intersection between this spur/dimple and the arcuate sulcus was located at the level of the rostral limit of the optic chiasma in both macaques and baboons (see fig. S3 for description of anatomical landmarks). At this anatomical level, we identified the intersection between the superior segment of the inferior precentral sulcus (IPRS-S) and the posterior segment of the inferior precentral sulcus (IPRS-P) in chimpanzee and human brains. Furthermore, the caudal limit of the arcuate spur in old-world monkeys was observed at the level of the anterior commissure; however it is located at the caudal limit of the IPRS-S in chimpanzees and humans. Note that, in our sample, the arcuate spur was present either in the form of a spur or a dimple in 100 and 93.75% of hemispheres in baboon

and macaque brains, respectively (fig. S4). The variability across studies in the frequency of occurrence of the arcuate spur in the macaque brain (20) is likely to be driven by the criteria used to define the presence or not of this arcuate spur, i.e., the inclusion or not of an arcuate spur with a dimple morphology. In our sample, we observe that, in macaques, the arcuate spur is observed as a spur, a dimple, or absent in 50, 44, and 6% of hemispheres, respectively (fig. S4C). Together, these data converge toward homologies between (i) the spur/dimple observed below the genu of the arcuate sulcus in old-world monkeys and the IPRS-P in chimpanzees and humans and (ii) the part of the arcuate sulcus extending from the caudal-most part of the arcuate spur to the IPRS-S/IPRS-P intersection in old-world monkeys and IPRS-S in chimpanzees and humans. The frequency of occurrence of IPRS-S and IPRS-P was identical across the four species examined {IPRS-S presence: $F = 0.803$, numerator degree of freedom (NumDF) = 3, denominator degree of freedom (DenDF) = 226.06, $P < 0.4931$ [nonsignificant (ns)]; IPRS-P presence: $F = 2.44$, NumDF = 3, DenDF = 386.38, $P < 0.06$ (ns), generalized linear mixed-effects model (GLMM) with species as fixed effect and subject ID as random effect; Fig. 2B}.

Second, the junction between IPRS-S in old-world monkeys and the part of the arcuate sulcus running dorsally and rostrally in the frontal cortex was tightly linked with the rostral part of the optic chiasma. Its rostral-most part was observed at the level of the middle part of the genu of the corpus callosum. In the human and chimpanzee brains, these two landmarks did correspond to

Table 1. Old world-monkeys: Correspondence between sulci defined with the traditional versus the revised nomenclature used here based on homologies with sulcal organization in the human brain.

Old nomenclature	Human-based nomenclature	
Precentral dimple	SPR-S	Superior precentral sulcus
Arcuate sulcus and spur	PMFS-P	Posterior segment of the posterior middle frontal sulcus
	IPRS-S	Superior segment of the inferior precentral sulcus
	IPRS-P	Posterior segment of the inferior precentral sulcus
Principal sulcus	IPRS-I	Inferior segment of the inferior precentral sulcus
	PMFS-I	Intermediate segment of the posterior middle frontal sulcus
	PMFS-A	Anterior segment of the posterior middle frontal sulcus
Inferior frontal dimple	IMFS-H	Horizontal ramus of the intermediate frontal sulcus
	IFS	Inferior frontal sulcus

Table 2. Chimpanzees: Correspondence between sulci defined with the traditional versus the revised nomenclature used here based on homologies with sulcal organization in the human brain.

Old nomenclature	Human-based nomenclature	
Superior precentral sulcus (prcs)	SPR-S	Superior precentral sulcus
Inferior precentral sulcus (prci)	IPRS-S	Superior segment of the inferior precentral sulcus
	IPRS-P	Posterior segment of the inferior precentral sulcus
	IPRS-I	Inferior segment of the inferior precentral sulcus
Superior frontal sulcus (fs)	SFS-A	Anterior superior frontal sulcus
	SFS-P	Posterior superior frontal sulcus
Inferior frontal sulcus (fi)	IFS	Inferior frontal sulcus
Middle frontal sulcus (fm)	PMFS-P	Posterior segment of the posterior middle frontal sulcus
	PMFS-I	Intermediate segment of the posterior middle frontal sulcus
	PMFS-A	Anterior posteromedial frontal sulcus
	IMFS-H	Horizontal ramus of the intermediate frontal sulcus
Frontomarginal sulcus (fma)	IMFS-V	Vertical ramus of the intermediate frontal sulcus

the caudal and rostral limit of the posterior posteromedial frontal sulcus (PMFS-P), respectively. The PMFS-P is present in 100% of

hemispheres in all species (Fig. 2C). It corresponds in chimpanzees to the caudal-most part of middle frontal sulcus (fm; Fig. 1B), but we observed that this sulcus most often splits into several segments, rather than being a continuous unique sulcus as previously described (17, 18). Critically, we observed a gradient regarding the morphological pattern of the PMFS-P/IPRS-S junction: Whereas PMFS-P is detached from the IPRS-S in 54% of hemispheres in humans, it is detached in 34% of hemispheres in chimpanzees and in 3% in baboons, and it is never detached in macaques ($F = 76.84$, NumDF = 3, DenDF = 352.03, $P < 2.2 \times 10^{-16}$, GLMM; Fig. 2C and fig. S5). Our data thus strongly point toward homologies between the human PMFS-P, the caudal-most part of the chimpanzee fm, and the dorsal part of the arcuate sulcus in old-world monkeys (Fig. 1D). The arcuate spur, when present, is formed when PMFS-P joins IPRS-S anterior to IPRS-S's caudal extremity. As such, together with evidence regarding the anatomical location of the caudal and rostral borders of IPRS-S, the arcuate spur appears to belong to IPRS-S and is not an additional sulcus (Fig. 2 and figs. S4 and S5).

Last, the ventral branch of the arcuate sulcus running below the IPRS-S/IPRS-P junction presents a dimple pointing rostrally in the frontal cortex in 27 and 13% of baboon and macaque hemispheres, respectively (Fig. 2D). The intersection between the ventral branch of the arcuate sulcus and this rostrally pointing dimple can be understood as the homolog of the junction between inferior segment of the inferior precentral sulcus (IPRS-I) and inferior frontal sulcus (IFS) in human and chimpanzee brains. First, both the ventral branch of the arcuate sulcus in old-world monkeys, the inferior part of prci in chimpanzees, and IPRS-I in humans occur in 100% of hemispheres (Fig. 2D and fig. S7). In addition, the intersection between IPRS-I/prci and IFS/fi in humans/chimpanzees is located at the level of the caudal part of the genu of the corpus callosum, exactly where the intersection between the ventral arcuate sulcus and the spur/dimple emerging rostrally is observed in old-world monkeys (Figs. 1 and 2D). This spur/dimple therefore corresponds to the precursor of the caudal part of the IFS. Topographically, in front of the ventral branch of the arcuate sulcus, only the inferior frontal dimple is observed (in 99% of baboon hemispheres and 74% of macaque hemispheres; Figs. 1A and 2D and fig. S7), and the assessment of its location revealed a tight relationship with the rostral part of the genu of the corpus callosum. However, in human and chimpanzee brains, the IFS always rostrally ends in a fork (Fig. 2D and fig. S7), which is also observed at the level of the rostral part of the genu of the corpus callosum. As such, one may hypothesize that the inferior frontal dimple is the homolog of the rostral-most part of the IFS in human and chimpanzee brains. This hypothesis finds support in our results showing that the IPRS-I/IFS pattern displays a gradient from the last common ancestor of humans and old-world monkeys to the last common ancestor of humans and apes, i.e., an IFS displaying a consistent rostral limit and rarely joining IPRS-I in old-world monkeys and a continuous sulcus displaying consistently a rostral sulcal fork and most often joining IPRS-I in hominids ($F = 194.09$, NumDF = 3, DenDF = 451.9, $P < 2.2 \times 10^{-16}$, GLMM; Fig. 2D). The present hypothesis is also supported by the known cytoarchitectonic organization of the region in both macaques and humans: Specifically, both the IFS and the inferior frontal dimple are the limits of area 45 (below) and area 9/46 (above) (fig. S6) (21, 22).

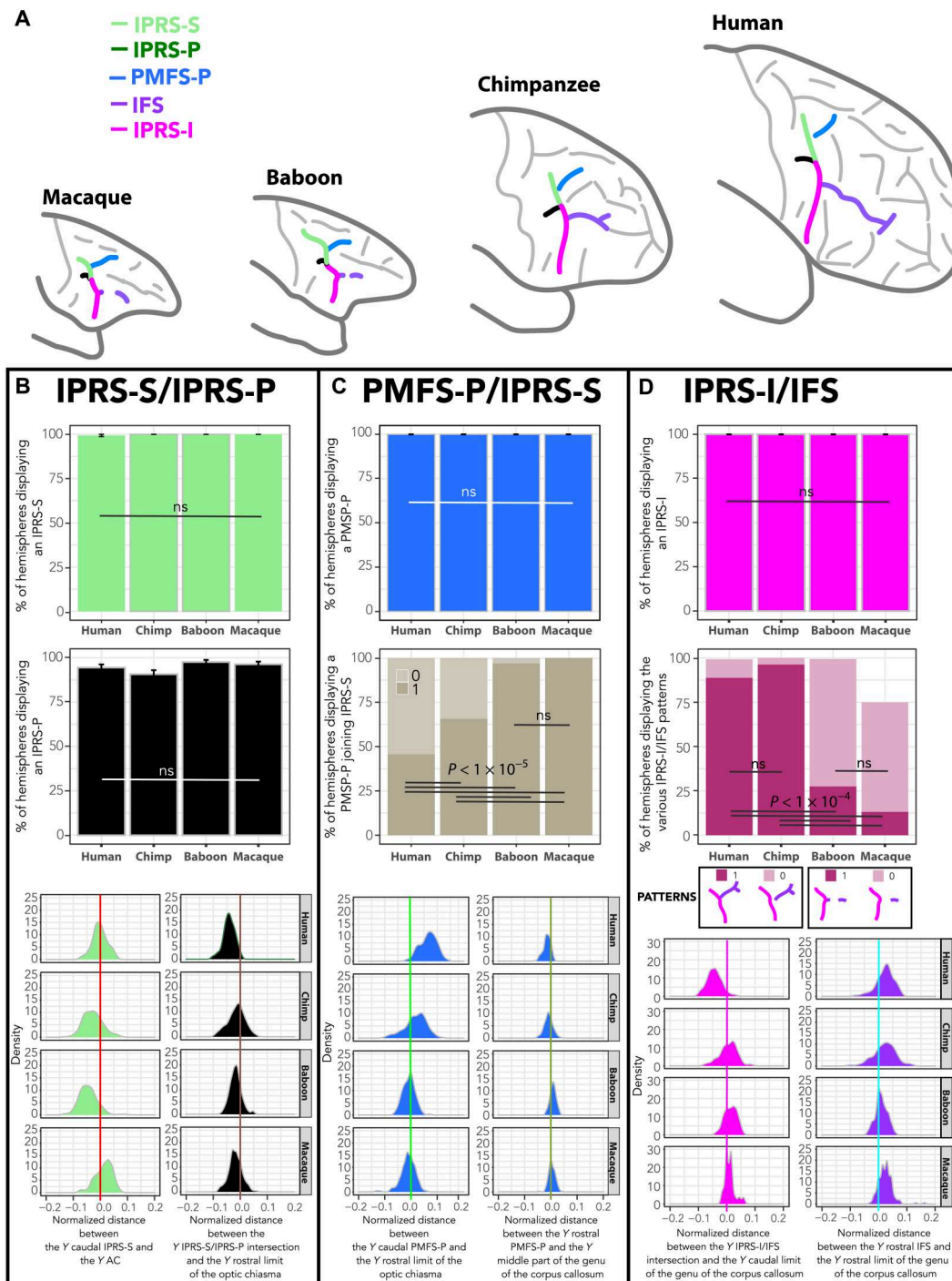


Fig. 2. Hominid sulcal correspondence to the arcuate sulcus in old-world monkeys. (A) Identification and location of the sulci forming the arcuate sulcus in old-world monkeys and their homologs in hominids. (B) Frequency of occurrence of IPRS-S and IPRS-P in brain hemispheres in all primates (top panels) and normalized distance between the anteroposterior (i) Y level of the caudal-most part of IPRS-S and Y level of the anterior commissure (AC) (light green) and (ii) Y level of the intersection between the caudal-most part of PMFS-P and Y level of the rostral limit of the optic chiasma (dark green) (bottom panel). (C) Frequency of occurrence of PMFS-P (top panel) and of hemispheres displaying a PMFS-P joining IPRS-S (middle panel) in all primates, as well as normalized distance between (i) the Y level of the caudal-most part of PMFS-P and the Y level of the rostral limit of the optic chiasma (blue) and (ii) Y level of the rostral-most part of PMFS-P and the Y level of the middle part of the genu of the corpus callosum (bottom panel). (D) Frequency of occurrence of IPRS-I and the various IPRS-I/IFS patterns in brain hemispheres in all primates (top panels) and normalized distance between the (i) Y level of the IPRS-I/IFS intersection and the Y level of the caudal part of the genu of the corpus callosum (pink) and (ii) Y level of the intersection between the rostral-most part of IFS and the Y level of the rostral limit of the genu of the corpus callosum (purple) (bottom panel). ns, nonsignificant. GLMM and/or Tukey post hoc tests at $P < 0.05$ (see Materials and Methods).

To sum up, our results suggest that the arcuate sulcus in old-world monkeys is composed of four segments: (i) PMFS-P, the dorsal part of the arcuate sulcus that detaches progressively in the primate phylogenetic tree; (ii) IPRS-P, the newly defined little spur/dimple below the genu of the arcuate sulcus; (iii) IPRS-S, which extends from the intersection between IPRS-P and the arcuate sulcus and the caudal end of the arcuate spur; and (iv) IPRS-I, i.e., the part of the inferior arcuate sulcus located ventral to the intersection between IPRS-P and IPRS-S.

Hominid correspondence of the supraprincipal dimples in old-world monkeys

Previous atlases had reported the existence of up to four dimples dorsal to the arcuate and principal sulci, but their relationship to human sulci had never been formally addressed before. First, we identified correspondence between the superior precentral sulcus (SPR-S) in human (SPR-S; Fig. 1A) and chimpanzee brains (prcs; Fig. 3B) and the caudal precentral dimple in the dorsal part of the frontal lobe in macaques and baboons (Fig. 3C). Topographically, this is the first dimple in front of the central sulcus and is considered to be the border between the primary hand motor cortical region and the dorsal premotor cortex (23–25). The sulcus with similar properties is prcs in chimpanzees and SPR-S in humans (Fig. 3A). In all species, the frequency of occurrence of this sulcus/dimple is highly preserved ($F = 1.23$, NumDF = 3, DenDF = 532.64, $P < 0.3$, GLMM; Fig. 3, A and B). Second, in the four species examined, the caudal-most part of SPR-S is located at the level of the rostral limit of the mammillary bodies, and the rostral-most limit of posterior superior frontal sulcus (SFS-P) is located at the level of the caudal limit of the rostrum of the corpus callosum (Fig. 3F). Here, we identified a gradient regarding SPR-S orientation from the last common ancestor of humans and old-world monkeys to the last common ancestor of humans and apes. In hominids, it always displays a vertical orientation compared to SFS (i.e., running parallel to the dorsal part of the central sulcus), and, in old-world monkeys, it can also present such an orientation, although more rarely ($F = 50.46$, NumDF = 3, DenDF = 512.78, $P < 2.2 \times 10^{-16}$, GLMM; Fig. 3D). Note that, as previously demonstrated with regard to the medial prefrontal cortex (12), the presence of gradients of sulcal organization in the four species studied is a marker of homologies.

In human and chimpanzee brains, SPR-S joins the superior frontal sulcus in 99% of hemispheres (SFS-P in human and fs in chimpanzee; Fig. 3, B and C). Topographically, in old-world monkeys, there is a dimple located just anterior to the precentral dimple (26) that is likely to correspond to the human SFS-P. First, its frequency of occurrence displays a gradient in the primate order ($F = 101.18$, NumDF = 3, DenDF = 506.08, $P < 2.2 \times 10^{-16}$, GLMM; Fig. 3C). Second, when assessing the configuration of this dimple, it appears to join the precentral dimple in old-world monkeys, more frequently in baboons (in 19% of hemispheres) than in macaques (in 4% of hemispheres), strongly indicative of a correspondence with SFS-P (Fig. 3E).

Furthermore, in old-world monkeys, two additional dimples are systematically observed dorsal to the principal sulcus and rostral to PMFS-P. The assessment of their location reveals that the caudal and rostral dimples are respectively located at the level of the rostral limit of the genu of the corpus callosum and of the supra-rostral (SUROS)/sus-orbitalis (SOS) junction located at the rostral-most part of the cingulate sulcus (CGS) (fig. S3). In

human brains, the caudal and rostral limits of anterior superior frontal sulcus (SFS-A) are also found at the same locations, respectively (fig. S8). In chimpanzees, the segmented fs suggests that it corresponds to SFS-P and SFS-A. In support of this hypothesis, we observed that the caudal and rostral limits of SFS-A in chimpanzees are located at the same anatomical levels as in human brains. Together, these data strongly suggest that the old-world monkey homolog of SFS-A is the two dimples described in this study and that the chimpanzee homolog of SFS-A is the anterior part of the sulcus previously referred to as fs (Fig. 1B).

Hominid correspondence of the principal sulcus in old-world monkeys

A major finding of the present study is that the principal sulcus of macaques and baboons and the fm in chimpanzees are not linear single sulci as previously considered. They are instead composed of distinct segments corresponding to known sulci in the human brain (Tables 1 and 2 and Fig. 4). Morphological features of nonlinearity are most notable within the depth of the sulcus but are sometimes apparent on the cortical surface (see examples in fig. S9). Three joining sulcal segments could be identified in old-world monkeys. Those segments are not contiguous in >20% of hemispheres in chimpanzees and in >50% of hemispheres in humans (Fig. 4, E and F). The extents of the caudal-most segment and of the rostral-most segment were located at the level of the caudal and rostral limits of the genu of the corpus callosum and at the level of the junction between the CGS and SUROS/SOS junction, respectively. At these anatomical levels, we identified the caudal-most parts of intermediate posteromedial frontal sulcus (PMFS-I), anterior posteromedial frontal sulcus (PMFS-A), and horizontal ramus of the intermediate frontal sulcus (IMFS-H) in humans and in chimpanzees (Fig. 4G). Furthermore, the frequency of occurrence of the three sulci is highly preserved across species (Fig. 4, B to D).

The existence of subdivisions along the principal sulcus is further supported by cytoarchitectonic differences of cortex of the dorsal bank of the principal sulcus in macaques. Changes at the interface between layer II and III could be observed along the rostro-caudal axis (fig. S10). Examination of connectivity with retrograde tracers also revealed heterogeneity of connections along the rostro-caudal axis (27, 28). The scarcity of functional evidence to provide further support for this view is mainly due to the focus of most electrophysiological investigations on the caudal half of the principal sulcus (fig. S11). Nevertheless, functional heterogeneity has been reported in the rare studies that have specifically addressed this question (29–31). Beyond the heterogeneity of area 46 in macaques, the existence of additional subdivisions along the principal sulcus is supported by awake rs-fMRI analysis in macaque monkeys (see Materials and Methods). Data-driven connectivity-based parcellation (see Materials and Methods) indicated that the optimal number of parcels is 3 (Fig. 4H). The borders of the parcels in both hemispheres did also correspond to the position of the morphological nonlinearity in the sulcus, corresponding to the junction between PMFS-I and PMFS-A and to the junction between PMFS-A and IMFS-H (Fig. 4I). Petrides and Pandya (21) have shown that three cytoarchitectonic areas lie along the caudo-rostral axis of the principal sulcus: area 9/46, area 46, and area 10. In human brains, respective homolog areas lie in PMFS-I, PMFS-A, and IMFS-H, the rostral-most part of this sulcus being located in area 10 (fig. S6),

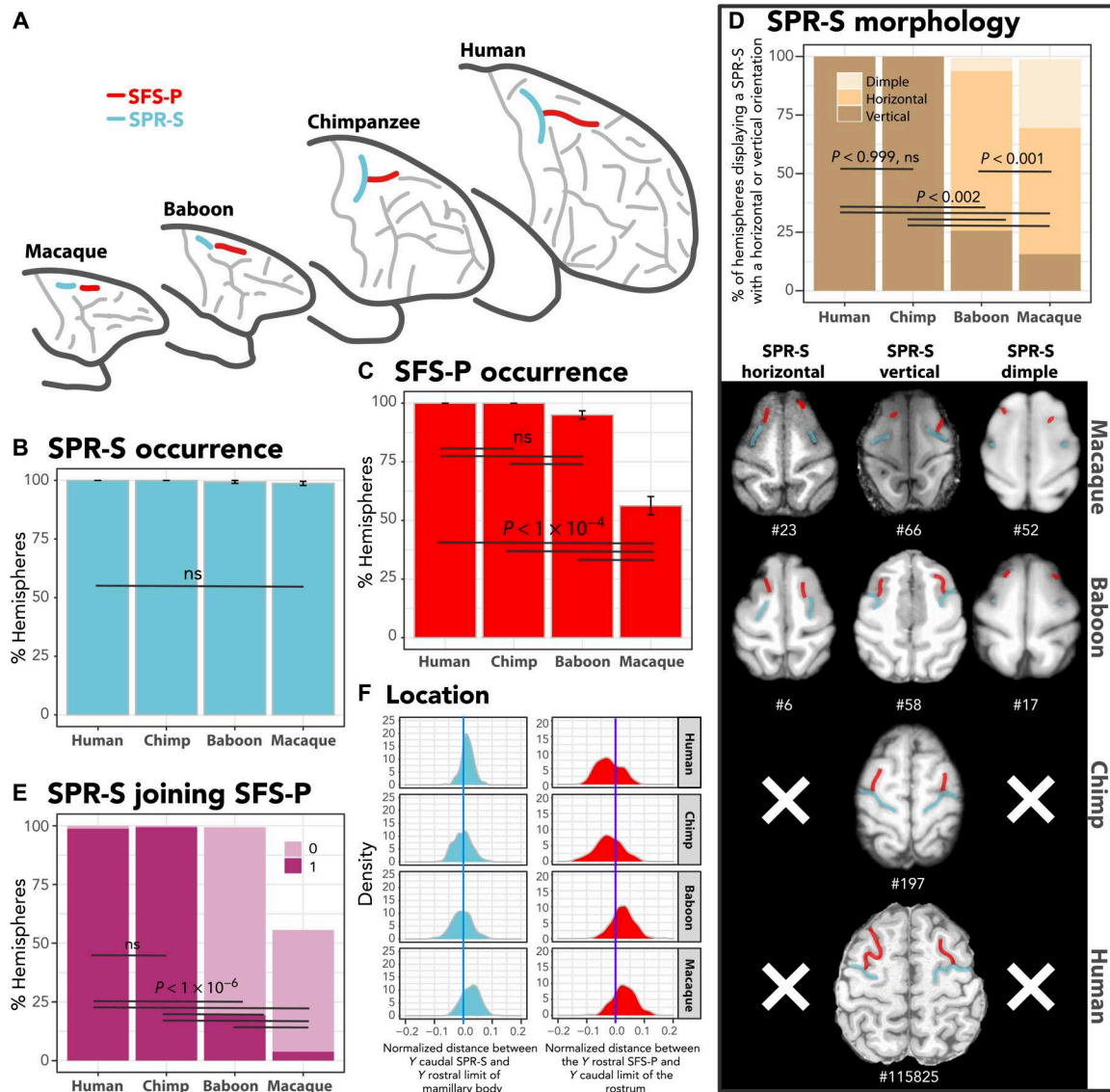


Fig. 3. Hominid correspondence to the precentral dimples in old-world monkeys. (A) Identification and location of the sulci forming the precentral dimples in old-world monkeys and their homologs in hominids. Frequency of occurrence of SPR-S (B) and SFS-P (C), and (D) of the various orientations of SPR-S (vertically or horizontally oriented to SFS-P or nonoriented dimple) in all primates. Whereas SPR-S is equally present in all species, SFS-P displays a decreased frequency of occurrence in macaques. The hominid-specific SPR-S vertical orientation can be observed in a few hemispheres in old-world monkeys. (E) Percentage of hemispheres in which SPR-S joins SFS-P. Whereas the SPR-S joins SFS-P in most of the hemispheres in hominids, it is rarely the case in old-world monkeys ($F = 528.9$, NumDF = 3, DenDF = 502.38, $P < 2.2 \times 10^{-16}$, GLMM). (F) Normalized distance between the (i) Y level of the caudal-most part of SPR-S and the Y level of the rostral limit of the mamillary bodies (blue) and (ii) Y level of the rostral-most part of SFS-P and the Y level of the caudal limit of the rostrum (red). GLMM and/or Tukey post hoc tests at $P < 0.05$ (see Materials and Methods).

reflecting the expansion of this area in apes and humans compared to old-world monkeys.

Alternative interpretations of the identity of the rostral-most segment of the principal sulcus are unlikely. First, IMFS-H is the only sulcus in the rostral part of the frontal cortex and spatially close enough to PMFS-A, which is highly preserved in chimpanzees. Second, dorsal paraintermediate frontal sulcus (PIMFS-D) and ventral paraintermediate frontal sulcus (PIMFS-V) display a drop in frequency of occurrence compared to humans (Fig. 5, A to C). Third, vertical ramus of the intermediate frontal sulcus (IMFS-V) is also present in chimpanzee and human brains

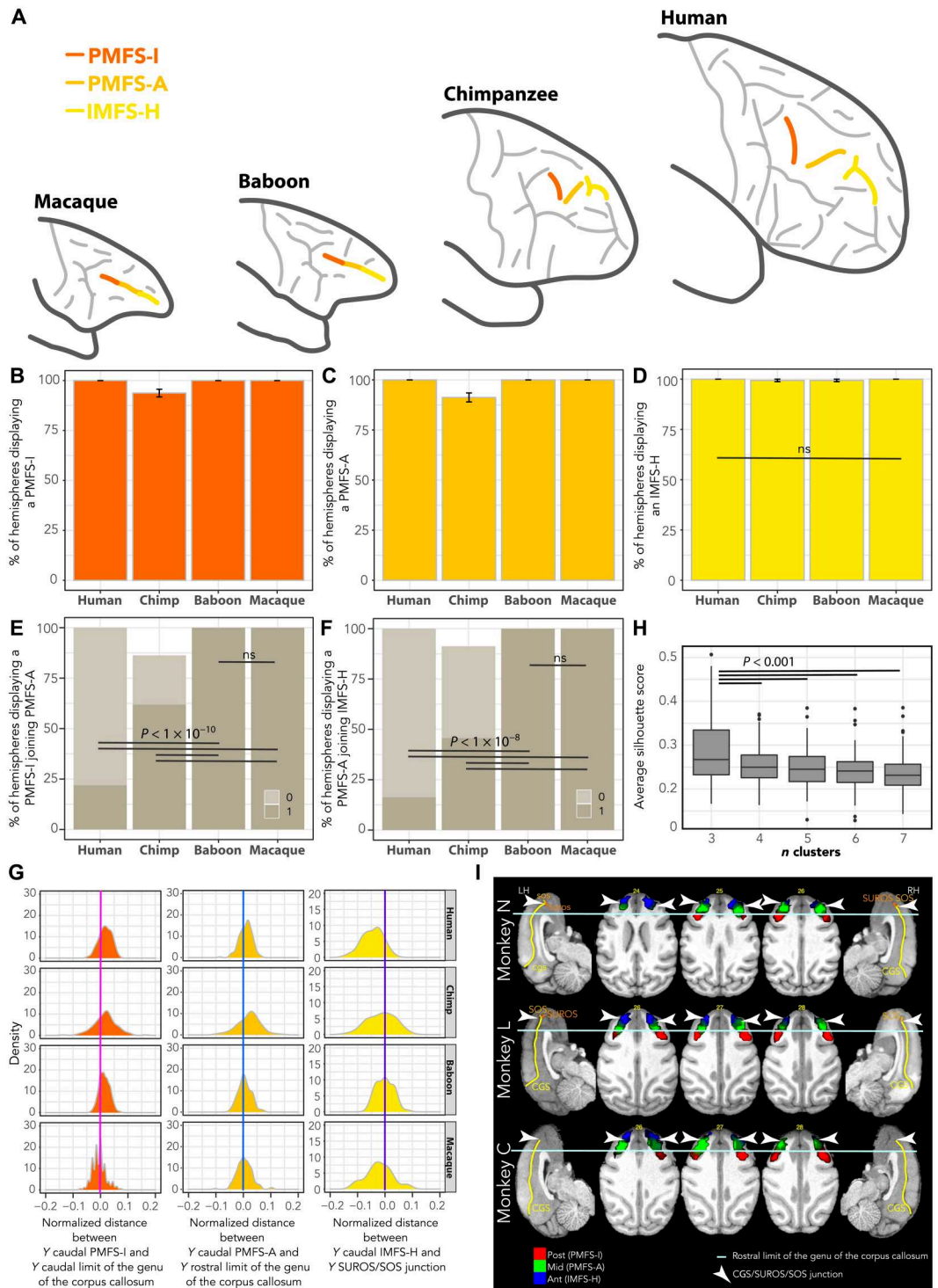
(Fig. 5D) but never joins PMFS-A in these two species. Rather, only PIMFS-D joins either IMFS-H (in human; Fig. 5E) or IMFS-V (in chimpanzee, Fig. 5F). Last, correspondence with the inferior and superior frontal sulci was excluded as candidates for the principal sulcus.

DISCUSSION

By combining sulcal pattern analysis with cytoarchitectonic analysis and rs-fMRI, the present study provides updated insights into the evolution of the frontal lobe across primates. Despite apparent

Fig. 4. Hominid correspondence to the principal sulcus in old-world monkeys.

(A) Identification and location of the sulci forming the principal sulcus in old-world monkeys and their homologs in hominids. Frequency of occurrence of PMFS-I (B), PMFS-A (C), and IMFS-H (D). (E) Percentage of hemispheres in which PMFS-I joins PMFS-A. (F) Percentage of hemispheres in which PMFS-A joins IMFS-H. (G) Normalized distance between the (i) Y level of the caudal-most part of PMFS-I and the Y level of the rostral limit of the genu of the corpus callosum (dark orange), (ii) Y level of the caudal-most part of PMFS-A and the Y level of the rostral limit of the genu of the corpus callosum (light orange), and (iii) Y level of the caudal-most part of IMFS-H and the Y level of the intersection between the CGS, SUROS, and SOS (yellow). (H) Average silhouette score across the two hemispheres of the three macaques performing 12 rs-fMRI runs (see Materials and Methods). The best number of clusters is 3. (I) Probability maps of these three clusters (Post, Mid, and Ant) across 12 runs for each macaque (N, L, and C). The borders of the three functional clusters correspond to anatomical landmarks, strongly suggesting that the posterior (post), middle (mid), and anterior (ant) clusters correspond to, respectively, PMFS-I, PMFS-A, and IMFS-H. GLMM and/or Tukey post hoc tests at $P < 0.05$ (see Materials and Methods). LH, left hemisphere; RH, right hemisphere.



discrepancies in the number of sulci, the lateral frontal lobe has a comparable organization across the primate order, complementing similar conclusions reached about the medial frontal cortex (12, 32, 33). Regardless of the phylogenetic distance between primate species (34), we observed an apparent relationship between brain size, gyrification, and similarity to human sulcal organization (Tables 1 and 2 and Fig. 1D). Only three sulci appeared in hominids reflecting the

expansion of the rostral prefrontal cortex (areas 10, 46, and 9): IMFS-V, PIMFS-D, and PIMFS-V. In all the frontal regions assessed in the present report, none appeared unique to the human brain. Despite suggestions that the lateral frontopolar cortex is uniquely human (32, 35, 36), the detailed analysis of sulcal morphology provides clear evidence for a common evolutionary history in

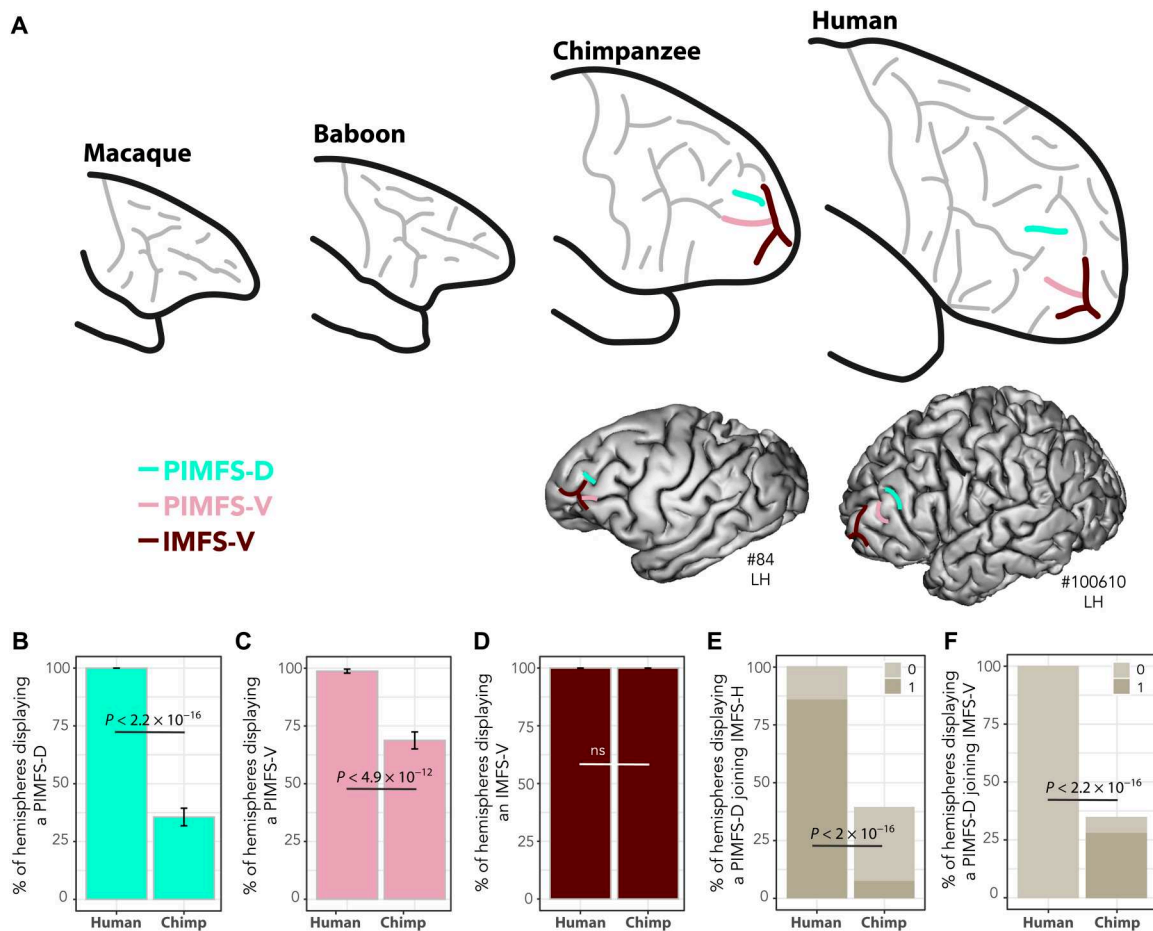


Fig. 5. Hominid-specific sulci. (A) Human correspondence of PIMFS-D, PIMFS-V, and IMFS-V in chimpanzees. (B) Frequency of occurrence of PIMFS-D is decreased in chimpanzees ($F = 225.85$, NumDF = 1, DenDF = 158, $P < 2.2 \times 10^{-16}$). (C) Frequency of occurrence of PIMFS-V is decreased in chimpanzees ($F = 55.9$, NumDF = 1, DenDF = 158, $P < 4.9 \times 10^{-12}$, GLMM). (D) Frequency of occurrence of IMFS-V is equal in humans and chimpanzees (ns at $P < 0.05$, GLMM). (E) PIMFS-D joins more frequently IMFS-H in humans than in chimpanzees ($F = 138.46$, NumDF = 1, DenDF = 141.72, $P < 2.2 \times 10^{-16}$, GLMM). (F) PIMFS-D joins more frequently IMFS-V in chimpanzees and never in humans ($F = 38.75$, NumDF = 1, DenDF = 214, $P < 2.51 \times 10^{-9}$, GLMM). GLMM and/or Tukey post hoc tests at $P < 0.05$ (see Materials and Methods).

hominids, with the lateral frontal cortex presenting a similar topological organization in human and chimpanzee brains.

The present study provides important clarifications about the macaque to human comparison of the frontal cortical organization. First, our results strongly suggest that PMFS-P does correspond to the border between the prefrontal and the premotor cortex, both in macaque and human brains. In macaque brains, it has been repeatedly shown that the dorsal part of the arcuate sulcus (i.e., PMFS-P in the human-based nomenclature; see Table 1) limits cytoarchitectonic area 6 from area 8 (fig. S6) (21). In human brains, although a formal cytoarchitectonic study should be conducted to provide a state-of-the-art demonstration, PMFS-P has also been suggested as being the limit between the frontal and the prefrontal cortex based on its functional connectivity profile (37). Second, a most notable and established functional aspect of the genu of the arcuate sulcus in macaque monkeys is the localization of the frontal eye field (FEF) in the anterior bank of the arcuate sulcus (38), i.e., at the intersection between PMFS-P and IPRS-S. By contrast, in humans, the FEF has largely been described as being located at the intersection between the SPRS and SFS-P (3, 5, 39). Although

these two FEFs have often been viewed as homologous (3, 5, 39), the present results support an alternative interpretation. Whereas only one FEF has been reported in macaques, two FEF have been observed in humans: a dorsal FEF, i.e., the most commonly described (see above), and a ventral one (called iFEF and located in IPRS-S), largely neglected so far (7, 8, 39). The present study points toward homologies between the macaque FEF and the human iFEF, in line with a recent hypothesis (20). Clarifying this critical question would require additional studies assessing the respective connectivity and function of FEF and iFEF in the human brain and identifying their homologs in macaques [for example, with spider matching techniques; (40)]. Last, our results emphasize that the principal sulcus does not correspond to the IFS, as previously suggested (41). Rather, we show that the anatomical and functional organization of the principal sulcus lies entirely in the dorsolateral prefrontal cortex, in line with the known cytoarchitectonic organization of this region in which areas 9/46 and 46 occupy both banks of the principal sulcus and expand ventrally to the inferior frontal dimple (21, 42).

A strong and highly reliable empirical result shown in the present and past studies (12, 37, 43–45) is the preserved topology of the sulcal organization of the cerebral cortex within and across primate species. Although the mechanisms supporting this conserved cortical folding pattern are not yet fully understood, such preservation is expected given the common developmental origin of the cortical areas in the primate order. First, it has been demonstrated that the cytoarchitectonic organization of the frontal cortex is topologically preserved in macaques and humans (20). Specifically, the frontal cortex is composed of several areas distinguished by their particular laminar organization, which display the same overall spatial location within and across primate species. The cortical laminar differentiation appears to be under the strong influence of genetic factors and governed by specific forces. Genetic factors appear to induce differential speeds of cell proliferation, thus creating heterogeneities in the ventricular zone that determine the endpoints of cortical neurons and the size of the cortical area [protomap hypothesis; (46)]. Then, the dual origin theory, originally developed by Sanides (40, 47), suggests that the cerebral cortex is formed during development through two progressive sequences of laminar differentiation emerging from two distinct cortical progenitors: a ventral one, the pyriform cortex, and a dorsal one, the indusium griseum. In the frontal cortex, the sequence running from the pyriform cortex induces ventral-to-lateral forces responsible for the formation of the orbitofrontal and ventrolateral cortex, whereas the one running from the indusium griseum induces dorsal-to-lateral forces responsible for the formation of the medial and dorsolateral cortex. Second, the cortical folding appears later during development and seems also governed by several factors (46, 48). Genetic influences, rather than pure external forces, seem to have a critical role in the formation of sulci and may explain the sulcal topology (46). The sulcal pits, i.e., the first location where a given sulcus develops (42), thought to relate closely to cytoarchitectonic areas (46, 49), have been shown to be under a strong genetic control (50–52) exerted regionally (53). By contrast, models suggesting that the sulcal formation is governed by sole mechanistic, geometric constraints (54–56) do not explain the extremely well-preserved topological organization of sulci across hemispheres, individuals, and primate species. Third, probably as a result of the two previous points, cortical sulci and cytoarchitectonic areas appear to display tight relationships. Although this point is still debated, we argue that the only proper way to assess this particular aspect is to section the brain perpendicular to the direction of each sulcus of interest to have access to the optimal laminar organization of the cortex located on each side of a particular sulcus (57). Studies assessing specifically the relationships between sulci and cytoarchitectonic areas have revealed that sulci are either limiting or axial to cytoarchitectonic areas (57). For instance, (i) the central sulcus is the limiting sulcus between the primary motor cortex (area 4) and the primary somatosensory cortex (area 3) both in macaques and humans (58–60), (ii) the inferior frontal dimple is the limiting sulcus between area 45 and area 9/46 (20, 21), and (iii) the CGS is limiting between area 24c' and 32' (61–63). Last, the cerebral cortex expands in the primate order around highly preserved subcortical structures, and we have shown in the present and past studies (12) that the landmarks of these subcortical structures (see fig. S3) are proxies for the topological organization of the sulcal cortical patterns. As the genome is highly similar across primate species (64, 65), one can thus hypothesize that identical genetic influences and

forces may constrain locally the sulcal expansion in all primates species and lead to conserved topological sulcal organization in the primate order. As such, the cortical expansion observed in the primate order should not result in sulci forming in widely distant places. Although our analysis needs to be expanded to the entire cerebral cortex to provide a definitive answer to this question, our empirical findings to date confirm this hypothesis.

In addition to inference about brain evolution, sulcal pattern analysis is an important tool for investigation brain function. In the human brain, the sulcal morphology of the frontal cortex has been associated with interindividual variability in the localization of brain activity (3, 5, 6, 66, 67) and in behavioral performances (68–70). Combined with the present study, these results suggest that the between-species interindividual sulcal cortical variability may be further interpreted in relation to the evolution of cognition. Specifically, whereas a preserved organization of the sulcal organization of a given cortical region across species may suggest that precursors of the abilities supported by this region were already present in the last common ancestors of hominids and old-world monkeys, a differential organization may suggest the emergence or the improvement of a given function.

To conclude, our work demonstrates the existence in macaque brains of the precursors of all the major sulci in the posterior frontal, dorsolateral, and frontopolar cortex of hominids, providing critical evidence for the value of the macaque primate brain in experimental, anatomical, and physiological neuroscience targeted to these regions. We expect that the present framework will allow a more accurate transfer of information from the nonhuman primate brain to the human brain.

MATERIALS AND METHODS

Neuroimaging T1 anatomical data of 80 human, 80 chimpanzee, 80 baboon, and 80 macaque brains were analyzed. Note that the source of the neuroimaging data and most of the procedures are described in details in our previous publication (12).

Anatomical neuroimaging data in human subjects

High-resolution anatomical scans of the human brain were obtained from the Human Connectome Project database (humanconnectome.org) (71). Acquisition parameters of T1 anatomical scans are the following: whole head, 0.7-mm³ isotropic resolution, TR (repetition time) = 2.4 s, TE (echo time) = 2.14 ms, and flip angle = 8° (details can be found on https://humanconnectome.org/storage/app/media/documentation/s1200/HCP_S1200_Release_Appendix_I.pdf). The full set of inclusion and exclusion criteria is detailed elsewhere (71). The experiments were performed in accordance with relevant guidelines and regulations, and all experimental protocols were approved by the Institutional Review Board (IRB) (IRB no. 201204036; Title: "Mapping the Human Connectome: Structure, Function, and Heritability"). All subjects provided written informed consent on forms approved by the IRB of Washington University in St. Louis.

Anatomical neuroimaging data in nonhuman primates

High-resolution anatomical scans of chimpanzee and baboon brains were obtained from the laboratories of W.D.H. and A.M., respectively. High-resolution anatomical scans of macaque brains were obtained from the laboratories of E.P., C.A., W.D.H., J.S.,

F.H.-B., and S.B.H. These data are now available in the PRIME-DE database (72–74). Data collected initially for studies on macaque monkeys and baboons were conducted under local ethics agreements [licenses from the U.K. Home Office; Provence and Lyon ethics committees] and in accordance with The Animals (Scientific Procedures) Act 1986 and with the European Union guidelines (EU Directive 2010/63/EU). Chimpanzee data collection was approved by the Institutional Animal Care and Use Committees at Yerkes National Primate Research Center (YNPRC) and University of Texas MD Anderson Cancer Center (UTMDACC) and also followed the guidelines of the Institute of Medicine on the use of chimpanzees in research.

Anatomical neuroimaging data analysis across species

Human and macaque brains were normalized in the human (www.bic.mni.mcgill.ca/ServicesAtlases/HomePage) and macaque (75) MNI stereotaxic coordinate systems, respectively. Chimpanzee and baboon brains were normalized in the chimpanzee (76) and the baboon (77) standard brain, respectively. Note that normalization of all primate brains consisted in linear registrations, which allow within-species comparisons between brains without altering relationships between sulci and gyri. As previously indicated (12), it is thus unlikely that such processing influences commonality and divergence of sulcal organization observed between species. Normalization of primate brains was performed with SPM12 (www.fil.ion.ucl.ac.uk/spm/software/spm12/) (12).

We examined the organization of sulci of the lateral frontal cortex in the entire dataset (80/160 brains/hemispheres for each species). This analysis consisted in the identification of the probability of occurrence of all sulci in the lateral frontal cortex and in the assessment of any relationships that may exist between these sulci and certain fixed anatomical landmarks across the species examined (see fig. S3 for description of these landmarks). Specifically, we assessed whether important characteristics of sulci (i.e., the caudal limit of SPRS-S, IPRS-S, IPRS-P, IFS, PMFS-P, PMFS-I, PMFS-A, and IMFS-H and the rostral limit of SFS-P, IFS, and PMFS-P) were located at the level of specific anatomical landmarks (i.e., rostral limit of the mammillary body, caudal limit of the rostrum, anterior commissure, rostral limit of the optic chiasma, caudal and rostral limit of the genu of the corpus callosum, and junction between the CGS and the fork composed of the SOS and the SUROS sulcus; see fig. S3). Toward that goal, we calculated the differences between the *Y* value of these sulcal characteristics and the *Y* value of the various anatomical landmarks. Note that we did not have any specific hypothesis regarding the spatial relationship between a given anatomical landmark and a particular sulcal characteristic. Following procedures previously described by Amiez *et al.* (12), these differences were calculated in all four species on the normalized T1 data and then normalized to take into account the different anteroposterior extent of the brains of the four species (i.e., 175, 110, 85, and 60 mm, respectively, in the human, chimpanzee, baboon, and macaque brains). The normalization performed within species was obtained by dividing the *Y* coordinate of the sulcus of interest, measured on brains registered linearly in the species-specific standard space, by the anteroposterior extent of the standard brain. For a given sulcal characteristic (e.g., the caudal-most part of PMFS-P), we calculated, in all individuals of each species, the normalized difference between the anteroposterior level (*Y* coordinate) of this characteristic with the anteroposterior

level (*Y* coordinate) of each anatomical landmarks used in the present study (fig. S3). The sulcal characteristic associated with the median the closest to 0 was assigned as being located at the level of this anatomical landmark. The add-on of baboon data is of considerable interest (although this species belongs to old-world monkeys) because the baboon brain is bigger and more gyrified than the macaque brain, and, as shown in (12), the slightly more gyrified brain of the baboon exhibits a tendency toward the hominid sulcal configuration in comparison with the macaque brain that is slightly less gyrified. The sulcus labeling was performed by C.A., and difficult cases were discussed with J.S. and M.P., as described by Amiez *et al.* (12).

We tested the influence of species on the probability of occurrence of a sulcus with logistic regressions. In the statistical models, “species” (human, chimpanzee, baboon, and macaque) was the independent variable, and “presence” (0, 1) of a sulcus was the dependent variable. To assess whether the probability of observing the various sulci was similar or different in each species, we performed GLMM in each species with these sulci as independent variable and the subject ID as random factor, i.e., formula: $\text{sulcus presence} \sim \text{species} + (1 | \text{ID})$. *F*, *P*, NumDF, and DenDF values from the GLMM are reported. Post hoc Tukey tests were then applied. These data are presented in dataset S1. All statistics were performed with R software, R Development Core Team (78) under R Studio (79).

rs-fMRI experiment in awake macaques

The aim was to identify any subdivisions of the principal sulcus in macaques using a data-driven approach, blind from local morphological variability in the sulcus. Because we have recently shown that the frontal cortical connectivity is highly affected by anesthesia (80), we restricted our analysis of rs-fMRI data obtained in awake macaques.

Data acquisition

Three rhesus monkeys (*Macaca mulatta*) were included in the study (two females: monkeys C, 21 years old, and N, 9.5 years old; one male: monkey L, 9.5 years old; weight, 5 to 8 kg). Animals were maintained on a water and food regulation schedule, individually tailored to maintain a stable level of performance for each monkey. All procedures follow the guidelines of European Community on animal care (European Community Council, directive no. 86-609, 24 November 1986) and were approved by French Animal Experimentation Ethics Committee no. 42 (CELYNE). Scanning was performed on a 3T Siemens Magnetom Prisma MRI Scanner (Siemens Healthcare, Germany). All detailed information about awake monkey training, surgery, and experimental rs-fMRI setup can be found in (80). The rs-fMRI acquisition parameters were the following: TR = 1800 ms, TE = 27 ms, flip angle = 75°, field of view (FOV) = 480 mm by 336 mm, voxel size = 1.8 mm isotropic, and 30 slices. For each macaque, 12 runs of 400 volumes were acquired.

Data analysis

Preprocessing steps were carried out using MATLAB toolbox SPM12, AFNI software [Analysis of Functional NeuroImages; (81)], and FSL software [FMRIB Software Library; (82)]. The preprocessing procedure is described in detail in (80). Both anatomical and functional images were registered in a common atlas space, i.e., the CHARM atlas [https://afni.nimh.nih.gov/pub/dist/doc/html/doc/nonhuman/macaque_tempatl/atlas_charm.html]; (83,

84)], to ensure optimized intersession and intersubject comparisons.

All rs-fMRI processing steps were realized with AFNI software. A temporal filtering was applied to extract the spontaneous slowly fluctuating brain activity (0.01 to 0.1 Hz). Linear regression was used to remove nuisance variables (the six parameter estimates for head motion, the cerebrospinal fluid, and white matter signals from the segmentation). Last, a spatial smoothing with a 4-mm full-width half maximum Gaussian kernel was applied to the output of the regression.

We then performed a data-driven parcellation of the principal sulcus. The first step was to identify and manually draw a mask covering the entire principal sulcus, separately in the left and right hemispheres of each macaque on the basis of the anatomical MRI scan. Visualization and drawing were performed with AFNI software. Each resulting principal sulcus mask was resampled from anatomical (voxel size = 0.5 mm³) to functional dimensions (voxel size = 1.8 mm isotropic). We computed, in each hemisphere, each macaque, and each run, Pearson's correlation (r) between the time course of each voxel of the principal sulcus mask and the time course of each voxel composing the gray matter of the whole brain. These r values were then transformed to z scores. The output was, for each subject, n three-dimensional (3D) matrix with n being the number of voxels in the principal sulcus mask. Each 3D matrix was flattened to reach an n -by- m 2D matrix representing z scores between each voxel of the principal sulcus mask (n rows) and each voxel of the rest of the gray matter of entire brain (m columns).

On the basis of previous work (85, 86), we applied a clustering algorithm to this matrix to classify voxels depending on their z score profile with voxels composing the gray matter of the entire brain. Clustering algorithms aim at joining elements displaying the same features into the same group, element with dissimilarities being included into other groups. Thus, we expected that voxels of the principal sulcus mask displaying similar connectivity profiles would be clustered together and would correspond to a particular principal sulcal subregion associated with a particular whole-brain connectivity profile. We applied spectral clustering algorithms because of their reliance on graph theory, which is known to reflect well brain connectivity (87). From the previous 2D matrix representing the whole-brain connectivity profile of each voxel of the principal sulcus mask, we computed the adjacency matrix measured by the correlation between rows. We then used the k -nearest neighbor to extract the similarity matrix. From this latter matrix, the Laplacian matrix and its spectral decomposition were computed, and we applied the K -means algorithm on the eigenvalues matrix to obtain the clusters (88). Results showed that highly connected voxels in the principal sulcus mask were grouped together. All clustering procedures were built with Python 3.8.10 and following libraries: scikit-learn (89) for all the clustering part, pandas (90) for the data management, numpy (91) for calculation and matrix building and operation, and nibabel (92) for NiFTi file management.

To identify the optimal number of clusters composing each principal sulcal mask based on a pure data-driven approach, we used silhouette index scores. This score measures the ratio of the sum of between-cluster and within-cluster dispersions for all clusters (where dispersion is defined as the sum of distances squared) and is higher when clusters are dense and well separated. We tested the influence of the number of parcels on silhouette index scores across macaques with mixed general linear model GLMMs in which

"number of parcels" (1→7) was the independent variable, "silhouette index scores" was the dependent variable, and subject and run ID are random factors. Post hoc Tukey tests were then applied. The resulting optimal number of clusters ($n = 3$, see results) was then used to parcellate the CGS mask of each hemisphere and in each macaque and each run. Last, for each macaque and each hemisphere, a probability map over the 12 runs was computed. These data are presented in dataset S2. All statistics were performed with R software, R Development Core Team under R Studio (79).

Cytoarchitectonic analysis of the dorsal principal sulcus in macaques

Three brains were initially perfused with saline solution followed by a formalin solution to ensure the fixation of the tissue. Before sectioning the tissue using cryotome, the entire brain was placed in a phosphate-buffered saline 20% sucrose solution. The brain was then sectioned along the anterior-posterior axis, with consecutive 40- μ m slices processed for different staining protocols and with one of the six sections taken for cresyl violet staining. Sections were then scanned using an AxioScan, Leica. Qualitative analyses of obtained images were then conducted by J.S. and V.M.-L. Results are presented in fig. S10.

Meta-analysis of electrophysiological studies

A PubMed search revealed 211 recording studies published between 1990 and 2020 on the dorsolateral or dorsal prefrontal cortex in monkeys. Of those studies, only 67 were included in the meta-analysis because they provided numerical values along the anterior-to-posterior axis of the actual recording sites or the localization of the recording chamber. If data from an animal were included in several studies, then only one study was considered. One study (93) was excluded from the analysis because of the large discrepancy (>10 mm) between the single-subject coordinates and the atlas used for reference (94). Figure S11 reports the distribution of recording sites in the principal sulcus (and adjacent dorsal region) of the dorsolateral prefrontal cortex in macaque monkeys. Studies included in the meta-analysis are provided in the Supplementary Materials.

Supplementary Materials

This PDF file includes:

Figs. S1 to S12

Legends for data S1 and S2

Other Supplementary Material for this

manuscript includes the following:

Data S1 and S2

[View/request a protocol for this paper from Bio-protocol.](#)

REFERENCES AND NOTES

1. C. Amiez, J. Sallet, J. Novek, F. Hadj-Bouziane, C. Giacometti, J. Andersson, W. D. Hopkins, M. Petrides, Chimpanzee histology and functional brain imaging show that the paracingulate sulcus is not human-specific. *Commun. Biol.* **4**, 54 (2021).
2. C. Amiez, R. Neveu, D. Warrot, M. Petrides, K. Knoblauch, E. Procyk, The location of feed-back-related activity in the midcingulate cortex is predicted by local morphology. *J. Neurosci.* **33**, 2217–2228 (2013).
3. C. Amiez, P. Kostopoulos, A.-S. Champod, M. Petrides, Local morphology predicts functional organization of the dorsal premotor region in the human brain. *J. Neurosci.* **26**, 2724–2731 (2006).
4. C. Amiez, M. G. Wutte, I. Faillenot, M. Petrides, B. Burle, E. Procyk, Single subject analyses reveal consistent recruitment of frontal operculum in performance monitoring. *Neuroimage* **133**, 266–278 (2016).

5. C. Amiez, M. Petrides, Functional rostro-caudal gradient in the human posterior lateral frontal cortex. *Brain Struct. Funct.* **223**, 1487–1499 (2018).
6. K. K. Loh, E. Procyk, R. Neveu, F. Lambertson, W. D. Hopkins, M. Petrides, C. Amiez, Cognitive control of orofacial motor and vocal responses in the ventrolateral and dorsomedial human frontal cortex. *Proc. Natl. Acad. Sci. U.S.A.* **117**, 4994–5005 (2020).
7. J. Derrfuss, V. L. Vogt, C. J. Fiebach, D. Y. von Cramon, M. Tittgemeyer, Functional organization of the left inferior precentral sulcus: Dissociating the inferior frontal eye field and the inferior frontal junction. *Neuroimage* **59**, 3829–3837 (2012).
8. J. Derrfuss, M. Brass, D. Y. von Cramon, G. Lohmann, K. Amunts, Neural activations at the junction of the inferior frontal sulcus and the inferior precentral sulcus: Interindividual variability, reliability, and association with sulcal morphology. *Hum. Brain Mapp.* **30**, 299–311 (2009).
9. F. Tomaiuolo, F. Giordano, Cerebral sulci and gyri are intrinsic landmarks for brain navigation in individual subjects: An instrument to assist neurosurgeons in preserving cognitive function in brain tumour surgery (Commentary on Zlatkina et al.). *Eur. J. Neurosci.* **43**, 1266–1267 (2016).
10. V. Zlatkina, C. Amiez, M. Petrides, The postcentral sulcal complex and the transverse postcentral sulcus and their relation to sensorimotor functional organization. *Eur. J. Neurosci.* **43**, 1268–1283 (2016).
11. C. Amiez, P. Kostopoulos, A.-S. Champod, D. L. Collins, J. Doyon, R. Del Maestro, M. Petrides, Preoperative functional magnetic resonance imaging assessment of higher-order cognitive function in patients undergoing surgery for brain tumors. *J. Neurosurg.* **108**, 258–268 (2008).
12. C. Amiez, J. Sallet, W. D. Hopkins, A. Meguerditchian, F. Hadj-Bouziane, S. Ben Hamed, C. R. E. Wilson, E. Procyk, M. Petrides, Sulcal organization in the medial frontal cortex provides insights into primate brain evolution. *Nat. Commun.* **10**, 3437 (2019).
13. T. M. Preuss, Do rats have prefrontal cortex? The rose-woolsey-akert program reconsidered. *J. Cogn. Neurosci.* **7**, 1–24 (1995).
14. S. P. Wise, Forward frontal fields: Phylogeny and fundamental function. *Trends Neurosci.* **31**, 599–608 (2008).
15. M. Petrides, *Atlas of the Morphology of the Human Cerebral Cortex on the Average MNI Brain* (Academic Press, ed. 1, 2018).
16. P. Bailey, G. Von Bonin, W. S. McCulloch, *The Isocortex of the Chimpanzee* (University of Illinois Press, 1950).
17. C. J. Connolly, The fissural pattern of the primate brain. *Am. J. Phys. Anthropol.* **21**, 301–422 (1936).
18. W. J. S. Krieg, *Interpretive Atlas of the Monkey's Brain* (Brain Books, 1975).
19. J. D. Schall, W. Zinke, J. D. Cosman, M. S. Schall, M. Paré, P. Pouget, On the evolution of the frontal eye field: Comparisons of monkeys, apes, and humans, in *Evolutionary Neuroscience*, J. H. Kaas, Ed. (Academic Press, ed. 2, 2020), pp. 861–890.
20. M. Petrides, D. N. Pandya, Comparative architectonic analysis of the human and the macaque frontal cortex, in *Handbook of Neuropsychology*, F. Boller, J. Grafman, Eds. (Elsevier, 1994), pp. 17–58.
21. M. Petrides, D. N. Pandya, Comparative cytoarchitectonic analysis of the human and the macaque ventrolateral prefrontal cortex and corticocortical connection patterns in the monkey. *Eur. J. Neurosci.* **16**, 291–310 (2002).
22. S. Geyer, M. Matelli, G. Luppino, K. Zilles, Functional neuroanatomy of the primate isocortical motor system. *Anat. Embryol.* **202**, 443–474 (2000).
23. M. Matelli, G. Luppino, G. Rizzolatti, Architecture of superior and mesial area 6 and the adjacent cingulate cortex in the macaque monkey. *J. Comp. Neurol.* **311**, 445–462 (1991).
24. A. Belmalih, E. Borra, M. Contini, M. Gerbella, S. Rozzi, G. Luppino, A multiarchitectonic approach for the definition of functionally distinct areas and domains in the monkey frontal lobe. *J. Anat.* **211**, 199–211 (2007).
25. G. Paxinos, X. Huang, A. W. Toga, *The Rhesus Monkey Brain in Stereotaxic Coordinates* (Academic Press, 1999).
26. M. Petrides, D. N. Pandya, Dorsolateral prefrontal cortex: Comparative cytoarchitectonic analysis in the human and the macaque brain and corticocortical connection patterns. *Eur. J. Neurosci.* **11**, 1011–1036 (1999).
27. E. Borra, C. G. Ferroni, M. Gerbella, V. Giorgetti, C. Mangiaracina, S. Rozzi, G. Luppino, Rostro-caudal connective heterogeneity of the dorsal part of the macaque prefrontal area 46. *Cereb. Cortex* **29**, 485–504 (2019).
28. H. Tanila, S. Carlson, I. Linnankoski, H. Kahila, Regional distribution of functions in dorso-lateral prefrontal cortex of the monkey. *Behav. Brain Res.* **53**, 63–71 (1993).
29. M. R. Riley, X.-L. Qi, C. Constantinidis, Functional specialization of areas along the anterior-posterior axis of the primate prefrontal cortex. *Cereb. Cortex* **27**, 3683–3697 (2017).
30. H. Tang, R. Bartolo, B. B. Averbach, Reward-related choices determine information timing and flow across macaque lateral prefrontal cortex. *Nat. Commun.* **12**, 894 (2021).
31. F.-X. Neubert, R. B. Mars, J. Sallet, M. F. S. Rushworth, Connectivity reveals relationship of brain areas for reward-guided learning and decision making in human and monkey frontal cortex. *Proc. Natl. Acad. Sci. U.S.A.* **112**, E2695–E2704 (2015).
32. J. Sallet, R. B. Mars, M. P. Noonan, F.-X. Neubert, S. Jbabdi, J. X. O'Reilly, N. Filippini, A. G. Thomas, M. F. Rushworth, The organization of dorsal frontal cortex in humans and macaques. *J. Neurosci.* **33**, 12255–12274 (2013).
33. L. Pozzi, J. A. Hodgson, A. S. Burrell, K. N. Sterner, R. L. Raauum, T. R. Disotell, Primate phylogenetic relationships and divergence dates inferred from complete mitochondrial genomes. *Mol. Phylogenet. Evol.* **75**, 165–183 (2014).
34. E. Koehlin, Frontal pole function: What is specifically human? *Trends Cogn. Sci.* **15**, 241–243 (2011).
35. F. A. Mansouri, E. Koehlin, M. G. P. Rosa, M. J. Buckley, Managing competing goals - a key role for the frontopolar cortex. *Nat. Rev. Neurosci.* **18**, 645–657 (2017).
36. J. A. Miller, W. I. Voorhies, D. J. Lurie, M. D'Esposito, K. S. Weiner, Overlooked tertiary sulci serve as a meso-scale link between microstructural and functional properties of human lateral prefrontal cortex. *J. Neurosci.* **41**, 2229–2244 (2021).
37. C. J. Bruce, M. E. Goldberg, Physiology of the frontal eye fields. *Trends Neurosci.* **7**, 436–441 (1984).
38. C. Amiez, M. Petrides, Anatomical organization of the eye fields in the human and non-human primate frontal cortex. *Prog. Neurobiol.* **89**, 220–230 (2009).
39. R. B. Mars, L. Verhagen, T. E. Gladwin, F.-X. Neubert, J. Sallet, M. F. S. Rushworth, Comparing brains by matching connectivity profiles. *Neurosci. Biobehav. Rev.* **60**, 90–97 (2016).
40. F. Sanides, Comparative architectonics of the neocortex of mammals and their evolutionary interpretation. *Ann. N. Y. Acad. Sci.* **167**, 404–423 (1969).
41. M. Petrides, Lateral prefrontal cortex: Architectonic and functional organization. *Phil. Trans. R. Soc. Lond. B Biol. Sci.* **360**, 781–795 (2005).
42. J. Régis, J.-F. Mangin, T. Ochiai, V. Frouin, D. Rivière, A. Cachia, M. Tamura, Y. Samson, "Sulcal root" generic model: A hypothesis to overcome the variability of the human cortex folding patterns. *Neur. Med. Chir. (Tokyo)* **45**, 1–17 (2005).
43. W. D. Hopkins, A. Meguerditchian, O. Coulon, S. Bogart, J.-F. Mangin, C. C. Sherwood, M. W. Grabowski, A. J. Bennett, P. J. Pierre, S. Fears, R. Woods, P. R. Hof, J. Vauclair, Evolution of the central sulcus morphology in primates. *Brain Behav. Evol.* **84**, 19–30 (2014).
44. C. J. Connolly, Development of the cerebral sulci. *Am. J. Phys. Anthropol.* **26**, 113–149 (1940).
45. D. Pandya, M. Petrides, P. B. Cipolloni, *Cerebral Cortex: Architecture, Connections, and the Dual Origin Concept* (Oxford Univ. Press, 2015).
46. P. Rakic, Specification of cerebral cortical areas. *Science* **241**, 170–176 (1988).
47. F. Sanides, D. Sanides, The "extraverted neurons" of the mammalian cerebral cortex. *Z. Anat. Entwickl. Gesch.* **136**, 272–293 (1972).
48. L. Vasung, C. K. Rollins, C. Velasco-Annis, H. J. Yun, J. Zhang, S. K. Warfield, H. A. Feldman, A. Gholipour, P. E. Grant, Spatiotemporal differences in the regional cortical plate and subplate volume growth during fetal development. *Cereb. Cortex* **30**, 4438–4453 (2020).
49. B. Fischl, N. Rajendran, E. Busa, J. Augustinack, O. Hinds, B. T. T. Yeo, H. Mohlberg, K. Amunts, K. Zilles, Cortical folding patterns and predicting cytoarchitecture. *Cereb. Cortex* **18**, 1973–1980 (2008).
50. G. Lohmann, D. Y. von Cramon, A. C. F. Colchester, Deep sulcal landmarks provide an organizing framework for human cortical folding. *Cereb. Cortex* **18**, 1415–1420 (2008).
51. Y. Le Guen, G. Auzias, F. Leroy, M. Noulhiane, G. Dehaene-Lambertz, E. Duchesnay, J.-F. Mangin, O. Coulon, V. Frouin, Genetic influence on the sulcal pits: On the origin of the first cortical folds. *Cereb. Cortex* **28**, 1922–1933 (2018).
52. K. Im, P. E. Grant, Sulcal pits and patterns in developing human brains. *Neuroimage* **185**, 881–890 (2019).
53. Y. Le Guen, F. Leroy, G. Auzias, D. Riviere, A. Grigis, J.-F. Mangin, O. Coulon, G. Dehaene-Lambertz, V. Frouin, The chaotic morphology of the left superior temporal sulcus is genetically constrained. *Neuroimage* **174**, 297–307 (2018).
54. D. C. Van Essen, A tension-based theory of morphogenesis and compact wiring in the central nervous system. *Nature* **385**, 313–318 (1997).
55. R. Toro, Y. Burnod, A morphogenetic model for the development of cortical convolutions. *Cereb. Cortex* **15**, 1900–1913 (2005).
56. T. Tallinen, J. Y. Chung, J. S. Biggins, L. Mahadevan, Gyrfication from constrained cortical expansion. *Proc. Natl. Acad. Sci. U.S.A.* **111**, 12667–12672 (2014).
57. J. Novek, T. Sprung-Much, E. Nolan, M. Petrides, Optimal blocking of the cerebral cortex for cytoarchitectonic examination: A neuronavigation-based approach. *Cereb. Cortex* **33**, 2704–2714 (2023).
58. K. Brodmann, Beiträge zur histologischen Lokalisation der Grosshirnrinde. II. Der Calcarinustyp. *J. Psychol. Neurol.* **2**, 133–159 (1903).
59. S. Geyer, G. Luppino, S. Rozzi, Motor cortex, in *The Human Nervous System*, J. K. Mai, G. Paxinos, Eds. (Academic Press, ed. 3, 2012), pp. 1012–1035.

60. K. Zilles, K. Amunts, Architecture of the cerebral cortex, in *The Human Nervous System*, J. K. Mai, G. Paxinos, Eds. (Academic Press, ed. 3, 2012), pp. 836–895.
61. B. A. Vogt, E. A. Nimchinsky, L. J. Vogt, P. R. Hof, Human cingulate cortex: Surface features, flat maps, and cytoarchitecture. *J. Comp. Neurol.* **359**, 490–506 (1995).
62. B. A. Vogt, L. Vogt, N. B. Farber, G. Bush, Architecture and neurocytology of monkey cingulate gyrus. *J. Comp. Neurol.* **485**, 218–239 (2005).
63. B. A. Vogt, Architecture, neurocytology and comparative organization of monkey and human cingulate cortices, in *Cingulate Neurobiology and Disease* (Oxford Univ. Press, 2009), pp. 65–93.
64. Rhesus Macaque Genome Sequencing and Analysis Consortium, R. A. Gibbs, J. Rogers, M. G. Katze, R. Bumgarner, G. M. Weinstock, E. R. Mardis, K. A. Remington, R. L. Strausberg, J. C. Venter, R. K. Wilson, M. A. Batzer, C. D. Bustamante, E. E. Eichler, M. W. Hahn, R. C. Hardison, K. D. Makova, W. Miller, A. Milosavljevic, R. E. Palermo, A. Siepel, J. M. Sikela, T. Attaway, S. Bell, K. E. Bernard, C. J. Buhay, M. N. Chandrabose, M. Dao, C. Davis, K. D. Delehaunty, Y. Ding, H. H. Dinh, S. Dugan-Rocha, L. A. Fulton, R. A. Gabisi, T. T. Garner, J. Godfrey, A. C. Hawes, J. Hernandez, S. Hines, M. Holder, J. Hume, S. N. Jhangiani, V. Joshi, Z. M. Khan, E. F. Kirkness, A. Cree, R. G. Fowler, S. Lee, L. R. Lewis, Z. Li, Y.-S. Liu, S. M. Moore, D. Muzny, L. V. Nazareth, D. N. Ngo, G. O. Okwuonon, G. Pai, D. Parker, H. A. Paul, C. Pfannkoch, C. S. Pohl, Y.-H. Rogers, S. J. Ruiz, A. Sabo, J. Santibanez, B. W. Schneider, S. M. Cook, E. Sodergren, A. F. Svatek, W. Utterback, S. Vattathil, W. Warren, C. S. White, A. T. Chinwalla, Y. Feng, A. L. Halpern, L. W. Hillier, X. Huang, P. Minx, J. O. Nelson, K. H. Pepin, X. Qin, G. G. Sutton, E. Venter, B. P. Walenz, J. W. Wallis, K. C. Worley, S.-P. Yang, S. M. Jones, M. A. Marra, M. Rocchi, J. E. Schein, R. Baertsch, L. Clarke, M. Csürös, J. Glasscock, R. A. Harris, P. Havlak, A. R. Jackson, H. Jiang, Y. Liu, D. N. Messina, Y. Shen, H. X.-Z. Song, T. Wyllie, L. Zhang, E. Birney, K. Han, M. K. Konkel, J. Lee, A. F. A. Smit, B. Ullmer, H. Wang, J. Xing, R. Burhans, Z. Cheng, J. E. Karro, J. Ma, B. Raney, X. She, M. J. Cox, J. P. Demuth, L. J. Dumas, S.-G. Han, J. Hopkins, A. Karimpur-Fard, Y. H. Kim, J. R. Pollack, T. Vinar, C. Addo-Quaye, J. Degenhardt, A. Denby, M. J. Hubsiz, A. Indap, C. Kosiol, B. T. Lahn, H. A. Lawson, A. Marklein, R. Nielsen, E. J. Vallender, A. G. Clark, B. Ferguson, R. D. Hernandez, K. Hirani, H. Kehrer-Sawatzki, J. Kolb, S. Patil, L.-L. Pu, Y. Ren, D. G. Smith, D. A. Wheeler, I. Schenck, E. V. Ball, R. Chen, D. N. Cooper, B. Giardine, F. Hsu, W. J. Kent, A. Lesk, D. L. Nelson, W. E. O'Brien, C. Prüfer, P. D. Stenson, J. C. Wallace, H. Ke, X.-M. Liu, P. Wang, A. P. Xiang, F. Yang, G. P. Barber, D. Haussler, D. Karolchik, A. D. Kern, R. M. Kuhn, K. E. Smith, A. S. Zwiig, Evolutionary and biomedical insights from the rhesus macaque genome. *Science* **316**, 222–234 (2007).
65. J. Rogers, R. A. Gibbs, Comparative primate genomics: Emerging patterns of genome content and dynamics. *Nat. Rev. Genet.* **15**, 347–359 (2014).
66. A. Lopez-Perser, L. Verhagen, C. Amiez, M. Petrides, J. Sallet, The human ventromedial prefrontal cortex: Sulcal morphology and its influence on functional organization. *J. Neurosci.* **39**, 3627–3639 (2019).
67. C. Amiez, M. Petrides, Neuroimaging evidence of the anatomo-functional organization of the human cingulate motor areas. *Cereb. Cortex* **24**, 563–578 (2014).
68. C. Amiez, C. R. E. Wilson, E. Procyk, Variations of cingulate sulcal organization and link with cognitive performance. *Sci. Rep.* **8**, 13988 (2018).
69. W. I. Voorhies, J. A. Miller, J. K. Yao, S. A. Bunge, K. S. Weiner, Cognitive insights from tertiary sulci in prefrontal cortex. *Nat. Commun.* **12**, 5122 (2021).
70. E. H. Willbrand, W. I. Voorhies, J. K. Yao, K. S. Weiner, S. A. Bunge, Presence or absence of a prefrontal sulcus is linked to reasoning performance during child development. *Brain Struct. Funct.* **227**, 2543–2551 (2022).
71. D. C. Van Essen, K. Ugurbil, E. Auerbach, D. Barch, T. E. J. Behrens, R. Bucholz, A. Chang, L. Chen, M. Corbetta, S. W. Curtiss, S. Della Penna, D. Feinberg, M. F. Glasser, N. Harel, A. C. Heath, L. Larson-Prior, D. Marcus, G. Michalareas, S. Moeller, R. Oostenveld, S. E. Petersen, F. Prior, B. L. Schlaggar, S. M. Smith, A. Z. Snyder, J. Xu, E. Yacoub; WU-Minn HCP Consortium, The Human Connectome Project: A data acquisition perspective. *Neuroimage* **62**, 2222–2231 (2012).
72. M. P. Milham, L. Ai, B. Koo, T. Xu, C. Amiez, F. Ballezeau, M. G. Baxter, E. L. A. Blezer, T. Brochier, A. Chen, P. L. Croxson, C. G. Damatac, S. Dehaene, S. Everling, D. A. Fair, L. Fleysher, W. Freiwald, S. Froudust-Walsh, T. D. Griffiths, C. Guedj, F. Hadj-Bouziane, S. B. Hamed, N. Harel, B. Hiba, B. Jarraya, B. Jung, S. Kastner, P. C. Klink, S. C. Kwok, K. N. Laland, D. A. Leopold, P. Lindenfors, R. B. Mars, R. S. Menon, A. Messinger, M. Meunier, K. Mok, J. H. Morrison, J. Nacef, J. Nagy, M. O. Rios, C. I. Petkov, M. Pinsk, C. Poirier, E. Procyk, R. Rajimehr, S. M. Reader, P. R. Roelfsema, D. A. Rudko, M. F. S. Rushworth, B. E. Russ, J. Sallet, M. C. Schmid, C. M. Schwiedrzik, J. Seidlitz, J. Sein, A. Shmuel, E. L. Sullivan, L. Ungerleider, A. Thiele, O. S. Todorov, D. Tsao, Z. Wang, C. R. E. Wilson, E. Yacoub, F. Q. Ye, W. Zarco, Y. Zhou, D. S. Margulies, C. E. Schroeder, An open resource for non-human primate imaging. *Neuron* **100**, 61–74 (2018).
73. PRIMatE Data and Resource Exchange (PRIME-DRE) Global Collaboration Workshop and Consortium; Electronic address: michael.milham@childmind.org; PRIMatE Data and Resource Exchange (PRIME-DRE) Global Collaboration Workshop and Consortium, Toward next-generation primate neuroscience: A collaboration-based strategic plan for integrative neuroimaging. *Neuron* **110**, 16–20 (2022).
74. PRIMatE Data Exchange (PRIME-DE) Global Collaboration Workshop and Consortium, Accelerating the evolution of nonhuman primate neuroimaging. *Neuron* **105**, 600–603 (2020).
75. S. Frey, D. N. Pandya, M. M. Chakravarty, L. Bailey, M. Petrides, D. L. Collins, An MRI based average macaque monkey stereotaxic atlas and space (MNI monkey space). *Neuroimage* **55**, 1435–1442 (2011).
76. W. D. Hopkins, B. B. Avants, Regional and hemispheric variation in cortical thickness in chimpanzees (*Pan troglodytes*). *J. Neurosci.* **33**, 5241–5248 (2013).
77. S. A. Love, D. Marie, M. Roth, R. Lacoste, B. Nazarian, A. Bertello, O. Coulon, J.-L. Anton, A. Meguerditchian, The average baboon brain: MRI templates and tissue probability maps from 89 individuals. *Neuroimage* **132**, 526–533 (2016).
78. R Core Team, R: A Language and Environment for Statistical Computing. R Foundation for Statistical Computing (Vienna, Austria, 2020).
79. RStudio Team, RStudio: Integrated Development for R (RStudio Inc., Boston, MA, 2016).
80. C. Giacometti, A. Dureux, D. Autran-Clavagnier, C. R. E. Wilson, J. Sallet, M. Dirheimer, E. Procyk, F. Hadj-Bouziane, C. Amiez, Frontal cortical functional connectivity is impacted by anaesthesia in macaques. *Cereb. Cortex* **32**, 4050–4067 (2022).
81. R. W. Cox, AFNI: Software for analysis and visualization of functional magnetic resonance neuroimages. *Comput. Biomed. Res.* **29**, 162–173 (1996).
82. M. Jenkinson, C. F. Beckmann, T. E. J. Behrens, M. W. Woolrich, S. M. Smith, FSL. *Neuroimage* **62**, 782–790 (2012).
83. B. Jung, P. A. Taylor, J. Seidlitz, C. Sponheim, P. Perkins, L. G. Ungerleider, D. Glen, A. Messinger, A comprehensive macaque fMRI pipeline and hierarchical atlas. *Neuroimage* **235**, 117997 (2021).
84. C. Reveley, A. Gruslys, F. Q. Ye, D. Glen, J. Samaha, B. E. Russ, Z. Saad, A. K. Seth, D. A. Leopold, K. S. Saleem, Three-dimensional digital template atlas of the macaque brain. *Cereb. Cortex* **27**, 4463–4477 (2017).
85. T. Blumensath, S. Jbabdi, M. F. Glasser, D. C. Van Essen, K. Ugurbil, T. E. J. Behrens, S. M. Smith, Spatially constrained hierarchical parcellation of the brain with resting-state fMRI. *Neuroimage* **76**, 313–324 (2013).
86. F.-X. Neubert, R. B. Mars, A. G. Thomas, J. Sallet, M. F. S. Rushworth, Comparison of human ventral frontal cortex areas for cognitive control and language with areas in monkey frontal cortex. *Neuron* **81**, 700–713 (2014).
87. L. Cheng, Y. Zhang, G. Li, J. Wang, C. Sherwood, G. Gong, L. Fan, T. Jiang, Connectional asymmetry of the inferior parietal lobule shapes hemispheric specialization in humans, chimpanzees, and rhesus macaques. *eLife* **10**, e67600 (2021).
88. U. von Luxburg, A tutorial on spectral clustering. arXiv:0711.0189 [cs.DS] (1 November 2007); <https://doi.org/10.48550/arXiv.0711.0189>.
89. F. Pedregosa, G. Varoquaux, A. Gramfort, V. Michel, B. Thirion, O. Grisel, M. Blondel, A. Müller, J. Nothman, G. Louppe, P. Prettenhofer, R. Weiss, V. Dubourg, J. Vanderplas, A. Passos, D. Cournapeau, M. Brucher, M. Perrot, É. Duchesnay, Scikit-learn: Machine learning in python. *J. M. Learn. Res.* **12**, 2825–2830 (2011).
90. W. McKinney, Data structures for statistical computing in python, in Proceedings of the 9th Python in Science Conference (SCIPY 2010), pp. 56–61.
91. C. R. Harris, K. J. Millman, S. J. van der Walt, R. Gommers, P. Virtanen, D. Cournapeau, E. Wieser, J. Taylor, S. Berg, N. J. Smith, R. Kern, M. Picus, S. Hoyer, M. H. van Kerkwijk, M. Brett, A. Haldane, J. F. Del Río, M. Wiebe, P. Peterson, P. Gérard-Marchant, K. Sheppard, T. Reddy, W. Weckesser, H. Abbasi, C. Gohlke, T. E. Oliphant, Array programming with NumPy. *Nature* **585**, 357–362 (2020).
92. M. Brett, C. J. Markiewicz, M. Hanke, M.-A. Côté, B. Cipollini, P. McCarthy, D. Jarecka, C. P. Cheng, Y. O. Halchenko, M. Cottaar, E. Larson, S. Ghosh, D. Wassermann, S. Gerhard, G. R. Lee, H.-T. Wang, E. Kastman, J. Kaczmarzyk, R. Guidotti, O. Duek, J. Daniel, A. Rokem, C. Madison, B. Moloney, F. C. Morency, M. Goncalves, R. Markello, C. Riddell, C. Burns, J. Millman, A. Gramfort, J. Leppäkangas, A. Sólón, J. J. F. van den Bosch, R. D. Vincent, M. Braun, K. Subramaniam, K. J. Gorgolewski, P. R. Raamana, J. Klug, B. N. Nichols, E. M. Baker, S. Hayashi, B. Pinsard, C. Haselgrove, M. Hymers, O. Esteban, S. Koudoro, F. Pérez-García, N. N. Oosterhof, B. Amirbekian, I. Nimmo-Smith, L. Nguyen, S. Reddigari, S. St-Jean, E. Panfilov, E. Garyfallidis, G. Varoquaux, J. H. Legarreta, K. S. Hahn, O. P. Hinds, B. Fauber, J.-B. Poline, J. Stutters, K. Jordan, M. Cieslak, M. E. Moreno, V. Haenel, Y. Schwartz, Z. Baratz, B. C. Darwin, B. Thirion, C. Gauthier, D. Papadopoulos Orfanos, I. Solovey, I. Gonzalez, J. Palasubramaniam, J. Lecher, K. Leinweber, K. Raktivan, M. Calábková, P. Fischer, P. Gervais, S. Gadde, T. Ballinger, T. Roos, V. R. Reddam, freec84, nipy/nibabel: 3.2.1, Zenodo (2020); <https://doi.org/10.5281/zenodo.4295521>.
93. A. H. Lara, J. D. Wallis, Executive control processes underlying multi-item working memory. *Nat. Neurosci.* **17**, 876–883 (2014).

94. K. S. Saleem, A. V. Avram, D. Glen, C. C.-C. Yen, F. Q. Ye, M. Komlos, P. J. Basser, High-resolution mapping and digital atlas of subcortical regions in the macaque monkey based on matched MAP-MRI and histology. *Neuroimage* **245**, 118759 (2021).

Acknowledgments

Funding: This work was funded by Human Frontier Science Program grant RGP0044/2014 (M.P., W.D.H., and C.A.); French National Research Agency, ANR-18-CE37-0012 (C.A.), ANR-12-PDOC-0014-01 (A.M.), ANR-15-CE37-0003 (F.H.-B.), and ANR-18-CE37-0016 (C.R.E.W.); Sir Henry Dale Wellcome Trust Fellowship, 105651/Z/14/Z (J.S.); Wellcome Trust core funding, 203139/Z/16/Z (Wellcome Centre for Integrative Neuroimaging); Canadian Institutes of Health Research (CIHR) Foundation, grant FDN-143212 (M.P.); European Research Council (ERC) under the European Union's Horizon 2020 research and innovation program, grant agreement no. 716931 - GESTIMAGE - ERC-2016-STG (A.M.); and National Institutes of Health, grants NS-042867, NS-073134, and NS-092988 (W.D.H.). **Author contributions:** Conceptualization: C.A., J.S., and M.P. Methodology: C.A., J.S., C.Gi., C.V., C.Ga., V.M.-L., E.P., C.R.E.W., and M.P. Investigation: C.A., J.S., C.Gi., C.V., C.Ga., V.M.-L., A.M., F.H.-B., S.B.H., W.D.H., E.P., and C.R.E.W. Visualization: C.A., J.S., C.Gi., C.V., C.Ga., V.M.-L., and M.P. Funding acquisition: C.A., J.S., M.P., A.M., F.H.-B., E.P., and W.D.H.

Writing—original draft: C.A., J.S., M.P., and C.R.E.W. Writing—review and editing: C.A., J.S., M.P., C.R.E.W., E.P., A.M., and F.H.-B. **Competing interests:** C.A., F.H.-B., S.B.H., A.M., and E.P. are employed by the Centre National de la Recherche Scientifique. The authors declare that they have no competing interests. **Data and materials availability:** All data needed to evaluate the conclusions in the paper are present in the paper and/or the Supplementary Materials. The source data are provided as source data file (dataset S1). Human and chimpanzee anatomical scans are available, respectively, from the Human Connectome Project database (www.humanconnectome.org/) and from the National Chimpanzee Brain Resource (www.chimpanzeebrain.org/). Note that a CC-BY public copyright license has been applied by the authors to the present document and will be applied to all subsequent versions up to the author-accepted manuscript arising from this submission, in accordance with the grant's open access conditions.

Submitted 22 November 2022

Accepted 14 April 2023

Published 19 May 2023

10.1126/sciadv.adf9445

A revised perspective on the evolution of the lateral frontal cortex in primates

Cline Amiez, Jrme Sallet, Camille Giacometti, Charles Verstraete, Cimence Gandraux, Valentine Morel-Latour, Adrien Meguerditchian, Fadila Hadj-Bouziane, Suliann Ben Hamed, William D. Hopkins, Emmanuel Procyk, Charles R.E. Wilson, and Michael Petrides

Sci. Adv., **9** (20), eadf9445.
DOI: 10.1126/sciadv.adf9445

View the article online

<https://www.science.org/doi/10.1126/sciadv.adf9445>



Permissions

<https://www.science.org/help/reprints-and-permissions>

Use of this article is subject to the [Terms of service](#)

Science Advances (ISSN) is published by the American Association for the Advancement of Science. 1200 New York Avenue NW, Washington, DC 20005. The title *Science Advances* is a registered trademark of AAAS.
Copyright © 2023 The Authors, some rights reserved; exclusive licensee American Association for the Advancement of Science. No claim to original U.S. Government Works. Distributed under a Creative Commons Attribution License 4.0 (CC BY).

Chimpanzee histology and functional brain imaging show that the paracingulate sulcus is not human-specific

Céline Amiez^{1,8}, Jérôme Sallet^{1,2,8}, Jennifer Novek³, Fadila Hadj-Bouziane⁴, Camille Giacometti¹, Jesper Andersson⁵, William D. Hopkins⁶ & Michael Petrides⁷

The paracingulate sulcus -PCGS- has been considered for a long time to be specific to the human brain. Its presence/absence has been discussed in relation to interindividual variability of personality traits and cognitive abilities. Recently, a putative PCGS has been observed in chimpanzee brains. To demonstrate that this newly discovered sulcus is the homologue of the PCGS in the human brain, we analyzed cytoarchitectonic and resting-state functional magnetic resonance imaging data in chimpanzee brains which did or did not display a PCGS. The results show that the organization of the mid-cingulate cortex of the chimpanzee brain is comparable to that of the human brain, both cytoarchitectonically and in terms of functional connectivity with the lateral frontal cortex. These results demonstrate that the PCGS is not human-specific but is a shared feature of the primate brain since at least the last common ancestor to humans and great apes ~6 mya.

¹Univ Lyon, Université Lyon 1, Inserm, Stem Cell and Brain Research Institute U1208, 69500 Bron, France. ²Wellcome Integrative Neuroimaging Centre, Department of Experimental Psychology, University of Oxford, Oxford OX1 3SR, UK. ³Montreal Neurological Institute, Department of Neurology and Neurosurgery, McGill University, Montreal, Quebec, Canada. ⁴Integrative Multisensory Perception Action & Cognition Team (ImpAct), INSERM U1028, CNRS UMR5292, Lyon Neuroscience Research Center (CRNL), Lyon, France, University of Lyon 1, Lyon, France. ⁵Wellcome Integrative Neuroimaging Centre, fMRIB, University of Oxford, Headington, UK. ⁶Department of Comparative Medicine, University of Texas MD Anderson Cancer Center, Bastrop, TX 78602, USA. ⁷Montreal Neurological Institute, Department of Neurology and Neurosurgery and Department of Psychology, McGill University, Montreal, Quebec, Canada. ⁸These authors contributed equally: Céline Amiez, Jérôme Sallet. ✉email: celine.amiez@inserm.fr

Understanding the mechanisms underlying brain evolution, and more specifically of the human brain, is still the topic of intense debates^{1–4}. Comparative neuroanatomical studies have demonstrated that ecological and social pressures are key factors that have driven the expansion of the neocortex in primates. But this expansion has differentially impacted brain circuits⁵. With the development of neuroimaging tools, one could address comparative neuroanatomy questions *in vivo* at different levels of analysis, from gross morphology (e.g., sulcal pattern analysis) to brain connectivity (e.g., resting-state functional Magnetic Resonance Imaging analysis). Comparative neuroimaging studies are principally relying on a comparison between human brains and a limited number of non-human primate models, namely macaques and marmosets^{6,7}, whose ancestors diverged from human ancestors 25 and 35 million years ago, respectively⁸. With a common evolutionary history until 7 million years ago, the chimpanzee is a key model for better understanding the evolution of brain regions that have largely expanded in the human brain, such as the medial prefrontal cortex⁹. Among the sulci that characterize the human medial frontal cortex, the paracingulate sulcus (PCGS) is a secondary sulcus running dorsal and parallel to the cingulate sulcus (CGS) in a rostro-caudal direction^{10,11} in the medial frontal cortex. The PCGS is observed in about 70% of subjects at least in one hemisphere^{10–13} and most

often starts at the intersection with the supra-orbitalis and the supra-rostral sulcus, in front and at the level of the anterior limit of the genu of the corpus callosum, where the anterior cingulate cortex (ACC) lies (Fig. 1a, b)^{13,14}. We are referring here to the cingulate subdivisions proposed by Vogt et al.¹⁵ (Fig. 1c). From the ACC, the PCGS runs caudally where the anterior mid-cingulate cortex (aMCC) lies, but it can also run as far posterior as the level of the anterior commissure (where the posterior mid-cingulate cortex (pMCC) lies) (Fig. 1). In the human brain, the impact of the presence of a PCGS on the cytoarchitectonic organization (i.e., the cellular organization of the cerebral cortex) of the aMCC is known¹⁰: when the PCGS is absent, areas 24c' and 32' occupy, respectively, the ventral and the dorsal banks of the CGS; however, when a PCGS is present, area 24c' occupies both banks of the CGS and area 32' occupies the PCGS (Fig. 1).

In the human brain, the morphological variability of the PCGS has been linked to personality traits^{16–18}, and pathologies^{19–23}, and has also been associated with higher-order cognitive processing, i.e., several so-called human-specific processes^{12,24–27}. These observations have led some investigators to suggest that cortical area 32' which occupies the PCGS when present and the dorsal bank of the CGS when the PCGS is absent, might be unique to the human brain^{28,29}. However, a recent study has shown, based on morphological observations of the sulcal

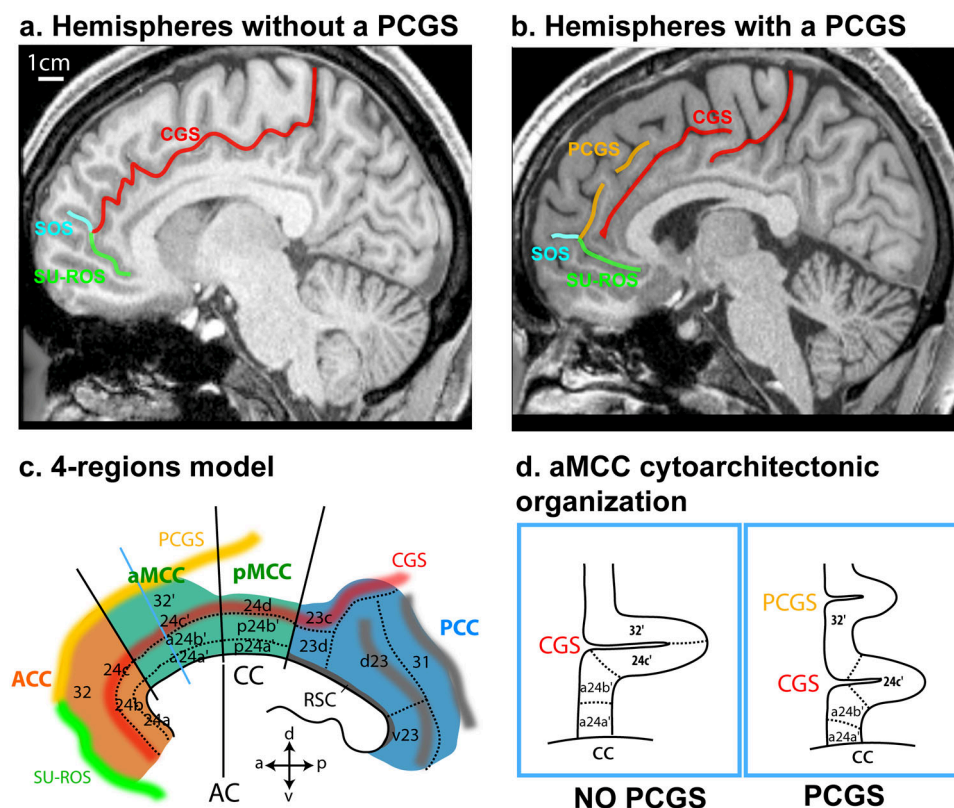


Fig. 1 Morphological and cytoarchitectonic organization of the cingulate cortex in hemispheres without or with a PCGS in the human brain. **a** In hemispheres displaying no PCGS, the CGS starts at the intersection with the supra-rostral sulcus (SUROS) and the sulcus sus-orbitalis (SOS) in front of the genu of the corpus callosum. **b** In hemispheres with a PCGS, it is the PCGS that starts rostrally at the intersection with the SUROS and the SOS^{13,14}. **c** The 4-regions model is represented in a hemisphere displaying a PCGS. This model identifies the limit between the ACC and the aMCC at the level of the anterior limit of the genu of the corpus callosum, the limit between the aMCC and the pMCC as being the anterior commissure. In the aMCC, when a PCGS is present, both banks of the CGS are occupied by area 24c' whereas the ventral bank of the PCGS is occupied by area 32'. When a PCGS is absent, the ventral and dorsal banks of the CGS are respectively occupied by area 24c' and 32'. **d** Cytoarchitectonic organization of the aMCC in hemispheres with and without a PCGS, as shown on coronal sections at the anteroposterior level displayed by the blue line in (c). a anterior, p posterior, d dorsal, v ventral, AC anterior commissure, cc corpus callosum, ACC anterior cingulate cortex, CGS cingulate sulcus, MCC mid-cingulate cortex, PCC posterior cingulate cortex, RSC retrosplenial cortex, PCGS paracingulate sulcus, SU-ROS supra-rostral sulcus, SOS sulcus sus-orbitalis. Figure 1c modified from Supplementary Fig. 3 in Amiez et al.¹³.

organization on structural MRI scans, the presence of a putative homologue of the human PCGS in 33.8% of chimpanzees, at least in one hemisphere¹³. Furthermore, opposing the view of a lack of area 32' in non-human primates, this transition area (i.e., area 32') between the cingulate cortex and cortex of the medial frontal gyrus has been shown in macaques³⁰. However, the statement that the PCGS is not human-specific and can be observed in chimpanzee brains must be supported by cytoarchitectonic evidence showing that the organization of this region in the chimpanzee brain is comparable to that in the human brain.

In the chimpanzee brain, it is not known whether, as in the human brain, the PCGS starts in the ACC and runs caudally to the midcingulate cortex (MCC)¹³. In the present study, we therefore first assessed the extent of the PCGS in both human and chimpanzee brains and hypothesized that, if the sulcus that we identified as a PCGS in the chimpanzee¹³ is homologous to the human PCGS, the mapping of the cytoarchitectonic organization of the aMCC in the chimpanzee should be comparable to that in the human brain.

It should be noted that, in the human brain, the functional connectivity within the MCC of seeds located in the PCGS and in the CGS, when the PCGS is absent, is similar. Specifically, Loh et al.³¹ have assessed the functional connectivity of the anterior rostral cingulate zone (RCZa) which is located within the anterior part of the MCC. Within the RCZa, there are limb and face motor representations with the limb motor representations lying within the CGS even when a PCGS is present; the face motor representations lie in the PCGS if present and in the CGS if the PCGS is absent³². Loh et al.³¹ have shown that the functional connectivity of the face motor representation of RCZa with lateral prefrontal and lateral motor regions of interest is similarly organized, regardless of whether it is located in the CGS in hemispheres without a PCGS or in the PCGS in hemispheres with a PCGS. The functional connectivity is stronger with anterior prefrontal regions and weaker with posterior motor regions³¹.

In the present study, we examined (1) the extent of the PCGS in both chimpanzee and human brains, (2) the cytoarchitectonic organization of the aMCC with a specific emphasis on the distribution of areas 24c' and 32' in three post-mortem chimpanzee brains which did or did not display a PCGS, and (3) in vivo functional connectivity of this region in four anesthetized chimpanzees based on the availability of resting-state functional magnetic resonance imaging (rs-fMRI) data. The results demonstrate that, in the chimpanzee brain, the impact the PCGS has on the cytoarchitectonic organization of the aMCC is comparable to that observed in the human brain. The results also show that the functional connectivity of the CGS and the PCGS is comparable to that observed in the human brain³¹. Altogether, these results demonstrate that the PCGS in chimpanzee brains is comparable in terms of cytoarchitecture and functional connectivity with the PCGS in human brains. These observations demonstrate that the PCGS is not human-specific and had already emerged in the brains of the last common ancestor with chimpanzees.

Results

Morphological study. We first re-analyzed data from Amiez et al.¹³ to assess the occurrence of a PCGS in the ACC versus the MCC in 197 human and 225 chimpanzee brains. Note that the ACC/MCC limit was identified using the probabilistic cytoarchitectonic map of the ACC from the JuBrain atlas (see "Methods")³³. This new analysis demonstrates that, in hemispheres displaying a PCGS (i.e., $n = 183$ human brain hemispheres, $n = 91$ chimpanzee brain hemispheres), the probability of observing a PCGS in the ACC is higher (89.6%) in human hemispheres than in chimpanzee (50.5%) hemispheres

(Fig. 2a, dependent variable: PCGS present (0/1), main effect species: $\chi^2 = 49.7$, $df = 1$, p -value = $1.79e-12$, logistic regression; source data are provided as Supplementary data 1).

By contrast, the probability of observing a PCGS in the MCC is comparable in human (78.7%) and chimpanzee (69.2%), i.e., it does not statistically differ between these two species (Fig. 2b) (dependent variable: PCGS present in MCC (0/1), main effect species: $\chi^2 = 2.9$, $df = 1$, p -value = 0.09, logistic regression). Finally, the probability of observing a PCGS in both the ACC and the MCC is significantly higher in human (in 68.3% of hemispheres displaying a PCGS) compared to chimpanzees (in 19.8% of hemispheres displaying a PCGS, Fig. 2c) (dependent variable: PCGS location (ACC/MCC), main effect species: $\chi^2 = 60.2$, $df = 1$, p -value = $8.48e-15$, logistic regression).

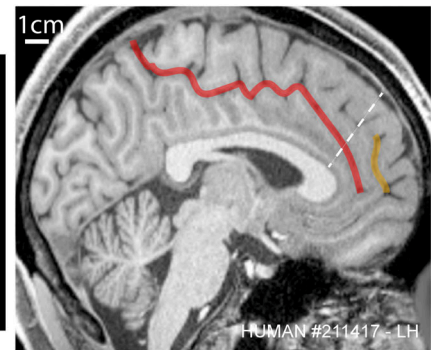
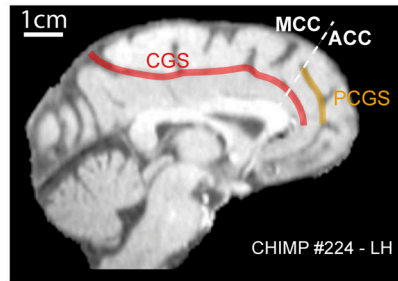
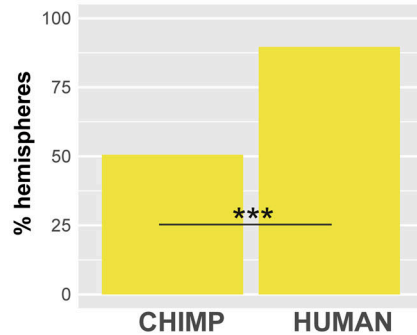
Cytoarchitectonic study. Note that our analysis is specifically focused on the distribution of area 24c' and area 32' and the impact of the presence/absence of a PCGS on it. Previous studies had already investigated the dorsal-ventral or rostral-caudal organization of the cingulate cortex and adjacent areas of the medial frontal region^{7,33–36}.

From the morphological inspection of the three chimpanzee brains included in the following cytoarchitectonic analysis, we selected four hemispheres. We analyzed the left hemisphere of CHIMP_1 and the right hemisphere of CHIMP_3 in which the PCGS was absent. We also selected the right hemisphere of CHIMP_1 and the left hemisphere of CHIMP_2 which displayed a PCGS. In CHIMP_2, the PCGS was present in the anteriormost part of the aMCC, but absent in the posterior part of the aMCC. Note that the remaining hemispheres (left hemisphere of CHIMP_3 and right hemisphere of CHIMP_2) displayed no PCGS.

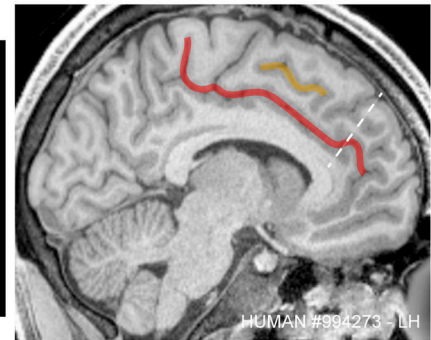
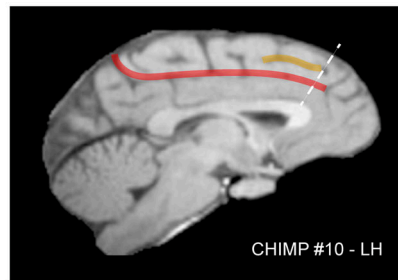
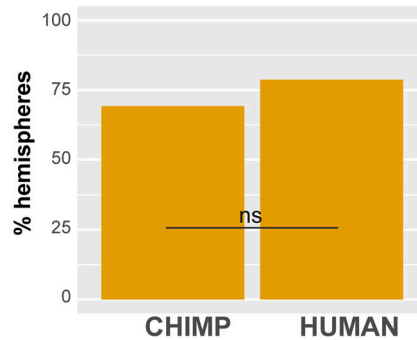
Hemispheres without a PCGS. We examined first the MCC within the left hemisphere of CHIMP_1, which did not display a PCGS. As shown in Fig. 3a, proceeding from the corpus callosum dorsally, we observed successively areas 24a' and 24b', respectively on the ventral and dorsal part of the gyrus of the cingulate cortex, and areas 24c' and 32', respectively in the ventral and dorsal bank of the CGS (for the cytoarchitectonic characteristics, see "Methods" section). Note that a transition zone was observed between each area (i.e. between areas 24a' and 24b', between areas 24b' and 24c', and between areas 24c' and 32'). Proceeding dorsally along the cingulate gyrus, the cytoarchitecture does not change abruptly, but rather a smooth reorganization is observed. We also examined the posterior part of the aMCC of CHIMP_2 (Fig. 4, slice 81) which does not display a PCGS (although the anterior part of the aMCC does possess a PCGS). The results demonstrated exactly the same cytoarchitectonic organization as in the left MCC of CHIMP_1.

Hemispheres with a PCGS. We examined the right hemisphere of CHIMP_1 and CHIMP_3, both of which display a PCGS in the MCC. In both chimpanzees, we observed successively from the corpus callosum in a dorsal direction towards the lateral cortical surface, area 24a' and area 24b', respectively on the ventral and dorsal parts of the cingulate gyrus, area 24c' in the ventral bank and in part of the dorsal bank of the CGS, and area 32' which extends from a part of the dorsal bank of the CGS to the ventral bank of the PCGS (for the cytoarchitectonic characteristics, see the "Methods" section). As in hemispheres in which the PCGS is absent, we observed small transition zones between adjacent areas (Fig. 3b). We also examined the anterior part of the aMCC in the left hemisphere of CHIMP_2 (Fig. 4, slices 141 and 701) which displays a PCGS. The results demonstrated exactly the same

a. PCGS presence in ACC



b. PCGS presence in MCC



c. PCGS presence both in ACC and MCC

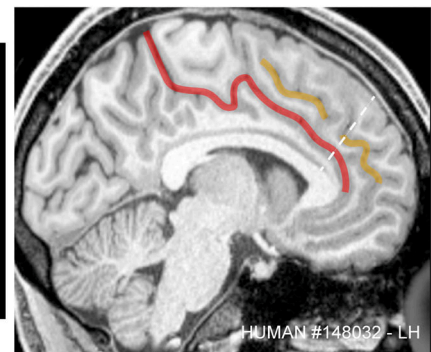
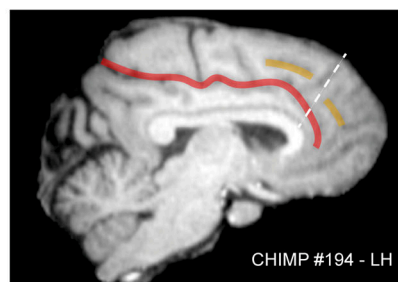
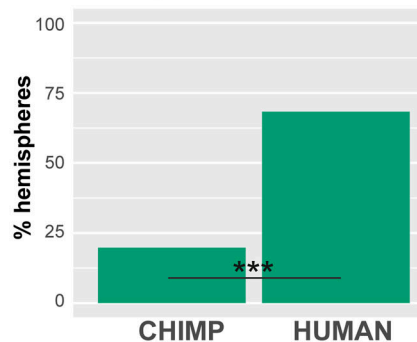


Fig. 2 Occurrence of the PCGS in the ACC and MCC in the chimpanzee and the human brains. Probability of occurrence of a PCGS in the ACC (a), the MCC (b), or in both ACC and MCC (c) in chimpanzee versus human brains. The putative limit between ACC and MCC is represented by the dashed line. CGS and PCGS correspond to the red and yellow lines, respectively. Left diagrams show that, in hemispheres displaying a PCGS (i.e., in $n = 183$ human brain hemispheres and $n = 91$ chimpanzee brain hemispheres), the probability of occurrence of a PCGS in the ACC as well as in both the ACC and the MCC is higher in human than in chimpanzee brains (dependent variable: PCGS present (0/1), main effect species: $\chi^2 = 49.7$, $df = 1$, p -value = $1.79e-12$, logistic regression). By contrast, the probability of occurrence of a PCGS in the MCC is similar in human and chimpanzee (dependent variable: PCGS present in MCC (0/1), main effect species: $\chi^2 = 2.9$, $df = 1$, p -value = 0.09 , logistic regression). ACC anterior cingulate cortex, LH left hemisphere, MCC mid-cingulate cortex, PCGS paracingulate sulcus, *** $p < 0.001$, logistic regression; ns non-significant logistic regression.

cytoarchitectonic organization as in the right MCC of CHIMP_1 and CHIMP_3.

Rs-fMRI study. From the morphological inspection of the four chimpanzee brains included in the following rs-fMRI analysis, we observed a PCGS in the left hemisphere of CHIMP_A, and in both the left and right hemispheres of CHIMP_C. The right hemisphere of CHIMP_A, and both hemispheres of CHIMP_B and CHIMP_D did not display a PCGS.

We first assessed, in hemispheres displaying a PCGS, the intra-hemispheric functional connectivity profiles of areas 24c' and 32' with Regions Of Interest (ROIs) located in the lateral frontal

cortex (Fig. 5a). To be able to conduct a comparison of connectivity fingerprints between species, ROIs were chosen for their known homologies between chimpanzee and human brains. The location of seeds and ROIs are displayed on the medial (left diagram) and the lateral cortical surface (right diagram) of a typical example (left hemisphere of CHIMP_C). The heat-maps reflecting the average correlation strength between each pair of seed-ROI clusters in the three hemispheres displaying a PCGS (see "Methods") are shown in Fig. 5a. The Boxplots further depict the average Z values of correlations between the two seeds and ROIs across the three hemispheres displaying a PCGS (see "Methods"). The results demonstrate how the activity of each seed is differentially correlated with the activity of lateral

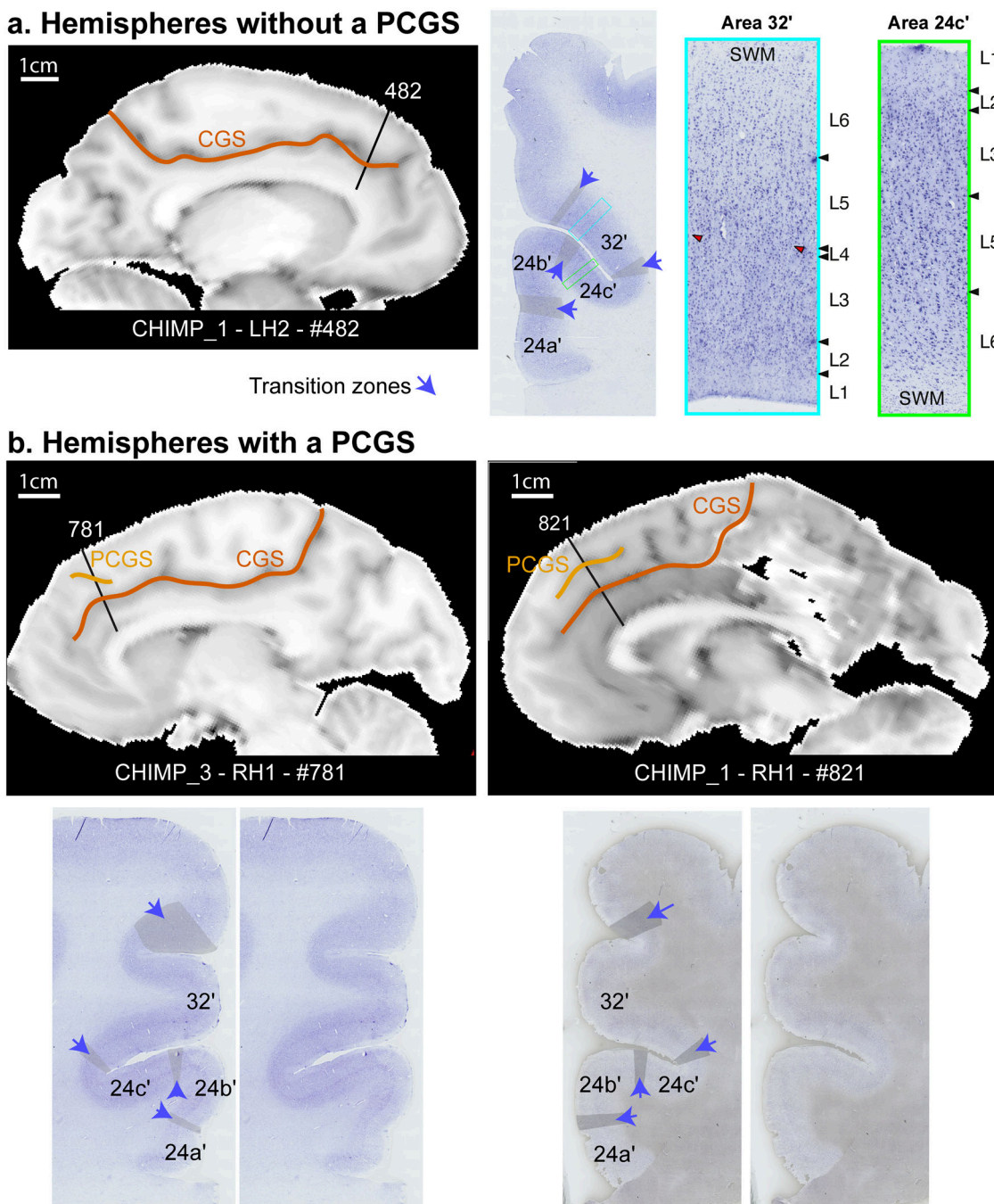


Fig. 3 Impact of the presence of a PCGS on the cytoarchitectonic organization of the anterior MCC. Cytoarchitectonic organization of the anterior MCC in hemispheres without (a) and with (b) a PCGS. **a** The MCC of the left hemisphere of CHIMP_1 is presented on a sagittal view of a post-mortem MRI scan (left panel). The CGS is marked in red. The coronal section presented on the middle panel corresponds to the antero-posterior level defined by a black line on the MRI image (slice 482). The right panels present the labeled and raw Nissl-stained slices. The black lines represent the limits between areas. The gray zones identified by a blue arrow correspond to transition zones between two adjacent cytoarchitectonic areas. Area 24c' occupies the ventral bank of the CGS and area 32' occupies the dorsal bank of the CGS. The photomicrographs of area 32' (corresponding to the region identified by a blue box on the coronal section) and area 24c' (corresponding to the region identified by a green box on the coronal section) are displayed on the right panels. Results show the presence of a dysgranular layer 4 (in red are displayed the granular patches) in area 32' and the absence of this layer in area 24c'. **b** The MCC of the right hemispheres of CHIMP_3 and CHIMP_1 are presented on sagittal views of post-mortem MRI scans. The CGS is marked in red, the PCGS in orange. The coronal sections presented on each Nissl-stained slice correspond to the antero-posterior levels defined by a black line on the MRI images (CHIMP_3: slice 781, CHIMP_1: slice 821). In both chimpanzees, area 24c' occupies the ventral bank, the fundus, and the lateral-most part of the dorsal bank of the CGS. Area 32' occupies the dorsal bank of the CGS, the gyrus between the CGS and the PCGS and the ventral bank of the PCGS. CGS cingulate sulcus, MRI magnetic resonance imaging, PCGS paracingulate sulcus, L1-6 cytoarchitectonic layers 1-6, SWM superficial white matter.

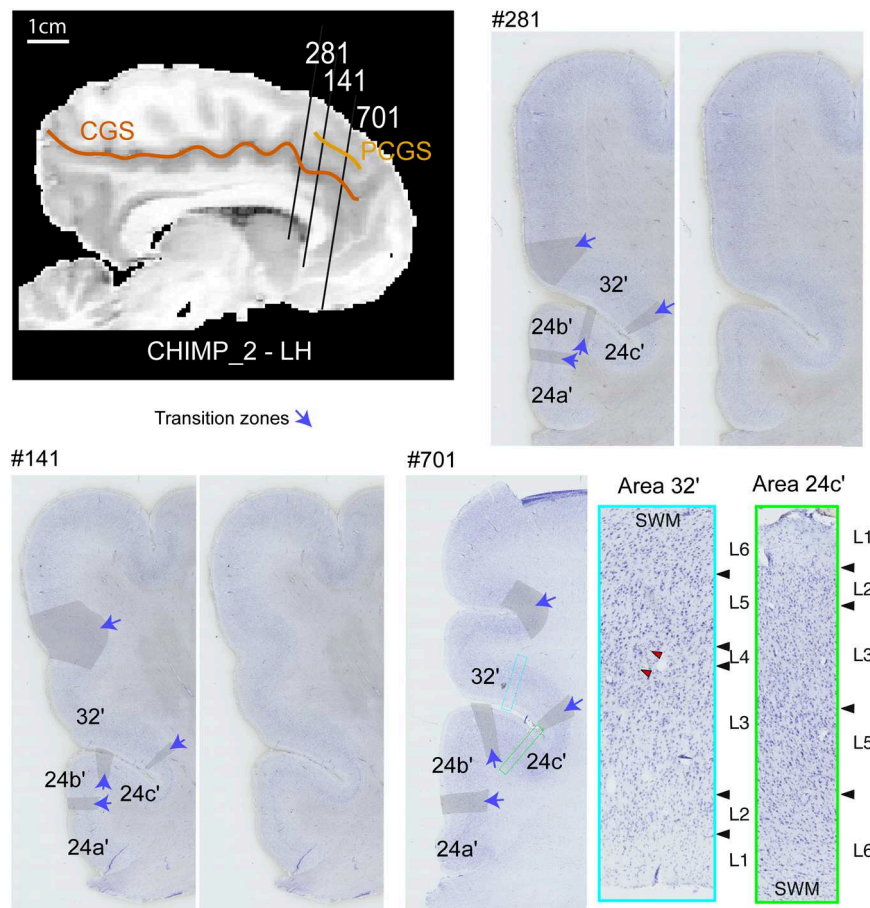


Fig. 4 Cytoarchitectonic organization of the anterior MCC of a hemisphere displaying a PCGS in its anterior part and no PCGS in its posterior part. The MCC of the left hemisphere of CHIMP_2 is presented on a sagittal view of a post-mortem MRI scan. The CGS is marked in red, the PCGS in orange. The Nissl-stained coronal sections presented correspond to the antero-posterior levels defined by a black line on the MRI images (slice 281 where the PCGS is absent, slices 141 and 701 where the PCG is present). On slice 281 where the PCGS is absent, (1) area 24c' occupies the ventral bank, the fundus, and the lateral-most part of the dorsal bank of the CGS, (2) area 32' occupies the dorsal bank of the CGS, the gyrus between the CGS and the PCGS and the ventral bank of the PCGS. On slices 141 and 701 where the PCGS is present, (1) area 24c' occupies the ventral bank, the fundus, and the lateral-most part of the dorsal bank of the CGS, (2) area 32' occupies the dorsal bank of the CGS, the gyrus between the CGS and the PCGS and the ventral bank of the PCGS. The gray zones identified by a blue arrow correspond to transition zones between two adjacent cytoarchitectonic areas. The photomicrographs of area 32' (corresponding to the region identified by a blue box on the coronal section of slice #701) and area 24c' (corresponding to the region identified by a green box on the coronal section of slice #701) are displayed on the right panels. Results show the presence of a dysgranular layer 4 (in red are displayed the granular patches) in area 32' and the absence of this layer in area 24c'. CGS cingulate sulcus, PCGS paracingulate sulcus, LH left hemisphere, L1–6 cytoarchitectonic layers 1–6, SWM superficial white matter.

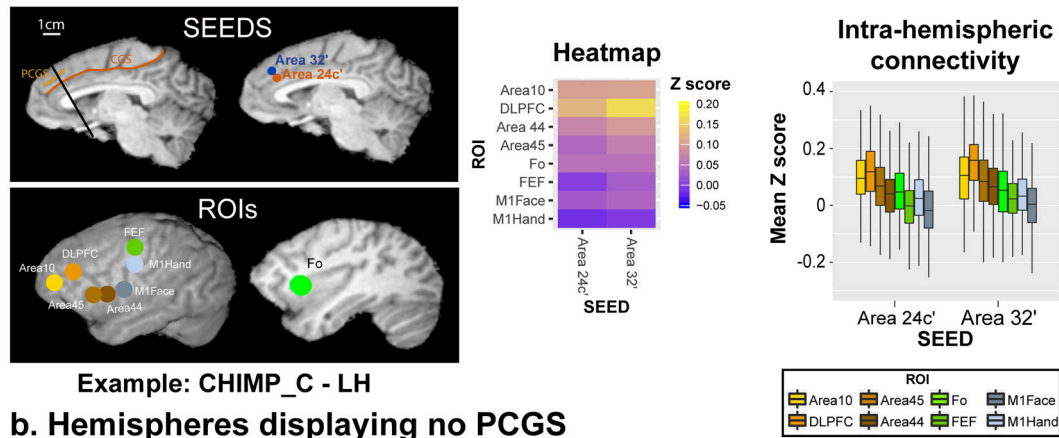
prefrontal/motor ROIs (see “Methods”). For each seed, we tested these differences in connectivity z values with a generalized linear model with ROI zones (prefrontal zones: Area 10, DLPFC (dorsolateral prefrontal cortex), Area 45, Area 44, and Fo (Frontal operculum), and motor zones: FEF (Frontal Eye Field), M1Face and M1Hand) as a fixed effect. To account for the variability observed across individuals, the chimpanzee ID was used as a random effect. The results indicated that, as in the human brain, the correlation strength between Area 24c' and Area 32' with the prefrontal cortex is significantly higher than with the motor zones (Area 24c': $df = 7$, $F = 154.8$, $p < 2.2e-16$; Area 32': $df = 7$, $F = 157$, $p < 2.2e-16$, ANOVA). We then assessed the linearity of correlation trends with lateral frontal areas along the rostro-caudal axis (Fig. 5c). To test and quantify these linear trends from anterior prefrontal to motor areas, we recoded the various lateral frontal ROIs into a numeric axis variable (ROLine) that corresponded to their relative posterior-to-anterior positions (see “Methods”). Based on this coding, the lowest value (1) corresponds to Area 10 (the most anterior ROI) and the highest

value (8) corresponds to the M1-Hand region (the most posterior ROI).

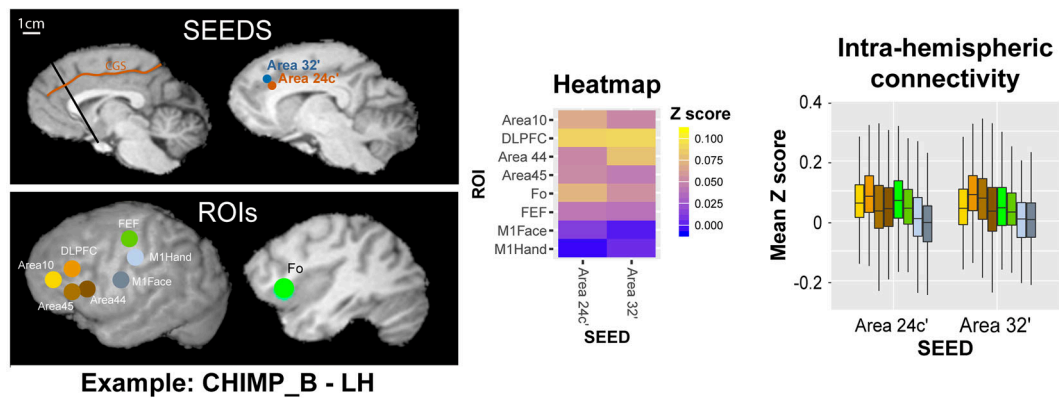
We performed the same analysis in hemispheres without a PCGS. The location of seeds and ROIs are displayed on the medial (left diagram) and the lateral cortical surface (right diagram) of a typical example (left hemisphere of CHIMP_B). The results indicated that, as in hemispheres displaying a PCGS, the correlation strength between Area 24c' and Area 32' with the prefrontal areas is significantly higher than with the motor zones as demonstrated by heat-maps and boxplots (Fig. 5b, Area 24c': $df = 7$, $F = 123.5$, $p < 2.2e-16$; Area 32': $df = 7$, $F = 110.1$, $p < 2.2e-16$, ANOVA; source data are provided as Supplementary data 2).

We then performed multiple linear regressions on the correlation values with seed identity, seed location, and ROline as predictors. A significant negative linear trend (slope) was observed for both seeds (stronger correlation with rostral prefrontal areas) and in both morphology types (presence or absence of a PCGS) (Fig. 5Cc. These negative slopes were

a. Hemispheres displaying a PCGS



b. Hemispheres displaying no PCGS



c. Linear trend of connectivity

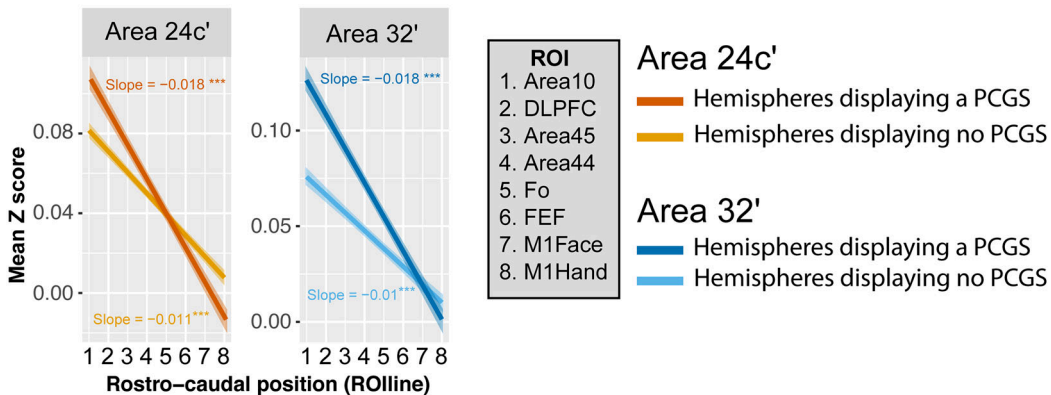


Fig. 5 Intra-hemispheric rostro-caudal functional organization between areas 24c' and 32' with the lateral frontal cortex in hemispheres displaying a PCGS (a, N = 3) and no PCGS (b, N = 5). **a** The location of each seed is shown in a typical example of a hemisphere displaying a PCGS (CHIMP_C - LH). The location of each region of interest (ROI) is shown on the cortical surface of the same hemisphere. The heat-map represents the averaged seed-ROI Z values in hemispheres displaying a PCGS. Boxplots displaying the mean ± SD Z-transformed connectivity between each seed (areas 24c' and 32') with the various ROIs in hemispheres displaying a PCGS. Results show that the correlation strength between Area 24c' and Area 32' with the prefrontal cortex is significantly higher than with the motor zones (Area 24c': $df = 7, F = 154.8, p < 2.2e-16$; Area 32': $df = 7, F = 157, p < 2.2e-16$, ANOVA). **b** The location of each seed is shown in a typical example of a hemisphere displaying no PCGS (CHIMP_B - LH). The heat-map represents the averaged seed-ROI Z values in hemispheres displaying a PCGS. Boxplots displaying the mean ± SD Z-transformed connectivity between each seed (areas 24c' and 32') with the various ROIs in hemispheres displaying no PCGS. Results show that the correlation strength between Area 24c' and Area 32' with the prefrontal areas is significantly higher than with the motor zones (Area 24c': $df = 7, F = 123.5, p < 2.2e-16$; Area 32': $df = 7, F = 110.1, p < 2.2e-16$, ANOVA). **c** Significant negative linear trend of connectivity (slope) of each seed with the rostro-caudal position of lateral frontal ROIs (ROIlines) in hemispheres displaying or not a PCGS. The ROIlines were obtained by recoding the ROIs in terms of their relative rostro-caudal rank: 1, Area 10; 2, DLPFC; 3, Area 45; 4, Area 44; 5, Fo; 6, FEF; 7, M1Face; 8, M1Hand. Results show that these negative slopes were statistically similar for both seeds (Area 24c' and Area 32') and for both morphologies (presence or absence of a PCGS) (interaction between seed identity, seed location, and ROIlines, $F = 3.03, p > 0.05$, ns, 3-ways ANOVA). LH left hemisphere; *** statistically significant at $p < 0.001$.

statistically similar for both seeds (Area 24c' and Area 32') and for both morphologies (presence or absence of a PCGS) (interaction between seed identity, seed location, and ROline, $F = 3.03$, $p = 0.08$, ns, 3-ways ANOVA).

Thus, the connectivity profiles of areas 24c' and 32' with the lateral frontal cortex regions follow the same pattern in hemispheres with a PCGS and those hemispheres that do not display a PCGS: both areas 24c' and 32' display equally stronger functional coupling with the lateral prefrontal cortex and weaker with the motor cortex.

Discussion

The present study demonstrates that the PCGS in the common chimpanzee (*Pan troglodytes*), as previously identified by morphological examination¹³, does correspond to the PCGS observed in the human (*Homo sapiens sapiens*)^{10,11}, both cytoarchitectonically and in term of functional connectivity.

When a PCGS is absent, the ventral and dorsal banks of the CGS are, respectively, occupied by areas 24c' and 32'; when a PCGS is present, we observed an expansion of area 32' on the medial wall above the CGS up to the fundus of the PCGS. Importantly, the functional connectivity of both areas 24c' and 32' with the lateral frontal cortex is similarly organized to that in the human brain³¹: both areas display equally stronger connectivity with rostral prefrontal areas than with caudal motor areas. Importantly, this gradient of functional connectivity can be observed despite the positioning of each ROI on the basis of the sulcal morphological organization in each chimpanzee brain (see "Methods" and Supplementary Fig. 1). Specifically, the positioning of each ROI was based on (1) the fMRI literature on the human brain concerning the precise relationship between the local sulcal organization and functional activity in the regions of interest^{37–41}, and (2) studies revealing that the sulcal organization between human and chimpanzee is well preserved^{13,37,42,43}. We chose this methodology because, for both ethical and methodological considerations, there is no study assessing the direct relationships between local sulcal morphology and functional activity in behaving chimpanzees. The present study strongly suggests that, in addition to preservation of the sulcal and cytoarchitectonic organization from the chimpanzee to the human brain, the sulcal-functional organization is also preserved. This is of importance because it indicates that the understanding of the sulcal organization in great apes may allow us to infer the functional organization of the brain in chimpanzees.

Based on the morphological sulcal organization of the medial prefrontal cortex¹³ and on the present study, three differences can be identified between the human and the chimpanzee cingulate organization: (1) the PCGS is present in fewer hemispheres in the chimpanzee (33.8% of chimpanzees display a PCGS at least in one hemisphere, compared to about 70% of humans); (2) the PCGS is more frequently observed in the left hemisphere than in the right hemisphere in the human but not in the chimpanzee brains; (3) the PCGS has a more caudal distribution in chimpanzee than in human brains, implying that the PCGS is more commonly found in the MCC compared to the ACC in chimpanzees.

The anatomo-functional organization of the cingulate cortex has received considerable attention. Along the rostral-caudal axis, several anatomical and functional subdivisions have been identified^{15,44–50}. Similarly, differences between the cingulate gyrus and the CGS have been demonstrated^{44,51–53}. One could identify similar functional properties of neurons in the ventral and dorsal banks of the CGS. For instance, neurons sensitive to distance to reward in a reward-guided sequential task have been recorded in both banks of the CGS^{54,55}. However, very few studies have directly investigated what might be the respective roles

of areas 24c' and 32' that occupy the banks of the CGS. In a rare study investigating the functional properties of the dorsal and ventral banks of the CGS in macaques, major differences were reported⁵⁶. Only neurons in the dorsal bank were modulated by the oculomotor saccade direction and, in addition, neurons in the dorsal bank were most active prior to the choice, while neurons in the ventral bank were most active at the outcome phase.

Sensorimotor properties of the human cingulate cortex have been well characterized⁵⁷. The aMCC contains a cingulate motor area (the anterior Rostral Cingulate Zone, RCZa) that is somatotopically organized. Whereas the face motor representations (mouth and eye) are located in the PCGS when present and in the CGS when the PCGS is absent (and, therefore, putatively in area 32'), the limb motor representations (hand and foot) are located in the CGS regardless of the presence or absence of the PCGS (and thus putatively in area 24c')^{31,32,37,50}. In exploratory situations in which the learning is driven by behavioral feedback, the analysis of visual, gustatory, and auditory feedback recruits a region located in the PCGS when present and in the CGS when the PCGS is absent^{37,38,40}, a region that is co-localized with the face motor area of RCZa^{37,50}. Altogether, these data led us to hypothesize that the role of the aMCC may be to perform an embodied analysis of feedback in exploratory situations, i.e. juice/visual/voice feedback recruit the face motor area of RCZa, whereas somatosensory feedback on the hand recruits the hand motor area of RCZa^{37,50}. Within this framework, areas 32' and 24c' might support effector specific comparable feedback-related functional processes in exploratory situations. In rhesus macaques, recordings from the ventral and dorsal banks of the CGS have highlighted the role of both structures in reward processing and behavioral adaptation^{54–56,58}. Given that both the cytoarchitectonic and the functional connectivity organization of the aMCC is comparable in macaque, chimpanzee and human brains, it is reasonable to hypothesize that the role of the aMCC in higher cognitive processing may also be preserved. However, in hemispheres displaying a PCGS, area 24c' occupies about half of the dorsal bank of the CGS in human brains^{10,44}, but it occupies only the fundus of the CGS and the most lateral part of the dorsal bank of the CGS in chimpanzee. One should be cautious in interpreting this difference as the boundaries between cingulate cortical areas 24c' and 32' in human brains are not consistent in the literature⁵⁹.

Unlike the human brain^{11,12,24,60}, we did not observe at the population level a left/right PCGS asymmetry in the chimpanzee. Although brain asymmetry is not a specifically human trait, its origins in a population have yet to be determined⁶¹. One hypothesis is that behavioral and brain asymmetry observed in primates might be related to the gradual evolution of language^{62–64}. At the individual subject level, future studies should aim at investigating a putative link between PCGS morphology and cognitive abilities in chimpanzees, as has been done in humans^{12,65}. Finally, another difference between human and chimpanzee brains is the prevalence of the PCGS in the ACC. While the PCGS is present in MCC in both chimpanzees and humans, the PCGS is more often observed in ACC in human brains. This finding suggests that differential evolutionary pressures impacted the ACC. This is a surprising result as some studies showed that the hotspot of cortical expansion in the primate medial frontal cortex may be located in the MCC rather than in the ACC^{66,67}. Other studies, however, showed that the ACC presents high structural variability across subjects in several primate species, contrasting with the MCC which presents less variability^{13,14,68}. The latter studies suggest that the ACC underwent greater expansion than the MCC during primate evolution. This expansion is however associated with a preserved cytoarchitectonic organization of the areas composing the ACC and adjacent ventromedial prefrontal cortex (vmPFC)^{30,35,47}.

Within the ACC, resting-state analyses have shown that area 24c has stronger coupling with the anterior insula, the striatum and the ventrolateral prefrontal cortex, while perigenual area 32 has stronger coupling with the dorsolateral prefrontal cortex, the amygdala, and the hippocampus³³. The ACC in the human brain has been associated with value-based computations in economic and social domains^{69–74}. Similar properties have been identified in the non-human primate brain^{52,75,76}. Implicit mentalizing abilities have been described in chimpanzees and macaques^{77,78}, and are affected by reversible lesions of the ACC in macaques⁷⁸. Recursive thinking and counterfactual manipulation of information to guide behavior have also been observed in macaques^{75,79}. Counterfactual reasoning was also impacted by reversible lesions of the ACC in macaques⁷⁵. However, human subjects have been shown to understand more complex relationships between social agents and their intentions than non-human primates^{70,80}. The more complex the information about intentionality of social agents a human subject can comprehend, the larger the gray matter volume in the ACC and vmPFC⁸¹. Altogether, these results suggest that the building blocks of a human ACC have been present since the last common ancestor to human and macaques, but its evolution might reflect the development of recursive thinking in hominids⁸².

To conclude, using multimodal data, the present study demonstrates that chimpanzee brains do possess a PCGS in the MCC that is comparable to that in the human brain in terms of cytoarchitecture and functional connectivity. The similarities between ACC and MCC in primates and rodents are still a matter of debate^{7,83}.

Methods

Subjects/specimens

Human subjects. The first step in this investigation was a reanalysis of the morphological organization of the PCGS in 197 human brains¹³ to refine our previous analysis by assessing the location and extent of the PCGS in the ACC and/or the MCC. High-resolution anatomical scans of these brains were obtained from the Human Connectome Project (HCP) database [<http://www.humanconnectome.org/>]. Only data from subjects with no family relationships were analyzed. The participants in the HCP study were recruited from the Missouri Family and Twin Registry that includes individuals born in Missouri⁸⁴. Acquisition parameters of T1 anatomical scans are the following: whole head, 0.7 mm³ isotropic resolution, TR = 2.4 s, TE = 2.14 ms, flip angle = 8° (more details can be found at [https://humanconnectome.org/storage/app/media/documentation/s1200/HCP_S1200_Release_Appendix_1.pdf]). The full set of inclusion and exclusion criteria is detailed elsewhere. Briefly, the HCP subjects are healthy individuals free from major psychiatric or neurological illnesses. They are drawn from ongoing longitudinal studies⁸⁴, in which they had received extensive assessments, including the history of drug use, and emotional and behavioral problems. The experiments were performed in accordance with relevant guidelines and regulations and all experimental protocols were approved by the Institutional Review Board (IRB) (IRB #201204036; Title: 'Mapping the Human Connectome: Structure, Function, and Heritability'). All subjects provided written informed consent on forms approved by the Institutional Review Board of Washington University in St Louis. In addition, the present study received approval (n°15-213) from the Ethics Committee of Inserm (IORG0003254, FWA00005831) and from the Institutional Review Board (IRB00003888) of the French Institute of Medical Research and Health.

Chimpanzee (*Pan troglodytes*). Three chimpanzee groups were examined in (1) the morphological sulcal organization of the medial frontal cortex (Group 1, $N = 225$), (2) in the cytoarchitectonic analysis of the MCC (Group 2, $N = 3$), and (3) in the functional connectivity analysis of the MCC (Group 3, $N = 4$, note that these four chimpanzees were also part of group 1).

Specifically, the morphological analysis aimed at refining our previous analysis on 225 chimpanzees¹³ by assessing the location and extent of the PCGS in the ACC and/or MCC. In the cytoarchitectonic analysis, we examined three post-mortem male chimpanzee brains that died from natural causes (CHIMP_1, CHIMP_2, and CHIMP_3; ages at death 38, 33, and 37 years, respectively). Within 14 h of each subject's death, the brain was removed and immersed in 10% formalin at necropsy. In the *in vivo* resting-state fMRI study, we analyzed the data obtained in four chimpanzees: three females (CHIMP_A, CHIMP_B, CHIMP_C, respectively 16, 17, and 27 years of age at the time of the experiment) and one male (CHIMP_D, 15 years of age). All four chimpanzees were captive born and were members of the

colony of apes housed at the Yerkes National Primate Research Center of Emory University.

The chimpanzees were all born in captivity and had all lived in social groups ranging from 2 to 13 individuals at the Yerkes National Primate Research Center and were housed according to institutional guidelines. Chimpanzee data collection was approved by the Institutional Animal Care and Use Committees at YNPRC and UTMACC and followed the guidelines of the Institute of Medicine in the use of chimpanzees in research. We note here that all *in vivo* MRI scans were obtained prior to changes in NIH policy on the acquisition of neuroimaging data from chimpanzees (Nov 2015).

MRI data acquisition

Structural MRI of post-mortem chimpanzee brains. Each post-mortem chimpanzee brain was scanned overnight in a 3 T Siemens Prisma MRI scanner to obtain structural T1 volumetric images (repetition time = 23 ms, echo time = 5.65 ms, voxel resolution = 0.4 × 0.4 × 0.4 mm). Each brain was scanned in a container filled with 10% formalin and supported with padding to prevent scanning artifacts from occurring near the edges of the container. 24, 4, and 36 repetitions of T1 scans of respectively CHIMP_1, CHIMP_2, and CHIMP_3 were obtained and averaged.

***In vivo* rs-fMRI acquisition in chimpanzee.** *In vivo* resting-state functional magnetic resonance imaging (rs-fMRI) data came from Dr Hopkins' laboratory. These data were acquired in early 2015 at the Yerkes National Primate Research Center (YNPRC) on the four adult chimpanzees at the time they were being surveyed for their annual physical examinations. Subjects were first immobilized by ketamine (10 mg/kg) or telazol (3–5 mg/kg) and subsequently anaesthetized with propofol (40–60 mg/[kg/h]) following standard procedures at the YNPRC. The subjects remained anaesthetized for the duration of the scans as well as the time needed to transport them between their home cage and the imaging facility (between 5 and 10 min). Chimpanzees were placed in the scanner chamber in a supine position with their head fitted inside the human-head coil.

They were scanned using a 3.0-T scanner (Siemens Trio; Siemens Medical Solutions USA, Inc., Malvern, PA, USA). T1-weighted images were collected using a three-dimensional gradient-echo sequence (repetition time = 2300 ms, echo time = 4.4 ms, number of signals averaged = 2, voxel resolution = 0.625 × 0.625 × 0.60 mm. In addition, 2 runs of 350 measurements each (16 min/session) of rs-fMRI scans were collected using a three-dimensional gradient-echo sequence (repetition time = 2683 ms, echo time = 25 ms, voxel resolution = 1.9 × 1.9 × 1.9 mm, right-left phase-encoding direction). An additional short run was performed with the same characteristics except that the phase-encoding was in the opposite direction (left-right). Scan duration was about 90 min.

After completing MRI procedures, the subjects were temporarily housed in a single enclosure for 6–12 h to allow the effects of the anesthesia to wear off before being returned to their social group.

Sulcal morphology of the medial frontal cortex. On the basis of structural T1 MRI scans of each hemisphere of all chimpanzee and human brains, we established the presence or absence of a PCGS in each cerebral hemisphere. A PCGS was marked as present if running parallel and dorsal to the CGS^{12,13}. We then examined whether this PCGS was located within the ACC, within the MCC, or extending along both regions. Note that the ACC-MCC limit was based on Vogt's four-region model (Fig. 1)^{15,45,85,86}.

Morphological analysis: occurrence and location of PCGS in human and chimpanzee. To establish the probability of occurrence of a PCGS in the MCC and the ACC in human and chimpanzee brains, we first reanalyzed the neuroimaging T1 anatomical data of 197 human brains and 225 chimpanzee brains from our previous study¹³. From this inspection, we identified 76 chimpanzees displaying a PCGS at least in one hemisphere (15, 29, and 32 displaying a PCGS in both hemispheres, only in the left hemisphere, and only in the right hemispheres, respectively), for a total of 91 hemispheres displaying a PCGS. We also identified 139 human brains displaying a PCGS at least in one hemisphere (45, 69, and 25 displaying a PCGS in both hemispheres, only in the left hemisphere, and only in the right hemispheres, respectively), for a total of 184 hemispheres displaying a PCGS. In these hemispheres, we then identified whether the PCGS was present in the ACC, the MCC, or in both the ACC and MCC. The limit between the ACC and the MCC was identified using the probabilistic cytoarchitectonic map of the ACC from the JuBrain atlas (<https://jubrain.fz-juelich.de/apps/cytoviewer2/cytoviewer-main.php#>)³³.

Cytoarchitectonic analysis: occurrence and location of PCGS in chimpanzee. From the morphological inspection of the three chimpanzee brains included in this analysis, we selected four hemispheres for the cytoarchitectonic analysis:

The left hemisphere of CHIMP_1, in which the PCGS is absent.

The right hemisphere of CHIMP_1, which displays a PCGS.

The left hemisphere of CHIMP_2, where a PCGS is present in the anterior-most part of the aMCC, but absent in the posterior part of the aMCC.

The right hemisphere of CHIMP_3, in which the PCGS is absent.

Note that the remaining hemispheres (left hemisphere of CHIMP_3 and right hemisphere of CHIMP_2) displayed no PCGS.

Rs-fMRI analysis: occurrence and location of PCGS in chimpanzee. We identified three hemispheres with a PCGS in the four chimpanzees included in this analysis:

Both the left and right hemispheres of CHIMP_C, and the left hemisphere of CHIMP_A, displayed a PCGS.

The right hemisphere of CHIMP_A, and both hemispheres of CHIMP_D and CHIMP_B did not display a PCGS.

Blocking and histological processing. Based on the averaged structural MRI data of the chimpanzee brains and using a neuronavigation system (Brainsight), each selected brain was cut in several blocks to obtain histological sections optimal for the study of the architecture of the regions of interest (see Novek et al.⁸⁷ for the method used). The blocks including the MCC were optimized to allow for histological sections that were perpendicular to the orientation of both the cingulate and/or paracingulate sulci. Note that the remaining blocks were processed for ongoing studies aiming to assess cytoarchitectonic areas of various regions of the chimpanzee cortex. All blocks were cryoprotected by immersion in buffered sucrose solutions from 10 to 30% until they sank, frozen to -60°C in a bath of 2-methylbutane chilled by a surrounding mixture of dry ice and ETOH, then stored at -80°C until use, where the block was kept surrounded by dry ice on a frozen microtome stage during sectioning. The histological sections were cut at a thickness of $30\ \mu\text{m}$, three out of every ten sections were kept, and a photograph was taken before each set of the kept sections throughout the entire blocks to aid with 3D reconstructions.

Cytoarchitectonic analysis. The detailed cytoarchitectonic analysis of the mid-cingulate cortex of the selected blocks was carried out from the sections that were cut in a coronal orientation. Every tenth section was mounted on $2'' \times 3''$ coated slides and stained with cresyl violet, a Nissl cell body stain, for cytoarchitectonic analysis; the remaining sections are being used in ongoing studies.

The architectonic organization of the MCC and, more specifically, the boundaries between the cytoarchitectonic areas composing the MCC, were identified on high-resolution tilted images of the entire region of interest from the cresyl violet sections, obtained under bright field with a Zeiss Axio Scan.Z1 at $\times 10$ magnification.

The assessment of the architectonic organization of the MCC was based on prior studies of this region in both the human¹⁰ and in the macaque monkey^{30,88} brains. Proceeding from the corpus callosum in a dorsal direction towards the lateral surface of the frontal lobe, the following areas were identified in the cingulate region: area 24a', area 24b', area 24c', and area 32'. Note that, dorsal to these cingulate cortical areas, the medial frontal areas 6, 8, and 9 are located. Area 24a' is an agranular area located on the gyrus just dorsal to the corpus callosum. It is characterized by a clear layer II, a thick layer III, a dense layer V, and a poorly defined layer VI. Area 24b' is an agranular area located dorsal to area 24a' and ends where the CGS starts. It is characterized by a broad layer III containing distinct layers IIIa, b, and c, as well as a highly prominent layer V composed of large pyramidal neurons. Area 24c' is an agranular area located in the ventral bank of the CGS and is characterized by thin layers II and III, as well as the presence of more densely packed large pyramidal neurons in layer V in comparison with area 24b'. Finally, area 32' is a dysgranular cingulo-frontal transitional area located dorsal to area 24c' in the dorsal bank of the CGS when there is no PCGS in the human brain and located within the PCGS if present¹⁰. In the macaque, area 32' (labeled as 32/6 or 32/8 in macaque) is located in the dorsal bank of the CGS^{30,88}. It displays a wide layer IIIc containing large pyramidal neurons, a dysgranular layer IV, and a thinner and less dense layer V than in area 24c'.

Rs-fMRI data analysis. Data were collected using 2 phase-encoding directions (2 full runs in Right-Left, and a shorter 3d run in Left-Right directions). It resulted in two pairs of images with distortions going in opposite directions (pair 1: 1st run in right-left and 3d run in left-right direction; pair 2: 2^d run in right-left and 3d run in left-right direction). Distortions were corrected using TOPUP's FSL tool. First, TOPUP estimated from these pairs the susceptibility-induced off-resonance field using a method similar to that described by Andersson et al.⁸⁹ as implemented in FSL⁹⁰. Once estimated, the images were then combined into corrected ones. Two runs, corrected for distortions, resulted from this analysis and were further preprocessed.

The preprocessing of resting-state scans was then performed with SPM 12. The first 5 volumes of each run were removed to allow for T1 equilibrium effects. The head motion correction was applied using rigid body realignment and we then applied a slice timing correction using the time center of the volume as reference. Then, using the AFNI software⁹¹, the segmentation of each brain was performed on skull-stripped brains. A temporal filtering was then applied to extract the spontaneous slowly fluctuating brain activity (0.01–0.1 Hz). Finally, linear regression was used to remove nuisance variables (the cerebrospinal fluid and white matter signals from the segmentation) and spatial smoothing with a 4-mm FWHM Gaussian kernel was applied to the output of the regression.

Seed selection in the MCC. The seeds consisted of 2.5-mm radius spheres and were positioned in the aMCC at the same antero-posterior level as in the cytoarchitectonic study as follows:

In hemispheres displaying no PCGS ($N = 5$): a seed assigned to area 24c' was positioned in the ventral bank of the CGS and a seed assigned to area 32' was positioned in the dorsal bank of the CGS.

In hemispheres displaying a PCGS ($N = 3$): a seed assigned to area 24c' was positioned in the CGS and a seed for area 32' was positioned in the ventral bank of the PCGS.

In both cases, the two seeds were positioned on an imaginary line going through the posterior limit of the genu of the corpus callosum and perpendicular to the axis on which the CGS and PCGS are running (see Supplementary Fig. 1 for positioning of seeds in all chimpanzees and hemispheres). In hemispheres displaying no PCGS, the two seeds (area 24c' and area 32') displayed a small overlap. This overlap was removed before performing the ROI-based resting-state data analysis.

Selection of regions of interest (ROIs). For a stricter comparison of the present results with results obtained in our previous study which assessed the functional connectivity of the CGS and PCGS in the anterior part of the human MCC³¹, we used the same ROIs (see below and Supplementary Fig. 1 for positioning of ROIs in all chimpanzees and hemispheres). Each ROI consisted of a sphere with a 5-mm radius.

ROIs selection in motor cortical areas. For each subject, 3 ROIs within the motor cortex of both hemispheres were identified based on sulcal morphology. These included the hand motor region (the precentral knob) within the central sulcus –M1Hand⁴³ and the primary face motor region within the ventral part of the posterior part of the precentral gyrus –M1Face⁹². We also included the frontal eye field –FEF-. In the human brain, this region is located within the ventral branch of the superior precentral sulcus³⁹. As the chimpanzee presents the same sulcal pattern in this region, including a ventral branch of the superior precentral sulcus, we tentatively included this ROI in our analysis.

Selection of ROIs in the prefrontal cortex. For each subject, 6 ROI locations within the left prefrontal cortex were identified based on the local anatomy. On a rostro-caudal axis:

The frontopolar cortex –Area 10–. In the human brain, this region is located at the intersection between the vertical segment of the intermediate frontal sulcus, the lateral and the medial frontomarginal sulcus, see⁴¹. Because chimpanzee brains display a similar sulcal pattern, we hypothesized that Area 10 most likely lies at the same location.

The dorsolateral prefrontal cortex –DLPFC–. In the human brain, area 9/46 of the DLPFC lies at the rostral level of the genu of the corpus callosum, above the inferior frontal sulcus. Because the chimpanzee displays also an inferior frontal sulcus that is also present at the level of the rostral level of the genu of the corpus callosum, we hypothesized that area 9/46 lies at the same location.

Broca's region: The two cytoarchitectonic areas that comprise Broca's region, namely area 44 and area 45, have been shown to be located in the chimpanzee brain between the inferior precentral sulcus and the fronto-orbital sulcus, and anterior to the fronto-orbital sulcus^{42,93}.

The frontal operculum –Fo– (intersection between the frontal operculum and the circular sulcus, see ref. ³⁸).

Statistics and reproducibility. The mean signal from Seeds and ROI regions was then extracted using AFNI software. For each chimpanzee brain, correlation coefficients between the two seeds with the various ROIs in the prefrontal cortex and the motor cortex were computed and normalized using the Fisher's r -to- z transform formula. The significant threshold at the individual subject level was $Z = 0.1$ ($p < 0.05$). These normalized correlation coefficients, which corresponded to the functional connectivity strength between each seed and each ROI in individual chimpanzee brains, were subsequently processed with R statistical software (<https://www.r-project.org/>) for all the following analyses.

To compare the connectivity profile of each seed with the various lateral frontal ROIs, we constructed boxplots corresponding to the correlation strength of each seed location with each of the ROIs. Based on these boxplots, it can be discerned that both Area 24c' and Area 32' seeds have stronger connectivity with prefrontal regions and weaker connectivity with premotor and motor areas (see "Results"). We then characterized this rostro-caudal functional axis based on the correlation profiles of Area 24c' and Area 32', when a PCGS is present and also when it is not present, with the lateral frontal cortex by estimating linear trends in the correlation strength for each seed with the rostro-caudal lateral frontal ROIs (for details, see "Methods" in Loh et al.³¹). The 8 ROIs were first ranked along a rostro-caudal axis based on their average Y coordinate values across chimpanzee brains and recoded into a numeric axis variable (ROLine): Area 10 (most anterior)-1, DLPFC-2, Area 45-3, Area 44-4, Fo-5, FEF-6, M1Face-7, M1Hand (most posterior)-8. We then performed multiple linear regressions on the correlation z values with seed identity (area 24c' and area 32'), sulcal morphology (PCGS absent or present), and the linear axis variable (ROLine) as predictors. We assessed whether the linear trends

(slopes) observed for each seed were identical or not in each sulcal morphology using a 3-ways ANOVA.

Reporting summary. Further information on research design is available in the Nature Research Reporting Summary linked to this article.

Data availability

The source data underlying Figs. 1 and 5 are provided as Source Data file (respectively Supplementary Data 1 and Supplementary Data 2). Human anatomical MRI scans are available from the Human Connectome Project database [<http://www.humanconnectome.org/>]⁹⁴, and Chimpanzee anatomical MRI and rs-fMRI scans are available from Dr. W. Hopkins [<http://www.chimpanzeebrain.org/>]⁹⁵. A reporting summary for this Article is available as a Supplementary Information file.

Received: 1 September 2020; Accepted: 25 November 2020;

Published online: 08 January 2021

References

- Dunbar, R. I. M. & Shultz, S. Why are there so many explanations for primate brain evolution? *Phil. Trans. R. Soc. B* **372**, 20160244 (2017).
- Barton, R. A. & Montgomery, S. H. Proportional versus relative size as metrics in human brain evolution. *Proc. Natl Acad. Sci. USA* **116**, 3–4 (2019).
- DeCasien, A. R., Williams, S. A. & Higham, J. P. Primate brain size is predicted by diet but not sociality. *Nat. Ecol. Evol.* **1**, 112 (2017).
- Mars, R. B. et al. Primate comparative neuroscience using magnetic resonance imaging: promises and challenges. *Front. Neurosci.* **8**, 298 (2014).
- DeCasien, A. R. & Higham, J. P. Primate mosaic brain evolution reflects selection on sensory and cognitive specialization. *Nat. Ecol. Evol.* **3**, 1483–1493 (2019).
- Sallet, J. et al. The organization of dorsal frontal cortex in humans and macaques. *J. Neurosci.* **33**, 12255–12274 (2013).
- Schaeffer, D. J. et al. Divergence of rodent and primate medial frontal cortex functional connectivity. *Proc. Natl Acad. Sci. USA* **117**, 21681–21689 (2020).
- Schrage, C. G. & Russo, C. A. M. Timing the origin of New World monkeys. *Mol. Biol. Evol.* **20**, 1620–1625 (2003).
- Passingham, R. How good is the macaque monkey model of the human brain? *Curr. Opin. Neurobiol.* **19**, 6–11 (2009).
- Vogt, B. A., Nimchinsky, E. A., Vogt, L. J. & Hof, P. R. Human cingulate cortex: surface features, flat maps, and cytoarchitecture. *J. Comp. Neurol.* **359**, 490–506 (1995).
- Paus, T. et al. Human cingulate and paracingulate sulci: pattern, variability, asymmetry, and probabilistic map. *Cereb. Cortex* **6**, 207–214 (1996).
- Amiez, C., Wilson, C. R. E. & Procyk, E. Variations of cingulate sulcal organization and link with cognitive performance. *Sci. Rep.* **8**, 13988 (2018).
- Amiez, C. et al. Sulcal organization in the medial frontal cortex provides insights into primate brain evolution. *Nat. Commun.* **10**, 3437 (2019).
- Lopez-Perssem, A., Verhagen, L., Amiez, C., Petrides, M. & Sallet, J. The human ventromedial prefrontal cortex: sulcal morphology and its influence on functional organization. *J. Neurosci.* **39**, 3627–3639 (2019).
- Vogt, B. A., Berger, G. R. & Derbyshire, S. W. G. Structural and functional dichotomy of human midcingulate cortex. *Eur. J. Neurosci.* **18**, 3134–3144 (2003).
- Mériaux, K. et al. A neural network reflecting individual differences in cognitive processing of emotions during perceptual decision making. *Neuroimage* **33**, 1016–1027 (2006).
- Whittle, S. et al. Variations in cortical folding patterns are related to individual differences in temperament. *Psychiatry Res.* **172**, 68–74 (2009).
- Kanai, R. & Rees, G. The structural basis of inter-individual differences in human behaviour and cognition. *Nat. Rev. Neurosci.* **12**, 231–242 (2011).
- Yücel, M. et al. Paracingulate morphologic differences in males with established schizophrenia: a magnetic resonance imaging morphometric study. *Biol. Psychiatry* **52**, 15–23 (2002).
- Yücel, M. et al. Anterior cingulate dysfunction: implications for psychiatric disorders? *J. Psychiatry Neurosci.* **28**, 350–354 (2003).
- Le Provost, J.-B. et al. Paracingulate sulcus morphology in men with early-onset schizophrenia. *Br. J. Psychiatry* **182**, 228–232 (2003).
- Shim, G. et al. Reduced cortical folding of the anterior cingulate cortex in obsessive-compulsive disorder. *J. Psychiatry Neurosci.* **34**, 443–449 (2009).
- Meredith, S. M. et al. Anterior cingulate morphology in people at genetic high-risk of schizophrenia. *Eur. Psychiatry* **27**, 377–385 (2012).
- Fornito, A. et al. Individual differences in anterior cingulate/paracingulate morphology are related to executive functions in healthy males. *Cereb. Cortex* **14**, 424–431 (2004).
- Buda, M., Fornito, A., Bergström, Z. M. & Simons, J. S. A specific brain structural basis for individual differences in reality monitoring. *J. Neurosci.* **31**, 14308–14313 (2011).
- Borst, G. et al. Folding of the anterior cingulate cortex partially explains inhibitory control during childhood: a longitudinal study. *Dev. Cogn. Neurosci.* **9**, 126–135 (2014).
- Cachia, A. et al. Longitudinal stability of the folding pattern of the anterior cingulate cortex during development. *Dev. Cogn. Neurosci.* **19**, 122–127 (2016).
- Cole, M. W., Yeung, N., Freiwald, W. A. & Botvinick, M. Cingulate cortex: diverging data from humans and monkeys. *Trends Neurosci.* **32**, 566–574 (2009).
- Vogt, B. A. Architecture, Neurocytology and Comparative Organization of Monkey and Human Cingulate Cortices. In *Cingulate Neurobiology and Disease*. (ed. Vogt, B. A.) 65–93 (Oxford University Press, 2009).
- Petrides, M. & Pandya, D. N. Comparative architectonic analysis of the human and the macaque frontal cortex. In *Handbook of Neuropsychology*, (eds. Boller, F. & Grafman, J.), 9, 17–58 (Amsterdam, Elsevier, 1994).
- Loh, K. K., Hadj-Bouziane, F., Petrides, M., Procyk, E. & Amiez, C. Rostro-caudal organization of motor areas and lateral frontal regions. *Front. Neurosci.* **11**, 753 (2018).
- Amiez, C. & Petrides, M. Neuroimaging evidence of the anatomo-functional organization of the human cingulate motor areas. *Cereb. Cortex* **24**, 563–578 (2014).
- Palomero-Gallagher, N. et al. Human pregenual anterior cingulate cortex: structural, functional, and connective heterogeneity. *Cereb. Cortex* **29**, 2552–2574 (2019).
- Mackey, S. & Petrides, M. Architecture and morphology of the human ventromedial prefrontal cortex. *Eur. J. Neurosci.* **40**, 2777–2796 (2014).
- Mackey, S. & Petrides, M. Quantitative demonstration of comparable architectonic areas within the ventromedial and lateral orbital frontal cortex in the human and the macaque monkey brains. *Eur. J. Neurosci.* **32**, 1940–1950 (2010).
- Vogt, B. A. Regions and Subregions of the Cingulate Cortex. In *Cingulate Neurobiology and Disease*. (ed. Vogt, B. A.) 3–30 (Oxford University Press, 2009).
- Loh, K. K. et al. Cognitive control of orofacial motor and vocal responses in the ventrolateral and dorsomedial human frontal cortex. *Proc. Natl Acad. Sci. USA* **117**, 4994–5005 (2020).
- Amiez, C. et al. The location of feedback-related activity in the midcingulate cortex is predicted by local morphology. *J. Neurosci.* **33**, 2217–2228 (2013).
- Amiez, C., Kostopoulos, P., Champod, A.-S. & Petrides, M. Local morphology predicts functional organization of the dorsal premotor region in the human brain. *J. Neurosci.* **26**, 2724–2731 (2006).
- Amiez, C. et al. Single subject analyses reveal consistent recruitment of frontal operculum in performance monitoring. *Neuroimage* **133**, 266–278 (2016).
- Petrides, M. *The Human Cerebral Cortex. An MRI Atlas of the Sulci and Gyri in MNI Stereotaxic Space*. (Academic Press, New York, 2012).
- Schenker, N. M. et al. Broca's area homologue in chimpanzees (Pan troglodytes): probabilistic mapping, asymmetry, and comparison to humans. *Cereb. Cortex* **20**, 730–742 (2010).
- Hopkins, W. D. et al. Evolution of the central sulcus morphology in primates. *Brain Behav. Evol.* **84**, 19–30 (2014).
- Palomero-Gallagher, N., Mohlberg, H., Zilles, K. & Vogt, B. Cytology and receptor architecture of human anterior cingulate cortex. *J. Comp. Neurol.* **508**, 906–926 (2008).
- Palomero-Gallagher, N., Vogt, B. A., Schleicher, A., Mayberg, H. S. & Zilles, K. Receptor architecture of human cingulate cortex: evaluation of the four-region neurobiological model. *Hum. Brain Mapp.* **30**, 2336–2355 (2009).
- Alexander, W. H. & Brown, J. W. Medial prefrontal cortex as an action-outcome predictor. *Nat. Neurosci.* **14**, 1338–1344 (2011).
- Neubert, F.-X., Mars, R. B., Sallet, J. & Rushworth, M. F. S. Connectivity reveals relationship of brain areas for reward-guided learning and decision making in human and monkey frontal cortex. *Proc. Natl Acad. Sci. USA* **112**, E2695–E2704 (2015).
- Heilbronner, S. R. & Hayden, B. Y. Dorsal anterior cingulate cortex: a bottom-up view. *Annu. Rev. Neurosci.* **39**, 149–170 (2016).
- Kolling, N. et al. Value, search, persistence and model updating in anterior cingulate cortex. *Nat. Neurosci.* **19**, 1280–1285 (2016).
- Procyk, E. et al. Midcingulate motor map and feedback detection: converging data from humans and monkeys. *Cereb. Cortex* **26**, 467–476 (2016).
- Rudebeck, P. H., Buckley, M. J., Walton, M. E. & Rushworth, M. F. S. A role for the macaque anterior cingulate gyrus in social valuation. *Science* **313**, 1310–1312 (2006).
- Chang, S. W. C., Gariépy, J.-F. & Platt, M. L. Neuronal reference frames for social decisions in primate frontal cortex. *Nat. Neurosci.* **16**, 243–250 (2013).
- Apps, M. A. J., Rushworth, M. F. S. & Chang, S. W. C. The anterior cingulate gyrus and social cognition: tracking the motivation of others. *Neuron* **90**, 692–707 (2016).
- Procyk, E., Tanaka, Y. L. & Joseph, J. P. Anterior cingulate activity during routine and non-routine sequential behaviors in macaques. *Nat. Neurosci.* **3**, 502–508 (2000).

55. Shidara, M. & Richmond, B. J. Anterior cingulate: single neuronal signals related to degree of reward expectancy. *Science* **296**, 1709–1711 (2002).
56. Cai, X. & Padoa-Schioppa, C. Neuronal encoding of subjective value in dorsal and ventral anterior cingulate cortex. *J. Neurosci.* **32**, 3791–3808 (2012).
57. Picard, N. & Strick, P. L. Imaging the premotor areas. *Curr. Opin. Neurobiol.* **11**, 663–672 (2001).
58. Amiez, C., Joseph, J. P. & Procyk, E. Reward encoding in the monkey anterior cingulate cortex. *Cereb. Cortex* **16**, 1040–1055 (2006).
59. Ding, S.-L. et al. Comprehensive cellular-resolution atlas of the adult human brain. *J. Comp. Neurol.* **524**, 3127–3481 (2016).
60. Wei, X. et al. Paracingulate sulcus asymmetry in the human brain: effects of sex, handedness, and race. *Sci. Rep.* **7**, 42033 (2017).
61. Vallortigara, G., Chiandetti, C. & Sovrano, V. A. Brain asymmetry (animal). *Wiley Interdiscip. Rev. Cogn. Sci.* **2**, 146–157 (2011).
62. Gentilucci, M. & Corballis, M. C. From manual gesture to speech: a gradual transition. *Neurosci. Biobehav. Rev.* **30**, 949–960 (2006).
63. Iturria-Medina, Y. et al. Brain hemispheric structural efficiency and interconnectivity rightward asymmetry in human and nonhuman primates. *Cereb. Cortex* **21**, 56–67 (2011).
64. Meguerditchian, A. & Vaclair, J. Baboons communicate with their right hand. *Behav. Brain Res.* **171**, 170–174 (2006).
65. Del Maschio, N. et al. ACC Sulcal patterns and their modulation on cognitive control efficiency across lifespan: a neuroanatomical study on bilinguals and monolinguals. *Cereb. Cortex* **29**, 3091–3101 (2019).
66. Sneve, M. H. et al. High-expanding regions in primate cortical brain evolution support supramodal cognitive flexibility. *Cereb. Cortex* **29**, 3891–3901 (2019).
67. Chaplin, T. A., Yu, H.-H., Soares, J. G. M., Gattass, R. & Rosa, M. G. P. A conserved pattern of differential expansion of cortical areas in simian primates. *J. Neurosci.* **33**, 15120–15125 (2013).
68. Croxson, P. L., Forkel, S. J., Cerliani, L. & Thiebaut de Schotten, M. Structural variability across the primate brain: a cross-species comparison. *Cereb. Cortex* **28**, 3829–3841 (2018).
69. Amodio, D. M. & Frith, C. D. Meeting of minds: the medial frontal cortex and social cognition. *Nat. Rev. Neurosci.* **7**, 268–277 (2006).
70. Coricelli, G. & Nagel, R. Neural correlates of depth of strategic reasoning in medial prefrontal cortex. *Proc. Natl Acad. Sci. USA* **106**, 9163–9168 (2009).
71. Nicolle, A. et al. An agent independent axis for executed and modeled choice in medial prefrontal cortex. *Neuron* **75**, 1114–1121 (2012).
72. Bartra, O., McGuire, J. T. & Kable, J. W. The valuation system: a coordinate-based meta-analysis of BOLD fMRI experiments examining neural correlates of subjective value. *Neuroimage* **76**, 412–427 (2013).
73. Vassena, E., Krebs, R. M., Silvetti, M., Fias, W. & Verguts, T. Dissociating contributions of ACC and vmPFC in reward prediction, outcome, and choice. *Neuropsychologia* **59**, 112–123 (2014).
74. Juechems, K. et al. A network for computing value equilibrium in the human medial prefrontal cortex. *Neuron* **101**, 977–987.e3 (2019).
75. Fouragnan, E. F. et al. The macaque anterior cingulate cortex translates counterfactual choice value into actual behavioral change. *Nat. Neurosci.* **22**, 797–808 (2019).
76. Hunt, L. T. et al. Triple dissociation of attention and decision computations across prefrontal cortex. *Nat. Neurosci.* **21**, 1471–1481 (2018).
77. Krupenye, C., Kano, F., Hirata, S., Call, J. & Tomasello, M. Great apes anticipate that other individuals will act according to false beliefs. *Science* **354**, 110–114 (2016).
78. Hayashi, T. et al. Macaques exhibit implicit gaze bias anticipating others' false-belief-driven actions via medial prefrontal cortex. *Cell. Rep.* **30**, 4433–4444.e5 (2020).
79. Ferrigno, S., Cheyette, S. J., Piantadosi, S. T. & Cantlon, J. F. Recursive sequence generation in monkeys, children, U.S. adults, and native Amazonians. *Sci. Adv.* **6**, eaaz1002 (2020).
80. Powell, J. L., Lewis, P. A., Dunbar, R. I. M., García-Fiñana, M. & Roberts, N. Orbital prefrontal cortex volume correlates with social cognitive competence. *Neuropsychologia* **48**, 3554–3562 (2010).
81. Lewis, P. A., Rezaie, R., Brown, R., Roberts, N. & Dunbar, R. I. M. Ventromedial prefrontal volume predicts understanding of others and social network size. *NeuroImage* **57**, 1624–1629 (2011).
82. Corballis, M. C. *The Recursive Mind: the origins of human language, thought, and civilization*. (Princeton University Press, 2011).
83. van Heukelum, S. et al. Where is cingulate cortex? A cross-species view. *Trends Neurosci.* **43**, 285–299 (2020).
84. Van Essen, D. C. et al. The Human Connectome Project: a data acquisition perspective. *Neuroimage* **62**, 2222–2231 (2012).
85. Vogt, B. A. & Vogt, L. Cytology of human dorsal midcingulate and supplementary motor cortices. *J. Chem. Neuroanat.* **26**, 301–309 (2003).
86. Vogt, B. A., Vogt, L. & Laureys, S. Cytology and functionally correlated circuits of human posterior cingulate areas. *Neuroimage* **29**, 452–466 (2006).
87. Novak, J., Sprung-Much, T., Nolan, E., Frey, S. & Petrides, M. Optimal cutting of the cortex for cytoarchitectonic visualization: a neuronavigation-based approach. in vol. Organization for Human Brain Mapping (OHBM), Abstract M854 (2019).
88. Morecraft, R. J. et al. Cytoarchitecture and cortical connections of the anterior cingulate and adjacent somatomotor fields in the rhesus monkey. *Brain Res. Bull.* **87**, 457–497 (2012).
89. Andersson, J. L. R., Skare, S. & Ashburner, J. How to correct susceptibility distortions in spin-echo echo-planar images: application to diffusion tensor imaging. *Neuroimage* **20**, 870–888 (2003).
90. Smith, S. M. et al. Advances in functional and structural MR image analysis and implementation as FSL. *Neuroimage* **23**, S208–S219 (2004).
91. Cox, R. W. AFNI: software for analysis and visualization of functional magnetic resonance neuroimages. *Comput. Biomed. Res.* **29**, 162–173 (1996).
92. Bailey, P., Von Bonin, G. & McCulloch, W. S. *The Isocortex of the Chimpanzee*. (University of Illinois Press, 1950).
93. Keller, S. S., Roberts, N. & Hopkins, W. A comparative magnetic resonance imaging study of the anatomy, variability, and asymmetry of Broca's area in the human and chimpanzee brain. *J. Neurosci.* **29**, 14607–14616 (2009).
94. Human Connectome Project database, <http://www.humanconnectome.org/>.
95. Chimpanzee MRI database, <http://www.chimpanzeebrain.org/>.

Acknowledgements

This work was supported by the Human Frontier Science Program (RGP0044/2014). C.A. received funding from the French National Research Agency (ANR-18-CE37-0012-01). J.S. was supported by a Sir Henry Dale Wellcome Trust Fellowship (105651/Z/14/Z) and IDEXLYON “IMPULSION” 2020 grant (IDEX/IMP/2020/14). The Wellcome Centre for Integrative Neuroimaging is supported by core funding from the Wellcome Trust (203139/Z/16/Z). C.A. and J.S. were also supported by Laboratoire d'excellence (LabEx) CORTEX ANR-11-LABX-0042 of Université de Lyon. W.D.H. is supported by NIH grants NS-042867, NS-073134, and NS-092988. M.P. was supported by the Canadian Institutes of Health Research (CIHR) Foundation grant FDN-143212. C.A. is employed by the Centre National de la Recherche Scientifique. We thank Sarah Lefebvre, Kristina Drudik, and Ilana Ruth Leppert for technical assistance in histology and scanning the tissue in the MRI. We also thank Franck Lambertson for help with analysis of rs-fMRI data obtained in chimpanzee.

Author contributions

C.A. organized the project and coordinated the consortium to gather the dataset. C.A., J.S., and M.P. interpreted data and wrote the article. J.N. and M.P. acquired post-mortem structural MRI scans in chimpanzees. C.A., J.S., J.N., and M.P. performed the blocking and histological processing of post-mortem chimpanzee brains. C.A., J.S., F.H.-B., C.G., and J.A. performed the analysis of chimpanzee rs-fMRI data. W.D.H. provided in vivo chimpanzee T1 and rs-fMRI data.

Competing interests

The authors declare no competing interests.

Additional information

Supplementary information is available for this paper at <https://doi.org/10.1038/s42003-020-01571-3>.

Correspondence and requests for materials should be addressed to C.A.

Reprints and permission information is available at <http://www.nature.com/reprints>

Publisher's note Springer Nature remains neutral with regard to jurisdictional claims in published maps and institutional affiliations.



Open Access This article is licensed under a Creative Commons Attribution 4.0 International License, which permits use, sharing, adaptation, distribution and reproduction in any medium or format, as long as you give appropriate credit to the original author(s) and the source, provide a link to the Creative Commons license, and indicate if changes were made. The images or other third party material in this article are included in the article's Creative Commons license, unless indicated otherwise in a credit line to the material. If material is not included in the article's Creative Commons license and your intended use is not permitted by statutory regulation or exceeds the permitted use, you will need to obtain permission directly from the copyright holder. To view a copy of this license, visit <http://creativecommons.org/licenses/by/4.0/>.

© The Author(s) 2021